Universidad de La Laguna

Departamento de Ingeniería Química y Tecnología Farmacéutica

Tesis Doctoral:

Estrategias para regeneración ósea en osteoporosis: estructuras 3D y liberación controlada

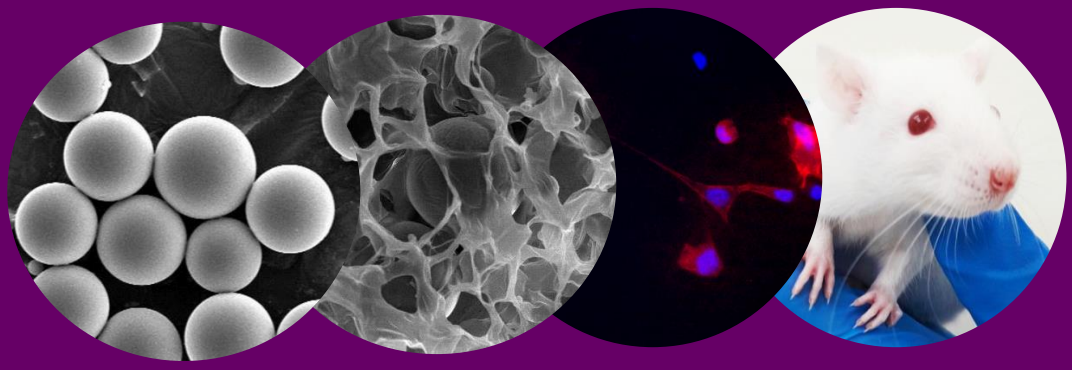

Patricia García García

Julio 2021

Universidad de La Laguna

Departamento de Ingeniería Química y Tecnología Farmacéutica

Memoria para optar al grado de Doctor en Ciencias de la Salud.

ESTRATEGIAS PARA REGENERACIÓN ÓSEA EN OSTEOPOROSIS: ESTRUCTURAS 3D Y LIBERACIÓN CONTROLADA

Directora: Araceli Delgado Hernández
Codirectora: Carmen Évora García.

Autora: Patricia García García.
Julio 2021

Departamento de Ingeniería Química y Tecnología Farmacéutica
Universidad de La Laguna

Araceli Delgado Hernández y **Carmen Évora García** Profesora Titular y Catedrática, respectivamente, del área de Farmacia y Tecnología Farmacéutica del Departamento de Ingeniería Química y Tecnología Farmacéutica,

Hacen constar:

1. Que Dª **Patricia García García**, Graduada en Farmacia ha realizado este trabajo de Tesis Doctoral que lleva por título: "Estrategias para regeneración ósea en osteoporosis: estructuras 3D y liberación controlada"

2. Que una vez revisada la memoria de Tesis Doctoral y, previo informe favorable de la Comisión Académica del Programa de Doctorado de Ciencias de la Salud, expresan su conformidad para que sea defendida ante el Tribunal correspondiente designado al efecto, ya que reúne los requisitos necesarios para optar al grado de Doctor.

Para que conste y surta los efectos oportunos, firman el presente documento en San Cristóbal de La Laguna, a 29 de junio de 2021

Dra. Araceli Delgado Hernández
Directora

Dra. Carmen Évora García
Codirectora

This thesis has been supported by the Ministry of Economy and Competitive (MAT2014-55657). Patricia García García acknowledges the predoctoral grant “Contratos predoctorales para la formación de Doctores M-ULL”

"Todo aquello que el hombre es capaz de imaginar es susceptible de llegar a suceder"

Eiichirō Oda

Aunque probablemente nunca vayas a leerlo, esto es para ti abuela

También para alguien que lo leyó con muchísimo interés, para Patri Díaz

Agradecimientos

Me atrevería a decir que todas las personas que hacen una tesis esperan que llegue este momento porque significa que has sido capaz de terminar, sorteando las adversidades, yo a veces echo la vista a atrás y pienso en cómo empezó toda esta historia y cómo he llegado hasta acabar una tesis. Todo empezó un día que La *Dra. Carmen (May)* me vio por el pasillo y literalmente gritó: ¡¡¡Ahora tenemos una tesis!!!, ¿por qué no vienes?, a lo que yo pensé, pues total, tampoco es que tenga nada mejor que hacer. Tal como se esperaba, aquella tesis se defendió sin percances y obtuvo un Sobresaliente Cum Lauden, y yo salí de aquella defensa de tesis de la cual no había entendido absolutamente nada, pero si tenía una cosa clara, me fascinó completamente. Gracias *May*, cuando estaba perdida, con unas simples palabras me encauzaste al camino que quiero seguir por el resto de mi vida y me sigues ayudando a encontrarme todos los días.

Gracias a la *Dra. Carmen Évora (May)* que no sólo me enseñó ciencia, sino que uno vale lo que esté dispuesto a trabajar, que si trabajas duro eres capaz de cualquier cosa y arreglar los "errores" del pasado. Gracias por darme una oportunidad a pesar de no ser alumno "brillante" y gracias por contagiarme tu actitud de arriesgar, tu espíritu trabajador y divertido.

Gracias a la *Dra. Araceli*, aunque más de una vez te hice perder la paciencia, gracias por todos sus consejos desde el primer día, su apoyo siempre que fue necesario y todo lo que me ha enseñado hasta ahora, por enseñarme a trabajar bien y con cabeza, y por supuesto, por forjarme el carácter.

Gracias a las dos por permitirme formar parte de esta pequeña familia que forma el grupo de investigación y guiarme siempre en esta aventura de la tesis. A las dos, mil gracias.

A la *Dra. Patricia Díaz*, gracias por todo lo que me has aportado tanto a nivel profesional como personal, me siento muy muy muy afortunada de haber podido trabajar contigo y de nuestra amistad, he de decir, que por mucho que me esfuerce son incapaz de expresar con palabras todo mi agradecimiento hacia a ti. Por estar siempre ahí para darme una colleja cuando me la merecía para enseñarme a que tengo que creer más en mí misma, para echarme siempre una mano en el laboratorio, por transmitirme tu pasión por lo que uno hace y por supuesto, ¡por todos los refraneros gallegos que aprendí! Y por último, gracias por enseñarme lo más importante que he aprendido hasta ahora, el uso del pensamiento crítico. ¡Gracias *Patricia*, nuestra señora de la Ciencia!

A todos los profesores del área de tecnología Farmacéutica, gracias por hacerme sentir este sitio como mi casa. Especialmente al *Dr. Alexia Oliva* que siempre

estuviste desde tu islita como dices tú, animándome, y a la *Dra. Mabel Soriano* que venía todas las tardes a animarme con la escritura de la tesis. No puedo olvidarme de la inestimable ayuda de *Laura Barroso* y de por supuesto, de *Margarita de la Rosa*, que siempre estuvo ahí, para un subsanar un documento, para buscar soluciones, para un darme consejo, para cada mañana un café lleno de contagiosa alegría y optimismo….

A alguien sin quien esta tesis no estaría, gracias al *Dr. Ricardo Reyes* por toda su ayuda, enseñanzas de técnicas que desconocía y por su disposición en cualquier momento.

Aunque fueron pocos, gracias a los compañeros de laboratorio, al *Dr. Javier Suárez* el "colega del otro lado" por sus ánimos y compañía, a la Dra. *Elisabet Segredo* por su apoyo constante, antes, durante y después, y la *Dra. Itxaso García* por introducirme en los mundos del laboratorio. Añadir a este agradecimiento a todos los TFGs con los cuales he podido compartir tardes, aprender cosas y disfrutar, gracias a los chiquillos como yo les decía, especialmente a *Sergio y Sara*.

A todo el personal del Estabulario Central de la Universidad, por su ayuda, sus ánimos y enseñanzas en especial a la *Dra. María Rosa*. Muchas gracias por todo lo que me has enseñado a lo largo de estos años de trabajo, daba gusto pasar las mañanas en el quirófano contigo. Gracias por todo lo que me has enseñado, por todo lo que te queda por enseñarme y por contagiarme tu optimismo, alegría y positivismo.

A esa pequeña "secta" del grupo de genética que me "adoptó" como una más, en especial a la *Dra. Teresa (Teresita)* y la *predoctora Ana (Anita)*, por contagiarme sus risas y sus locuras, y por enseñarme que lo mío es de ellas y lo de ellas es mío (dejen de sustraerme el DMEM por favor). *Ana*, te doy gracias por todo, por todo lo que eres, gracias por ser tú y por todas esas cosas que me aportas como amiga y compañera, también por todos esos ratitos y por las anécdotas de cuando se nos complicaban las noches de cañas y los domingos de chándal que había que subir a "dar de comer a toda esa gente".

A todos mis amigos, a mis pequeños *"cáncamos"*, por esas reuniones que me daban la vida, que me aguantaron todos esos días que llegaba hasta el gorro y los días que llegaba emocionada por la ciencia y que me aguantaron cada vez que se me nublaba la vista o hablaba del alambrito. A mis amigas con algo más de fundamento, *Kelly* gracias por tu sabiduría y optimismo, *Cele*, gracias por lo loca que estás y lo divertida que eres. A todos los demás gracias.

A dos personas especiales que están desde que empezamos juntos la aventura de la carrera de Farmacia y espero que estén ahí cuando empecemos la del asilo de jubilados. A mi "K: constante de eliminación" *(Pablo)*, con nuestros más y

nuestros menos siempre estuviste para escucharme, animarme y hacerme reír. Y a *Nere*, gracias por soportarme durante estos 10 estupendos años, nos alegramos y estuvimos tristes juntas, te hice perder la paciencia más de una vez, pero pasara lo que pasara siempre creíste en mí. Gracias.

A *Davi*, por sus cada vez que se acordaba de mi agobio constante y me mandaba un tupper de comida casera, o me hacía terapia con "Margarito perrito terapeuta".

A *Marcos, Juan Luis, Emma y Judith* por su infinita paciencia conmigo, a esta tesis le faltarían parte sin su ayuda.

A la gente de botánica, *Nere, Sharay, Ana y Marta*, por tener siempre unas palabras de ánimo.

A mis compañeros de Orfan, gracias por todas las cosas que aprendí trabajando allí, en especial a *Alicia* por tu amistad que no tiene precio.

A Dr. *Bruno Sarmento* por una fructífera, aunque breve estancia en su laboratorio, a todos los chicos por hacerme sentir una más. A *Giulia* y *William* por los buenos momentos.

A *David*, por apoyarme, por estar a mi lado en los malos momentos, y disfrutar de los buenos con tu alegría.

A toda mi familia, que siempre me apoyó, apoya y apoyará, sin la ayuda de todos no habría llegado hasta donde estoy ahora, además de la "Beca de estudios familia García-Umpiérrez". *A mi madre*, por enseñarme siempre a disfrutar de lo que uno hace, disfrutando del presente y por todo tu sacrificio para ayudarme a convertirme en quien soy ahora. Y por supuesto, a mi abuela, *Doña Margarita*, por demostrarme que pase lo que pase hay que ser fuerte y optimista, y por enfadarte por dejar a mis ratitas solas en vacaciones.

A todos aquellos a los que encontré por este camino, muchísimas gracias por contribuir a la persona que soy ahora. Por último y no menos importante me gustaría decir: ¡¡¡Allá va una tesis más para levantar la pantalla del ordenador de la Dra. Carmen Évora!!!

Glossary

α-ER: α-estrogen receptor

AdT: adipose tissue

ALD: alendronate

ALP: alkaline phosphatase

BCIP: 5-bromo-4-chloro-3-indolyl

BLT: bone like tissue

BMa: bone marrow

BSA: bovine serum albumin

BMP: bone morphogenetic protein (proteína morfogenética ósea)

CEIBA: Ethics Committee for Animal Care of the University of La Laguna

CB: cortical bone

CBT: cortical bone thickness

CCM: completed culture media

CHT: chitosan (quitosano)

CT: connective tissue

Ct.Wi: cortical bone thickness

DPI: 4′,6-diamidino-2-phenylindole

DCC: N, N’-dicyclohexylcarbodiimide

DCM: methylene chloride

DEX: dexametasone 21-isonicotinate

DMEM: Dubelcco’s modified Eagle’s medium

DMSO: dimethyl sulfoxide

DPBS: Dulbecco's modified phosphate buffered saline

DS: defect site

DSC: differential scanning calorimetry

ECM: extracellular matrix

FBS: fetal bovine serum

FDA: Food and Drug Administration

FGF: fibroblast growth factor (factor de crecimiento fibroblástico)

GF: growth factor (factor de crecimiento)

EMA: European Medicines Agency

HAP: hidroxiapatite (hidroxiapatita)

HBSS: Hank's balanced salt solution

HFIP: hexafluoroisopropanol

HP-γ-CD: 2-Hidroxipropil γ-Ciclodextrin

HT: hyaline tissue

IB: inmature bone

ICS: intercortical space

IGF: insulin-like growth factor (factor de crecimiento insulínico)

IM: intramuscular

IP: intraperitoneal

IST: intercortical space thickness

M: material

MAR: mineral apposition rates

MB: mature bone

MeOH: methanol

MMP10: metalloproteinase 10

MSC: mesenchymal stem cell (células madre mesenquimales)

Mw: molecular weight

NB: newly formed bone

NBT: tetrazolium chloride

NHS: N-hydroxysuccinamide

Non-OP: non osteoporotic

OCN: osteocalcin

OD: ovariectomy and dexametasone treatment

OP: osteoporosis

OPG: osteoprotegerin (osteoprotegerina)

OPA: o-pthaldialdehyde

OS: osteoid

PBS: phosphate buffer solution

PDGF: platelet derived growth factor (factores derivados de plaquetas)

PEG: polyethylene glycol

PLA: poly (lactide acid) (ácido poli-láctico)

PLGA: poly (lactide-co-glycolide acid) (ácido poli-lactico-co-glicólico)

PVA: poly (vinyl alcohol)

RB: rivoflavin

rhBMP-2: recombinant human bone morphogenetic protein

rhPDGF-BB: recombinant human platelet derived growth factor (factor de crecimiento recombinante derivado de plaquetas)

ROI: region of interest

SC: subcutaneous

SDF-1: factor derivado del estroma 1

SEM: scanning electron microscopy

SLS: sodium lauryl sulfate

STPP: pentabasic sodium tripolyphosphate

TB: trabecular bone

TBS: tris-buffered saline

Tb.N: trabecular number

Tb.Th: trabecular thickness

Tb.Ts: trabecular separation

Tg: glass transition temperature

TGF-β1: Transforming Growth Factor beta 1 (factor de crecimiento transformante beta)

OVX: ovariectomy (ovariectomía)

Índice:

Resumen

.

Resumen

En el presente trabajo se desarrollaron sistemas de distinta naturaleza conteniendo microesferas cargadas con sustancias activas para la regeneración ósea en osteoporosis empleando un defecto crítico de calvaria en osteoporosis. En todos los sistemas se empleó la proteína morfogenética ósea 2 (BMP-2) incluida en microesferas que fue combinada con otras sustancias activas. El primer sistema desarrollado fue un gel a base de quitosano y colágeno cargado con 17β-estradiol (en microesferas, films, o disperso) y nano-hidroxiapatita que se implantó en animales sanos y osteoporóticos. *In vivo s*e cedió aproximadamente un 70% de la BMP-2 cargada durante las primeras 6 semanas. Los datos indicaron la regeneración de aproximadamente un 50% del defecto en todos los grupos sin observarse diferencias entre los diferentes perfiles de liberación del 17β-estradiol asociado a las diferentes estrategias empleadas para su incorporación. Estos resultados denotaron la necesidad de retrasar la cesión de la BMP-2 y desarrollar estructuras tridimensionales más efectivas. De esta manera, en una siguiente aproximación se desarrollaron dos estructuras de igual composición, pero diferente consistencia, un hidrogel y una esponja, ambos de alginato. Además, se probó a estudiar el efecto de la incorporación de células madre mesenquimales (MSC) de ratas osteoporóticas sembradas en la estructura tridimensional previo a la implantación. Aunque no se observó ningún efecto sinérgico entre las MSCs y la BMP-2, sí que se obtuvieron resultados de regeneración muy prometedores, un 80% del defecto, pero sin alcanzar un nivel adecuado de mineralización. Por ello, en el último ensayo se optó por hacer una esponja a base de quitosano incorporando, además de BMP-2, otras moléculas terapéuticas para mejorar la mineralización, un bifosfonato (alendronato) y la metaloproteinasa 10 (MMP10). Los resultados sugieren que la estructura desarrollada es adecuada para la regeneración en animales osteoporóticos. Sin embargo, al contrario de lo que se puede esperar, no resulta óptima para animales sanos. Esto señala que es necesario llegar a un equilibrio entre la estructura tridimensional diseñada, las sustancias activas a utilizar y la cinética de liberación de las mismas para alcanzar la respuesta terapéutica deseada.

Abstract

.

Abstract

In the present work, systems of different nature were developed containing microspheres loaded with active substances to induce bone regeneration in a critical calvaria defect in osteoporosis. Bone morphogenetic protein 2 (BMP-2) was included in microspheres and combined with other active substances. The first developed system was a chitosan and collagen gel loaded with 17β-estradiol (in microspheres, films, or dispersed) and nano-hydroxyapatite that was implanted in healthy and osteoporotic animals. Approximately, 70% of the loaded BMP-2 was released *in vivo* during the first 6 weeks. The experimental data indicated a regeneration of approximately 50% of the defect in all groups independently of the obtained 17β-estradiol release profiles, associated with the different incorporation strategies used. These results denoted the need to further delay the release of BMP-2 and develop other more effective three-dimensional structures. In this way, in a following approach, two structures of the same composition, but different consistency, were developed, a hydrogel and a solid system (sponge), both made of alginate. In addition, the effect of the incorporation of mesenchymal stem cells (MSC) from osteoporotic rats seeded in the three-dimensional structure prior to implantation on bone regeneration was tested. Although no synergistic effect was observed between MSCs and BMP-2, very promising regeneration results were obtained, 80% of the defect size was regenerated, but without reaching an adequate level of mineralization in osteoporotic rats. For this reason, in the last study chitosan-based sponges incorporating, in addition to BMP-2, other therapeutic molecules to improve mineralization, a bisphosphonate (alendronate) and metalloproteinase-10 (MMP-10). The results suggest that the developed structure is suitable for bone regeneration in osteoporotic animals. However, contrary to expected, these systems were not adequate to treat critical bone defects in healthy animals. Therefore, to obtain a suitable bone regeneration is necessary to reach a balance between the designed three-dimensional structure, the active substances to be used and their release kinetics.

Introducción

.

Introducción

1. El hueso y su proceso regenerativo

El tejido óseo se encuentra en constante remodelación a lo largo de la vida adulta mediante un complejo proceso fisiológico en el cual intervienen células, citoquinas y factores de crecimiento. A diferencia de otros tejidos, las lesiones óseas se pueden curar dando lugar a un tejido indistinguible del hueso adyacente, poseyendo las mismas propiedades que el tejido original. El mecanismo seguido por el organismo para la reparación de una fractura se muestra de manera esquemática en la figura 1. Cuando se produce una fractura se produce un complejo proceso fisiológico para la reparación. En primer lugar, se produce una inflamación aguda, pérdida de integridad del tejido, destrucción de vasos sanguíneos con la consiguiente formación de un hematoma que es una fuente rica en citoquinas inductoras de inflamación y factores de crecimiento (GF) procedentes de plaquetas. Además, macrófagos y otras células inflamatorias se infiltran en el hematoma y liberan citoquinas y GF formándose una matriz provisional de fibrina rica en fibronectica. Los GF y la fibronectica regulan el crecimiento de capilares y la formación de un tejido de granulación. Los GF liberados atraen más leucocitos, que a su vez reclutan fibroblastos y MSC del periostio, de médula ósea o de la circulación adyacentes. Las MSC proliferan, se condensan y se diferencian para formar condrocitos que junto con los fibroblastos forman lo que se denomina callo blando, estabilizando el sitio de la fractura. El callo blando se remodela gradualmente por diferenciación de MSC a osteoblastos, dando lugar a la formación de la matriz proteico-mineral de baja calidad y estructuralmente desordenada en un proceso denominado osificación endocondral hasta que finalmente se produce la maduración del hueso (remodelado) que va reemplazando al callo duro y mejorando sus propiedades mecánicas hasta obtener las de un hueso sano (Sathyendra & Darowish, 2013).

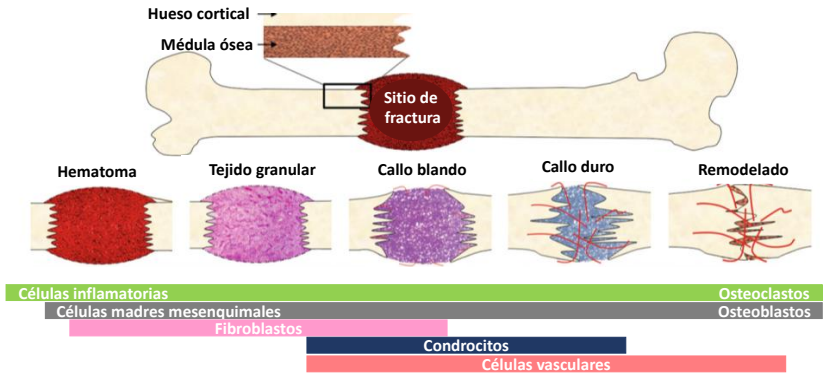

Figura 1. Esquema de las fases de curación de la fractura, desde la formación del hematoma proinflamatorio hasta el hueso remodelado. Pasando por los intermedios de tejido granular, callo blando y callo duro. Se señalan los diversos tipos celulares implicados en cada una de las etapas. Adaptada (Lackington & Thompson, 2020).

La remodelación es un proceso complejo mediante el cual el hueso viejo dañado se reemplaza por hueso nuevo. Este ciclo de remodelación se compone de tres fases principales:

1- Fase de resorción ósea mediada por osteoclastos, durante la cual se disuelven tanto las matrices minerales como las de colágeno.

2- El período de reversión, proceso de formación de nuevo tejido, que coincide en tiempo con el proceso de reabsorción.

3- Deposición de la nueva matriz ósea por acción de los osteoblastos.

1.1. Células implicadas en el proceso

Los componentes celulares implicados en este ciclo son principalmente las células precursoras osteogénicas, osteoblastos, osteoclastos, osteocitos y elementos hematopoyéticos de la médula ósea. Siendo las células madre

mesenquimales (MSC) la población de células madre osteoprogenitoras adultas ubicadas en el hueso.

1.1.1. Osteoclastos

Los osteoclastos son células multinucleadas responsables de la resorción ósea: disolución de la fase inorgánica de la matriz ósea y degradación de las proteínas del colágeno, proceso controlado por mecanismos celulares y hormonales como los estrógenos. En particular, RANKL (ligando activador del receptor del factor nuclear B) es expresado por osteoblastos, como forma unida a membrana o liberado como citoquina; se une a su receptor RANK en precursores de osteoclastos y osteoclastos, regulando su diferenciación, supervivencia y actividad. En la interacción RANKL / RANK, la citoquina osteoprotegerina (OPG) ejerce una función fundamental ya que es un receptor señuelo soluble para RANKL, evitando su unión a RANK, inhibiendo la osteoclastogénesis y protegiendo así de la resorción ósea excesiva. Muy importante para la remodelación ósea.

1.1.2. Osteoblastos

Los osteoblastos son células maduras, metabólicamente activas y desempeñan un papel fundamental en el proceso de formación de hueso representando del 4 al 6% de la población celular. Estas células se derivan de las MSC que, después de comprometerse con el linaje osteogénico, se diferencian en progenitores de osteoblastos que expresan los genes Runx2 (factor de transcripción) y Col1a1 (colágeno 1α1). Estos preosteoblastos evolucionan a osteoblastos maduros que experimentan cambios morfológicos aumentando de tamaño y transformándose en células cuboidales. Esta transición está relacionada con la síntesis de la matriz ósea que se produce en dos pasos: el depósito del material celular seguido de su posterior mineralización, en esta etapa los osteoblastos maduros pueden sufrir apoptosis o convertirse en osteocitos o en células de revestimiento óseo.

1.1.3. Osteocitos

Los osteocitos representan el último estado de diferenciación de los osteoblastos que permanecen incrustados en la matriz ósea, residiendo en lagunas. Los osteocitos son células clave para las funciones esqueléticas normales, desempeñando un papel fundamental en el mantenimiento de la homeostasis ósea, actuando como mecanosensores, regulando la homeostasis del fosfato y orquestando el proceso de remodelación ósea a través de interacciones intercelulares en respuesta al entorno local.

2. Problemas en la regeneración ósea

Este es el mecanismo por el que se resuelven habitualmente las fracturas que no son críticas, es decir, el hueso es capaz de regenerarse por sí mismo sin la acción de ningún agente externo. Sin embargo, cuando hay una pérdida de masa ósea muy elevada el tejido no es capaz de regenerarse por sí mismo y se considera un defecto crítico (Fayaz et al., 2011). Para la reparación de estos defectos es necesario recurrir a una intervención quirúrgica y emplear material de relleno (Janicki & Schmidmaier, 2011; Pape et al., 2010). Habitualmente se emplean injertos óseos, que son utilizados en procedimientos ortopédicos y maxilofaciales, entre los injertos óseos el estándar es el auoinjerto, que consiste en la extracción de hueso del propio paciente, usualmente de las crestas ilíacas anterior y posterior de la pelvis, para injertar en la zona afectada. Los autoinjertos combinan los 3 pilares para una óptima regeneración, son osteoinductores (contienen factores de crecimiento y proteínas morfogenéticas óseas), osteogénicos (contienen células osteoprogenitoras) y osteoconductores (actúan como soporte para el nuevo tejido) (Bauer & Muschler, 2000; Fayaz et al., 2011; Janicki & Schmidmaier, 2011). Aunque los autoinjertos tienen numerosas ventajas, también presentan ciertos inconvenientes entre los que podemos incluir el procedimiento quirúrgico que conlleva la extracción del injerto con sus posibles complicaciones y molestias al paciente, aumentando además el tiempo de hospitalización y el gasto sanitario (Ahlmann et al., 2002; St John et al., 2003). Una alternativa a los autoinjertos son los aloinjertos, procedentes de donantes vivos o cadáveres, poseen las ventajas de que se pueden obtener en gran cantidad y los xenoinjerto obtenidos a partir de animales son otras alternativas, sin

embargo, sus propiedades osteoinductoras y osteoprogenitoras están disminuidas debido al proceso previo de esterilización que deben sufrir y las posibilidades de rechazo o reacciones inmonológicas son mayores (Janicki & Schmidmaier, 2011; Shibuya & Jupiter, 2015). Como se ha puesto de manifiesto, la reparación de un defecto crítico conlleva un proceso complejo para pacientes sanos, pero en el caso de pacientes con enfermedades el proceso de regeneración se complica, como en la osteoporosis.

La osteoporosis es una enfermedad esquelética sistémica caracterizada por una disminución de la masa ósea y un deterioro de la microarquitectura ósea, lo que conduce a una mayor fragilidad del esqueleto y, por tanto, a un incremento del riesgo de fractura. Las fracturas de cadera asociadas a la osteoporosis son más costosas y están asociadas a una mayor tasa de mortalidad (Armas & Recker, 2012). Se estima que aproximadamente de los 15 millones de fracturas de cadera que se producen al año un 10-15% dan como resultado una curación deficiente (Cheung et al., 2016) este porcentaje aumenta hasta un 50% cuando la fractura ocurre junto con una lesión vascular grave (Bahney et al., 2015). Esto sumado al aumento del envejecimiento de la población hace que la osteoporosis pueda convertirse en un problema de salud grave con un elevado costo sanitario. La reparación en fracturas osteoporóticas presenta un patrón más complejo que en hueso sano, se produce la formación de un tejido más débil con poca cantidad de hueso esponjoso y cortical, lo que complica la fijación ósea de los implantes (Giannoudis et al., 2007; Nikolaou et al., 2009). Estudios, tanto en humanos como en animales, demuestran que la osteoporosis retrasa la consolidación de fracturas (Namkung-Matthai et al., 2001; Nikolaou et al., 2009; Xu et al., 2003) ya que tanto la formación del callo como la osificación endocondral están retardados (Giannoudis et al., 2007; Yingjie et al., 2007).

En definitiva, a pesar de la elevada capacidad de autoregeneración del hueso, hay situaciones complejas como la osteoporosis en las que es necesario el desarrollo de nuevas estrategias basadas en ingeniería de tejidos para promover la regeneración de defectos críticos, combinando el uso de molécula terapéuticas, estructuras tridimensionales y células madre.

3. Ingeniería de tejidos en osteoporosis

La ingeniería de tejidos aplica los principios de la biomedicina y la ingeniería para lograr reparar un tejido dañado mediante el uso de sustitutos que inducirán la respuesta natural del tejido, sus aplicaciones incluyen regeneración de cartílago (P. Lee et al., 2014), tejido hepático (Takeda & Vacanti, 1995) y tejido cardíaco (Engelmayr et al., 2008) además de la regeneración ósea. En todos los casos se busca estimular y acelerar la propia respuesta curativa del paciente (Chen & Liu, 2016). Para lograr este objetivo es indispensable el adecuado desarrollo de una estructura tridimensional biocompatible (que posee compatibilidad biológica) capaz de cargar y ceder fármacos (Chen & Liu, 2016; Chocholata et al., 2019; García-García et al., 2020; O'Brien, 2011).

3.1. Moléculas terapéuticas

Algunas sustancias activas como el uso del 17β-estradiol puede mejorar la formación de hueso induciendo la apoptosis de osteoclastos, implicados en el proceso de degradación de hueso. Ya que, en la OP posmenopáusica hay un retraso en la consolidación de la fractura debido a la deficiencia de estrógenos. Este estrógeno, además, induce la transcripción de la fosfatasa alcalina y estimula la expresión de la BMP-2 regulando la diferenciación a osteoblastos (Krum, 2011). Otras sustancias que actúa al mismo nivel que el 17β-estradiol son los bifosfonatos, como por ejemplo el alendronato. Estos bifosfonatos se utilizan de manera habitual en el tratamiento de la osteoporosis posmenopáusica (Otto et al., 2021).

El uso de factores de crecimiento ha ido tomando importancia en las últimas décadas debido a su potencial para la regeneración de tejidos. Los factores de crecimiento son secretados por los osteoblastos y las células madre mesenquimales y actúan como moléculas de señalización uniéndose a receptores específicos de membrana para activar cascadas de señalización que tienen como objetivo inducir un complejo sistema de transducción de señales. (Heldin et al., 1997; Lee et al., 2011; Lieberman et al., 2002). Se

ha descrito que existen numerosos factores de crecimientos expresados durante el proceso de curación de una fractura ósea, destacando por su potencial como agentes terapéuticos el factor de crecimiento insulínico (IGF), el factor de crecimiento fibroblástico (FGF), factores derivados de plaquetas (PDGF), y los factores de crecimiento transformados-beta (TGF-β) (De Witte et al., 2018; Lieberman et al., 2002).

Las proteínas morfogenéticas óseas (BMPs) son factores de crecimientos pertenecientes a la superfamilia del TGF-β, se han descrito unas 25 BMPs diferentes (Crane & Cao, 2014), entre ellas las que presentan un papel más importante en la morfogénesis ósea son la BMP-2, BMP-4, BMP-6, BMP-7 y la BMP-9. Fue en 1971 cuando se acuño por primera vez el nombre de BMPs por Urits, y se demostró que podían inducir la formación de hueso ectópico en animales adultos (Urist & Strates, 1971).

La BMP-2 es la que presenta un papel más prometedor en la regeneración ósea, su uso fue aprobado por la FDA en 2002, 2004 y 2007 para el tratamiento de la fusión espinal intersomática, fracturas de tibia abierta y para la elevación del seno y aumento de la cresta alveolar en defectos asociados a su extracción. Simultáneamente en 2002 fue aprobado por la EMA para su uso en fracturas de tibia (Schmidt-Bleek et al., 2016). Las BMPs son junto con los factores de necrosis tumoral (TNF) de los principales quimioatrayentes de MSC al sitio del defecto. Tanto la BMP-2 como la BMP-7 inducen la migración de las MSC y junto con la BMP-4, BMP-5 y BMP-6 inducen la diferenciación a osteoblastos (Fiedler et al., 2002), por tanto, la señalización de las BMPs conduce a la activación y expresión de los genes necesarios para la diferenciación de las MSC a osteoblastos y la consecuente osteogénesis (Chen et al., 2012; Song et al., 2009) como se muestra en la figura 2.

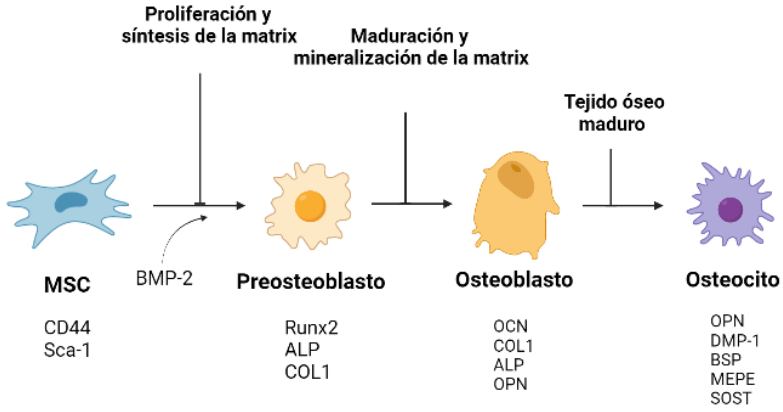

Figura 2. Proceso de diferenciación de MSC a osteoblastos. Esquema de la formación. Las células MSC inducidas por la BMP-2 se diferencian a preostoeblastos y según los estímulos adecuados osteoblasto y osteocito. Al final de la formación ósea algunos osteoblastos permanecen fijados a la matriz calcificada en forma de osteocitos. Runx2: Factor de transcripción RunX2, ALP: fosfatasa alcalina; COL1: colágeno tipo 1; OCN: osteoclacina; OPN: osteopontina; BSP: sialoproteína ósea; DMP-1: fosfoproteína ácida de matriz de dentina 1; SOST: esclerostina; MEPE: fosfoglicoproteína extracelular de matriz.

En general los huesos osteoporóticos, con poco hueso cortical y esponjoso, presentan una capacidad de autoreparación de fracturas reducida y un patrón de fractura más complejo, dando lugar a problemas para su fijación. Si combinamos la autoreparación deficiente con la disminución de la actividad anabólica del hueso y de la expresión génica de la BMP-2 por parte de las MSC osteoporóticas (Van Lieshout & Alt, 2016), la BMP-2 resulta un factor prometedor para el tratamiento de fracturas osteoporóticas. Hasta ahora la evidencia clínica es prometedora, si bien, como diversos autores citan la preocupación son las elevadas dosis de BMP-2 que son necesarias para inducir la regeneración ósea. Otro problema a tener en cuenta con el uso de las BMPs es su vida media tan corta. Por ello, es necesario un adecuado vehículo para mantener concentraciones eficaces y evitar concentraciones elevadas fuera del lugar a tratar que produzcan efectos no deseados. (Khattar et al., 2019; Rosenberg et al., 2019; Zheng et al., 2021).

Más recientemente se ha demostrado que en la homeostasis y adecuada curación de la fractura intervienen más sustancias activas, como las metaloproteinasas (MMPs). Alguno estudios demuestran una sobreexpresión de la metalorpoteinasa-10 (MMP-10) en osteoblastos y condorcitos durante la formación de hueso (Mao et al., 2013). Esto junto con estudios que demuestran una mejora de la mineralización en su uso en combinación con la BMP-2 en un defecto crítico de calota de ratón sano (Reyes et al., 2018) la hacen una sustancia candidata para promover la regeneración ósea en osteoporosis.

3.2. Estructuras tridimensionales

En el caso específico de la regeneración ósea se recurre al uso de estructuras 3D también denominados andamios (scaffolds) que hagan de guía al hueso nuevo en formación y permitan la encapsulación de principios activos y una liberación controlada de los mismos para mantener concentraciones óptimas en el sitio del defecto. Para este fin una estructura debe cumplir una serie de requisitos generales: 1) debe degradarse o reabsorberse para dejar espacio al tejido nuevo que se va formando; 2) ser biocompatible (De Witte et al., 2018), es decir, que no produzca una respuesta inflamatoria ni inmunológica (Porter et al., 2009); 3) idealmente tener unas adecuadas propiedades mecánicas, que le permitan adaptarse a la presión que sufre el tejido sin producir un ambiente que impida la supervivencia de las células del tejido (Garg et al., 2012); 4) tener una porosidad y tamaño de poro interno adecuado, permitiendo el adecuado transporte de los nutrientes y de productos de desecho, que facilite la migración celular y la revascularización del tejido, un tamaño de poro demasiado pequeño impide la penetración celular mientras que un poro demasiado grande dificulta la proliferación (Lyons et al., 2008; Rider et al., 2018) por ello el tamaño de poro ideal para regeneración ósea oscila entre 150 y 300 µm (De Witte et al., 2018) y 5) servir de guía y soporte al hueso, degradándose a medida que este comienza a crecer, para permitir al hueso nuevo ocupar el sitio.

La estructura debe fabricarse con una arquitectura interna-externa adecuada y con una gran superficie específica para facilitar la adhesión, proliferación y la migración celular (Chung & Park, 2007; Khang et al., 2006). Por último

y no menos importante, actuar como sistema de liberación controlada de factores de crecimiento y/o fármacos.

A la hora de seleccionar un material para el desarrollo de un andamio se debe tener en cuenta, además de sus propiedades mecánicas, degradabilidad y biocompatibilidad, su capacidad osteoconductora (facilitan la colonización celular y conducen la formación de hueso) y osteoinductora (promueven la formación de hueso). Para la fabricación de estructuras 3D para regeneración ósea se utilizan materiales de diversa naturaleza, que fundamentalmente se clasifican en polímeros de origen natural, polímeros sintéticos o materiales inorgánicos como cerámicas o metales. En el caso de algunos materiales de origen inorgánico como la hidroxiapatita (HAP) o el fosfato tricálcico beta (β-TCP) pueden tener capacidad osteoinductora. Estos compuestos se diferencian en su tiempo de permanencia y degradabilidad, la HAP posee una baja biodegradabilidad mientras que el β-TCP se degrada en un tiempo más corto, por ello, tienden a combinarse para forma andamios que promueven la regeneración de hueso.

3.2.1. Materiales

3.2.1.1. Polímeros naturales

Los polímeros de origen natural podemos clasificarlos típicamente en dos grupos: proteínicos (colágeno, seda, gelatina, fibronectina, …) y de base polisacarídica (ácido hialurónico, celulosa, alginato, quitosano, …) (Chen & Liu, 2016). Los materiales de origen proteico habitualmente son aislados de animales, mientras que los de base polisacarídica se obtienen comúnmente de algas, como el caso del alginato, de caparazones de moluscos, como el quitosano, o de recursos microbianos como el dextrano y derivados. Las principales ventajas de los polímeros naturales son su biocompatibilidad, su capacidad para permitir la adhesión y proliferación celular, pero por lo general, poseen malas propiedades mecánicas y al ser obtenidos a partir de productos naturales son susceptibles de variabilidad en el proceso de producción dando lugar a diferencias entre lotes.

A continuación, se describen con mayor profundidad algunos de los polímeros de origen natural que han sido utilizados durante el desarrollo experimental de esta tesis, incluidos el colágeno I, el alginato sódico y el quitosano.

- *Colágeno*

Existen más de 29 tipos de colágenos (Sorushanova et al., 2019) aunque, el más utilizado para desarrollo de estructuras para regeneración ósea es el colágeno tipo I, el cual se utiliza para la fabricación de hidrogeles, esponjas liofilizadas o implantes de electrohilado. El colágeno tipo I es el más abundante en la mayoría de los tejidos conectivos, está formado por una cadena 2α y dos cadenas 1α. El colágeno tipo I tiene una excelente biocompatibilidad y biodegradabilidad además de flexibilidad, alta resistencia a la tracción y alta afinidad por el agua y con buenas propiedades osteoinductoras (Lauritano et al., 2020). Habitualmente se combina con agentes inorgánicos como β-TCP (Kato et al., 2014), precursores de la hidroxiapatita (HAP) (Kajii et al., 2018; Kawai et al., 2017) e HAP (Ding et al., 2019; Gupta et al., 2016; Semyari et al., 2018) para mejorar sus pobres propiedades mecánicas. Para el uso del colágeno como biomaterial para el desarrollo de estructuras 3D comúnmente se recurre a la reticulación de sus fibras ya sea utilizando métodos físicos o químicos (Sorushanova et al., 2019). Entre los agentes químicos más utilizados están los aldehídos como el glutaraldehído que estabilizan las cadenas de colágeno debido a su capacidad de autopolimerización. Sin embargo, el glutaraldehído sin reaccionar, así como sus productos de degradación pueden quedar unidos a la matriz del material dando lugar a toxicidad (Delgado et al., 2017; Lee et al., 2001). Con respecto a los métodos físicos, estos son más lábiles que los químicos, pero carecen de toxicidad. Uno de los métodos físicos empleados es el uso de radiación ultravioleta en combinación con algún agente fotoreactivo como la rivoflabina (Ibusuki et al., 2007). No obstante, se debe ser cuidadoso en controlar esta reticulación puesto que los métodos físicos se asocian con la posible desnaturalización del colágeno (Sorushanova et al., 2019).

- *Alginato*

Durante las últimas décadas otros polímeros de origen natural como el alginato y el quitosano han sido ampliamente utilizados. El alginato es extraído de las algas pardas, se utiliza en ingeniería de tejidos, en la fabricación de sistemas de liberación de fármacos y la encapsulación de células debido a su biocompatibilidad y biodegradabilidad, baja toxicidad e inmonogenicidad además de su reticulación controlada (Lee & Mooney, 2012; Tønnesen & Karlsen, 2002). El alginato tiene un carácter muy hidrofílico y comparado con otros materiales como el colágeno, posee la ventaja de que permite la encapsulación encapsular células vivas, por contraparte, posee como es habitual en los polímeros de origen natural, unas pobres propiedades mecánicas y tiene una degradación no controlada (Lauritano et al., 2020). El alginato se compone de dos unidades de monómeros, el ácido β-D-manurónico y del ácido α-L-gulurónico. Para el desarrollo de estructuras basadas en alginato habitualmente se recurre a entrecruzar sus cadenas utilizando cationes divalentes como por ejemplo el Ca^{2+}, formando geles por gelificación iónica, por el contrario en presencia de cationes monovalentes se forman sales solubles (Tønnesen & Karlsen, 2002). La interacción entre el catión divalente y los grupos carboxilos y los hidroxilos terminales del α-L-gulurónico forma enlaces que dan lugar a estructuras que se conocen como “caja de huevos” (Grassi et al., 2006; H.-R. Lin et al., 2004). Los alginatos que poseen una mayor cantidad de bloques gulurónicos que de manurónico dan lugar a estructuras de una consistencia y resistencia mayor, debido a que los residuos de gulurónico tienen mayor afinidad por los cationes divalentes que los residuos de manurónico (Tønnesen & Karlsen, 2002). Habitualmente el alginato se utiliza para fabricar hidrogeles, además de para la elaboración de sistemas de liberación controlada de fármacos como pueden ser microesferas (Gainza et al., 2013; Zhai et al., 2015), pero también se ha utilizado en la fabricación de esponjas, fibras de electrohilado (Zamani et al., 2019).

- *Quitosano*

El quitosano procede del tratamiento industrial de caparazones de crustáceos. Es biocompatible, biodegradable, bioactivo (produce una

respuesta positiva en contacto con organismo), antibacteriano, y no inmonogénico (Lauritano et al., 2020). El quitosano tiene una similitud estructural con a la celulosa, está formado por unidades de 2-acetamino-2-desoxi-β-D-glucosa. Entre las desventajas del quitosano, como es habitual en los polímeros de origen natural, se incluyen sus malas propiedades mecánicas y que en función de su grado de acetilación y su peso molecular se puede retardar en exceso su degradación (Croisier & Jérôme, 2013; Rodríguez-Vázquez et al., 2015). Además, dependiendo del tipo de quitosano, también se pueden presentar problemas de solubilidad (Preethi Soundarya et al., 2018). Habitualmente para su uso en regeneración ósea se recurre a su combinación con hidroxiapatita u óxidos de silicio y de titanio, para formar estructuras de mejores propiedades mecánicas (Li et al., 2018; Pallela et al., 2012). La carga positiva del quitosano permite la reticulación de sus cadenas mediante el proceso denominado gelificación iónica, el compuesto que usualmente se utiliza para ello es el tripolifosfato sódico (Bugnicourt & Ladavière, 2016). Las estructuras a base de quitosano que se utilizan normalmente son esponjas liofilizadas de quitosano, hidrogeles, films y mallas de electrohilado.

3.2.1.2. Polímeros sintéticos

Con respecto a los polímeros sintéticos algunos de los más utilizados son la ε-policaprolactona (ε-PCL) los ácidos polilácticos (PLA) y polilácticos-co-glicólicos (PLGA) e incluso el polietilen glicol (PEG). La principal ventaja que presentan estos polímeros es su síntesis controlada y su mayor reproducibilidad con respecto a las propiedades mecánicas y físicas. Además, tienen una serie de características fácilmente modificables como su cristalinidad, peso molecular y grupos terminales y controlando estas características se puede obtener una estructura tridimensional adecuada (Porter et al., 2009; Stratton et al., 2016).

Los PLGAs y PLAs se obtienen por copolimerización de unidades de ácido láctico solo o con ácido glicólico, como en el caso del PLGA. La viscosidad inherente del polímero es dependiente del peso molecular (Kapoor et al., 2015). Habitualmente ambos tipos de polímeros se pueden sintetizar poseyendo en su extremo terminal un grupo éster o un grupo carboxilo, los

terminados en grupo éster tienen una mayor resistencia a la degradación, importante para controlar la biodegradabilidad de la estructura. Es conocido que el PLGA con una proporción 50:50 de ambas unidades se hidroliza más rápido que aquellos que posee más unidades de una clase que de otra (Mir et al., 2017). Hay que tener en cuenta todos estos factores si se pretende desarrollar una nueva estructura o controlar la velocidad de liberación de un fármaco. El uso más extendido de los PLGAs y PLAs es la fabricación de sistema de cesión controlada de fármacos en diversas formas, microesferas, nanopartículas, nanocapsulas, nanofibras, etc. La liberación del fármaco, proteína o factor de crecimiento encapsulado se produce por difusión a través de la cubierta, por erosión y formación de poros en la misma o por una combinación de ambos mecanismos (Kumari et al., 2010).

La estrategia más utiliza hoy en día para el desarrollo de estructuras 3D para ingeniería de tejidos es combinar polímeros naturales con polímeros de origen sintético, permitiendo aumentar la hidrofilia, biodegradabilidad y adhesión celular de estos últimos y en el caso de los naturales, la combinación con un polímero sintético mejora las propiedades mecánicas, además de la reproducibilidad del proceso de fabricación (Chen & Liu, 2016; Chocholata et al., 2019; Rezvani Ghomi et al., 2021).

3.2.2. Características morfológicas de las estructuras

Con respecto a las estructuras en sí, hay infinidad de diseños, desde hidrogeles, a esponjas sólidas (Geiger, 2003; Granito et al., 2017) espumas de poliuretano (Rodríguez-Évora et al., 2013), diseños elaborados por lixiviación de partículas (Crane & Cao, 2014) y por impresión 3D (Bahraminasab, 2020), espumas de vidrio de fosfato cálcico (Sanzana et al., 2014), fibras de electrohilado (Garcia-Orue et al., 2019), etc.

- *Hidrogeles*

A partir de los años 60 se ha incrementado el uso de los hidrogeles como sistemas para regeneración de tejidos debido a su semejanza estructural y en composición con la matriz extracelular (Shevach et al., 2014).

Los hidrogeles son redes reticuladas de polímeros, comúnmente naturales como alginato, quitosano, ácido hialurónico, pero también se han fabricado de polímeros sintéticos como el polietilenglicol, pluronic, tetronic, etc (Gibbs et al., 2016; Rodríguez-Évora et al., 2013). Se caracterizan por ser altamente porosos, hidrofílicos y en ocasiones poseen características de inyectabilidad. La alta porosidad y su carácter acuoso les permite su integración en la mayoría de los tejidos además de la aceptación por parte de las células nativas de ese tejido (Hoffman, 2012). En los hidrogeles inyectables esta propiedad supone una ventaja, ya que no requiere de un proceso quirúrgico para su administración y supone un ahorro económico y mayor comodidad para el paciente. Los hidrogeles inyectables poseen la capacidad al inyectarse de cubrir toda la zona del defecto, alcanzando los bordes de este, es decir, la zona donde comienza la regeneración.

Parece lógico optar por estos hidrogeles como candidatos para la regeneración de tejidos, si bien, existen algunas desventajas como puede ser su poco tiempo de permanencia en un defecto, que es necesario prolongar según el tipo de lesión.

- *Esponjas*

Algunas de las alternativas a los hidrogeles son la bioimpresión 3D, o la fabricación esponjas o espumas de mayor consistencia utilizando diferentes polímeros. Una manera sencilla de fabricar una estructura tipo esponja es por moldeado y posterior liofilización (De la Riva et al., 2010; García-García et al., 2020). La liofilización permite fabricar andamios, utilizando distintos tipos de polímeros, con una estructura interna porosa con poros interconectados. En función del tipo de polímero se pueden obtener estructuras con una menor o mayor tasa de degradabilidad, además de controlar las propiedades mecánicas (J. Sun & Tan, 2013). El objetivo es llegar a un punto medio, lograr una estructura que permanezca el tiempo necesario para la regeneración y se degrade a la velocidad adecuado, para permitir que el nuevo tejido vaya ocupando su espacio.

3.3. Sinergia entre células y materiales en la regeneración ósea

Como se ha descrito anteriormente es fundamental desarrollar una adecuada estructura 3D pero además, la utilización de células osteoprogenitoras puede incrementar la efectividad del sistema. Originariamente la ingeniería de tejidos surgió como una solución prometedora para superar las limitaciones de las técnicas convencionales de regeneración de hueso, como los autoinjertos y aloinjertos. Las estrategias basadas en el uso de MSC requieren de una abundante cantidad de células mesenquimales multipotentes con potencial osteogénico que liberen los factores de crecimiento para inducir la diferenciación a osteoblastos además de un andamio con las características específica comentadas anteriormente (Zhang et al., 2020).

El término MSC fue acuñado por primera vez por Caplan en 1991 (Caplan, 1991) el cual las definió como células progenitoras pluripotentes que al dividirse dan lugar a tejidos esqueléticos como cartílago, hueso, tendón, ligamentos y tejido conectivo. Hoy en día se sabe que las MSC se pueden extraer de diversas fuentes como médula ósea, paredes de vasos, tejido adiposo, músculo, tendón, etc (X. Wang et al., 2013). En la ingeniería de tejidos el uso de células mesenquimales se está implementando debido a su potencial regenerativo. Las MSC carecen de inmunogenicidad *in vitro*, no expresan moléculas estimuladoras del complejo II de histocompatibilidad como CD40, CD80 y CD86 y más importante aún, no inducen la proliferación de linfocitos (H. Lin et al., 2019; X. Wang et al., 2013). Algunos autores manifiestan que la combinación de diferentes materiales con MSC y factores de crecimiento produce un aumento significativo de la formación de hueso, por ejemplo, la combinación con BMP y β-TCP produjo formación de hueso en músculo de perros (Yuan, 2001) o la combinación con BMP-2 y Factor derivado del estroma 1 (SDF-1) aumentó la migración y diferenciación de las MSC y en consecuencia la curación de la fractura (Granero-Moltó et al., 2009). Además la HAP no posee efectos tóxicos sobre las MSC y se ha puesto de manifiesto que aumenta la formación de hueso cuando se utiliza estructuras 3D de HAP en combinación con MSC en modelos *in vivo* de conejo (H. Wang et al., 2007). También es habitual ver descritos andamios compuestos por HAP y

colágeno tipo I como se mencionó con anterioridad (Ferreira et al., 2012). El colágeno permite la diferenciación de MSC y la osteogénesis, favorece un ambiente ideal para la formación de hueso.

En cuanto a los polímeros sintéticos derivados del ácido poliláctico, hemos de decir que las estructuras elaboradas con PLA presembradas con MSC no afectan a la actividad metabólica de las células ni a su viabilidad, además, diversos estudios muestran que no son tóxicos, sino que son capaces de permitir el crecimiento celular y la expresión génica osteogénica (Velioglu et al., 2019). Además, se ha puesto de manifiesto que los biomateriales compuestos por PLA combinado con HAP mostraron buena adhesión y proliferación celular produciendo un aumento de la diferenciación a osteoblastos y de la actividad de la fosfatasa alcalina (S.-S. Kim et al., 2006). Los PLGAs al contrario que los PLAs presentan una baja tasa de adhesión celular y pobre capacidad de osteoinducción (Zhang et al., 2020). Sin embargo, tanto los PLAs como los PLGAs combinados con materiales que aumentan su hidrofilia como el ácido hialurónico mejoran la biocompatibilidad, osteoconducción y diferenciación osteogénica (Ramesh et al., 2018). Las estructuras que utilizan PLGAs combinado con quitosano cargados con BMP-2 y presembrados con MSC humanas inducen un aumento de la proliferación celular con el tiempo y un incremento del grado de mineralización a los 21 días de cultivo (Zhang et al., 2020).

El uso de MSC hasta ahora ha dado lugar a resultados muy prometedores, pero sigue existiendo una serie de brechas que solventar. Entre ellos la mejora de las técnicas de cultivo, el desarrollo de mejores estructuras para asegurar su viabilidad y actividad terapéutica. Una nueva línea de trabajo es el empleo de MSC modificadas genéticamente. Actualmente estas técnicas se encuentran en desarrollo y a la espera de la realización de un mayor número de estudios de toxicidad a corto y largo plazo (Qin et al., 2014).

3.4. Estado actual de la regeneración ósea en osteoporosis

Para concluir se pone de manifiesto que aún queda un camino largo que recorrer en la regeneración de defectos críticos en situaciones de osteoporosis. Durante los últimos 10 años el grupo de investigación al que me he incorporado ha trabajado en la regeneración de defectos críticos de tejido óseo, y ha testado distintos hidrogeles bioactivos cargados con micropartículas con BMP-2 en modelos de rata osteoporótica por ovariectomía. Entre ellos se ha estudiado la combinación de Tetronic®1307 con alginato, reconstituido en plasma rico en factores de crecimiento (PRGF), y Tetronic®1307 combinado con Pluronic®F127 y α-Ciclodextrina. Ambos estudios pusieron de manifiesto que tanto en animales osteoporóticos como animales sanos se formaba nuevo hueso, sin embargo, en animales osteoporóticos se trataba de un hueso muy poco mineralizado (Segredo-Morales, García-García, et al., 2018; Segredo-Morales, Reyes, et al., 2018), y no se observó mejoría con el uso del PRGF. Algunos autores han estudiado otros factores de crecimiento en combinación con la BMP-2 como es el caso del factor de crecimiento recombinante derivado de plaquetas (rhPDGF-BB) y tampoco se encontraron mejorías en la formación de hueso en un defecto crítico en ratas osteoporóticas (H. J. Kim et al., 2021).

La hidroxiapatita es otro material que se ha testado en combinación con terapia celular para resolver defectos críticos en animales osteoporóticos. Youhao Tang y colaboradores utilizaron una estructura tridimensional de HAP presembrada con MSC transfectadas y demostraron que a las 4 semanas se formaba hueso en un defecto mandibular de rata osteoporótica (Tang et al., 2008). En otros estudios, andamios de HAP combinada con sulfato de calcio para la cesión de BMP-2, zoledronato y exosomas aislados de MSC, fueron evaluados en un modelo de defecto en cuello del fémur de rata osteoporótica poniendo de manifiesto que esta combinación mejoró las propiedades mecánicas. Los resultados indicaron además que el uso de exosomas en situaciones de osteoporosis, permite la disminución en las dosis de BMP-2 necesarias para la regeneración ósea (Qayoom et al., 2020). Otro fármaco, aunque convencional pero no menos estudiado por su papel en la regeneración ósea es la simvastatina. Recientemente, se ha

observado que la combinación de esta estatina con HAP resulta eficaz para el relleno de un defecto óseo mandibular en rata OP y rata diabética (Camacho-Alonso et al., 2020).

Otra estrategia prometedora utilizada para curar defectos en osteoporótica es el uso de membranas bioactivas. Tingfan Sun y colaboradores desarrollaron una membrana de submucosa del intestino delgado heparinizada, previamente mineralizada como vehículo para el péptido P28 derivado de BMP-2. Esta estructura promovió *in vitro* la proliferación y viabilidad celular, la actividad de la fosfatasa alcalina y la expresión de RNAm de genes relacionados con la osteogénesis en cultivos de MSC aisladas de médula ósea de rata osteoporótica. La evaluación de este sistema en un defecto crítico en calota de ratas ovacteriomizadas mostró un importante incremento de la regeneración del defecto (T. Sun et al., 2018).

Otra vía abierta es la identificación de alteraciones genéticas en ciertas patologías para poder actuar sobre ellas y regular su expresión. En este sentido, se ha identificado que la desmetilasa 5A específica de lisina (KDM5A) está sobre expresada en humanos y ratonas OP que a su vez también muestran una disminución de Runx2. Los autores concluyeron que la disminución de la diferenciación osteogénica inducida por la BMP-2 observada en MSC osteroporóticas puede ser consecuencia en parte de la sobreexpresión de KDM5A. Además, observaron en un modelo de ratona OP que al silenciar KDM5A se recupera parcialmente la pérdida de masa ósea (C. Wang et al., 2016).

Con esta somera revisión hemos querido poner de manifiesto que, aunque se ha trabajado mucho en la regeneración de defectos óseos sigue siendo escaso el interés en el desarrollo de estrategias para situaciones específicas como la OP teniendo en cuenta el gran porcentaje de población que afecta.

4. Referencias

Ahlmann, E., Patzakis, M., Roidis, N., Shepherd, L., & Holtom, P. (2002). Comparison of anterior and posterior iliac crest bone grafts in terms of harvest-site morbidity and functional outcomes. *The Journal of*

Bone and Joint Surgery-American Volume, *84*(5). https://doi.org/10.2106/00004623-200205000-00003

Armas, L. A. G., & Recker, R. R. (2012). Pathophysiology of Osteoporosis. *Endocrinology and Metabolism Clinics of North America*, *41*(3). https://doi.org/10.1016/j.ecl.2012.04.006

Bahney, C. S., Hu, D. P., Miclau, T., & Marcucio, R. S. (2015). The Multifaceted Role of the Vasculature in Endochondral Fracture Repair. *Frontiers in Endocrinology*, *6*. https://doi.org/10.3389/fendo.2015.00004

Bahraminasab, M. (2020). Challenges on optimization of 3D-printed bone scaffolds. *BioMedical Engineering OnLine*, *19*(1). https://doi.org/10.1186/s12938-020-00810-2

Bauer, T. W., & Muschler, G. F. (2000). Bone Graft Materials. In *CLINICAL ORTHOPAEDICS AND RELATED RESEARCH Number* (Vol. 371). http://journals.lww.com/clinorthop

Bugnicourt, L., & Ladavière, C. (2016). Interests of chitosan nanoparticles ionically cross-linked with tripolyphosphate for biomedical applications. *Progress in Polymer Science*, *60*. https://doi.org/10.1016/j.progpolymsci.2016.06.002

Camacho-Alonso, F., Martínez-Ortiz, C., Plazas-Buendía, L., Mercado-Díaz, A. M., Vilaplana-Vivo, C., Navarro, J. A., Buendía, A. J., Merino, J. J., & Martínez-Beneyto, Y. (2020). Bone union formation in the rat mandibular symphysis using hydroxyapatite with or without simvastatin: effects on healthy, diabetic, and osteoporotic rats. *Clinical Oral Investigations*, *24*(4). https://doi.org/10.1007/s00784-019-03180-9

Caplan, A. I. (1991). Mesenchymal Stem Cells*. In *Journal of Orthopaedic Research* (Vol. 9). Orthopaedic Research Society.

Chen, F.-M., & Liu, X. (2016). Advancing biomaterials of human origin for tissue engineering. *Progress in Polymer Science*, *53*. https://doi.org/10.1016/j.progpolymsci.2015.02.004

Chen, G., Deng, C., & Li, Y.-P. (2012). TGF-β and BMP Signaling in Osteoblast Differentiation and Bone Formation. *International Journal of Biological Sciences*, *8*(2). https://doi.org/10.7150/ijbs.2929

Cheung, W. H., Miclau, T., Chow, S. K.-H., Yang, F. F., & Alt, V. (2016). Fracture healing in osteoporotic bone. *Injury*, *47*. https://doi.org/10.1016/S0020-1383(16)47004-X

Chocholata, P., Kulda, V., & Babuska, V. (2019). Fabrication of Scaffolds for Bone-Tissue Regeneration. *Materials*, *12*(4). https://doi.org/10.3390/ma12040568

Chung, H. J., & Park, T. G. (2007). Surface engineered and drug releasing pre-fabricated scaffolds for tissue engineering. *Advanced Drug Delivery Reviews*, *59*(4–5). https://doi.org/10.1016/j.addr.2007.03.015

Crane, J. L., & Cao, X. (2014). Bone marrow mesenchymal stem cells and TGF-β signaling in bone remodeling. *Journal of Clinical Investigation*, *124*(2). https://doi.org/10.1172/JCI70050

Croisier, F., & Jérôme, C. (2013). Chitosan-based biomaterials for tissue engineering. *European Polymer Journal*, *49*(4). https://doi.org/10.1016/j.eurpolymj.2012.12.009

De la Riva, B., Sánchez, E., Hernández, A., Reyes, R., Tamimi, F., López-Cabarcos, E., Delgado, A., & Évora, C. (2010). Local controlled release of VEGF and PDGF from a combined brushite–chitosan system enhances bone regeneration. *Journal of Controlled Release*, *143*(1). https://doi.org/10.1016/j.jconrel.2009.11.026

De Witte, T.-M., Fratila-Apachitei, L. E., Zadpoor, A. A., & Peppas, N. A. (2018). Bone tissue engineering via growth factor delivery: from scaffolds to complex matrices. *Regenerative Biomaterials*, *5*(4). https://doi.org/10.1093/rb/rby013

Delgado, L. M., Fuller, K., & Zeugolis, D. I. (2017). <sup/> Collagen Cross-Linking: Biophysical, Biochemical, and Biological Response Analysis. *Tissue Engineering Part A*, *23*(19–20). https://doi.org/10.1089/ten.tea.2016.0415

Ding, M., Koroma, K. E., Sorensen, J. R., Sandri, M., Tampieri, A., Jespersen, S. M., & Overgaard, S. (2019). Collagen-hydroxyapatite composite substitute and bone marrow nuclear cells on posterolateral spine fusion in sheep. *Journal of Biomaterials Applications*, *34*(3). https://doi.org/10.1177/0885328219851315

Engelmayr, G. C., Cheng, M., Bettinger, C. J., Borenstein, J. T., Langer, R., & Freed, L. E. (2008). Accordion-like honeycombs for tissue engineering of cardiac anisotropy. *Nature Materials*, *7*(12). https://doi.org/10.1038/nmat2316

Fayaz, H. C., Giannoudis, P. V., Vrahas, M. S., Smith, R. M., Moran, C., Pape, H. C., Krettek, C., & Jupiter, J. B. (2011). The role of stem cells

in fracture healing and nonunion. *International Orthopaedics*, *35*(11). https://doi.org/10.1007/s00264-011-1338-z

Ferreira, A. M., Gentile, P., Chiono, V., & Ciardelli, G. (2012). Collagen for bone tissue regeneration. *Acta Biomaterialia*, *8*(9). https://doi.org/10.1016/j.actbio.2012.06.014

Fiedler, J., Röderer, G., Günther, K.-P., & Brenner, R. E. (2002). BMP-2, BMP-4, and PDGF-bb stimulate chemotactic migration of primary human mesenchymal progenitor cells. *Journal of Cellular Biochemistry*, *87*(3). https://doi.org/10.1002/jcb.10309

Gainza, G., Aguirre, J. J., Pedraz, J. L., Hernández, R. M., & Igartua, M. (2013). rhEGF-loaded PLGA-Alginate microspheres enhance the healing of full-thickness excisional wounds in diabetised Wistar rats. *European Journal of Pharmaceutical Sciences*, *50*(3–4). https://doi.org/10.1016/j.ejps.2013.07.003

García-García, P., Reyes, R., Pérez-Herrero, E., Arnau, M. R., Évora, C., & Delgado, A. (2020). Alginate-hydrogel versus alginate-solid system. Efficacy in bone regeneration in osteoporosis. *Materials Science and Engineering C*, *115*, 111009. https://doi.org/10.1016/j.msec.2020.111009

Garcia-Orue, I., Gainza, G., Garcia-Garcia, P., Gutierrez, F. B., Aguirre, J. J., Hernandez, R. M., Delgado, A., & Igartua, M. (2019). Composite nanofibrous membranes of PLGA/Aloe vera containing lipid nanoparticles for wound dressing applications. *International Journal of Pharmaceutics*, *556*. https://doi.org/10.1016/j.ijpharm.2018.12.010

Garg, T., Singh, O., Arora, S., & Murthy, R. S. R. (2012). Scaffold: A Novel Carrier for Cell and Drug Delivery. *Critical Reviews™ in Therapeutic Drug Carrier Systems*, *29*(1). https://doi.org/10.1615/CritRevTherDrugCarrierSyst.v29.i1.10

Geiger, M. (2003). Collagen sponges for bone regeneration with rhBMP-2. *Advanced Drug Delivery Reviews*, *55*(12). https://doi.org/10.1016/j.addr.2003.08.010

Giannoudis, P. V., Einhorn, T. A., & Marsh, D. (2007). Fracture healing: The diamond concept. *Injury*, *38*. https://doi.org/10.1016/S0020-1383(08)70003-2

Gibbs, D. M. R., Black, C. R. M., Dawson, J. I., & Oreffo, R. O. C. (2016). A review of hydrogel use in fracture healing and bone regeneration. *Journal of Tissue Engineering and Regenerative Medicine*, *10*(3).

https://doi.org/10.1002/term.1968

Granero-Moltó, F., Weis, J. A., Miga, M. I., Landis, B., Myers, T. J., O'Rear, L., Longobardi, L., Jansen, E. D., Mortlock, D. P., & Spagnoli, A. (2009). Regenerative Effects of Transplanted Mesenchymal Stem Cells in Fracture Healing. *Stem Cells*, *27*(8). https://doi.org/10.1002/stem.103

Granito, R. N., Custódio, M. R., & Rennó, A. C. M. (2017). Natural marine sponges for bone tissue engineering: The state of art and future perspectives. *Journal of Biomedical Materials Research Part B: Applied Biomaterials*, *105*(6). https://doi.org/10.1002/jbm.b.33706

Grassi, G., Crevatin, A., Farra, R., Guarnieri, G., Pascotto, A., Rehimers, B., Lapasin, R., & Grassi, M. (2006). Rheological properties of aqueous Pluronic–alginate systems containing liposomes. *Journal of Colloid and Interface Science*, *301*(1). https://doi.org/10.1016/j.jcis.2006.04.068

Gupta, V., Lyne, D. V., Barragan, M., Berkland, C. J., & Detamore, M. S. (2016). Microsphere-based scaffolds encapsulating tricalcium phosphate and hydroxyapatite for bone regeneration. *Journal of Materials Science: Materials in Medicine*, *27*(7). https://doi.org/10.1007/s10856-016-5734-1

Heldin, C.-H., Miyazono, K., & ten Dijke, P. (1997). TGF-β signalling from cell membrane to nucleus through SMAD proteins. *Nature*, *390*(6659). https://doi.org/10.1038/37284

Hoffman, A. S. (2012). Hydrogels for biomedical applications. In *Advanced Drug Delivery Reviews* (Vol. 64, Issue SUPPL., pp. 18–23). Elsevier. https://doi.org/10.1016/j.addr.2012.09.010

Ibusuki, S., Halbesma, G. J., Randolph, M. A., Redmond, R. W., Kochevar, I. E., & Gill, T. J. (2007). Photochemically Cross-Linked Collagen Gels as Three-Dimensional Scaffolds for Tissue Engineering. *Tissue Engineering*, *13*(8). https://doi.org/10.1089/ten.2006.0153

Janicki, P., & Schmidmaier, G. (2011). What should be the characteristics of the ideal bone graft substitute? Combining scaffolds with growth factors and/or stem cells. *Injury*, *42*. https://doi.org/10.1016/j.injury.2011.06.014

Kajii, F., Iwai, A., Tanaka, H., Matsui, K., Kawai, T., & Kamakura, S. (2018). Single-dose local administration of teriparatide with a octacalcium phosphate collagen composite enhances bone

regeneration in a rodent critical-sized calvarial defect. *Journal of Biomedical Materials Research Part B: Applied Biomaterials*, *106*(5). https://doi.org/10.1002/jbm.b.33993

Kapoor, D. N., Bhatia, A., Kaur, R., Sharma, R., Kaur, G., & Dhawan, S. (2015). PLGA: a unique polymer for drug delivery. *Therapeutic Delivery*, *6*(1). https://doi.org/10.4155/tde.14.91

Kato, E., Lemler, J., Sakurai, K., & Yamada, M. (2014). Biodegradation Property of Beta-Tricalcium Phosphate-Collagen Composite in Accordance with Bone Formation: A Comparative Study with Bio-Oss Collagen® in a Rat Critical-Size Defect Model. *Clinical Implant Dentistry and Related Research*, *16*(2). https://doi.org/10.1111/j.1708-8208.2012.00467.x

Kawai, T., Suzuki, O., Matsui, K., Tanuma, Y., Takahashi, T., & Kamakura, S. (2017). Octacalcium phosphate collagen composite facilitates bone regeneration of large mandibular bone defect in humans. *Journal of Tissue Engineering and Regenerative Medicine*, *11*(5). https://doi.org/10.1002/term.2110

Khang, G., Lee, S. J., Kim, M. S., & Lee, H. B. (2006). Biomaterials: Tissue Engineering and Scaffolds. In *Encyclopedia of Medical Devices and Instrumentation*. John Wiley & Sons, Inc. https://doi.org/10.1002/0471732877.emd029

Khattar, V., Lee, J. H., Wang, H., Bastola, S., & Ponnazhagan, S. (2019). Structural determinants and genetic modifications enhance BMP2 stability and extracellular secretion. *FASEB BioAdvances*, *1*(3). https://doi.org/10.1096/fba.2018-00023

Kim, H. J., Kim, K.-H., Lee, Y.-M., Ku, Y., Rhyu, I.-C., & Seol, Y.-J. (2021). In ovariectomy-induced osteoporotic rat models, BMP-2 substantially reversed an impaired alveolar bone regeneration whereas PDGF-BB failed. *Clinical Oral Investigations*. https://doi.org/10.1007/s00784-021-03915-7

Kim, S.-S., Sun Park, M., Jeon, O., Yong Choi, C., & Kim, B.-S. (2006). Poly(lactide-co-glycolide)/hydroxyapatite composite scaffolds for bone tissue engineering. *Biomaterials*, *27*(8). https://doi.org/10.1016/j.biomaterials.2005.08.016

Krum, S. A. (2011). Direct transcriptional targets of sex steroid hormones in bone. *Journal of Cellular Biochemistry*, *112*(2). https://doi.org/10.1002/jcb.22970

Kumari, A., Yadav, S. K., & Yadav, S. C. (2010). Biodegradable polymeric nanoparticles based drug delivery systems. *Colloids and Surfaces B: Biointerfaces*, *75*(1). https://doi.org/10.1016/j.colsurfb.2009.09.001

Lackington, W. A., & Thompson, K. (2020). Fracture Healing and Progress Towards Successful Repair. In *Racing for the Surface*. Springer International Publishing. https://doi.org/10.1007/978-3-030-34471-9_10

Lauritano, D., Limongelli, L., Moreo, G., Favia, G., & Carinci, F. (2020). Nanomaterials for Periodontal Tissue Engineering: Chitosan-Based Scaffolds. A Systematic Review. *Nanomaterials*, *10*(4). https://doi.org/10.3390/nano10040605

Lee, C. ., Grodzinsky, A. ., & Spector, M. (2001). The effects of cross-linking of collagen-glycosaminoglycan scaffolds on compressive stiffness, chondrocyte-mediated contraction, proliferation and biosynthesis. *Biomaterials*, *22*(23). https://doi.org/10.1016/S0142-9612(01)00067-9

Lee, K., Silva, E. A., & Mooney, D. J. (2011). Growth factor delivery-based tissue engineering: general approaches and a review of recent developments. *Journal of The Royal Society Interface*, *8*(55). https://doi.org/10.1098/rsif.2010.0223

Lee, K. Y., & Mooney, D. J. (2012). Alginate: Properties and biomedical applications. *Progress in Polymer Science*, *37*(1). https://doi.org/10.1016/j.progpolymsci.2011.06.003

Lee, P., Tran, K., Chang, W., Shelke, N. B., Kumbar, S. G., & Yu, X. (2014). Influence of Chondroitin Sulfate and Hyaluronic Acid Presence in Nanofibers and Its Alignment on the Bone Marrow Stromal Cells: Cartilage Regeneration. *Journal of Biomedical Nanotechnology*, *10*(8). https://doi.org/10.1166/jbn.2014.1831

Li, Y., Zhang, Z., & Zhang, Z. (2018). Porous Chitosan/Nano-Hydroxyapatite Composite Scaffolds Incorporating Simvastatin-Loaded PLGA Microspheres for Bone Repair. *Cells Tissues Organs*, *205*(1). https://doi.org/10.1159/000485502

Lieberman, J. R., Daluiski, A., & Einhorn, T. (2002). The role of Growth Factors in the repair of bone. *The Journal of Bone and Joint Surgery-American Volume*, *84*(6). https://doi.org/10.2106/00004623-200206000-00022

Lin, H.-R., Sung, K. C., & Vong, W.-J. (2004). In Situ Gelling of

Alginate/Pluronic Solutions for Ophthalmic Delivery of Pilocarpine. *Biomacromolecules*, *5*(6). https://doi.org/10.1021/bm0496965

Lin, H., Sohn, J., Shen, H., Langhans, M. T., & Tuan, R. S. (2019). Bone marrow mesenchymal stem cells: Aging and tissue engineering applications to enhance bone healing. *Biomaterials*, *203*. https://doi.org/10.1016/j.biomaterials.2018.06.026

Lyons, F., Partap, S., & O'Brien, F. J. (2008). Part 1: Scaffolds and Surfaces. *Technology and Health Care*, *16*(4). https://doi.org/10.3233/THC-2008-16409

Mao, L., Yano, M., Kawao, N., Tamura, Y., Okada, K., & Kaji, H. (2013). Role of matrix metalloproteinase-10 in the BMP-2 inducing osteoblastic differentiation. *Endocrine Journal*, *60*(12), 1309–1319. https://doi.org/10.1507/endocrj.EJ13-0270

Mir, M., Ahmed, N., & Rehman, A. ur. (2017). Recent applications of PLGA based nanostructures in drug delivery. *Colloids and Surfaces B: Biointerfaces*, *159*. https://doi.org/10.1016/j.colsurfb.2017.07.038

Namkung-Matthai, H., Appleyard, R., Jansen, J., Hao Lin, J., Maastricht, S., Swain, M., Mason, R. ., Murrell, G. A. ., Diwan, A. ., & Diamond, T. (2001). Osteoporosis influences the early period of fracture healing in a rat osteoporotic model. *Bone*, *28*(1). https://doi.org/10.1016/S8756-3282(00)00414-2

Nikolaou, V. S., Efstathopoulos, N., Kontakis, G., Kanakaris, N. K., & Giannoudis, P. V. (2009). The influence of osteoporosis in femoral fracture healing time. *Injury*, *40*(6). https://doi.org/10.1016/j.injury.2008.10.035

O'Brien, F. J. (2011). Biomaterials & scaffolds for tissue engineering. *Materials Today*, *14*(3). https://doi.org/10.1016/S1369-7021(11)70058-X

Otto, S., Aljohani, S., Fliefel, R., Ecke, S., Ristow, O., Burian, E., Troeltzsch, M., Pautke, C., & Ehrenfeld, M. (2021). Infection as an Important Factor in Medication-Related Osteonecrosis of the Jaw (MRONJ). *Medicina*, *57*(5). https://doi.org/10.3390/medicina57050463

Pallela, R., Venkatesan, J., Janapala, V. R., & Kim, S.-K. (2012). Biophysicochemical evaluation of chitosan-hydroxyapatite-marine sponge collagen composite for bone tissue engineering. *Journal of Biomedical Materials Research Part A*, *100A*(2).

https://doi.org/10.1002/jbm.a.33292

Pape, H. C., Evans, A., & Kobbe, P. (2010). Autologous Bone Graft: Properties and Techniques. *Journal of Orthopaedic Trauma*, *24*(Supplement 1). https://doi.org/10.1097/BOT.0b013e3181cec4a1

Porter, J. R., Ruckh, T. T., & Popat, K. C. (2009). Bone tissue engineering: A review in bone biomimetics and drug delivery strategies. *Biotechnology Progress*. https://doi.org/10.1002/btpr.246

Preethi Soundarya, S., Haritha Menon, A., Viji Chandran, S., & Selvamurugan, N. (2018). Bone tissue engineering: Scaffold preparation using chitosan and other biomaterials with different design and fabrication techniques. *International Journal of Biological Macromolecules*, *119*. https://doi.org/10.1016/j.ijbiomac.2018.08.056

Qayoom, I., Teotia, A. K., & Kumar, A. (2020). Nanohydroxyapatite Based Ceramic Carrier Promotes Bone Formation in a Femoral Neck Canal Defect in Osteoporotic Rats. *Biomacromolecules*, *21*(2). https://doi.org/10.1021/acs.biomac.9b01327

Qin, Y., Guan, J., & Zhang, C. (2014). Mesenchymal stem cells: mechanisms and role in bone regeneration. *Postgraduate Medical Journal*, *90*(1069). https://doi.org/10.1136/postgradmedj-2013-132387

Ramesh, N., Moratti, S. C., & Dias, G. J. (2018). Hydroxyapatite-polymer biocomposites for bone regeneration: A review of current trends. *Journal of Biomedical Materials Research Part B: Applied Biomaterials*, *106*(5). https://doi.org/10.1002/jbm.b.33950

Reyes, R., Rodríguez, J. A., Orbe, J., Arnau, M. R., Évora, C., & Delgado, A. (2018). Combined sustained release of BMP2 and MMP10 accelerates bone formation and mineralization of calvaria critical size defect in mice. *Drug Delivery*, *25*(1). https://doi.org/10.1080/10717544.2018.1446473

Rezvani Ghomi, E., Nourbakhsh, N., Akbari Kenari, M., Zare, M., & Ramakrishna, S. (2021). Collagen-based biomaterials for biomedical applications. *Journal of Biomedical Materials Research Part B: Applied Biomaterials*. https://doi.org/10.1002/jbm.b.34881

Rider, P., Kačarević, Ž., Alkildani, S., Retnasingh, S., Schnettler, R., & Barbeck, M. (2018). Additive Manufacturing for Guided Bone Regeneration: A Perspective for Alveolar Ridge Augmentation. *International Journal of Molecular Sciences*, *19*(11).

https://doi.org/10.3390/ijms19113308

Rodríguez-Évora, M., Delgado, A., Reyes, R., Hernández-Daranas, A., Soriano, I., San Román, J., & Évora, C. (2013). Osteogenic effect of local, long versus short term BMP-2 delivery from a novel SPU–PLGA–βTCP concentric system in a critical size defect in rats. *European Journal of Pharmaceutical Sciences*, *49*(5). https://doi.org/10.1016/j.ejps.2013.06.008

Rodríguez-Vázquez, M., Vega-Ruiz, B., Ramos-Zúñiga, R., Saldaña-Koppel, D. A., & Quiñones-Olvera, L. F. (2015). Chitosan and Its Potential Use as a Scaffold for Tissue Engineering in Regenerative Medicine. *BioMed Research International*, *2015*. https://doi.org/10.1155/2015/821279

Rosenberg, M., Shilo, D., Galperin, L., Capucha, T., Tarabieh, K., Rachmiel, A., & Segal, E. (2019). Bone Morphogenic Protein 2-Loaded Porous Silicon Carriers for Osteoinductive Implants. *Pharmaceutics*, *11*(11). https://doi.org/10.3390/pharmaceutics11110602

Sanzana, E. S., Navarro, M., Ginebra, M.-P., Planell, J. A., Ojeda, A. C., & Montecinos, H. A. (2014). Role of porosity and pore architecture in the *in vivo* bone regeneration capacity of biodegradable glass scaffolds. *Journal of Biomedical Materials Research Part A*, *102*(6). https://doi.org/10.1002/jbm.a.34845

Sathyendra, V., & Darowish, M. (2013). Basic Science of Bone Healing. *Hand Clinics*, *29*(4). https://doi.org/10.1016/j.hcl.2013.08.002

Schmidt-Bleek, K., Willie, B. M., Schwabe, P., Seemann, P., & Duda, G. N. (2016). BMPs in bone regeneration: Less is more effective, a paradigm-shift. *Cytokine & Growth Factor Reviews*, *27*. https://doi.org/10.1016/j.cytogfr.2015.11.006

Segredo-Morales, E., García-García, P., Reyes, R., Pérez-Herrero, E., Delgado, A., & Évora, C. (2018). Bone regeneration in osteoporosis by delivery BMP-2 and PRGF from tetronic–alginate composite thermogel. *International Journal of Pharmaceutics*, *543*(1–2), 160–168. https://doi.org/10.1016/j.ijpharm.2018.03.034

Segredo-Morales, E., Reyes, R., Arnau, M. R., Delgado, A., & Évora, C. (2018). In situ gel-forming system for dual BMP-2 and 17β-estradiol controlled release for bone regeneration in osteoporotic rats. *Drug Delivery and Translational Research*, *8*(5), 1103–1113. https://doi.org/10.1007/s13346-018-0574-9

Semyari, H., Salehi, M., Taleghani, F., Ehterami, A., Bastami, F., Jalayer, T., Semyari, H., Hamed Nabavi, M., & Semyari, H. (2018). Fabrication and characterization of collagen–hydroxyapatite-based composite scaffolds containing doxycycline via freeze-casting method for bone tissue engineering. *Journal of Biomaterials Applications*, *33*(4). https://doi.org/10.1177/0885328218805229

Shevach, M., Soffer-Tsur, N., Fleischer, S., Shapira, A., & Dvir, T. (2014). Fabrication of omentum-based matrix for engineering vascularized cardiac tissues. *Biofabrication*, *6*(2). https://doi.org/10.1088/1758-5082/6/2/024101

Shibuya, N., & Jupiter, D. C. (2015). Bone Graft Substitute. *Clinics in Podiatric Medicine and Surgery*, *32*(1). https://doi.org/10.1016/j.cpm.2014.09.011

Song, B., Estrada, K. D., & Lyons, K. M. (2009). Smad signaling in skeletal development and regeneration. *Cytokine & Growth Factor Reviews*, *20*(5–6). https://doi.org/10.1016/j.cytogfr.2009.10.010

Sorushanova, A., Delgado, L. M., Wu, Z., Shologu, N., Kshirsagar, A., Raghunath, R., Mullen, A. M., Bayon, Y., Pandit, A., Raghunath, M., & Zeugolis, D. I. (2019). The Collagen Suprafamily: From Biosynthesis to Advanced Biomaterial Development. *Advanced Materials*, *31*(1). https://doi.org/10.1002/adma.201801651

St John, T., Vaccaro, A., Sah, A., Schaefer, M., Berta, S., Albert, T., & Hilibrand, A. (2003). Physical and monetary costs associated with autogenous bone graft harvesting. *The American Journal of Orthopedics*, *32*(1), 18–23.

Stratton, S., Shelke, N. B., Hoshino, K., Rudraiah, S., & Kumbar, S. G. (2016). Bioactive polymeric scaffolds for tissue engineering. *Bioactive Materials*, *1*(2). https://doi.org/10.1016/j.bioactmat.2016.11.001

Sun, J., & Tan, H. (2013). Alginate-Based Biomaterials for Regenerative Medicine Applications. *Materials*, *6*(4). https://doi.org/10.3390/ma6041285

Sun, T., Liu, M., Yao, S., Ji, Y., Shi, L., Tang, K., Xiong, Z., Yang, F., Chen, K., & Guo, X. (2018). Guided osteoporotic bone regeneration with composite scaffolds of mineralized ECM/heparin membrane loaded with BMP2-related peptide. *International Journal of Nanomedicine*, *Volume 13*. https://doi.org/10.2147/IJN.S152698

Takeda, T., & Vacanti, J. P. (1995). Hepatocyte Transplantation in the Dalmatian Dog Model of Hyperuricosuria. *Tissue Engineering*, *1*(4). https://doi.org/10.1089/ten.1995.1.355

Tang, Y., Tang, W., Lin, Y., Long, J., Wang, H., Liu, L., & Tian, W. (2008). Combination of bone tissue engineering and BMP-2 gene transfection promotes bone healing in osteoporotic rats. *Cell Biology International*, *32*(9). https://doi.org/10.1016/j.cellbi.2008.06.005

Tønnesen, H. H., & Karlsen, J. (2002). Alginate in Drug Delivery Systems. *Drug Development and Industrial Pharmacy*, *28*(6). https://doi.org/10.1081/DDC-120003853

Urist, M. R., & Strates, B. S. (1971). Bone Morphogenetic Protein. *Journal of Dental Research*, *50*(6). https://doi.org/10.1177/00220345710500060601

Van Lieshout, E. M. M., & Alt, V. (2016). Bone graft substitutes and bone morphogenetic proteins for osteoporotic fractures: what is the evidence? *Injury*, *47*. https://doi.org/10.1016/S0020-1383(16)30011-0

Velioglu, Z. B., Pulat, D., Demirbakan, B., Ozcan, B., Bayrak, E., & Erisken, C. (2019). 3D-printed poly(lactic acid) scaffolds for trabecular bone repair and regeneration: scaffold and native bone characterization. *Connective Tissue Research*, *60*(3). https://doi.org/10.1080/03008207.2018.1499732

Wang, C., Wang, J., Li, J., Hu, G., Shan, S., Li, Q., & Zhang, X. (2016). KDM5A controls bone morphogenic protein 2-induced osteogenic differentiation of bone mesenchymal stem cells during osteoporosis. *Cell Death & Disease*, *7*(8). https://doi.org/10.1038/cddis.2016.238

Wang, H., Li, Y., Zuo, Y., Li, J., Ma, S., & Cheng, L. (2007). Biocompatibility and osteogenesis of biomimetic nano-hydroxyapatite/polyamide composite scaffolds for bone tissue engineering. *Biomaterials*, *28*(22). https://doi.org/10.1016/j.biomaterials.2007.04.014

Wang, X., Wang, Y., Gou, W., Lu, Q., Peng, J., & Lu, S. (2013). Role of mesenchymal stem cells in bone regeneration and fracture repair: a review. *International Orthopaedics*, *37*(12). https://doi.org/10.1007/s00264-013-2059-2

Xu, S., Yu, R., Zhao, G., & Wang, J. (2003). Early period of fracture healing in ovariectomized rats. *Chinese Journal of Traumatology*, *6*,

160–166.

Yingjie, H., Ge, Z., Yisheng, W., Ling, Q., Hung, W. Y., Kwoksui, L., & Fuxing, P. (2007). Changes of microstructure and mineralized tissue in the middle and late phase of osteoporotic fracture healing in rats. *Bone*, *41*(4). https://doi.org/10.1016/j.bone.2007.06.006

Yuan, H. (2001). Bone formation induced by calcium phosphate ceramics in soft tissue of dogs: a comparative study between porous alpha-TCP and beta-TCP. *Journal of Materials Science: Materials in Medicine*, *12*(1). https://doi.org/10.1023/A:1026792615665

Zamani, D., Moztarzadeh, F., & Bizari, D. (2019). Alginate-bioactive glass containing Zn and Mg composite scaffolds for bone tissue engineering. *International Journal of Biological Macromolecules*, *137*. https://doi.org/10.1016/j.ijbiomac.2019.06.182

Zhai, P., Chen, X. B., & Schreyer, D. J. (2015). PLGA/alginate composite microspheres for hydrophilic protein delivery. *Materials Science and Engineering: C*, *56*. https://doi.org/10.1016/j.msec.2015.06.015

Zhang, Y., Wu, D., Zhao, X., Pakvasa, M., Tucker, A. B., Luo, H., Qin, K. H., Hu, D. A., Wang, E. J., Li, A. J., Zhang, M., Mao, Y., Sabharwal, M., He, F., Niu, C., Wang, H., Huang, L., Shi, D., Liu, Q., … El Dafrawy, M. (2020). Stem Cell-Friendly Scaffold Biomaterials: Applications for Bone Tissue Engineering and Regenerative Medicine. *Frontiers in Bioengineering and Biotechnology*, *8*. https://doi.org/10.3389/fbioe.2020.598607

Zheng, X., Liu, Y., Liu, Y., Pan, Y., & Yao, Q. (2021). Novel three-dimensional bioglass functionalized gelatin nanofibrous scaffolds for bone regeneration. *Journal of Biomedical Materials Research Part B: Applied Biomaterials*, *109*(4). https://doi.org/10.1002/jbm.b.34720

Objetivos

Objetivos

El objetivo global de este trabajo de investigación ha sido diseñar, caracterizar y evaluar *in vitro* e *in vivo* estructuras tridimensionales conteniendo sustancias osteoreguladoras y estimulantes de la mineralización ósea para mejorar la calidad y contenido mineral del hueso que por la acción de distintas estrategias se forma en un defecto crítico en calota de animales osteoporóticos.

Para ello, se han abordado los siguientes objetivos específicos:

1. Definir el modelo de inducción de la osteoporosis de rata y ratón, incidiendo en la valoración de las transformaciones que se producen en fémures y calota, hueso en el que se realiza el defecto.

2. Estudiar el efecto regenerativo en ratas normales y osteoporóticas de un hidrogel inyectable compuesto por colágeno, quitosano, hidroxipropil γ-ciclodextrina y PEG, cargado con nano-hidroxiapatita y conteniendo BMP-2 y 17β-estradiol con perfiles de liberación variable.

3. Evaluar la influencia del tiempo de permanencia y estructura de sistemas basados en alginato cargados con BMP-2 y 17-βestradiol, conteniendo o no células mesenquimales, sobre la regeneración ósea en rata osteoporótica.

4. Estudiar el efecto de la combinación BMP-2 con MMP10 frente a BMP-2 y alendronato sobre la mineralización del hueso formado en un defecto crítico en ratones normales y osteoporóticos, empleando un andamio de quitosano.

Chapter 1

PLGA-BMP-2 and PLA-17β-estradiol microspheres reinforcing a composite hydrogel for bone regeneration in osteoporosis

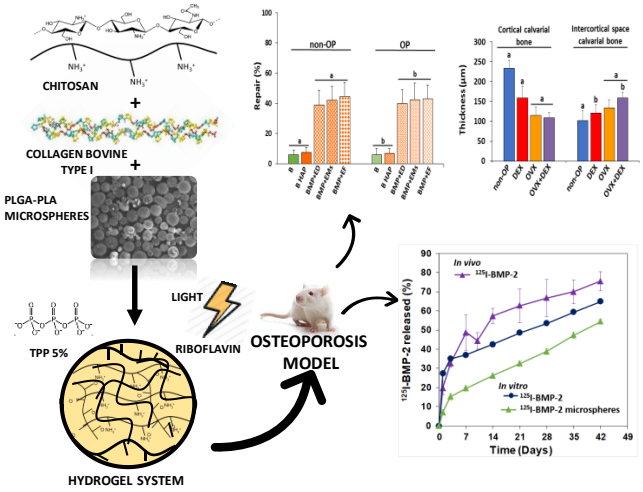

Regen Biomater. 2019 Jun;6(3):149-162

Pharmaceutics. 2019 Dec 3;11(12):648

.

1. Introduction

Bone tissue is under continuous remodelling throughout our lifetime. However, its regeneration capacity is limited by defects size, blood perfusion, age and metabolic disorders (Michalski & McCauley, 2017). Craniofacial bone defects or craniofacial congenital malformations generally require surgery and defects to be refilled with natural or synthetic biomaterials to promote bone healing. Often scaffolds are not enough to induce osteogenesis, and the contribution of other key elements such as progenitor cells or signalling molecules is required to ensure clinical success. In addition, the defect size and the comorbidity with other diseases altering bone tissue metabolism, compromise complete bone healing. Specifically, osteoporosis (OP) is characterized by an imbalance between the processes of bone formation and resorption and, consequently, by a delay in bone defects regeneration (Russow et al., 2018).

Bone morphogenetic proteins (BMPs) are a well-known growth factors family with osteo- and chondroinductive properties. Particularly, recombinant human BMP-2 (rhBMP-2) has shown a strong osteoinductive effect when incorporated in local delivery carriers placed in the injury site (Quinlan et al., 2015). Postmenopausal osteoporosis is related to multiple factors, emphasizing the decreased levels of estrogens. These molecules play a key role in bone cell metabolism through estrogen receptor α (ERα). Estrogens inhibit osteoclastic bone resorption, via increasing osteoclast apoptosis, reducing osteoblastic production of receptor activator of nuclear factor κB ligand (RANKL) and increasing osteoprotegerin production (Lyritis et al., 2010).

Among the several natural polymers used for bone regeneration, chitosan (CHT) is a biomaterial frequently used for scaffold preparation. In a recent extensive review (Venkatesan et al., 2017) focused on CHT for bone tissue regeneration, different advantages were highlighted and discussed such as biocompatibility, capacity for BMPs sustained release, improvement of cell proliferation and increased *in vitro* and *in vivo* stem cells differentiation

and mineralization. However, to obtain a bone graft material able to simulate bone composition, collagen, the major extracellular matrix (ECM) of bone tissue, and hydroxyapatite (HAP), the mineral component of the bone, have also been widely studied (Ma et al., 2016; Teotia et al., 2017; Venkatesan et al., 2017). HAP has been incorporated in scaffolds in micro and nanoparticles to improve protein adsorption, cell adhesion and osteoinductivity (Teotia et al., 2017). The addition of HAP nanoparticles surface-grafted with poly (lactide acid) (PLA) to poly (lactide-co-glycolide acid) (PLGA) scaffolds enhanced the osteogenesis and the mineralization of the formed bone in critical size defects (B. Zhang et al., 2017; P. Zhang et al., 2009). Also, scaffolds prepared with microspheres of PLGA encapsulating tricalcium phosphate/HAP mixtures enhanced the expression of osteogenic markers in mesenchymal stem cells cultures (Gupta et al., 2016). Collagen/HAP scaffolds, loaded with PLGA microspheres containing bone active substances, have also been tested to accelerate bone regeneration (Quinlan et al., 2015; Wang et al., 2017).

Although the aforementioned studies indicated positive results, their application in OP conditions have not always been successful (Segredo-Morales et al., 2017). According to already published reports, the low level of estrogen in OP alters the evolution of calvarial bone repair due to estrogen, Transforming Growth Factor beta 1 (TGF-β1) and α-estrogen receptor (α-ER) interaction (Giovanini et al., 2018). Previous reports of our research group revealed that local implantation of scaffolds, loaded with combinations of BMP-2 and 17β-estradiol formulated in microspheres of PLA or PLGA in rat calvaria critical defects, increased the bone repair in OP rats but the new bone that refilled the defect was less mineralized compared to non-OP groups (Segredo-Morales, García-García, et al., 2018; Segredo-Morales, Reyes, et al., 2018).

2. Objectives

Taking into account that: 1) estrogens are involved in the control of bone resorption; 2) post-menopausal OP is associated with an estrogen deficiency and 3) BMP-2 is involved in bone formation by stimulating mesenchymal stem cells (MSC) differentiation to osteoblast, in the first part of this research work we proposed a loaded BMP-2 and 17β-estradiol sandwich like system including HAP nanoparticles to regenerate a calvarial critical defect in OP rats. This sandwich system is composed by two polymeric external films and a core of a biocomposite hydrogel containing collagen, chitosan (CHT), citrate-coated carbonated apatite nanoparticles (nano-HAP) to improve mineralization, polyethylene glycol (PEG-400), 2-Hidroxipropil γ-Ciclodextrin (HP-γ-CD) and microspheres to provide sustained release of active substances. The core hydrogel was previously characterized in terms of behaviour and mass-transfer (Pérez-Herrero et al., 2019). In the present study, we aim to study the influence of the release rate of 17β-estradiol on the osteogenic effect after sandwich like system implantation in OP rats. Therefore, 17β-estradiol was incorporated into the system in 3 forms: dispersed in the core, encapsulated in microspheres prepared with a mixture of PLA and PLGA dispersed within the hydrogel and, lastly, included in the PLGA films shell prepared by electrospun.

To do this, the first step was to develop and select an adequate osteoporotic model in rat. OP was induced in the rats through three procedures: ovariectomy (OVX), dexametasone (DEX) chronic treatment and a combination of OVX and DEX (OD). The bones were histologically analyzed. Then, the bone repair obtained by the combination of BMP-2 in PLGA microspheres with 17β-estradiol in different formulations was quantified in OP and non-OP rats.

3. Materials and methods

3.1. Microspheres preparation and characterization

BMP-2 microspheres were prepared by the double emulsion method (w/o/w) as previously described (Hernández et al., 2012). Briefly 200 µL of 0.2% poly(vinyl alcohol) (PVA, Mw:30,000-70,000 KDa, 87-90% hydrolysed, Sigma-Aldrich) containing recombinant human bone morphogenetic protein 2, (Biomedal Life Sciences) (260µg) was emulsified with 1 mL of a [4:1] poly (lactide-co-glycolide) acid (PLGA) mixture (150 mg); PLGA-RG504 (PLGA 50:50, Resomer® RG504, 0.58 dL/g, Evonik Industries):PLGA-RG858 (PLGA 85:15 Resomer®, 1.5 dL/g, RG858-S Evonik Industries) dissolved in methylene chloride (DCM, Sigma-Aldrich) by vortexing for 1 min (Genie® Industries 2, Sciences Industries Inc.). Then, this emulsion was poured into 10 mL of a 0.2% PVA solution, vortexed 15 seconds, poured into 100 mL of 0.1% PVA and kept under magnetic stirring for 1 hour for solvent evaporation.

The 17β-estradiol (Sigma-Aldrich) microspheres were prepared by a modified emulsion solvent evaporation method as previously described (Segredo-Morales, Reyes, et al., 2018). The method is based on the emulsification of a 17β-estradiol (4mg) solution containing poly (lactide acid) (PLA-S, Resomer® RG203-S, Evonik Industries) (160 mg) and PLGA-RG858 (40 mg) in 0.6 mL of DCM:Methanol (DCM:MeOH) (80:20) with 4 mL of 1% PVA aqueous solution by vortexing 1 min .Then this emulsion was added to 96 mL of 0.16% PVA solution, under magnetic stirring to allow organic solvent evaporation for 1 hour.

Both types of microspheres were washed with double distilled water and collected by filtration (pore size 45 µm, Pall Corporation), lyophilized and stored at 4°C until use. Microspheres were characterized in terms of size (Mastersizer 2000, Malvern Instruments) and morphology by scanning electron microscopy after silver coating (SEM, Jeol JSM-6300).

To determine BMP-2 encapsulation efficiency and to carry out BMP-2 release assays, some microspheres batches were prepared with ^{125}I-BMP-2. BMP-2 was labelled with ^{125}INa (PerkinElmer) by the iodogen method (Fraker & Speck, 1978). Briefly, in 50 µg Iodogen coated tubes (Pierce® Pre-coated Iodination Tube, Thermo Scientific) 25 µL of the protein solution (1mg/mL) was mixed with 10 µL of ^{125}INa (≈1 mCi) and taken to a final volume of 100 µL with phosphate buffer solution (PBS, 0.5M pH = 7). This mixture was kept at room temperature for 15 minutes under continuous stirring (120 rpm), then, 50 µL of a saturated tyrosine (Sigma-Aldrich) solution in PBS was added to remove any unreacted ^{125}I, the solution was adjusted to a final volume of 200 µL with PBS. Labelled proteins were purified using Zeba™ Spin Desalting Column (Thermo Scientific). Labelling yields and stability were evaluated by instant thin layer chromatography (iTLC) using 11.5 x 0.8 cm silica gel coated strips (Varian Iberica SL) to which 5 µL of the labelled protein was added (30,000-40,000 cpm), using 85% methanol in water as mobile phase. A gamma counter (Cobra II, Packard®) was used to measure free ^{125}I (R_f=1) and labelled proteins (R_f=0) as previously published (De la Riva et al., 2009).

To evaluate microspheres encapsulation efficiency radioactivity was measured on 3 microspheres aliquots using a gamma counter (Cobra II, Packard®) and compared to the total protein reactivity.

On the other hand, the content of 17β-estradiol in the microspheres was determined spectrophotometrically at λ= 280 nm by dissolving an accurate amount of microspheres (10 mg) in a mixture of DCM:MeOH (80:20).

To study the dispersion state of 17β-estradiol in the polymer matrix of the microspheres, differential scanning calorimetry (DSC 025, TA Instruments), was performed. 17β-estradiol and lyophilized microspheres were analyzed after drying in an oven at 37°C overnight. In addition, polymer blends (RG 203-S and RG 858, [4:1]) and polymer blends with 17β-estradiol (8.5%) were dissolved in DCM: MeOH (80:20) and kept in a

hood for 24 hours. Then, samples were placed in a vacuum desiccator for 48 hours to complete the evaporation of the organic solvent. The analysis of all samples was performed with the same settings using two thermal cycles under nitrogen atmosphere (50 mL/min). In the first cycle temperature was increased form RT to 40°C (10°C/min) and then cooled to -20°C (5°C/min) to avoid possible water interference. Once the samples were stabilized, they underwent a final heating cycle from -20°C to 270°C at 10°C/min.

3.2. Film fabrication and characterization

The polymer film was fabricated by a previously described electrospinning method (García-García et al., 2020). Briefly, 7 mg of 17β-estradiol and 300 mg of a mixture of PLGAs, PLGA-RG755-S (PLGA 75:25, Resomer® RG755-S, Evonik Industries) and RG858 [4:1] were dissolved in 2 mL of hexafluoroisopropanol (HFIP, Sigma-Aldrich) and loaded into a Luer-lock syringe (Norm-Ject) equipped with a 18G needle. This solution was ejected at a continuous flow of 3 mL/h using a syringe pump (Harvard Apparatus, MA®) under an electric field of 7 KV. Fibers were collected on a cylindrical metal collector that rotates at 200 rpm located at a 10 cm distance from the syringe. The process took place at room temperature and 65% of relative humidity.

Films were characterized in terms of thickness, porosity and fiber diameter. Mean fiber diameter was obtained measuring 50 fibers for each sample after silver coating using SEM images (SEM, Jeol JSM-6300) at a 1,500 magnification by an image analysis software (ImageJ v1.52, National Institute of Health). Film thickness was obtained using stereomicroscope images (Leica M205 C, Leica LAS, v3 software).

Real mesh density was obtained by helium pycnometry (Micromeritics, AccuPyc 1330) while apparent density was calculated from the weight and estimated volume. The volume was obtained from the length, width and

thickness as described in equation 1. Total porosity was calculated using real density and apparent density values as shown in equation 2.

$$Apparent\ density = \frac{weight}{(lenght \cdot width \cdot thickness)} \quad \text{(eq. 1)}$$

$$Porosity\ (\%) = \frac{real\ density - apparent\ density}{real\ density} \cdot 100 \quad \text{(eq. 2)}$$

3.3. Core system preparation and characterization

Four solutions were used as follows: 1) 10 mg/mL type I collagen (bovine collagen type I, Mw: 376.37 Da, Sigma-Aldrich) cold solution in acetic acid (Merck) 0.043 M; 2) 0.43 g/mL aqueous solution of 2-Hidroxipropil γ-Ciclodextrin (HP-γ-CD, CAVASOL® W8 HP, Wacker Chemical) with riboflavin (RB, Sigma-Aldrich) (5 mg/mL); 3) 20 mg/mL aqueous solution of chitosan (CHT, 150 mPa.s, Protasan® UP-CL-213, NovaMatrix, Ultrapure Polymer Systems) and 4) poly (ethylene glycol) 400 (PEG 400, density: 1.128 g/mL, Sigma-Aldrich). The hydrogel was prepared by mixing the above-mentioned components by vortex to obtain the following final concentrations: 5 mg/mL of collagen, 34 mg/mL of HP-γ-CD (0.4 mg/mL of RB), 5 mg/mL of CHT and 150 mg/mL of PEG 400. To prepare the core system 20 mg of microspheres were dispersed in 50 µL of the hydrogel. Also, when nano citrate-coated carbonated apatite nanoparticles (nano-HAP, kindly donated by Jaime Gómez-Morales, PhD, Laboratory of Crystallographic Studies, CSIC, Spain) were used an adequate amount of nanoparticles were added to the hydrogel. Afterwards, this hydrogel was cross-linked with 5% w/v pentabasic sodium tripolyphosphate (STPP; Sigma-Aldrich) sterile aqueous solution (0.5 µL/µL of hydrogel) under blue visible light at 468 nm (Dental device, quartz-tungsten halogen Hilux UltraPlus, Benlioglu Dental Inc) for 3 min (Pérez-Herrero et al., 2019). The dose of BMP-2 was 6 µg for each scaffold in microspheres and the total 17β-estradiol dose was 200 µg/system in three different forms: electrospun films, microspheres or dispersed into the gel.

Hydrogels porosity, with and without microspheres, was calculated using the equation 1 using freeze-dried samples. To avoid collapse during freeze-drying, the hydrogel was maintained in a mold and quickly frozen with liquid nitrogen before being exposed to a high-vacuum lyophilization process.

In addition, water uptake and mass loss assays were carried out for the core hydrogel by incubation of 300 µL hydrogel aliquots with 5 mL of sterile MilliQ water (37ºC) under orbital agitation (25 rpm). At specific times, six samples were withdrawn, the excess of water was removed, samples were weighted and freeze-dried. Then, three samples were visualized by SEM (Jeol JSM-6300) to see the evolution of the internal structure after incubation and the other three samples were used to record the dried weight and calculate the percentage of mass loss and water uptake applying equations 3 and 4, respectively.

$$Mass\ loss(\%) = \frac{(W_0 - W_d)}{W_0}\ x\ 100 \qquad \text{(eq. 3)}$$

$$Water\ uptake(\%) = \frac{(W_w - W_d)}{W_d}\ x\ 100 \qquad \text{(eq. 4)}$$

Where W_o was the estimated initial sample weight, and W_w and W_d were the weights of the wet and dried sample respectively, at the different times tested.

Viscoelastic and thixotropic behaviors of the core hydrogel were obtained with a Bohlin CVOD 100 rheometer at 37ºC by means of a Peltier system, using cone-plate and parallel geometries with a diameter for the fixed lower plate of 60 mm and a gap between the fixed and rotating part of 1 mm. The evolution of viscosity with shear rate (from 0.071 to 30 s^{-1}) was acquired by cone-plate geometry (diameter of cone 40 mm, angle 4º). The evolution of elastic (G') and viscous moduli (G'') with frequency (from 0.128 to 4.015 Hz) was acquired by a parallel plate geometry (diameter of rotating upper plate 20 mm) at a constant shear stress of 0.2387 Pa.

To test the healing of the core system two syringes of 1 mL were loaded with the hydrogel including 17β-estradiol microspheres, up to 0.5 mL. Then, 4 doses of 50 µL each were unloaded from both syringes assayed for fluidity through a 20G needle and dose uniformity. For this, the discharged samples were lyophilized, and the 17β-estradiol content was evaluated by spectrophotometry at 280 nm after dissolution in DCM: MeOH (80:20).

3.4. In vitro release assays

BMP-2 *in vitro* release assays were carried out by incubating 3 mg of ^{125}I-BMP-2 microspheres in sterile MilliQ water at 37ºC and 25 rpm. The amount of BMP-2 released was calculated by measuring the radioactivity of the supernatants with a gamma counter at pre-set timepoints (Cobra® II, Packard).

The *in vitro* release of 17β-estradiol from the different formulations (dispersed in the core system, included in microspheres incorporated to the core system and inside electrospun films) was carried out at 37°C and 25 rpm using two release media: an aqueous solution of 1% sodium lauryl sulfate (SLS, Sigma-Aldrich) (The United States Pharmacopeial Convention, 2014) and MeOH:water (50:50) (Birnbaum et al., 2000; Zaghloul A, 2006). The 17β-estradiol released was measured in the supernatant using the spectrophotometric method. The effective diffusion coefficient, D_{eff} in the matrix of the microspheres and the mass transfer coefficient of the drug in the boundary layer *h*, were calculated according to the non-steady-state Fick law, as previously described in detail (Pérez-Herrero et al., 2019). The released fraction of 17β-estradiol from the microspheres dispersed or not in the core system was analyzed and equations 5 to 8 were applied for D_{eff} and *h* calculation.

$$\frac{M_t}{M_\infty} = 1 - \sum_{n=1}^{\infty} \frac{6\,L^2}{\beta_n^2\,(\beta_n^2 + L^2 - L)}\, exp\left(-\frac{\beta_n^2}{R^2}\, D_{eff}\, t\right) \qquad \text{(eq. 5)}$$

Where M_t and M_∞ are the total mass of drug released to the media at time *t* and at the end of the experiment, respectively. The β_ns are the infinite roots (eigenvalues) of the equation 6:

$$\beta_n \cot \beta_n + L - 1 = 0 \qquad \text{(eq. 6)}$$

L is the dimensionless mass transfer Biot number, equation 7:

$$L = \frac{h\,R}{D_{eff}} \qquad \text{(eq. 7)}$$

For large values of *L*, the roots of equation 6 are multiple of the number *pi* and equation 4 can be simplified in the equation 8 that is a simplified solution of non-steady-state Fick law:

$$\frac{M_t}{M_\infty} = 1 - \frac{6}{\pi^2}\sum_{n=1}^{\infty}\frac{1}{n^2}\,exp\left(-\frac{n^2\,\pi^2}{R^2}\,D_{eff}\,t\right) \qquad \text{(eq. 8)}$$

As previously described, to minimize the residual sum of squares "genetic algorithms" already implanted in R software (R Foundation for Statistical Computing, version 3.6.1., 2019) were used (Pérez-Herrero et al., 2019).

3.5. Animal experiments

All animal experiments were carried out in conformity with the European Directive (2010/63UE) on Care and Use in Experimental Procedures. Furthermore, the animal protocols were approved on November 5th, 2014 by the Ethics Committee for Animal Care of the University of La Laguna (CEIBA) with identification code CEIBA2014-0128. All surgical procedures were made under aseptic conditions.

3.5.1 Animal model development

40 female adult Sprague-Dawley rats approximately 12 weeks old, weighing 200-250 g, were divided in 4 groups of 10 each. The experimental osteoporosis was induced in 3 groups by three different protocols,

ovariectomy (OVX), chronic administration of dexamethasone (DEX) and ovariectomy + dexamethasone (OD). The fourth group was the sham, non osteoporotic control group (non-OP). A bilateral ovariectomy was carried out under isoflurane anaesthesia via dorsal approach for animals of OVX and OD groups. Analgesia consisted in buprenorphine administered subcutaneously (0.05 mg/kg) before surgery and paracetamol (70 mg/100mL) in the water, for 3 days post-surgery. The DEX group received 0.3 mg/kg body weight of dexamethasone-21-isonicotinate (Deyanil retard, Fatro Ibérica) administered subcutaneously once every two weeks (Govindarajan et al., 2013) for up to the time of euthanasia. Then, two weeks after the ovariectomy the OD group rats were chronically treated with DEX as the DEX group. The 40 rats were sacrificed after 12 weeks and the calvaria and femurs were extracted to be histologically analyzed. The results of these analyzes were used to evaluate the 3 protocols tested to induce OP.

3.5.2. In vivo evaluation of the systems

50 female Sprague-Dawley rats (12 weeks old), weighing 200-250 g, were dividing in 2 groups of 25 each, OP and non-OP. The OP group rats were ovariectomized as described for (OVX) and the non-OP group rats underwent similar surgery, but the ovaries were not resected. 12 weeks post-surgery, 8 mm critical size cranial defects were surgically created with a trephine burr under isoflurane anaesthesia and the systems were placed into the defects (Rodríguez-Évora et al., 2013).

Afterwards rats were again divided in 5 groups of 5 rats each, and the regenerative treatment was applied as reflected in Table 1. The implantation of the system was carried out following a two-step procedure. First, a layer of film (bottom film), previously soaked with the blood produced during the surgery, was placed in the defect then 50 µL of the hydrogel mixed with the microspheres and partially crosslinked with UV light, was discharged on the defect. Secondly, the hydrogel was completely crosslinked by dripping 25 µL of STPP to form the core system, after 5

min, a second layer of film (soaked in blood) was placed on the top, like a sandwich and the wound was then closed with surgical clips.

Table 1. Experimental groups to evaluate regenerative efficiency

Group designations	Treatment
Blank I (B)	System loaded with blank microspheres and blank films
Blank II (B HAP)	System loaded with blank microspheres and 5 mg of nano-HAP and blank films
BMPβeF	System loaded with 6 µg of BMP-2 in microspheres and 200 µg of 17β-estradiol in the 2 films + 5 mg nano-HAP
BMPβeMs	System loaded with 6 µg of BMP-2 in microspheres and 200 µg of 17β-estradiol in microspheres, blank films + 5 mg nano-HAP
BMPβeD	System loaded with 6 µg of BMP-2 and 200 µg of 17β-estradiol dispersed, blank films + 5 mg nano-HAP

3.5.3. ^{125}I-BMP-2 in vivo release assay

The BMP-2 release kinetics was monitored periodically by measuring the remaining ^{125}I-BMP-2 at the rat calvarial defect site using an external probe-type gamma counter (Captus®, Nuclear Iberica), as previously described and validated (Delgado et al., 2006). Briefly, at each sampling time point, five 1-min readings were taken at the ^{125}I emission peak (27 KeV) and the mean value was calculated and considered the remaining radioactivity. The initial measure (time = 0) is considered the administered dose (100%). After 6 weeks, the rats (n = 5) were sacrificed.

3.6. Rat mesenchymal stem cells (rMSCs) osteogenic differentiation

rMSCs were obtained from the bone marrow of the femur of OVX female Sprague-Dawley rats by centrifugal isolation as previously described (Dobson et al., 1999). Briefly, the cells were resuspended in Dulbecco's modified Eagle's medium (DMEM, HyClone®) supplemented with 10%

fetal bovine serum (FBS, Biowest, South America Origin), 1% penicillin-streptomycin (Sigma-Aldrich) and 2 mM L-Glutamine (Biowest) (Complete Culture Medium, CCM). Then, cells were cultured in flasks of 75 cm^2 at 37°C and 5% CO_2. The culture medium was changed every 2-3 days.

To test the osteogenic differentiation, 50,000 cells (passage 2) in 20 µL of CCM were added over aliquots of 300 µL of the core system (hydrogel with microspheres) with and without nano-HAP and incubated at 37°C and 5% CO_2 for 1.5 hours to facilitate cell adhesion. The cell distribution was checked by light microscopy. Afterwards, 500 µL of CCM were added to each well, and, after 3 days of incubation the medium was changed to CCM supplemented with 10 mM β-glycerol phosphate (Sigma-Aldrich), 10^{-7}M dexamethasone (Sigma-Aldrich) and 50 µM ascorbate-2-phosphate (Sigma-Aldrich) to induce osteogenic differentiation. At 7, 14 and 21 days of culture, three wells of each sample were washed (2 times) with Hank's balanced salt solution (HBSS) cooled at 4°C. Then, 500 µL of 0.1 M buffer Tris-HCl, 0.1M NaCl and 0.05M magnesium chloride hexahydrate ($MgCl_2$, Merck) (pH = 9.2-9.5) containing nitro blue tetrazolium chloride (NBT, Roche Diagnostics) and 5-bromo-4-chloro-3-indolyl phosphate (BCIP, Roche Diagnostics) were added and cells were incubated at 37°C and 5% CO_2 under soft agitation for 1.5 hours. Then the NBT/BCIP was removed, and cells were fixed with a solution of 3.7-4% p-formaldehyde buffered to pH = 7.0 (PFA, Panreac®) during 30 min. After this, the formaldehyde was removed, and the wells were washed 3 times with HBBS. Immediately after this, cells were visualized by stereo microscopy (Leica M205C, Leica Las, v3 sofware). Afterwards, samples were dehydrated in a graded series of ethanol before being embedded in Paraplast® and cut using a microtome (Shandon Finesse 325), sections were observed by light microscopy (Leica DM 4000B).

3.7. Histological, immunohistochemical and histomorphometrical evaluation

First, to check the osteoporotic-like condition, 12 weeks after the 10 rats underwent the different protocols were sacrificed and the femurs and calvaria were analysed. The femurs and calvaria were fixed with PFA, decalcified in Histofix® Decalcifier (Panreac) and prepared for histological analysis as previously described (Hernández et al., 2012; Rodríguez-Évora et al., 2013).

Bone morphology was analysed by hematoxylin-erythrosin staining. The histomorphometric analysis was carried out in femurs by measuring the following parameters: thickness of the cortical bone (Ct.Wi) and number (Tb.N), width (Tb.Wi) and separation (Tb.Sp) of the trabeculae in cancellous bone. In the calvaria bone, the histomorphometric analysis was carried out by measuring the following parameters, cortical bone thickness (CBT) and intercortical space thickness (IST) occupied by trabecular bone in transversal sections of calvaria.

To determine the capacity of the systems to regenerate the critical size defect practiced in the calvaria of the rats, samples of the 10 groups of 5 rats each were examined.

Samples were processed as previously described (Hernández et al., 2012). New bone formation was identified by hematoxylin-erythrosin staining. Bone mineralization was assessed with VOF trichrome stain, in which red and brown staining indicates advanced mineralization, whereas less mineralized, newly formed bone stains blue (Martínez-Sanz et al., 2011). Sections were analysed by light microscopy (Leica DM 4000B). Computer based image analysis software (Leica Q-win V3 Pro-Image Analysis System) was used to evaluate all sections. A region of interest (ROI) within the defect (50 mm^2) for quantitative evaluation of new bone formation was defined. The ROI consisted of a circular region of 50 mm^2, the centre of which coincided with that of the defect site. New bone formation was

expressed as a percentage of repair with respect to the original defect area within the ROI, applying the equation 9.

$$\%\, repair = \frac{new\ bone\ area}{original\ defect\ area\ within\ the\ ROI} \times 100 \qquad \text{(eq. 9)}$$

From the total bone repair, the areas of mature bone (MB) and immature bone (IB) were determined and the MB/IB ratio for each experimental group as well as between non-osteoporotic and osteoporotic-like animals, was calculated.

For immunohistochemical analysis, sections were deparaffined and rehydrated in Tris-buffered saline (TBS, pH 7.4, 0.01 M Trizma base, 0.04 M Tris-HCl, 0.15 M NaCl), which was used for all further incubations and rinse steps. Sections were incubated in citrate buffer (pH 6) at 90ºC for antigen retrieval, followed by incubation in 0.3% hydrogen peroxide in TBS buffer for 20 min. After a rinse step, sections were blocked with 2% FBS in TBS–0.2% Triton X-100 (blocking buffer). The indirect immunohistochemical procedure was carried out by incubating the sections with osteocalcin (OCN) polyclonal antiserum (1:100) (Millipore, Barcelona) in blocking buffer overnight at 4 ºC. Sections were the rinsed three times, incubated with biotin-SP-conjugated donkey anti-rabbit F(ab) fragment (1:200) (Millipore, Barcelona) in blocking buffer for 1 h followed by, after another rinse step, a incubation in peroxidase-conjugated streptavidin (1:300) (Millipore, Barcelona) for 1 h. Peroxidase activity was revealed in Tris–HCl buffer (0.05 M, pH = 7.6) containing 0.05% of 3,3'-diaminobenzidine tetrahydrochloride (Sigma, Poole, UK) and 0.004% hydrogen peroxide. Reaction specificity was confirmed by replacing the specific antiserum with normal serum or by pre-adsorption of the specific antiserum with the corresponding antigen.

OCN staining was evaluated using computer-based image analysis software (ImageJ, v1.52, National Institute of Health). OCN staining was measured by applying a fixed threshold to select for positive staining within the ROI. Positive pixel areas were divided by the total surface size (mm^2)

of the ROI. Values were normalized to those measured from blank scaffolds and are reported as relative staining intensities.

Statistical analysis was performed with SPSS version 25 software. We compared the distinct treatments by means of a one-way analysis of variance (ANOVA) with a Tukey multiple comparison post-test. Significance was set at $p<0.05$ unless otherwise stated. Results are expressed as means ± SD.

4. Results

4.1. Systems characterization

The characteristics of the developed microspheres, electrospun film and core system are shown in table 2.

Table 2. Characteristics of the sandwich-like system components. Microspheres: size (µm) and encapsulation efficiency (EE). Electrospun film: thickness, porosity and average diameter of the fibers. Core system: porosity, water uptake and mass loss fresh and after incubation in MilliQ water, 37°C and 25 rpm for 7 or 28 days.

Microspheres	Size (µm)			E.E. (%)
17β-estradiol	101.4 (10% < 29.73, 90% < 198.31)			83.5 ± 1.84
BMP-2	112.1 (10%<60.3, 90% <174.8)			71 ± 7
Film	Thickness (µm)	Fiber diameter (µm)		Porosity (%)
	63.4 ± 4.3	1.2 ± 0.26		71.9 ± 0.41
Core system	Porosity (%)	Incubation time	Water uptake (%)	Mass loss (%)
(Hydrogel + microspheres)	72	7 days	135.9 ± 2.6	18.85 ± 7
		28 days	138.9 ± 11.0	29.19 ± 4.88

The hydrogel porosity without microspheres was 81.62 ± 2.25% and decreased down to 69.98 ± 3.07% after microspheres addition (core system). The integrity of the system was assayed throughout 4 weeks. Figure 1 shows the morphology of the microspheres (Fig. 1A), the hydrogel (Fig. 1B, C) and the core system by SEM (fig. D-F). The images of the hydrogel internal structure (Fig. 1B, C), the core system freshly prepared (Fig. 1D) and after 4 weeks of incubation showed that the microspheres were homogeneously dispersed in the hydrogel while being trapped in the core system (Fig. 1E, F). The core system absorbed a significant amount of water during the first days of incubation which was maintained over time. On the contrary, the system lost less than 20% of the mass weight during the first week and approximately 35% after 4 weeks (Table 2).

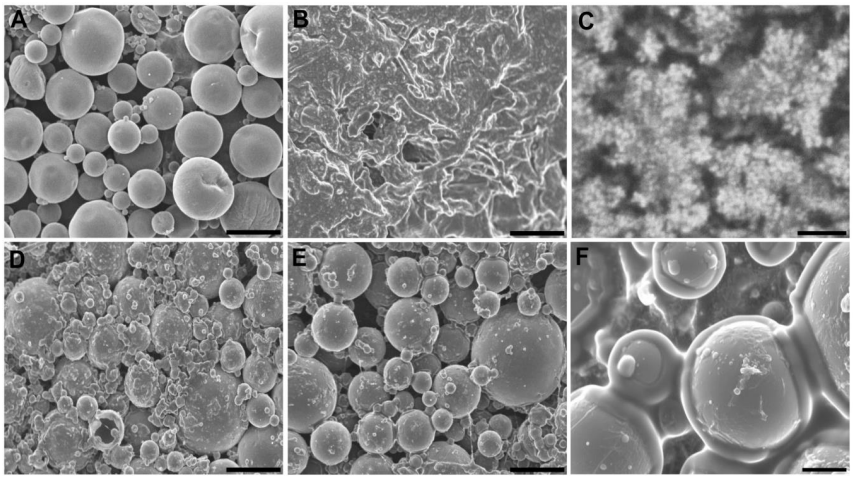

Figure 1. SEM images (A) microspheres; (B) hydrogel; (C) hydrogel high magnification detail; (D) core system freshly prepared; (E) internal structure of the core system after 4 weeks incubation in water at 37°C and 25 rpm and (F) high magnification detail of Fig. 1E. Scale bars (A, B, D, E) 100 µm, (C) 1 µm, (F) 20 µm.

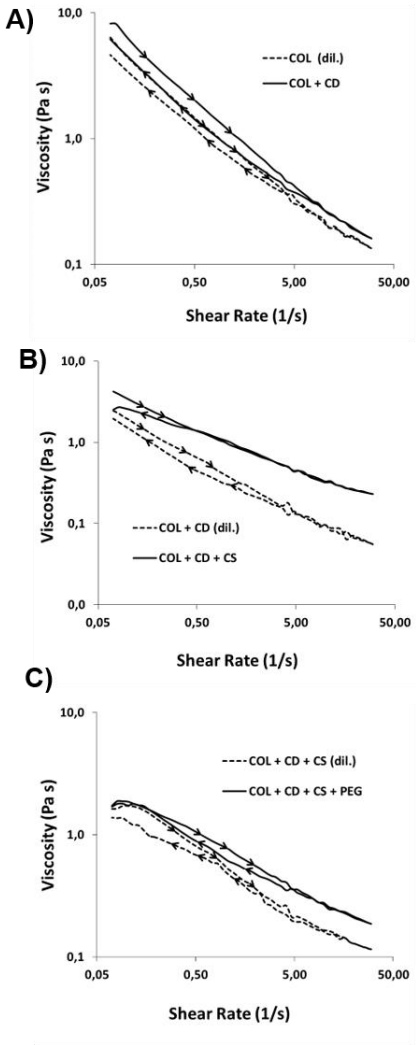

Figure 2. Evolution of the viscoelastic behavior of collagen with the incorporation of cyclodextrin, chitosan and PEG. (A) Variation of viscosity with shear rate in collagen (COL) versus a mixture of collagen and cyclodextrin (COL+CD) with a mass ratio equal to that in the core system. (B) Variation of viscosity with share rate in collagen–cyclodextrin mixture (COL+CD) versus a collagen–cyclodextrin–chitosan mixture (COL+CD+CS) with a mass ratio equal to that in the core system. (C) Variation of viscosity with shear rate in collagen–cyclodextrin–chitosan mixture (COL+CD+CS) versus the complete gel (COL+CD+CS+PEG) with a mass ratio equal to that in the core system.

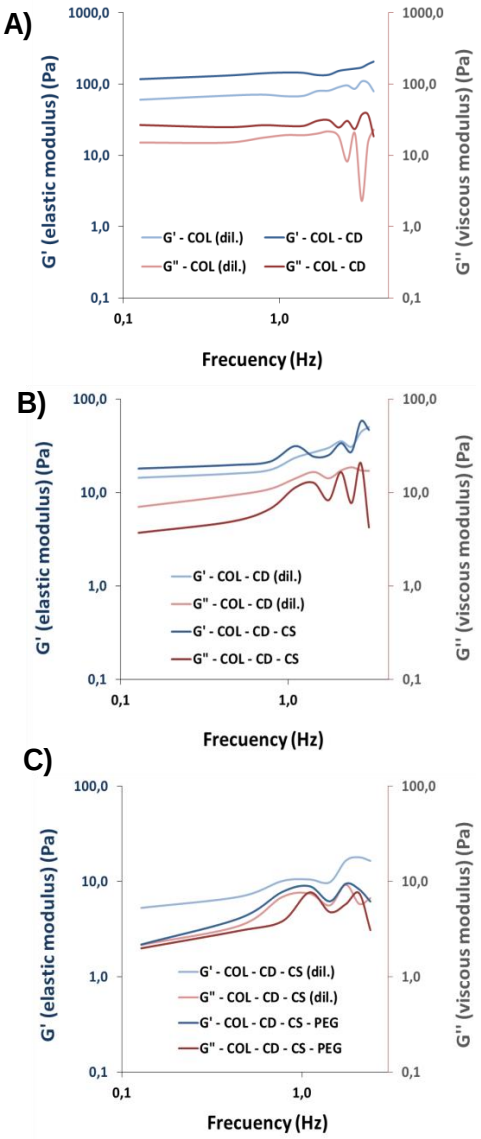

Figure 3. Evolution of the viscoelastic behavior of collagen with the incorporation of cyclodextrin, chitosan and PEG. (A) Viscous moduli against frequency of collagen (COL) versus a mixture of collagen and cyclodextrin (COL+CD) with a mass ratio equal to that in the core system. (B) Viscous moduli against frequency in collagen–cyclodextrin mixture (COL+CD) versus a collagen–cyclodextrin–chitosan mixture (COL+CD+CS) with a mass ratio equal to that in the core system. (C) Viscous moduli against frequency in collagen–cyclodextrin–chitosan mixture (COL+CD+CS) versus the complete gel (COL+CD+CS+PEG) with a mass ratio equal to that in the core system.

Fig. 2A and 3A represents the variation in viscosity with the shear rate and the elastic and viscous moduli with the frequency, respectively, for a

collagen solution (COL) and a mixture of collagen and cyclodextrin (COL+CD). In this regard, the incorporation of cyclodextrin to the collagen solution increases the viscosity values (Fig. 2A) and the gel behavior of collagen (both modulus increase, although the elastic to a greater extent, staying above in both cases) (Fig. 3A). Chitosan was added to the collagen–cyclodextrin mixture to harden the hydrogel by crosslinking with TPP, this addition further increased the viscosity of the system (COL+CD). Moreover, the incorporation of chitosan (COL+CD+CS) increased the difference between elastic and viscous modulus (Fig. 2B, 3B). Note that the comparison between COL+CD and COL+CD+CS was performed at the same conditions as Fig. 2A and 3A. The PEG addition increased the viscosity (Fig. 2C). At low frequencies, the big difference between the elastic and viscous moduli of the collagen–cyclodextrin–chitosan mixture decreased when PEG is incorporated, as shown in Figure 3C.

Moreover, the core system (COL+CD+CS+PEG) presented a thixotropic behavior. The forward and backward curves did not overlap, being the area between both (or hysteresis loop) (Fig. 2C) an indication of the magnitude of the thixotropic behavior. This characteristic allows the implantation of the core system in a minimally invasive way and facilitate the adjustment to the shape of the defect. In fact, the core system flew well through a 20 G needle and the average dose discharged was uniformed, 83.5 ± 6% of the loaded dose.

The differential scanning calorimetry thermograms of the 17β-estradiol microspheres and components plotted in Fig. 4 allows to analyse the state of 17β-estradiol in the microsphere's polymeric matrix. The glass transition temperature (Tg) of the RG 203-S and RG 858 [4:1] polymers mixture was located at 52-58 °C, between the Tg of PLA (RG203-S) and PLGA (RG858). The DSC analysis of pure 17β-estradiol showed three endothermic peaks (Fig. 4A), the first two at 118.1 °C and 174.4 °C were previously attributed to the partial and complete loss of hydrogen-bound water and reticular water, respectively. The third peak, located at 179.4 °C corresponds to the melting point (Turek et al., 2016). This last peak,

characteristic of the crystalline structure of 17β-estradiol, was neither detected for the polymer blend+17β-estradiol, nor in the microspheres thermogram (Fig. 4B). These results indicated that 17β-estradiol was dissolved in the polymer by at least 8.5%.

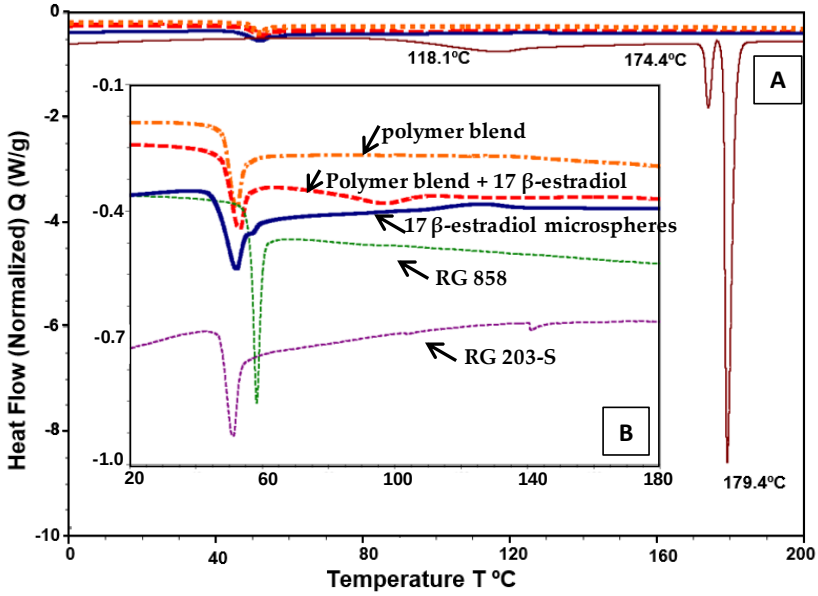

Figure 4. Differential scanning calorimetry thermograms of (A) pure 17β-estradiol and (B) PLA (RG203-S); PLGA (RG858), polymer blend (RG203-S:RG858, [4:1]) and polymer blend with 8.5% of 17β-estradiol, previously dissolved in DCM:MeOH (80:20) and the curve of the microspheres of 17β-estradiol.

4.2. Osteogenic differentiation

The count of rMSCs alkaline phosphatase positive cells (ALP +), cultured in the hydrogels with osteogenic differentiation culture medium, showed a discrete and progressive increase between 7 and 21 days of culture in the hydrogels without and with nano-HAP. However, the number of positive

cells was significantly higher in those hydrogels containing nano-HAP (Fig. 5). Likewise, qualitatively, the cells cultured in the hydrogels with nano-HAP, presented greater intensity of color, suggesting greater ALP activity (Fig. 5) than without nano-HAP.

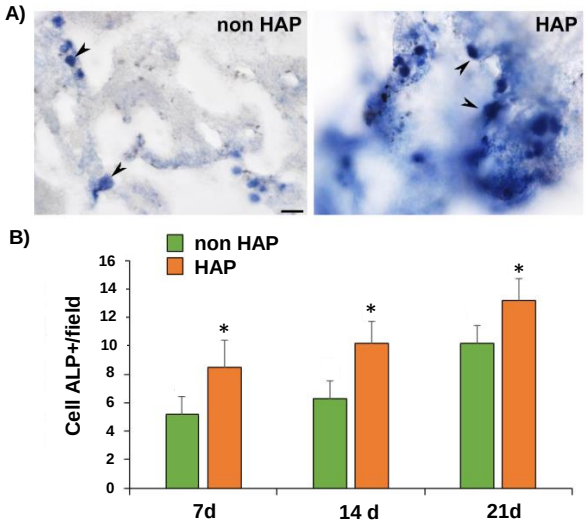

Figure 5. Alkaline phosphatase (ALP) activity in rMSCs cultures. (A) Representative images from hydrogels 21 days after cultured showing the APL positive (ALP+) cells morphology (arrowheads) culture in hydrogels without (Non HAP) and with nano-hydroxyapatite (HAP). (B) Number of APL+ cells/ microscopic field at different time points (7, 14 and 21 days). Scale bar = 20 µm. (*) Denotes statistical differences to non HAP group at each point, $p<0.01$.

4.3. Release profiles of ^{125}I-BMP-2 and 17β-estradiol

Figure 6 shows the release profile of BMP-2. Although the hydrogel provoked a strong reduction of the burst effect, the *in vitro* release of BMP-2 from the microspheres and from the core system showed a biphasic profile. During the first 24 hours approximately 7% of the protein was release from the core system *versus* 27% from the microspheres directly

dispersed in the medium. Afterwards, the release rate was kept in the range of 60-55 ng/day (Fig. 6). The *in vivo* release profile was also biphasic, with a first phase that lasted up to 7 days and approximately 50% of the protein released. Then the release rate was reduced to 70 ng/day, slightly higher than the *in vitro* rate.

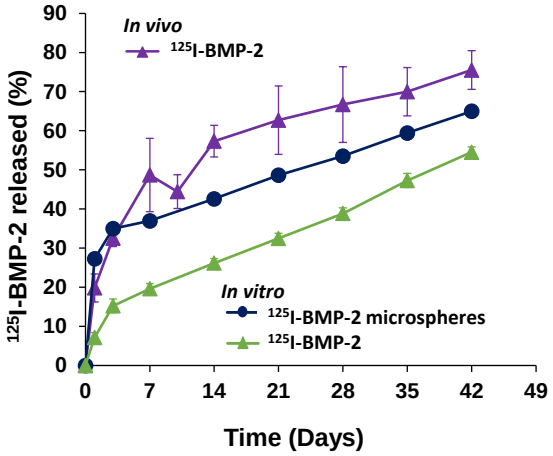

Figure 6. BMP-2 Release assays. *In vivo* release profile of ^{125}I-BMP-2 from PLGA-microspheres in the system after implantation in the rat calvaria defect (n=5). *In vitro* release of ^{125}I-BMP-2 (incubation in water at 37ºC and 25 rpm) from PLGA-microspheres and from the PLGA microspheres dispersed in the core system.

The *in vitro* release rate of 17β-estradiol in the aqueous medium depended on the formulation (Fig. 7A). At the end point of the study 4 week 100% of the 17β-estradiol dispersed in the core system was released. On the other hand, for the same time point only 70% of the drug loaded in the electrospun films was released. The release profile was characterized by a high burst effect, approximately half of the dose was released during the first day. By contrast, the 17β-estradiol release rate was extremely slow for the microspheres alone and the microspheres included in the hydrogel (core system). Both release profiles were similar, less than 20% was delivered,

in 4 weeks. However, when the MeOH: water (50:50) medium was used, there were no differences in the transfer profiles. The presence of MeOH modified the solubility of 17β-estradiol, leading to a strong burst effect of 70-85% of the dose released in the first 24 hours (Fig. 7A).

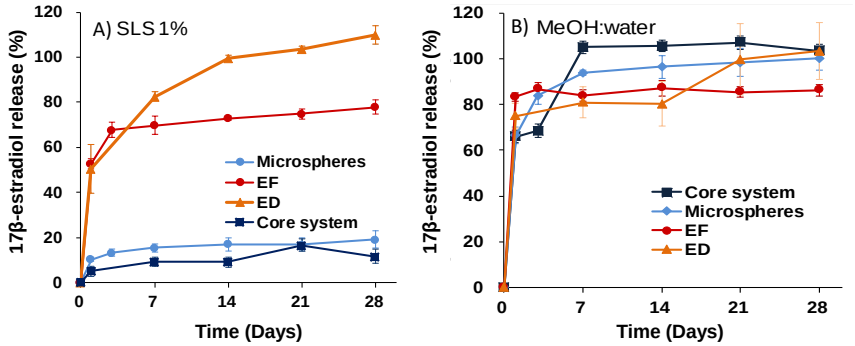

Figure 7. *In vitro* 17-βestradiol release profiles in different release media at 37ºC and 25 rpm. (A) in MeOH:water (50:50) and (B) in aqueous solution of SLS 1%. ED: 17β-estradiol dispersed in the core system; EF: 17β-estradiol in the electrospun film; microspheres: 17β-estradiol pre-encapsulated in microspheres and core system: 17β-estradiol microspheres in the hydrogel.

The estimated values of D_{eff} and h for 17β-estradiol release in the different media are show in Table 3. Although the value of D_{eff} for 17β-estradiol in SLS was significantly lower compared to the MeOH:water (50:50), there were no differences for h regardless of the release media used. h is the contribution of hydrogel, as part of the boundary layer, to the whole mass transfer process, and the value of this coefficient should not change by varying the release media. The values of R^2 (Table 3), together with the comparison of experimental and predicted values of the released fractions shows a good data fit to the proposed model for both release media.

Table 3. Estimated values of effective diffusion coefficient (D_{eff}) and mass transfer coefficient (h) for 17β-estradiol release in different media applying equations 5-8.

Release media	D_{eff} (m²/s)	h (m/s)	R^2 (%) value
MeOH:water (50:50)	$2.28 \cdot 10^{-15} \pm 5.00 \cdot 10^{-17}$	$7.56 \cdot 10^{-10} \pm 2.89 \cdot 10^{-10}$	95.47 ± 0.07
SLS 1%	$5.58 \cdot 10^{-16} \pm 9.81 \cdot 10^{-17}$	$4.01 \cdot 10^{-10} \pm 4.94 \cdot 10^{-10}$	92.49 ± 2.71

4.4. Histology, immunohistochemical and histomorphometrical evaluation

4.4.1. Osteoporotic model assessment

The osteoporotic models were assessed in both long bone (femur) and flat bone (calvaria). The histological analysis of calvaria showed evident changes in the structure and microarchitecture of the bone among the different experimental groups. While the non-OP animals showed a normal bone structure in cortical bone (CB), trabecular bone (TB) and intercortical space (ICS), in the different OP models (DEX, OVX and OD) (Fig. 8A) a progressive decrease in cortical bone thickness (CBT) and an increase in the intercortical space thickness (IST) was observed, being the group OD the one that presented greater alteration of the tissue bone structure (Fig. 8B).

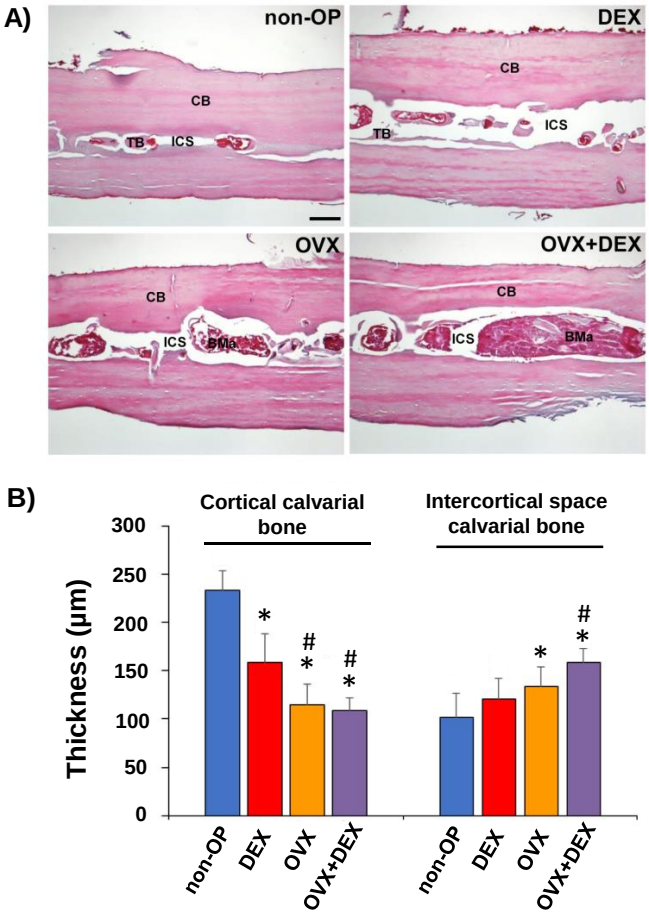

Figure 8. Validation of the OP model in calvarial bone. (A) Representative images in transversal section of calvaria in non-osteoporotic animals (non-OP) and in each of the different experimental models tested. (B) Histomorphometric analysis of the cortical bone thickness and intercortical space thickness evaluated in calvaria for the different models of osteoporosis. CB: cortical bone, BMa: bone marrow, ICS: intercortical space, TB: trabecular bone. Scale bar = 100 µm. (*) Denotes statistical differences to non-OP group. (#) Denotes statistical differences to DEX group.

The histological analysis of the femurs also showed evident changes in the structure and microarchitecture of the bone among the different experimental groups. While non-OP animals showed a normal bone structure, in the different OP models (DEX, OVX and OD) structural changes were observed, both at the level of cortical and cancellous bone, showing a less compact bone with a more porous structure (Fig. 9A). The histomorphometric analysis revealed differences in the measured cancellous bone parameters (Tb.N, Tb.Wi. and Tb.Sp.) with a significant reduction in all of them for the OVX and OD groups compared to the non-OP and DEX animals (Fig. 9 B, C, D). However, the cortical bone thickness (Ct.Wi.), although showing a slight reduction in the groups OVX and OD with respect to the non-OP and DEX groups, this effect was not significant (Fig. 9 E).

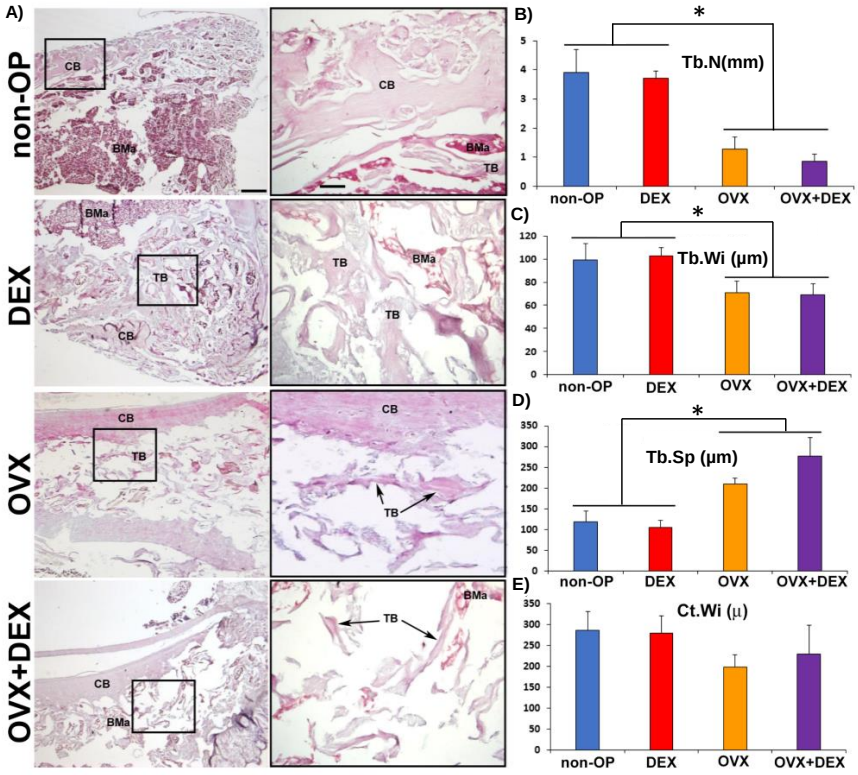

Figure 9. Validation of the OP model in long bone (femur). (A) The left column shows representative panoramic images of rat femur longitudinal sections in non-osteoporotic animals (non-OP) and in each of the different experimental models of osteoporosis tested. The right column shows high magnification images of the distal portion of the femur showing differences in the microarchitecture of the bone in the different models. Histomorphometric analysis of the different parameters evaluated in femur. (B) Tb. N (mm), (C) Tb. Wi (µm), (D) Tb. Sp. (µm) and (E) Ct. Wi (µm). CB: cortical bone, TB: Trabecular bone, BMa: bone marrow. Scale bars: Left column 250 µm. Right column 50 µm. (*) Denotes statistical differences between indicated groups. Fig. (B, C, D) $p<0.001$.

4.4.2. In vivo evaluation of the systems

The histological analysis at the level of the calvarial defect showed low new bone formation in the blank groups (B and B HAP), being limited to the margins of the defect in both, non-OP and OP groups (Fig. 10). The groups implanted with BMP-2 + 17β-estradiol in the three different formulations showed a greater area of newly formed bone not only in the margins but also in inner zone of the defect (Fig. 10). The newly formed bone in the different experimental groups in both, non-OP and OP animals, showed a normal morphology and VOF staining revealed areas of mineralization, slightly more in the non-OP animals groups (Fig. 10).

The histomorphometric analysis showed low repair response in the blank groups (B and B HAP) of non-OP and OP animals, with repair percentages between 6 and 8%. On the contrary, groups implanted with BMP-2 + 17β-estradiol in the three different formulations, showed a significantly higher repair response, with values between 38 and 45%, no differences were observed between non-OP and OP animals (Fig. 11A).

On the other hand, the analysis of mature and immature bone showed a higher quantity of mature bone and, therefore, a greater degree of mineralization, in the non-OP experimental groups with respect to OP animals. The ratio between mature and immature bone (MB/IB) showed individually higher values in all non-OP with respect to OP groups. Overall, the mean value of MB/IB for non-OP animals was 1.47 while for OP animals this value decreased to 0.99 (Fig. 11B, C).

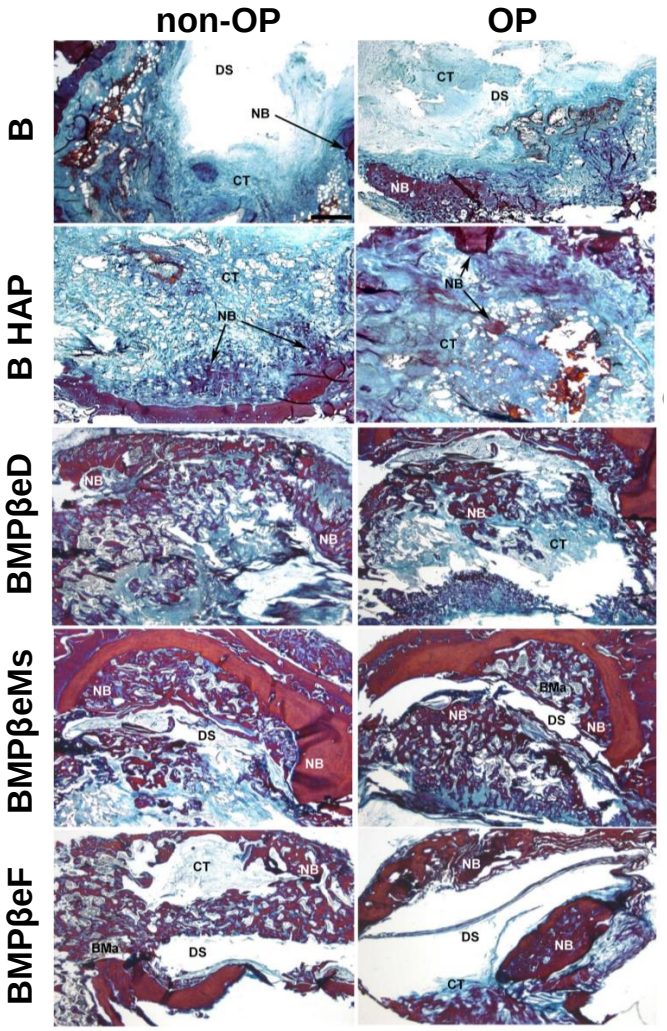

Figure 10. Repair process in calvarial defect. Representative images in horizontal section of calvarial critical size defects in non-OP and OP rats showing the repair response at the defect level in the different experimental groups 12 weeks post implantation. BMa: bone marrow, CT: connective tissue, NB: newly formed bone, DS: defect site. Scale bar = 1 mm.

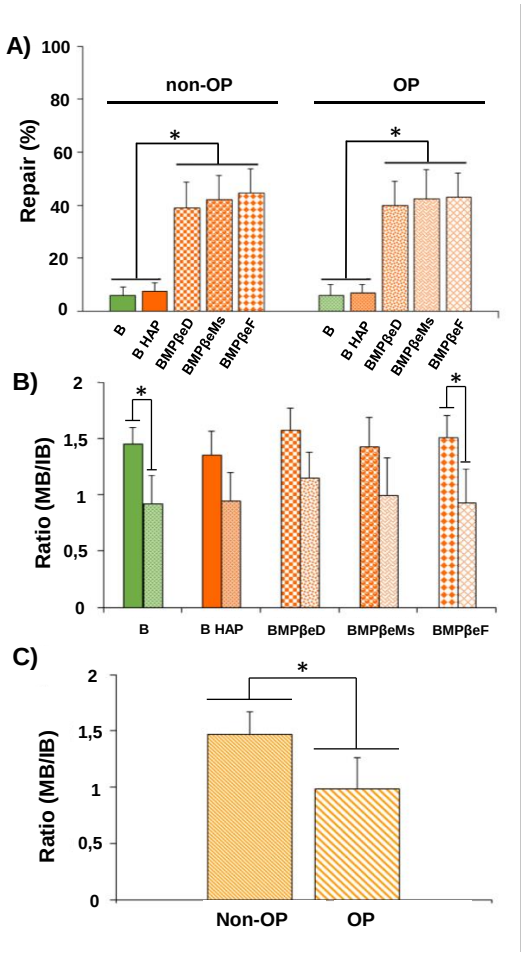

Figure 11. Repair process in calvarial defect. Histomorphometrical analysis (A) comparing the degrees of repair (%) among the different experimental groups in non-OP and OP rats 12 weeks post implantation. (B) Ratio overall between mature bone and inmature bone (MB/IB) among the different experimental groups, (C) and between non-OP and OP rats, estimated using VOF staining. Bars represent means ± SD (n=4). (*) Denotes statistical differences between indicated groups.

The immunohistochemical analysis of osteocalcin (OCN), a marker of late osteogenesis and mineralization, showed low immunoreaction for the blank groups (B and B HAP) in both, non-OP and OP animals, with no differences between them (Fig. 12). However, the immunoreaction was higher and more intense with respect to the blank groups for groups implanted with BMP-2+17β-estradiol in the three different formulations. Additionally, in this case, the response was slightly higher for the non-OP animals than for OP (Fig. 12). The histomorphometric analysis, showed slightly higher relative OCN staining values in the BMP-2 + 17β-estradiol groups in non-OP animals (Fig. 13).

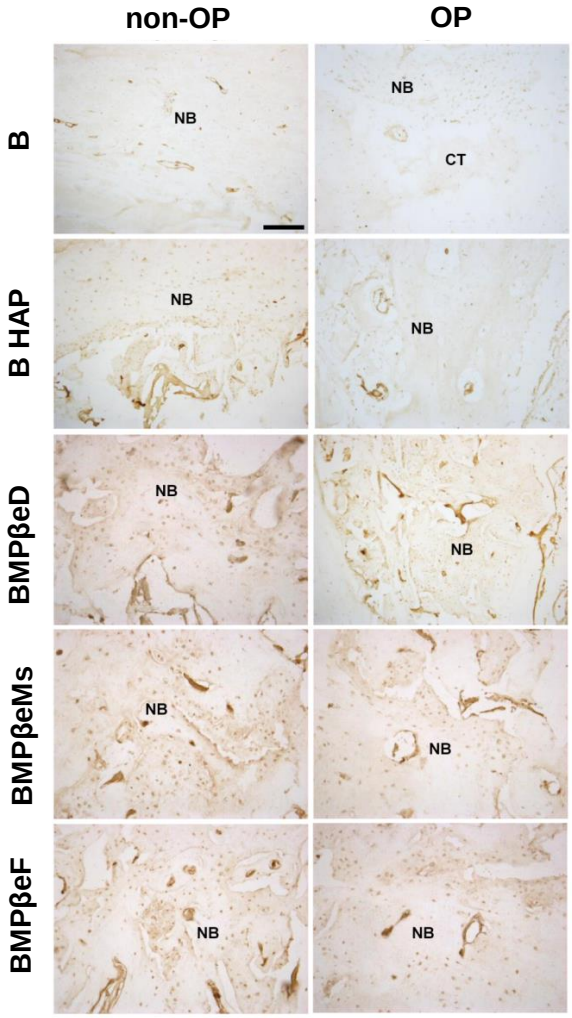

Figure 12. OCN relative expression. Representative images in horizontal sections of calvarial critical size defects in non-OP and OP rats showing OCN immunoreactivity in the different experimental groups 12 weeks post implantation. CT: connective tissue, NB: newly formed bone. Scale bar = 100 µm.

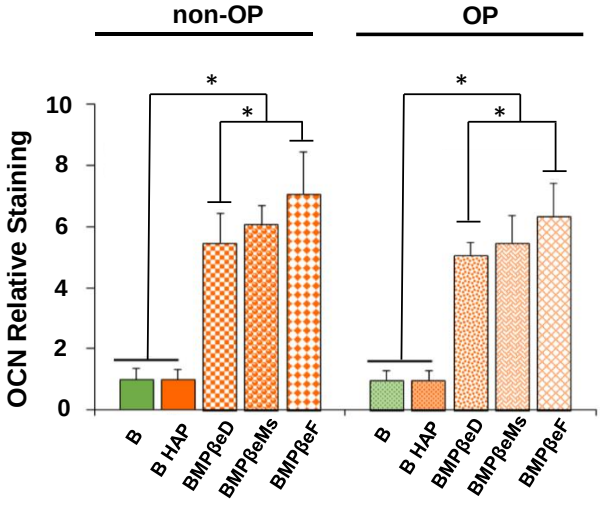

Figure 13. OCN relative expression. Histomorphometric analysis showing the relative staining values for OCN-ir. Bars represent means ± SD (n=4). (*) Denotes statistical differences between indicated groups.

5. Discussion

In this first study a BMP-2-17β-estradiol hydrogel system with a porosity of approximately 70% was evaluated for the regeneration of a critical size defect in rat calvaria. The hydrogel presented adequate characteristics in terms of cell adhesion, viability and proliferation of MSC isolated from rats (Pérez-Herrero et al., 2019). The thixotropic behavior of the hydrogel allows its injectability and the characterization has been completed by testing the water uptake and mass loss as well as performing osteoblastic differentiation studies with osteoporotic rMSCs. *In vitro* release profiles of 17β-estradiol in two media and the *in vitro* and *in vivo* release profile of BMP-2 form the developed systems, were also analyzed.

The osteogenic differentiation of osteoporotic rMSCs seeded on the systems was assessed to test the effect of the nano-HAP incorporation on

cell behavior. The results showed greater ALP activity and a greater number of differentiated cells when cells are cultured in the systems with nano-HAP. Therefore, nano-HAP systems were subsequently used in the *in vivo* experiments.

Despite the high number of OP studies and the several publications dedicated to tissue repair in non-OP specimens, very few reports devoted to bone defect regeneration in OP have been published. Therefore, as a first step to stablish an adequate OP model, a histological evaluation of the femur and calvaria of rats subjected to three different treatments for osteoporosis induction, was carried out. OP is a systemic bone disease characterized by the increase in bone porosity, loss of bone mass and changes in the microstructure of the skeletal tissue. Consequently, the OP population has an increased risk of fracture. As OP might be primary as post-menopausia, or secondary due to corticoid chronic administration, three animal models were used for OP induction: OVX, chronic glucocorticoid treatment and the combination of both.

The bone histological study of the different treatments used to generate OP aims to test if the induced bone damage is treatment dependent. In general, OP condition is established through the analysis of long bones and lumbar spine but few data of the effect on the calvaria of the animals used as OP models are available (Calciolari et al., 2017). Most of the publications focused on the regeneration of calvaria critical size defects in OP animals do not report the effects of OP in this bone (Durão et al., 2014; Engler-Pinto et al., 2019). In the present study, histomorphometric analysis of the femurs and calvarias after the three treatments revealed that the effect of OVX was similar to OD combination, except for the higher separation of trabeculae in cancellous bone (Tb.Sp) observed in OD animals. Here, because we wanted to test the effect of sandwich like system loaded with 17β-estradiol and to simplify the model and improve animal welfare, OVX was selected.

Given that some authors have observed a delay in bone consolidation of OVX rats (Cortet, 2011) and that, as we previously described, combinations of BMP-2 and 17β-estradiol formulated in microspheres applied to a critical calvaria defect improved bone healing in OP rats but the new bone was less mineralized (Segredo-Morales, García-García, et al., 2018; Segredo-Morales, Reyes, et al., 2018), we tried to prolong the active substances release to cover this delay. Hence, drugs were incorporated to the hydrogel system pre-encapsulated in microspheres for prolonged controlled release. To reduce the release rate of the therapeutic molecules, microspheres were prepared with a mixture of polymers, 20% of RG 858 was combinated with RG 504 for BMP-2 microspheres or with RG203-S for 17β-estradiol microspheres. RG 858 is a 85:15 PLGA, of high molecular weight with a degradation rate lower than RG 504 and RG203-S. The BMP-2 release profiles showed a two-phase behavior with a weak burst effect observed during the first week. However, the burst effect of BMP-2 that observed for from the microspheres was damped by the hydrogel, probably due to the interaction of the protein with the HAP chemical groups (Quinlan et al., 2015; Teotia et al., 2017). Afterwards, the second phases were practically parallel, which indicated a mass transfer process controlled by the access of water inside the microspheres, dissolution, and diffusion of the protein through the pores of the polymeric matrix.

To study the release profile of 17β-estradiol, two release media were used, MeOH:water (50:50) and an aqueous solution of SLS. The first selected media was used based on literature as the standard condition used for 17β-estradiol release. However, due to the lack of biological relevance of such ethanol:water solvent an aqueous solution of SLS was also tested. Moreover, this last media is the recommended by the American Pharmacopeia (The United States Pharmacopeial Convention, 2014). Agreement with our hypothesis, the release of 17β-estradiol in MeOH:water was fast regardless of the loading technique. However, the *in vitro* release of 17β-estradiol was formulation dependent when an aqueous medium was used, the release rate was slower when 17β-estradiol was

loaded in microspheres. According to the DSC results, 17β-estradiol formed a solid solution in the microspheres, indicating the release process takes place by molecular diffusion of 17β-estradiol within the microspheres and governed by the partition coeficient. In addition, the higher estimated values of D_{eff} in the MeOH:water compared with the aqueous medium, confirmed the dependency on the release media. The calorimetric analysis of the electrospun sheet was not carried out due to the low 17β-estradiol dose per fiber weight. Although 17β-estradiol is expected to be also dissolved in the polymer, the large specific surface area that microfibers have causes the fast release rate. Similarly, 17β-estradiol dispersed in the hydrogel was scarce maintained in the systems. Obviously, neither media are physiological, but it seems more correct to use an aqueous medium to predict *in vivo* release. Presumably, a slightly faster release rate is expected to take place *in vivo*, since the biological components present in the tissue could accelerate the drug release from the system.

Despite the beneficial role of the nano-HAP controlling BMP-2 burst effect as well as its positive effect on the proliferation and osteogenic differentiation of rMSC which justifies the use of nano-HAP in the system, the reparative effect of the blank scaffolds with and without nano-HAP was not enough to be considered useful. Unlike the observed in this study, other authors showed better new bone formation compared to untreated defects in metaphyseal regions of osteoporotic chinese mountain goat model with a nanoparticulated HAP system with and without collagen type-1 (Alt et al., 2016). By contrast, in another study, (Teotia et al., 2017) similarly to the our findings, the use of nano-HAP and calcium sulfate bone scaffolds loaded with BMP-2 combined with zolendronic acid in rat critical calvaria defect showed no effect on repair and mineralization at 8 and 12 weeks with respect to the empty defect (Teotia et al., 2017).

The three combinations of BMP-2 with 17β-estradiol showed the same effect at 12 weeks. However, the ratios of mature and immature bone in normal and osteoporotic animals showed significant differences, indicating

that the quality of the repaired bone, at least after 12 weeks, was better in non-OP animals.

6. Conclusions

The prepared core system resulted to be easily injectable allowing a reliable dose administration. The system helps to control the burst effect of BMP-2 pre-encapsuled in PLGA microspheres probably due to the presence pf nano-HAP. The release of 17β-estradiol from PLA-PLGA microspheres was intricated and governed by the partition coefficient of the drug which is in solid dissolution in the microspheres. The system was biocompatible both *in vitro* and *in vivo*. However, the regenerative effect detected was independent of the 17β-estradiol release profile, and, therefore, we hypothesize the bone defect regeneration observed in both OP and non-OP rats, was mainly due to the osteogenic effect of BMP-2 released in a controlled manner for 6 weeks. A delay in the mineralization of the newly formed bone in OP animals was observed. Consequently, new strategies and alternative drugs will be explored trying to accelerate the mineralization in osteoporosis.

7. References

Alt, V., Cheung, W. H., Chow, S. K. H., Thormann, U., Cheung, E. N. M., Lips, K. S., Schnettler, R., & Leung, K. S. (2016). Bone formation and degradation behavior of nanocrystalline hydroxyapatite with or without collagen-type 1 in osteoporotic bone defects - An experimental study in osteoporotic goats. *Injury*, *47*, S58–S65. https://doi.org/10.1016/S0020-1383(16)47010-5

Birnbaum, D. T., Kosmala, J. D., Henthorn, D. B., & Brannon-Peppas, L. (2000). Controlled release of b-estradiol from PLAGA microparticles: The effect of organic phase solvent on encapsulation and release. In *Journal of Controlled Release* (Vol. 65). www.elsevier.com/locate/jconrel

Calciolari, E., Mardas, N., Dereka, X., Kostomitsopoulos, N., Petrie, A., & Donos, N. (2017). The effect of experimental osteoporosis on bone regeneration: Part 1, histology findings. *Clinical Oral Implants Research*, *28*(9). https://doi.org/10.1111/clr.12936

Cortet, B. (2011). Bone repair in osteoporotic bone: postmenopausal and cortisone-induced osteoporosis. *Osteoporosis International*, *22*(6). https://doi.org/10.1007/s00198-011-1612-3

De la Riva, B., Nowak, C., Sánchez, E., Hernández, A., Schulz-Siegmund, M., Pec, M. K., Delgado, A., & Évora, C. (2009). VEGF-controlled release within a bone defect from alginate/chitosan/PLA-H scaffolds. *European Journal of Pharmaceutics and Biopharmaceutics*, *73*(1), 50–58. https://doi.org/10.1016/j.ejpb.2009.04.014

Delgado, J. J., Evora, C., Sánchez, E., Baro, M., & Delgado, A. (2006). Validation of a method for non-invasive in vivo measurement of growth factor release from a local delivery system in bone. *Journal of Controlled Release*, *114*(2), 223–229. https://doi.org/10.1016/j.jconrel.2006.05.026

Dobson, K. R., Reading, L., Haberey, M., Marine, X., & Scutt, A. (1999). Centrifugal Isolation of Bone Marrow from Bone: An Improved Method for the Recovery and Quantitation of Bone Marrow Osteoprogenitor Cells from Rat Tibiae and Femurae. *Calcified Tissue International*, *65*(5). https://doi.org/10.1007/s002239900723

Durão, S. F., Gomes, P. S., Colaço, B. J., Silva, J. C., Fonseca, H. M., Duarte, J. R., Felino, A. C., & Fernandes, M. H. (2014). The biomaterial-mediated healing of critical size bone defects in the ovariectomized rat. *Osteoporosis International*, *25*(5). https://doi.org/10.1007/s00198-014-2656-y

Engler-Pinto, A., Siéssere, S., Calefi, A., Oliveira, L., Ervolino, E., Souza, S., Furlaneto, F., & Messora, M. R. (2019). Effects of leukocyte- and

platelet-rich fibrin associated or not with bovine bone graft on the healing of bone defects in rats with osteoporosis induced by ovariectomy. *Clinical Oral Implants Research*, *30*(10). https://doi.org/10.1111/clr.13503

Fraker, P. J., & Speck, J. C. (1978). Protein and cell membrane iodinations with a sparingly soluble chloroamide, 1,3,4,6-tetrachloro-3a,6a-diphenylglycoluril. *Biochemical and Biophysical Research Communications*, *80*(4), 849–857. https://doi.org/10.1016/0006-291X(78)91322-0

García-García, P., Reyes, R., Pérez-Herrero, E., Arnau, M. R., Évora, C., & Delgado, A. (2020). Alginate-hydrogel versus alginate-solid system. Efficacy in bone regeneration in osteoporosis. *Materials Science and Engineering C*, *115*, 111009. https://doi.org/10.1016/j.msec.2020.111009

Giovanini, A. F., de Sousa Passoni, G. N., Göhringer, I., Deliberador, T. M., Zielak, J. C., Storrer, C. L. M., Costa - Casagrande, T. A., & Scariot, R. (2018). Prolonged use of alendronate alters the biology of cranial repair in estrogen-deficient rats' associated simultaneous immunohistochemical expression of TGF-β1+, α-ER+, and BMPR1B-. *Clinical Oral Investigations*, *22*(5). https://doi.org/10.1007/s00784-017-2292-y

Govindarajan, P., Khassawna, T., Kampschulte, M., B€ Ocker ‡, W., Huerter, B., D€ Urselen §, L., Faulenbach, M., & Heiss, C. (2013). *Implications of combined ovariectomy and glucocorticoid (dexamethasone) treatment on mineral, microarchitectural, biomechanical and matrix properties of rat bone*. https://doi.org/10.1111/iep.12038

Gupta, V., Lyne, D. V., Barragan, M., Berkland, C. J., & Detamore, M. S. (2016). Microsphere-based scaffolds encapsulating tricalcium

phosphate and hydroxyapatite for bone regeneration. *Journal of Materials Science: Materials in Medicine*, *27*(7). https://doi.org/10.1007/s10856-016-5734-1

Hernández, A., Reyes, R., Sánchez, E., Rodríguez-Évora, M., Delgado, A., & Évora, C. (2012). In vivo osteogenic response to different ratios of BMP-2 and VEGF released from a biodegradable porous system. *Journal of Biomedical Materials Research Part A*. https://doi.org/10.1002/jbm.a.34183

Lyritis, G. P., Georgoulas, T., & Zafeiris, C. P. (2010). Bone anabolic versus bone anticatabolic treatment of postmenopausal osteoporosis. *Annals of the New York Academy of Sciences*, *1205*(1). https://doi.org/10.1111/j.1749-6632.2010.05666.x

Ma, X., He, Z., Han, F., Zhong, Z., Chen, L., & Li, B. (2016). Preparation of collagen/hydroxyapatite/alendronate hybrid hydrogels as potential scaffolds for bone regeneration. *Colloids and Surfaces B: Biointerfaces*, *143*. https://doi.org/10.1016/j.colsurfb.2016.03.025

Martínez-Sanz, E., Ossipov, D. A., Hilborn, J., Larsson, S., Jonsson, K. B., & Varghese, O. P. (2011). Bone reservoir: Injectable hyaluronic acid hydrogel for minimal invasive bone augmentation. *Journal of Controlled Release*, *152*(2). https://doi.org/10.1016/j.jconrel.2011.02.003

Michalski, M. N., & McCauley, L. K. (2017). Macrophages and skeletal health. *Pharmacology & Therapeutics*, *174*. https://doi.org/10.1016/j.pharmthera.2017.02.017

Pérez-Herrero, E., García-García, P., Gómez-Morales, J., Llabrés, M., Delgado, A., & Évora, C. (2019). New injectable two-step forming hydrogel for delivery of bioactive substances in tissue regeneration. *Regenerative Biomaterials*, *6*(3). https://doi.org/10.1093/rb/rbz018

Quinlan, E., López-Noriega, A., Thompson, E., Kelly, H. M., Cryan, S. A., & O'Brien, F. J. (2015). Development of collagen–hydroxyapatite scaffolds incorporating PLGA and alginate microparticles for the controlled delivery of rhBMP-2 for bone tissue engineering. *Journal of Controlled Release*, *198*. https://doi.org/10.1016/j.jconrel.2014.11.021

Rodríguez-Évora, M., Delgado, A., Reyes, R., Hernández-Daranas, A., Soriano, I., San Román, J., & Évora, C. (2013). Osteogenic effect of local, long versus short term BMP-2 delivery from a novel SPU-PLGA-βTCP concentric system in a critical size defect in rats. *European Journal of Pharmaceutical Sciences*, *49*(5), 873–884. https://doi.org/10.1016/j.ejps.2013.06.008

Russow, G., Jahn, D., Appelt, J., Märdian, S., Tsitsilonis, S., & Keller, J. (2018). Anabolic Therapies in Osteoporosis and Bone Regeneration. *International Journal of Molecular Sciences*, *20*(1). https://doi.org/10.3390/ijms20010083

Segredo-Morales, E., García-García, P., Évora, C., & Delgado, A. (2017). BMP delivery systems for bone regeneration: Healthy vs osteoporotic population. Review. In *Journal of Drug Delivery Science and Technology* (Vol. 42, pp. 107–118). Editions de Sante. https://doi.org/10.1016/j.jddst.2017.05.014

Segredo-Morales, E., García-García, P., Reyes, R., Pérez-Herrero, E., Delgado, A., & Évora, C. (2018). Bone regeneration in osteoporosis by delivery BMP-2 and PRGF from tetronic–alginate composite thermogel. *International Journal of Pharmaceutics*, *543*(1–2), 160–168. https://doi.org/10.1016/j.ijpharm.2018.03.034

Segredo-Morales, E., Reyes, R., Arnau, M. R., Delgado, A., & Évora, C. (2018). In situ gel-forming system for dual BMP-2 and 17β-estradiol controlled release for bone regeneration in osteoporotic rats. *Drug*

Delivery and Translational Research, *8*(5), 1103–1113. https://doi.org/10.1007/s13346-018-0574-9

Teotia, A. K., Raina, D. B., Singh, C., Sinha, N., Isaksson, H., Tägil, M., Lidgren, L., & Kumar, A. (2017). Nano-Hydroxyapatite Bone Substitute Functionalized with Bone Active Molecules for Enhanced Cranial Bone Regeneration. *ACS Applied Materials & Interfaces*, *9*(8). https://doi.org/10.1021/acsami.6b14782

The United States Pharmacopeial Convention (Ed.). (2014). *The United States Pharmacopeia 37-The National Formulary 32, USP* (Baltimore, Vol. 32).

Turek, A., Olakowska, E., Borecka, A., Janeczek, H., Sobota, M., Jaworska, J., Kaczmarczyk, B., Jarząbek, B., Gruchlik, A., Libera, M., Liśkiewicz, A., Jędrzejowska-Szypułka, H., & Kasperczyk, J. (2016). Shape-Memory Terpolymer Rods with 17-β-estradiol for the Treatment of Neurodegenerative Diseases: an In Vitro and In Vivo Study. *Pharmaceutical Research*, *33*(12). https://doi.org/10.1007/s11095-016-2019-9

Venkatesan, J., Anil, S., Kim, S.-K., & Shim, M. S. (2017). Chitosan as a vehicle for growth factor delivery: Various preparations and their applications in bone tissue regeneration. *International Journal of Biological Macromolecules*, *104*. https://doi.org/10.1016/j.ijbiomac.2017.01.072

Wang, X., Wu, X., Xing, H., Zhang, G., Shi, Q., E, L., Liu, N., Yang, T., Wang, D., Qi, F., Wang, L., & Liu, H. (2017). Porous Nanohydroxyapatite/Collagen Scaffolds Loading Insulin PLGA Particles for Restoration of Critical Size Bone Defect. *ACS Applied Materials & Interfaces*, *9*(13). https://doi.org/10.1021/acsami.6b13566

Zaghloul A. (2006). beta-Estradiol biodegradable microspheres: effect of

formulation parameters on encapsulation efficiency and in vitro release. *Pharmazie . 2006 Sep;61(9):775-9.*, *9*(61), 775–779.

Zhang, B., Zhang, P., Wang, Z., Lyu, Z., & Wu, H. (2017). Tissue-engineered composite scaffold of poly(lactide-co-glycolide) and hydroxyapatite nanoparticles seeded with autologous mesenchymal stem cells for bone regeneration. *Journal of Zhejiang University-SCIENCE B*, *18*(11). https://doi.org/10.1631/jzus.B1600412

Zhang, P., Hong, Z., Yu, T., Chen, X., & Jing, X. (2009). In vivo mineralization and osteogenesis of nanocomposite scaffold of poly(lactide-co-glycolide) and hydroxyapatite surface-grafted with poly(l-lactide). *Biomaterials*, *30*(1). https://doi.org/10.1016/j.biomaterials.2008.08.041

Chapter 2

Alginate-hydrogel versus alginate-solid system. Efficacy in bone regeneration in osteoporosis

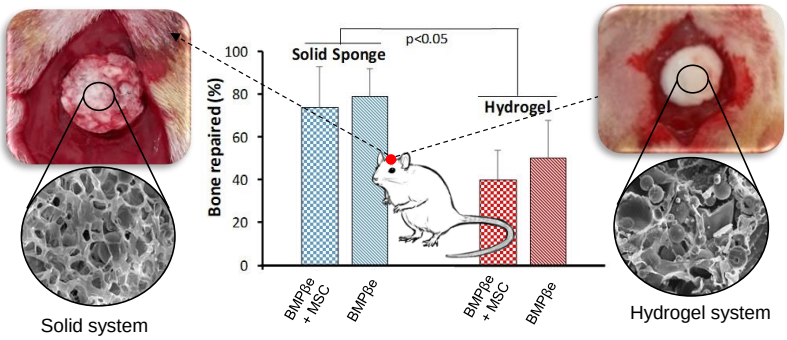

Mater Sci Eng C Mater Biol Appl. 2020 Oct;115:111009

1. Introduction

Scaffolds play an active role in bone regeneration as artificial extracellular matrix. Different biodegradable and/or osteointegrable materials of diverse nature (phosphates, bio-glass, natural and synthetic polymers) have been used to construct 3D-scaffolds. The design of these scaffolds is based on fulfilling several characteristics to facilitate tissue ingrowth, such as biocompatibility, porous structure with interconnected pores, permeability for blood perfusion, nutrients supply, cell adhesion and differentiation (Velasco et al., 2015). Hydrogels suit these characteristics, thus the development and preparation of biodegradable hydrogels for bone tissue engineering applications is currently of great interest (Hoffman, 2012; Peppas et al., 2006). In addition, scaffold bioactivity is required to successfully tackle critical size bone defect regeneration. One strategy to "activate" scaffolds is their loading with signalling molecules or cells involved in the remodelling event cascade such as growth factors, cytokines, hormones or mesenchymal stem cells (MSC). Particularly, BMP-2, is involved in most of the processes required for bone formation (Begam et al., 2017; Chen & Kawazoe, 2018; Fayaz et al., 2011; Hutmacher, 2000; Nauth et al., 2011; Vo et al., 2012). The benefits of rhBMP-2 have been already proven, nevertheless, the risk of adverse effects associated with the high dose required in the clinic and the inability of the carrier to retain the protein in the defect, site make necessary the development of scaffolds with controlled release capacity for greater efficacy and safety (El Bialy et al., 2017). Injectability and adaptability to the bone defect shape are among the most characteristic advantages of hydrogels (Hoffman, 2012; Peppas et al., 2006). However, their poor mechanical properties and short residence time in the defect could be a disadvantage depending on the type of bone lesion to be treated. Finally, their incapacity to regulate growth factors release has led to the development of different strategies to control drug release rate by increasing the drug binding to the hydrogel matrix (Agrawal & Sinha, 2017; Kondiah et al., 2016; Moreno et al., 2016) or combining hydrogels with sustained release platforms (Dorati et al., 2017; Kondiah et al., 2016; Moreno et al., 2016). As we already mentioned in chapter 1 our

previous studies with hydrogels of different composition shown that the regenerated bone was less mineralized in OP groups than in non-OP groups (Segredo-Morales, García-García, et al., 2018; Segredo-Morales, Reyes, et al., 2018). Also in chapter 1, we studied the regeneration induced in the calvarial critical defect of a hydrogel composed by collagen and HAP aimed to improve mineralization and control BMP-2 and 17β-estradiol release using microspheres. However, this strategy did not enhance the mineralization of the new bone filling in the defect. Given that all bone repair processes are impaired and bone healing time is delayed in OP (Cheung et al., 2016; Kubo et al., 1999; Namkung-Matthai et al., 2001; Oliver et al., 2013), to overcome the low mineralization observed in our previous studies we hypothesized that a longer residence time of the scaffold in the defect and a longer release of BMP-2 in OP is required.

2. Objectives

In this part, a new alginate hydrogel system, crosslinked in two steps and a solid sponge system with the same composition both loaded with 17β-estradiol and BMP-2 within microspheres were compared. The goal is to keep similar physical and chemical properties for both systems such as composition, hydrophilicity/hydrophobicity, water uptake, swelling behaviour, porosity and BMP-2 and 17β-estradiol release rates. Therefore, the expected different between both systems is the scaffold residence time in the critical size calvarial defect. Microspheres were elaborated from a combination of alginate and poly (lactide-co-glycolide) acid (PLGA) with different lactide to glycolide ratio and molecular weight (Mw). Therefore, two β-estradiol-BMP-2-Alginate-PLGA systems, hydrogel (HY) and solid sponge (SS), were developed and *in vitro* characterized. The quality of the regenerated bone using both systems alone or seeded with OP mesenchymal stem cells (MSCs) was compared in a critical size defect in OP rats

3. Materials and methods

3.1. Microsphere preparation and characterization

Alginate-PLGA microspheres of BMP-2 were prepared by modifying a previously described double emulsion (w/o/w) method (Gainza et al., 2013; Zhai et al., 2015). Briefly, an aqueous solution of 500 µL of rhBMP-2 (Biomedal Life Sciences) (500µg), 100 µL of 15% poly (vinyl alcohol) (PVA, Mw: 33,000-70,000 KDa, 87-90% hydrolysed, Sigma-Aldrich) and 300 µL of 6% sodium alginate (Protasan® UP MVG, Novamatrix) (w/v) was emulsified with 2 mL of a mixture of PLGA 75:25 (PLGA 75:25, Resomer® RG755, Evonik Industries) and PLGA 85:15 (PLGA 85:15, Resormer® RG858, Evonik Industries) [4:1] in methylene chloride solution (125 mg/mL, DCM) by vortexing (Genie® Industries 2, Sciences Industries Inc.) for 1 min. Then, 5.2 mL of an aqueous solution of 2.5 mL of PVA (10% w/v), 2.5 mL of NaCl (10% w/v) (Merck) and 200 µL of $CaCl_2$ (0.5M, Merck) was poured over the first emulsion and vortexed for 30 seconds (position 10). Finally, the organic solvent was evaporated in 100 mL of 0.25M $CaCl_2$ aqueous solution under constant magnetic stirring for 1.5 hours.

Microspheres of 17β-estradiol (Sigma-Aldrich) were prepared by the solvent evaporation method as in chapter 1 (section 3.1). Briefly a mixture of 17β-estradiol (6 mg), PLGA 75:25 (160 mg) and PLGA 85:15 (40 mg) dissolved in 0.6 mL DCM:methanol (DCM:MeOH) [80:20] solution was emulsified with 4 mL of 1% PVA aqueous solution by vortexing for 1 min, poured into 100 mL of PVA (0.15% w/v) aqueous solution and left under magnetic stirring for 1 hour.

Both types of microspheres were washed with double distilled water and collected by filtration (Supor®-450, 0.45 µm, 47 mm filters, Pall Corporation), lyophilized and conserved at 4ºC until use.

The encapsulation efficiency of both type of microspheres was determined as described in chapter 1 (section 3.1), using ^{125}I-BMP-2 as a tracer to determine rhBMP-2 or by spectrophotometry at λ= 280 nm for

17β-estradiol. Also, microspheres were characterized in terms of morphology and size distribution (see chapter 1, section 3.1).

3.2. Electrospinning film fabrication and characterization

The polymer film was fabricated by electrospinning as described in chapter 1 (section 3.2). A solution of 7 mg of 17β-estradiol, 240 mg of PLGA 75:25 and 60 mg of PLGA 85:15 in 2 mL of hexafluoroisopropanol (HFIP, Sigma-Aldrich) were electrospun using an 18G needle at a flow rate of 3 mL/h under 10 kV power supply and the collector rotating at 200 rpm at 10 cm from the needle.

The film quality and fiber diameter were analysed using SEM (Jeol, JSM-6300) images and the film thickness was measured by stereo-microscop (Leica M205C, Leica Las, v 3 sofware). The real density was measured in a helium pycnometer (AccuPyc 1330, Micromeritics) and the porosity was calculated (see equation 1 and 2, chapter 1 section 3.2).

Water uptake and mass loss assays were carried out, as described in chapter 1 (section 3.2). Samples square pieces of 3 x 3 cm of electrospun film were incubated in water (37ºC) under orbital agitation (25 rpm). At specific times, three samples were withdrawn, the excess of water removed, weighted and freeze-dried to record the dry weight. The percentages of mass loss and water uptake were calculated applying equation 3 and equation 4, (chapter 1, section 3.2), respectively.

3.3. Systems preparation and characterization

Solid system (SS). To prepare the alginate solid sponge system 15 mg of microspheres were dispersed in 100 µL of 2% alginate aqueous solution and freeze-dried. The alginate was then cross-linked by incubation with 100 µL of 1% $CaCl_2$ during 3 min and washed with 100 µL of sterile MilliQ water three times and freeze-dried. All the systems were stored at 4ºC until use.

Hydrogel system (HY). To prepare the alginate hydrogel system 4.5% w/w sodium alginate sterile aqueous solution was partially cross-linked by sufficient quantity of a 1% w/w $CaCl_2$ sterile aqueous solution to give a final concentration of 4% w/w of sodium alginate and 0.12% w/w of $CaCl_2$. Then, 15 mg of microspheres were dispersed in the partially cross-linked hydrogel (PC-HY). Afterwars, the hydrogel was cross-linked with 5% w/w $CaCl_2$ sterile aqueous solution (0.7 µL/ µL of hydrogel).

The systems were characterized in terms of porosity, water uptake and mass loss, as previously described in chapter 1 (section 3.2 and 3.3, equations 1-4). Morphology and structural characteristics were observed by SEM (Jeol JSM-6300). Described in chapter 1 (section 3.3).

In addition, the rheological characteristics of the PC-HY, freshly prepared with and without microspheres, and after 4 hours at rest (PC-HY +4h), were obtained with a Bohlin CVOD 100 rheometer at 20ºC and 37ºC by means of a Peltier system, using cone-plate and parallel geometries with a diameter of the fixed lower plate of 60 mm and a gap between the fixed and rotating part of 1 mm. The evolution of viscosity with shear rate (from 0.071 to 30 s^{-1}) was acquired by a cone-plate geometry (diameter of cone 40 mm, angle 4º). The evolution of elastic (G') and viscous moduli (G'') with frequency (0.128 a 6.93 Hz) was acquired by a parallel plate geometry (diameter of rotating upper plate 20 mm) at a constant shear stress of 0.2387 Pa.

The systems to be implanted were prepared under aseptic conditions and all contained 6 µg of BMP-2 in microspheres. In addition, the solid sponge systems were loaded with 300 µg of 17β-estradiol in microspheres (SS-BMPβe). However, in the hydrogel system the dose of 17β-estradiol was divided: 240 µg in microspheres dispersed in the hydrogel and 60 µg in two electrospun films placed forming a sandwich system (HY-BMPβe). Both systems, solid sponge and hydrogel, seeded with MSCs obtained from osteoporotic rats, SS-BMPβe-MSC and HY-BMPβe-MSC, were also implanted.

3.4. In vitro release assays

The rhBMP-2 *in vitro* release assays were carried out by incubating (37ºC, 25 rpm orbital stirring) each system in sterile MilliQ water. The amount of the ^{125}I-BMP-2 released was calculated by measuring the radioactivity of the supernatants (Cobra® II, Packard). The *in vitro* assays of 17β-estradiol from free microspheres, microspheres in the HY, microspheres in the SS and samples of the electrospun films were carried out in an aqueous solution of SLS (1% w/v), in MeOH:water (50:50) and in dimethyl sulfoxide (DMSO, Acofarma):water (40:60) at 37ºC with orbital stirring (25 rpm).

3.5. Cell isolation and culture

Osteoporotic bone marrow rat rMSC were obtained as described in chapter 1 (section 3.6) (Dobson et al., 1999). SS-BMPβe-MSC and HY-BMPβe-MSC systems were seeded with a $5x10^5$ rMSCs suspension in passage 2 (60 µL) approximately 20 min before implantation.

The 60 µL of the rMSC suspension were dropped on the solid sponge system or mixed with the hydrogel system. In previous *in vitro* studies we demonstrated that all materials are biocompatible and rMSCs allow their adhesion and viability (Reyes et al., 2013; Vayas et al., 2019).

3.6. Animal experiments

3.6.1. Surgical procedures

30 female Sprague-Dawley rats, weighing 250-300 g, underwent ovariectomy (OVX) and three months post-OVX, critical size (8 mm diameter) calvarial defects were created surgically. Surgeries were made under aseptic conditions described in chapter 1 (section 3.5.2).

3.6.2. In vivo evaluation of the systems

The 30 female rats pre-OVX were divided in 6 groups of 5 rats each, 2 groups of 5 OP rats each were implanted with SS-^{125}I-BMPβe and HY-^{125}I-BMPβe to determine the ^{125}I-BMP-2 release kinetics. After 6 weeks the rats were sacrificed.

The other four groups were used to evaluate the bone regeneration induced by a combination of BMP-2 and 17β-estradiol with and without rMSC in the two systems. 2 groups were implanted with the solid systems: SS-BMPβe (6 µg BMP-2 + 300 µg β-estradiol) or SS-BMPβe-MSC (6 µg BMP-2 + 300 µg 17β-estradiol + 5x10^5 rMSC, Passage 2) and 2 groups were implanted with the hydrogel system, HY-BMPβe or HY-BMPβe-MSC. The animals were sacrificed at 12 weeks post-implantation, and the defects enclosing samples were resected from the calvaria.

3.6.3. In vivo ^{125}I-BMP-2 release assays

In vivo ^{125}I-BMP-2 release assay was carried out with the non-invasive method used in chapter 1 (section 3.5.3).

3.7. Histology and histomorphometrical evaluation

The samples were fixed (10% formalin solution) decalcified in Histofix® Decalcifier (Panreac) and prepared for histological analysis, as previously described in chapter 1 (section 3.7). New bone formation and the presence of adipose and connective tissue was identified by hematoxylin-erythrosin staining based on their different morphological characteristics and the degree of new bone mineralization with VOF trichrome stain. Similarly, adipose or connective tissue were identified in the ROI and the percentage calculated from the ratio between the area occupied by each specific tissue and the area of the original defect.

Statistical analyses were performed using SPSS version 25 software. One-way analysis of variance (ANOVA) and a Tukey multiple comparison

post-test were used to compare the overall performance of the different groups. Results are expressed as mean ± standard deviation. Significance was set at $p < 0.05$ unless otherwise stated.

4. Results

4.1. Scaffolds Characterization

The mean volume diameters of the alginate-PLGA microspheres containing BMP-2 and PLGA microspheres with 17β-estradiol were 64.0 µm (10% <14.8 µm; 90% <111.6 µm) and 171.4 µm (10% <46.2 µm; 90% <286.0 µm) respectively. The encapsulation efficiency was 71% and 99% for the BMP-2 and 17β-estradiol, respectively.

Mentioned scaffolds were prepared by dispersing a mixture of the above microspheres in an alginate aqueous solution from which a final presentation of solid sponge or hydrogel was set. The SS scaffold presented a higher porosity (89.4 ± 1.8%) than the freeze-dried HY system (63 ± 2.2 %) (Fig. 1A, B). For *in vivo* administration the HY was assembled between two electrospun membranes (Fig. 1C). The characteristics of the film was: 63.4 ± 4.3 µm of thickness, microfiber diameter of 1.2 ± 0.26 µm and 71.4 ± 4.1% of porosity (Fig. 1C).

The incubation of the systems in water at 37ºC, showed most of the water uptake (Fig. 1D) and mass loss (Fig. 1E) occurred during the first days but in a different ratio depending on the system. The SS water uptake was more than double (500%) of that showed by HY (200%) or the film (150%). On the other hand, the HY suffered a very important mass loss (40%) compared with that detected in the other two systems (6%).

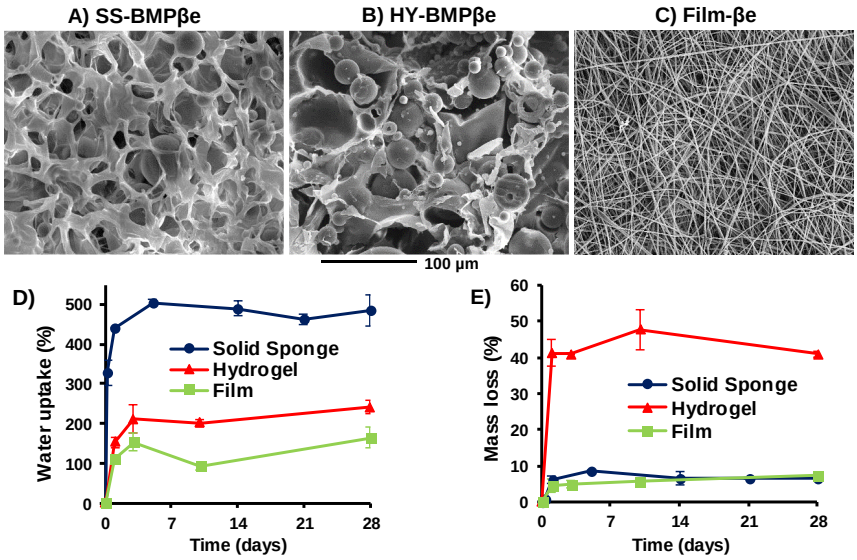

Figure 1. Scanning electron microscope images of alginate solid sponge (A) and cross-linked hydrogel (B) containing BMP-2 and 17β-estradiol microspheres as well as the PLGA electrospinning film (C) containing 17β-estradiol. Water uptake (D) and mass loss (E) of the above mentioned systems during incubation in water at 37ºC under orbital agitation (25 rpm).

4.2. Hydrogel viscoelastic behaviour

Viscoelastic behaviour of partially cross-linked alginate hydrogel freshly prepared (PC-HY) as well as after 4 hours at rest or containing microspheres analysed.

All the samples evaluated showed a progressive viscosity decrease with the shear rate (Fig. 2), characteristic of a pseudo-plastic material. However, the viscosity curves with the increase (forward curve) and decrease (backward curve) of the shear rate in the freshly prepared PC-HY and after 4h at rest, do not overlap, which reveals a thixotropic behaviour that was more evident at 20 ºC than at 37 ºC, according to a smaller hysteresis loop area recorded at this latter temperature. The area of the hysteresis loop characterizes the energy associated with the sol-gel

transition and the time for the material reorganization, hence the greater the area, the longer the time to recover its initial state after stress (Barbucci et al., 2008). The 4% w/w aqueous solution of alginate showed no thixotropic behaviour (Fig. 2).

The viscosity values of the freshly prepared PC-HY and after 4 h at rest or containing microspheres, were markedly superior to those of the alginate solution (4% w/w), especially at low shear rates (Fig. 2). In all the analysed samples, the viscosity was lower at 37°C than at 20°C (Fig. 2).

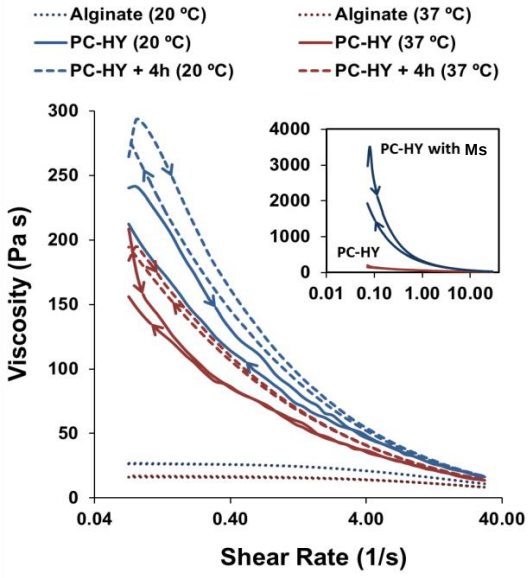

Figure 2. Evolution of the viscosity with shear rate at 20ºC and 37ºC, of pure alginate aqueous solution (4% w/w) and partially cross-linked hydrogel (4% w/w alginate and 0.12% w/w of $CaCl_2$) freshly prepared (PC-HY) and after 4 hours at rest (PC-HY + 4h). In the upper right part of the figure is shown the change in viscosity of the PC-HY with the inclusion of microspheres. The curve direction (forward and backward) is indicated by arrows.

For the different samples, the evolution of elastic (G') and viscous moduli (G'') with the frequency (Fig. 3) confirms the above results. The highest

G' and G'' values were found in the PC-HY containing microspheres, followed by PC-HY after 4h at rest and freshly prepared, the lowest values were obtained with the alginate aqueous solution (4% w/w). The alginate solution (4% w/w) showed a viscous behaviour, as indicated by G'' values being higher than those of G' throughout the studied frequency range, while in PC-HY systems an evolution towards more elastic behaviour was observed. Thus, the freshly prepared PC-HY presented similar values of both G' and G" moduli but after 4 hours at rest those values separated resulting in an elastic modulus higher than the viscous modulus. The inclusion of the microspheres further increased this difference between the elastic and the viscous moduli due to a greater predominance of a solid-like behaviour of the system.

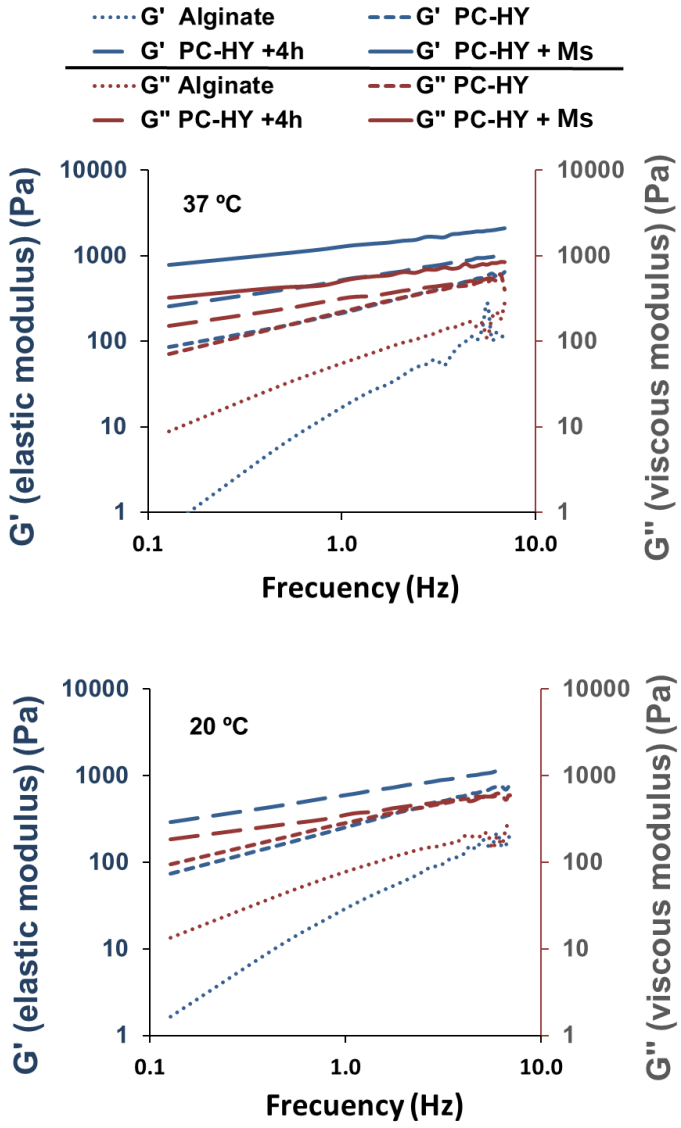

Figure 3. Viscoelastic behaviour at 20ºC and 37ºC, of pure alginate aqueous solution (4% w/w) and partially cross-linked hydrogel (4% w/w alginate and 0.12% w/w of $CaCl_2$) freshly prepared (PC-HY) and after 4 hours at rest (PC-HY +4h). Behaviour of PC-HY with the inclusion of microspheres (PC-HY + Ms) at 37ºC is also shown.

4.3. ^{125}I-BMP-2 and 17β-estradiol release profiles

The *in vivo* release profiles of BMP-2 from SS-^{125}I-BMP and HY-^{125}I-BMP were similar. During the first 24 h approximately 20% of the dose, equivalent to 1,2 µg of the BMP-2, was released (Fig. 4). At 6 weeks, the percentage of BMP-2 released was about 43-48%. However, the *in vitro* ^{125}I-BMP-2 release profiles were faster than *in vivo*. Around 15-20% was released in the first day reaching a 57-60% released at 6 weeks. A similar *in vitro* release profile (Fig. 4) was obtained from the microspheres alone dispersed in the medium, which indicates that the release profile of BMP-2 from both systems, SS and HY, is governed by the microspheres.

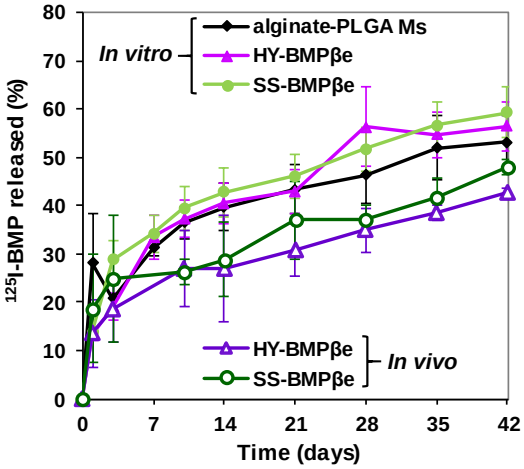

Figure 4. BMP-2 *in vitro* and *in vivo* release assays. Release profile of ^{125}I-BMP-2 from alginate-PLGA microspheres alone or included in the hydrogel (HY-BMPβe) and solid sponge (SS-BMPβe) systems in water at 37°C (n=3) or after implantation in the rat calvarial defect (n=5).

The 17β-estradiol release profiles showed a faster release rate from the film (Fig. 5D) than from the microspheres or the microspheres incorporated in HY or SS (Fig. 5A, B, C). After 4 weeks, 25% of the dose was released from microspheres and 78% from the film (Fig 5). Moreover, compared with the microspheres, the 17β-estradiol release rate

was slightly reduced during the first days by their incorporation in the SS or the HY.

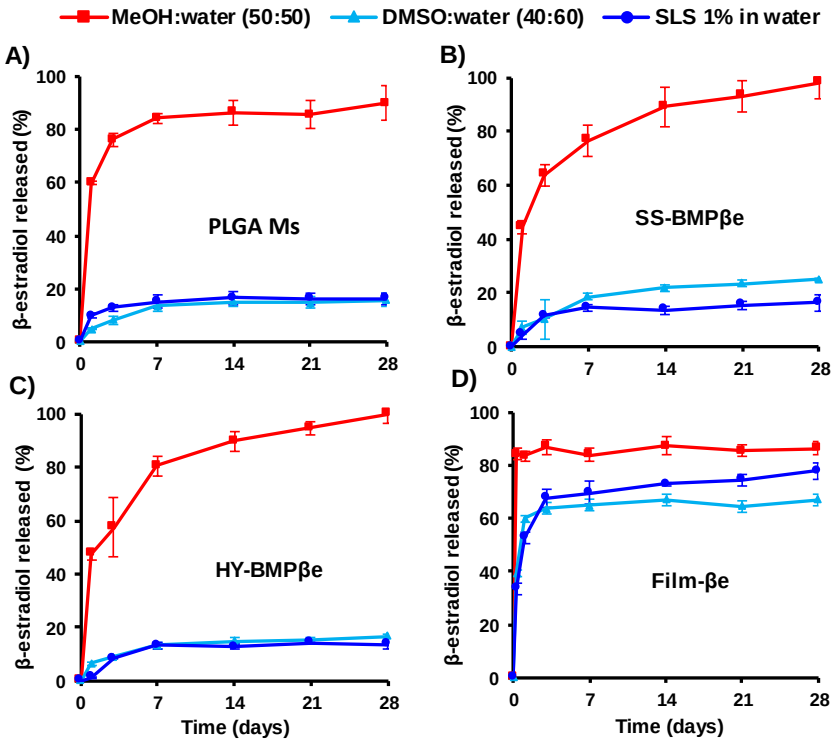

Figure 5. Release profiles of 17β-estradiol from PLGA microspheres alone (PLGA Ms) or included in the solid sponge (SS-BMPβe) or hydrogel (HY-BMPβe) systems as well as from the electrospinning film, at 37°C, in three different release media: methanol:water (50:50), dimethyl sulfoxide:water (40:60) and sodium lauryl sulphate 1% in water. (n=3).

4.4. Histological and histomorphometrical evaluation

Visual inspection of the SS and HY systems at 12 weeks post-implantation showed a different degree of the defect filling, being higher for groups implanted with the SS scaffold.

The macroscopic analysis of the calvaria showed that in groups implanted with the SS, the defect appeared completely filled with a homogeneous tissue of homogeneous aspect similar to the adjacent normal bone (Fig 6A). This was observed both in the groups treated with BMPβe and in those treated with BMPβe + MSC. The histological analysis confirmed the new bone formation (Fig. 6C, D). In all these experimental groups, the repair was observed not only in the margins but also inside the defect. However, a more detailed analysis showed that the repaired bone presented a somewhat fragmented appearance, with areas of bone surrounded by connective tissue and the presence of adipose tissue between both (Fig. 6G).

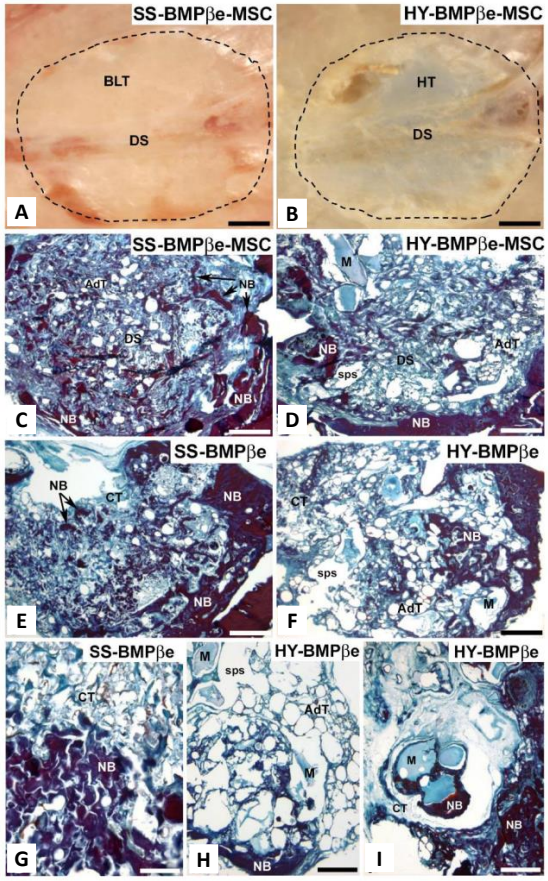

Figure 6. Histological evaluation of the implanted systems, solid system sponge (SS) or crosslinked alginate hydrogel in situ (HY), containing BMP-2 and β-estradiol (BMPβe) with and without MSCs in the calvarial defect of OP rats. (A, B). Macrophotographs of the defect area (dashed line) showing the characteristics of the repaired tissue; (C-F) horizontal photomicrographs showing the repaired bone and the presence of connective and adipose tissue in the defect; (G, H) details showing the morphological characteristics of the repaired tissue; (I) detail of the HY-BMPβe group showing remnants of the hydrogel surrounded by newly formed bone. AdT: adipose tissue; BLT: bone-like tissue; CT: connective tissue; DS: site of defect; HT: hyaline tissue; M: Material; NB. New bone; sps: spaces. Scale bars = a - f: 2 mm; g: 250 µm; h: 500 µm; i: 350 µm.

In the animals implanted with the HY, the macroscopic analysis of the calvaria allowed to clearly observe the morphology of the defect, filled with a tissue of semi-transparent hyaline appearance (Fig 6B). The histological analysis confirmed these results, the new bone formation in these animals was lower than that observed for the SS scaffold (Fig. 6D, F). The tissue repair in this case was mainly limited to the margins of the defect (Fig. 6D, F). The newly formed bone also showed a fragmented appearance, with a higher abundance of adipose tissue and numerous spaces of variable size that were sometimes occupied by what appeared to be rests of scaffold material (Fig. 6H, I).

The qualitative histological results were confirmed by the histomorphometrical analysis of the samples. A higher percentage of repair, between 74% in the group treated with BMPβe + MSC and 79% in that with BMPβe alone, was found in the animals implanted with the SS compared with those implanted with the HY, which ranged between 40% for the group treated with BMPβe + MSC and 50% in the group with BMPβe alone (Fig 7A). In fact, significant differences were found between the implanted systems, SS and HY, although no differences were observed between the applied treatments, with or without rMSC. On the other hand, in all animal groups, the proportion of mature bone, with a high degree of mineralization, was greater than the immature bone, independently of the treatment and the implanted system (Fig 7B). The mature bone/immature bone ratios ranged between 1.42 and 1.67, the animals implanted with the HY presenting the lower values. Nevertheless, the statistical analysis of the data did not show significant differences neither between treatments nor between the implanted system type (Fig 7B).

The analysis of adipose and connective tissues in the area of the defect, revealed the existence of slightly higher amounts of adipose (22% and 17% with HY and SS respectively) than of connective tissue (18% and 10% with HY and SS respectively), being the percentages of both tissues higher with the HY systems than with the SS systems. Consequently, the ratio of adipose or connective tissue to bone present in the defect area

(Fig 7C) were significantly higher in the HY systems compared to the SS systems for both tissues. Differences due to the treatment with BMPβe or withBMPβe +MSC were not found in any case.

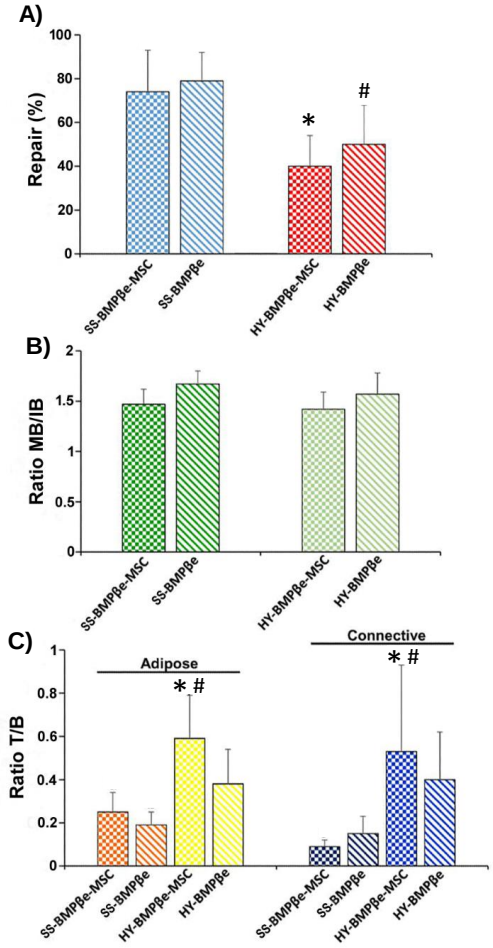

Figure 7. Histomorphometrical evaluation of the implanted systems: (A) Degree of bone repair (%); (B) the ratio of mature bone/immature bone (MB/IB) estimated using VOF staining and (C) the ratios of adipose or connective tissue/bone (T/B) in the different experimental groups. Bars represent means ± SD (n=3), $p<0.05$. (*) Denotes statistical differences with SS-BMPβe-MSC. (#) Denotes statistical differences with SS-BMPβe.

5. Discussion

This chapter is dedicated to evaluate the permanence time effect of BMP-2 and 17β-estradiol systems with and without rMSC, on an OP rats critical size bone defect regeneration. Since bone regeneration is slower in OP animals than in non-OP, the system permanency in the defect and the maintenance of local therapeutic concentrations of BMP-2 and 17β-estradiol may play an important role in tissue regeneration. The biomaterials osteointegration and/or degradation rate should ideally match the bone formation rate. Therefore, the preparation of two BMP-2-β-estradiol PLGA-alginate systems, a solid sponge and a hydrogel, with the same composition, were suitable to test our hypothesis. Both systems exhibited high porosity and great water uptake capacity, these characteristics facilitate the free diffusion of oxygen and nutrients including endogenous growth factors and other cytokines providing an optimum environment for bone tissue ingrowth. Furthermore, the release profiles of both drugs from the two systems were similar as the release rate was controlled by the microspheres. In comparison with the sponge, the hydrogel had better characteristics for minimally invasive administration. Immediately after the addition of a small amount of cross-linker, the alginate solution increases its viscosity forming a dense polymer network with thixotropic behaviour, especially at 20°C. Therefore, the viscosity of the material decreases when subjected to a certain mechanical stress, and gradually recovers at rest. This behaviour allows for the injection of highly viscous materials, even at room temperatures, and facilitate their adaptation to the target site. The incorporation of microspheres to the hydrogel increased the viscosity by 10 times while maintaining its thixotropic behaviour. To ensure formulations remain at the defect for a sufficient time, both hydrogel and sponge were placed between two electrospun polymer sheets forming a sandwich system. Despite of this, the hydrogel mass loss was greater than that of the sponge, hence its defect permanence time would be shorter. This characteristic probably prevents the hydrogel formulation from remaining long enough on the defect to guide tissue growth as reflected by the *in vivo* repair results.

Although the hydrogel formulation has the advantage of being easily injectable, sponges were also flexible and adapted perfectly to the defect edge. The histological analysis clearly showed the better efficiency of the sponge system, approximately 75% of defect was regenerated against the approximately 50% reached for the hydrogel. In addition, the architecture of the repaired tissue was different, the newly formed tissue in the defects treated with the hydrogel presented a more disorganized structure with large hollow spaces, probably due to the rapid and large hydrogel mass loss observed *in vitro*. Also, a greater presence of adipose tissue, typical of osteoporosis, was found, evidencing a lower quality of the repaired tissue in this group. By contrast, the implantation of sponges led to a more compact tissue, with a lower presence of connective tissue, probably as a consequence of the higher percentage of regeneration achieved, as this tissue plays an important role guiding and regulating the repair process at the initial steps of bone formation (Chermnykh et al., 2019; Reinke & Sorg, 2012).

As already reported, hydrogels of variable composition loaded with BMP-2 and 17β-estradiol within microsphere showed similar bone regeneration rate on calvarial defects in OP and non-OP rats. However, the mineralization process was tremendously reduced in OP rats (Segredo-Morales, García-García, et al., 2018; Segredo-Morales, Reyes, et al., 2018). For this reason, two new strategies were incorporated: the addition of rMSC and the microspheres composition modification to reduce the BMP-2 release rate. First, the use of polymers characterized by a relatively slow degradation rate and, second, the incorporation of negatively charged alginate, in the internal aqueous phase, to interact with the positive charge of the proteins and facilitate their retention inside the microspheres we reflected in an extension of the BMP-2 release time. After 6 weeks approximately 46% of the BMP-2 dose was released *in vivo*. For 17β-estradiol, as we already discussed in chapter 1, the unavailability of the radio labelled molecule (that allows to monitor the *in vivo* release kinetics) together with its low aqueous solubility makes difficult to predict the release profiles from the implanted system. However, an increase when compared to the *in vitro* release rate is

expected due to the continuous blood flow, which will increase as new tissue refills the defect. In any case, the *in vivo* release of 17β-estradiol from the microspheres would not be very fast because of the poor water solubility but would be supplemented by the rapid release of the drug incorporated in the electrospun polymer sheets due to the large specific surface area of the fibers as described in chapter 1.

Unfortunately, none of the tools applied accelerated the mineralization of the formed bone. No differences were observed in the mineralization degree with either of the scaffolds with or without rMSC. The addition of rMSC to the systems pre-loaded with BMP-2 did not improve neither the regeneration rate nor the mineralization of the new bone tissue. The osteogenic effect of rMSC and BMP-2 is widely documented in the literature in different animal models. Furthermore, the synergistic effect of the combination of these two elements has been demonstrated in a calvarial defect (Aquino-Martínez et al., 2017; Del Rosario et al., 2015; He et al., 2014; Ho et al., 2016; Keller et al., 2015; Kim et al., 2015; Kong et al., 2019; Li et al., 2019; Stephan et al., 2010; Zhang et al., 2019) which is the animal model used in this study. The different composition and architecture of scaffolds, and the BMP-2 doses used by some authors together with the lack of literature (PubMed database) referred to the osteoporotic rMSC and BMP-2 combination efficacy for bone regeneration in osteoporosis, hinders direct comparison of our data with previous works. To the best of our knowledge, this is the first time that the combination of BMP-2 and osteoporotic rMSC has been assayed in an osteoporotic rat critical defect. The molecular alterations of osteoporotic rMSC are reflected on a proliferative capacity decrease (Tsiridis et al., 2007), production of type I collagen-deficient matrix and a tendency to adipogenic differentiation (Rodríguez et al., 2000) leading to significant deficiencies in self-repair and an impaired differentiation.

6. Conclusion

In this work, two physically different PLGA-alginate scaffolds, SS and HY, have been successfully elaborated presenting the same BMP-2 and 17β-estradiol release rate. Both systems promoted bone regeneration in a critical size calvarial defect in OP rats, although SS showed a significantly higher percentage of bone formation. Moreover, SS promoted the formation of bone with better quality, in terms of lower proportion of adipose and connective tissue. Since the active substances release rate was similar, this difference in bone regeneration can be related to the shorter permanence time of HY in the defect and highlights the importance of the scaffold's physical configuration to optimize the effect of the sustained delivery of active molecules. Finally, the incorporation of osteoporotic MSCs in the scaffolds did not improve the bone regeneration process in any case.

7. References

Agrawal, V., & Sinha, M. (2017). A review on carrier systems for bone morphogenetic protein-2. *Journal of Biomedical Materials Research Part B: Applied Biomaterials*, *105*(4). https://doi.org/10.1002/jbm.b.33599

Aquino-Martínez, R., Artigas, N., Gámez, B., Rosa, J. L., & Ventura, F. (2017). Extracellular calcium promotes bone formation from bone marrow mesenchymal stem cells by amplifying the effects of BMP-2 on SMAD signalling. *PLOS ONE*, *12*(5). https://doi.org/10.1371/journal.pone.0178158

Barbucci, R., Pasqui, D., Favaloro, R., & Panariello, G. (2008). A thixotropic hydrogel from chemically cross-linked guar gum: synthesis, characterization and rheological behaviour. *Carbohydrate Research*, *343*(18). https://doi.org/10.1016/j.carres.2008.08.029

Begam, H., Nandi, S. K., Kundu, B., & Chanda, A. (2017). Strategies for delivering bone morphogenetic protein for bone healing. *Materials Science and Engineering: C*, *70*.

https://doi.org/10.1016/j.msec.2016.09.074

Chen, G., & Kawazoe, N. (2018). *Porous Scaffolds for Regeneration of Cartilage, Bone and Osteochondral Tissue*. https://doi.org/10.1007/978-3-319-76711-6_8

Chermnykh, E. S., Kiseleva, E. V., Rogovaya, O. S., Rippa, A. L., Vasiliev, A. V., & Vorotelyak, E. A. (2019). Tissue-engineered biological dressing accelerates skin wound healing in mice via formation of provisional connective tissue. *Histology and Histopathology*, *33*(11), 1189–1199. https://doi.org/10.14670/HH-18-006

Cheung, W. H., Miclau, T., Chow, S. K.-H., Yang, F. F., & Alt, V. (2016). Fracture healing in osteoporotic bone. *Injury*, *47*. https://doi.org/10.1016/S0020-1383(16)47004-X

Del Rosario, C., Rodríguez-Évora, M., Reyes, R., Delgado, A., & Évora, C. (2015). BMP-2, PDGF-BB, and bone marrow mesenchymal cells in a macroporous β-TCP scaffold for critical-size bone defect repair in rats. *Biomedical Materials (Bristol)*, *10*(4). https://doi.org/10.1088/1748-6041/10/4/045008

Dobson, K. R., Reading, L., Haberey, M., Marine, X., & Scutt, A. (1999). Centrifugal Isolation of Bone Marrow from Bone: An Improved Method for the Recovery and Quantitation of Bone Marrow Osteoprogenitor Cells from Rat Tibiae and Femurae. *Calcified Tissue International*, *65*(5). https://doi.org/10.1007/s002239900723

Dorati, R., DeTrizio, A., Modena, T., Conti, B., Benazzo, F., Gastaldi, G., & Genta, I. (2017). Biodegradable scaffolds for bone regeneration combined with drug-delivery systems in osteomyelitis therapy. In *Pharmaceuticals* (Vol. 10, Issue 4). MDPI AG. https://doi.org/10.3390/ph10040096

El Bialy, I., Jiskoot, W., & Reza Nejadnik, M. (2017). Formulation, Delivery and Stability of Bone Morphogenetic Proteins for Effective Bone Regeneration. *Pharmaceutical Research*, *34*(6). https://doi.org/10.1007/s11095-017-2147-x

Fayaz, H. C., Giannoudis, P. V., Vrahas, M. S., Smith, R. M., Moran, C.,

Pape, H. C., Krettek, C., & Jupiter, J. B. (2011). The role of stem cells in fracture healing and nonunion. *International Orthopaedics*, *35*(11). https://doi.org/10.1007/s00264-011-1338-z

Gainza, G., Aguirre, J. J., Pedraz, J. L., Hernández, R. M., & Igartua, M. (2013). rhEGF-loaded PLGA-Alginate microspheres enhance the healing of full-thickness excisional wounds in diabetised Wistar rats. *European Journal of Pharmaceutical Sciences*, *50*(3–4). https://doi.org/10.1016/j.ejps.2013.07.003

He, X., Liu, Y., Yuan, X., & Lu, L. (2014). Enhanced healing of rat calvarial defects with MSCs loaded on BMP-2 releasing chitosan/alginate/hydroxyapatite scaffolds. *PLoS ONE*, *9*(8). https://doi.org/10.1371/journal.pone.0104061

Ho, S. S., Vollmer, N. L., Refaat, M. I., Jeon, O., Alsberg, E., Lee, M. A., & Leach, J. K. (2016). Bone Morphogenetic Protein-2 Promotes Human Mesenchymal Stem Cell Survival and Resultant Bone Formation When Entrapped in Photocrosslinked Alginate Hydrogels. *Advanced Healthcare Materials*, *5*(19), 2501–2509. https://doi.org/10.1002/adhm.201600461

Hoffman, A. S. (2012). Hydrogels for biomedical applications. In *Advanced Drug Delivery Reviews* (Vol. 64, Issue SUPPL., pp. 18–23). Elsevier. https://doi.org/10.1016/j.addr.2012.09.010

Hutmacher, D. W. (2000). Scaffolds in tissue engineering bone and cartilage. *Biomaterials*, *21*(24). https://doi.org/10.1016/S0142-9612(00)00121-6

Keller, L., Eap, S., Schiavi, J., Huck, O., Jacomine, L., Gauthier, C., Sebastian, V., Schwinté, P., Jessel, N., & Fioretti, F. (2015). A living thick nanofibrous implant bifunctionalized with active growth factor and stem cells for bone regeneration. *International Journal of Nanomedicine*. https://doi.org/10.2147/IJN.S72670

Kim, B. S., Choi, M. K., Yoon, J. H., & Lee, J. (2015). Evaluation of bone regeneration with biphasic calcium phosphate substitute implanted with bone morphogenetic protein 2 and mesenchymal stem cells in a rabbit calvarial defect model. *Oral Surgery, Oral*

Medicine, Oral Pathology and Oral Radiology, *120*(1), 2–9. https://doi.org/10.1016/j.oooo.2015.02.017

Kondiah, P., Choonara, Y., Kondiah, P., Marimuthu, T., Kumar, P., du Toit, L., & Pillay, V. (2016). A Review of Injectable Polymeric Hydrogel Systems for Application in Bone Tissue Engineering. *Molecules*, *21*(11). https://doi.org/10.3390/molecules21111580

Kong, Y., Zhao, Y., Li, D., Shen, H., & Yan, M. (2019). Dual delivery of encapsulated BM-MSCs and BMP-2 improves osteogenic differentiation and new bone formation. *Journal of Biomedical Materials Research Part A*, *107*(10). https://doi.org/10.1002/jbm.a.36737

Kubo, T., Shiga, T., Hashimoto, J., Yoshioka, M., Honjo, H., Urabe, M., Kitajima, I., Semba, I., & Hirasawa, Y. (1999). Osteoporosis influences the late period of fracture healing in a rat model prepared by ovariectomy and low calcium diet. *Journal of Steroid Biochemistry and Molecular Biology*, *68*(5–6), 197–202. https://doi.org/10.1016/S0960-0760(99)00032-1

Li, X., Zhang, R., Tan, X., Li, B., Liu, Y., & Wang, X. (2019). Synthesis and Evaluation of BMMSC-seeded BMP-6/nHAG/GMS Scaffolds for Bone Regeneration. *International Journal of Medical Sciences*, *16*(7). https://doi.org/10.7150/ijms.31966

Moreno, M., H. Amaral, M., M. Sousa Lobo, J., & C. Silva, A. (2016). Scaffolds for Bone Regeneration: State of the Art. *Current Pharmaceutical Design*, *22*(18), 2726–2736. https://doi.org/10.2174/1381612822666160203114902

Namkung-Matthai, H., Appleyard, R., Jansen, J., Hao Lin, J., Maastricht, S., Swain, M., Mason, R. ., Murrell, G. A. ., Diwan, A. ., & Diamond, T. (2001). Osteoporosis influences the early period of fracture healing in a rat osteoporotic model. *Bone*, *28*(1). https://doi.org/10.1016/S8756-3282(00)00414-2

Nauth, A., Ristevski, B., Li, R., & Schemitsch, E. H. (2011). Growth factors and bone regeneration: How much bone can we expect? *Injury*, *42*(6). https://doi.org/10.1016/j.injury.2011.03.034

Oliver, R. A., Yu, Y., Yee, G., Low, A. K., Diwan, A. D., & Walsh, W. R. (2013). Poor histological healing of a femoral fracture following 12 months of oestrogen deficiency in rats. *Osteoporosis International*, *24*(10). https://doi.org/10.1007/s00198-013-2345-2

Peppas, N. A., Hilt, J. Z., Khademhosseini, A., & Langer, R. (2006). Hydrogels in Biology and Medicine: From Molecular Principles to Bionanotechnology. *Advanced Materials*, *18*(11). https://doi.org/10.1002/adma.200501612

Reinke, J. M., & Sorg, H. (2012). Wound Repair and Regeneration. *European Surgical Research*, *49*(1), 35–43. https://doi.org/10.1159/000339613

Reyes, R., Pec, M., Sánchez, E., del Rosario, C., Delgado, A., & Évora, C. (2013). Comparative, osteochondral defect repair: Stem cells versus chondrocytes versus Bone Morphogenetic Protein-2, solely or in combination. *European Cells and Materials*, *25*. https://doi.org/10.22203/eCM.v025a25

Rodríguez, J. P., Montecinos, L., Ríos, S., Reyes, P., & Martínez, J. (2000). Mesenchymal stem cells from osteoporotic patients produce a type I collagen-deficient extracellular matrix favoring adipogenic differentiation. *Journal of Cellular Biochemistry*, *79*(4). https://doi.org/10.1002/1097-4644(20001215)79:4<557::AID-JCB40>3.0.CO;2-H

Segredo-Morales, E., García-García, P., Reyes, R., Pérez-Herrero, E., Delgado, A., & Évora, C. (2018). Bone regeneration in osteoporosis by delivery BMP-2 and PRGF from tetronic–alginate composite thermogel. *International Journal of Pharmaceutics*, *543*(1–2), 160–168. https://doi.org/10.1016/j.ijpharm.2018.03.034

Segredo-Morales, E., Reyes, R., Arnau, M. R., Delgado, A., & Évora, C. (2018). In situ gel-forming system for dual BMP-2 and 17β-estradiol controlled release for bone regeneration in osteoporotic rats. *Drug Delivery and Translational Research*, *8*(5), 1103–1113. https://doi.org/10.1007/s13346-018-0574-9

Stephan, S. J., Tholpady, S. S., Gross, B., Petrie-Aronin, C. E., Botchway,

E. A., Nair, L. S., Ogle, R. C., & Park, S. S. (2010). Injectable tissue-engineered bone repair of a rat calvarial defect. *The Laryngoscope*. https://doi.org/10.1002/lary.20624

Tsiridis, E., Upadhyay, N., & Giannoudis, P. (2007). Molecular aspects of fracture healing:Which are the important molecules? *Injury*, *38*(1). https://doi.org/10.1016/j.injury.2007.02.006

Vayas, R., Reyes, R., Arnau, M. R., Évora, C., & Delgado, A. (2019). Injectable Scaffold for Bone Marrow Stem Cells and Bone Morphogenetic Protein-2 to Repair Cartilage. *CARTILAGE*. https://doi.org/10.1177/1947603519841682

Velasco, M. A., Narváez-Tovar, C. A., & Garzón-Alvarado, D. A. (2015). Design, Materials, and Mechanobiology of Biodegradable Scaffolds for Bone Tissue Engineering. *BioMed Research International*, *2015*. https://doi.org/10.1155/2015/729076

Vo, T. N., Kasper, F. K., & Mikos, A. G. (2012). Strategies for controlled delivery of growth factors and cells for bone regeneration. *Advanced Drug Delivery Reviews*, *64*(12). https://doi.org/10.1016/j.addr.2012.01.016

Zhai, P., Chen, X. B., & Schreyer, D. J. (2015). PLGA/alginate composite microspheres for hydrophilic protein delivery. *Materials Science and Engineering: C*, *56*. https://doi.org/10.1016/j.msec.2015.06.015

Zhang, R., Li, X., Liu, Y., Gao, X., Zhu, T., & Lu, L. (2019). Acceleration of Bone Regeneration in Critical-Size Defect Using BMP-9-Loaded nHA/ColI/MWCNTs Scaffolds Seeded with Bone Marrow Mesenchymal Stem Cells. *BioMed Research International*, *2019*. https://doi.org/10.1155/2019/7343957

Chapter 3

The bone regeneration capacity of BMP-2+MMP-10 loaded scaffolds depends on the tissue status

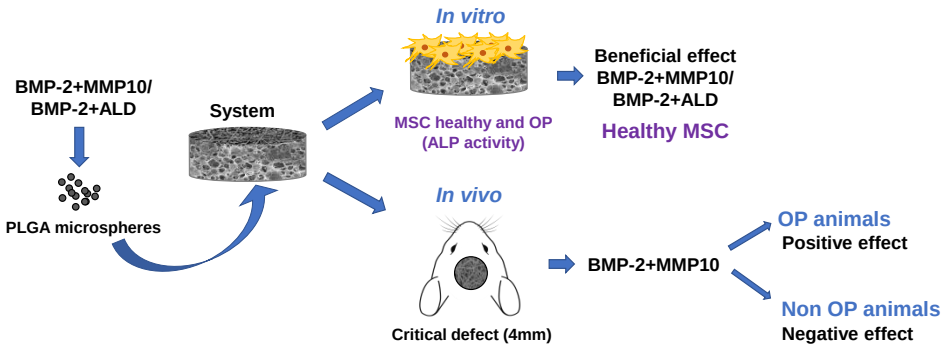

Pharmaceutics. 2021 Jun 29; 13:979

1. Introduction

In previous chapters, scaffolds loaded with combinations of BMP-2 and 17β-estradiol formulated in microspheres were tested in an osteoporotic rat calvarial bone critical defect. Experimental results showed the new bone formed in OP rats was less mineralized than in non-OP rats as we have already observed other strategies (García-García et al., 2020; Segredo-Morales, García-García, et al., 2018; Segredo-Morales, Reyes, et al., 2018). On the other hand, bisphosphonates are routinely used for OP treatment. These antiosteoclastic agents systemically administrated or integrated into scaffolds of different nature have been reported to support bone defects regeneration in both OP and non-OP animals (Hur et al., 2016; Kim et al., 2016; Mardas et al., 2017; van Houdt et al., 2018; Wang et al., 2018). Yet, some authors stated no bisphosphonates effect in the regeneration of calvarial bone defects (Toker et al., 2012).

Moreover, BMPs have been combined with different bisphosphonates to reduce the excessive osteoclastogenesis that they induce consequence of their strong osteogenesis (Huntley et al., 2019). This combination formulated in local release systems generally caused a remarkable improvement in the bone defect regeneration induced by BMP-2 (Little et al., 2005; Raina et al., 2018). However, very few publications are devoted to study the effect of this combination in osteoporotic animals. In fact, only two reports were found describing the effect of an IV or subcutaneous zoledronate single dose on the regeneration of a calvarial defect or a mid-diaphyseal open femoral fracture treated with a local release of BMP-2 or BMP-7, respectively (Lee et al., 2015; Mathavan et al., 2018).

The outcomes of both studies were different, the combination of a BMP-2 embedded collagen carrier with IV zoledronate had initially a negative effect in bone quantity and quality induced by rhBMP-2. Although this undesirable effect disappeared at long term assessments, the combination did not exceed the regeneration capacity of BMP-2 alone (Lee et al., 2015). Conversely, the local implantation of BMP-7 incorporated in a collagen putty combined with zolendronate injected subcutaneously,

suggested the hypothesis that osteoporosis is a disease that delays or hinders bone regeneration is incorrect (Mathavan et al., 2018). However, the aforementioned studies are complicated to compare as defect models, experimental designs and the BMPs used were different.

Lastly, Matrix metalloproteinases (MMPs) are enzymes that play pivotal roles in tissue remodelling, by degrading a wide variety of matrix or nonmatrix substrates. MMPs expression, detected in osteoblasts and osteoclasts, has been shown to be required for bone homeostasis and proper fracture healing. In fact, altered cartilage remodelling and vascularization leading to impaired fracture repair has been reported in murine models with genetic deficiency in MMP9 (Colnot et al., 2003) or MMP13 (Kosaki et al., 2007; Stickens et al., 2004), while delayed bone remodelling has been observed in MMP2-KO mice (Lieu et al., 2011). Among them, MMP-10 has been shown to be expressed in osteoblasts and chondrocytes during bone formation in humans (Bord et al., 1998). Interestingly, this MMP can enhance the *in vitro* osteoblastic differentiation of myoblastic cells induced by BMP-2 (Mao et al., 2013). Moreover, we have recently demonstrated that MMP-10 is overexpressed in calcified human aortic valves (AVs) and active MMP-10 promotes calcification of valvular interstitial cells isolated from human AVs, through Akt phosphorylation (Matilla et al., 2020). Besides, we have also shown that MMP-10 accelerates bone repair by enhancing BMP-2 induced bone healing and improving the mineralization rate in a murine model of calvaria critical size defect (Reyes et al., 2018).

2. Objectives

Taking into account the previous results regarding better quality of the bone regenerated with the alginate sponge than with the hydrogel in OP rats, together with the higher mineralization observed with the combination of BMP-MMP in non-OP animals, the aim of this last part of this work is to further analyze the *in vitro* and *in vivo* MMP-10 pro-mineralization effect when combined with BMP-2 on a solid 3D scaffold. To do so, different MMP-10 doses were tested. Moreover, the MMP-10+BMP-2 activity was compared to scaffolds incorporating alendronate,

a bisphosphonate, and BMP-2. Both proteins and bisphosphonate were formulated on microspheres and embedded on a crosslinked chitosan foam. The obtained foams were then surrounded by electrospun meshes loaded or not with alendronate to form the final scaffold with a sandwich-like structure. The *in vitro* promotion of ALP activity and *in vivo* mineralization using a critical size calvarial defect was assessed in both healthy and osteoporotic conditions.

3. Materials and methods

3.1 Microspheres preparation and characterization

3.1.1. Microspheres Preparation

Different drug-loaded poly (lactide-co-glycolide acid) (PLGA) microspheres were designed for the experiment and prepared following different protocols (Table 1). PLGA microspheres loaded with BMP-2 and MMP-10 were prepared by a double emulsion method (w/o/w). To obtain loaded microspheres 35 µg of BMP-2 (GenScript) and 2.1 µg or 8.5 µg rhMMP-10 (obtained equally to (Orbe et al., 2011)) as described in Table 1 were dissolved in 200 µL of 0.8% poly (vinyl alcohol) (PVA, Mw: 30,000-70,000 KDa, 87-90% hydrolysed, Sigma-Aldrich). This aqueous phase was added to 1 mL of oil phase formed by the PLGA-RG755 (PLGA, 75:25, Resomer® RG755, 0.54 dL/g, Evonik Industries) and PLGA-RG858 (PLGA 85:15, Resomer® RG858, 1.5 dL/g, Evonik Industries) mixture at 9 to 1 ratio at 150mg/mL in methylene chloride (DCM, Sigam-Aldrich) and homogenized for 1 minute by vortex. Then, 3mL of a second aqueous solution prepared with 2.5% PVA was added to the first emulsion and homogenized for one minute. Finally, the solvent was evaporated as previously described.

Alendronate (ALD; Sigma-Aldrich) microspheres were prepared by a double emulsion method as described above with slight modifications. An internal aqueous phase (450 µL) was prepared containing PVA at 0.8%, chitosan (CHT, 150mPa.s, Protasan® UP-CL-213, NovaMatrix, Ultrapure Polymer Systems) at 1% and 75 µg ALD. The oil phase prepared as

described above was added to this aqueous phase and homogenized for one minute. The second aqueous phase was added as previously described and the solvent was evaporated by pouring the microspheres in 100 mL of 0.1% PVA and 2.5% of pentabasic sodium tripolyphosphate (STPP; Sigma-Aldrich) for one hour under continuous stirring.

The obtained microspheres were washed with double distilled water, filtered through a 0.45 µm pore size filter (Pall Corporation, Sigma-Aldrich), freeze-dried and stored at 4ºC until use. Then, the microspheres were characterized as described in chapter 1 (section 3.1).

Table 1. Developed PLGA microspheres and drug amounts used per batch.

Microspheres type	**BMP-2 (µg)**	**ALD (µg)**	**MMP-10 (µg)**
Blank PLGA	-	-	-
PLGA-BMP-2	35 µg	-	-
PLGA/Chitosan-BMP-2+ALD	35 µg	75 µg	-
PLGA-BMP-2+Low MMP-10	35 µg	-	2.1 µg
PLGA-BMP-2+High MMP-10	35 µg	-	8.5 µg

3.1.2. Microspheres loading efficiency

Protein loading efficiencies were evaluated using radiolabeled BMP-2 (^{125}I-BMP-2) as described in chapter 1 (section 3.1).

ALD loading efficiency was evaluated on microspheres loaded with ^{99m}Technetium radiolabeled ALD. Drug labelling was performed as described by Gundogdu and coworkers (Gundogdu et al., 2018). In Brief, 5 mg of ALD was mixed with 1 mg of ascorbic acid and 0.5 mg of tin chloride dihydrate ($SnCl_2 \cdot 2H_2O$) and kept under inert atmosphere. Afterwards, 0.5 mL of ultrapure water was added (MilliQ). Once dissolved, 100 µL of the generator eluate (≈0.5-1 mCi) was added and the solution was stirred (120 rpm) at room temperature for 15 minutes.

Labelling yields and stability were evaluated by instant thin layer chromatography (iTLC) using 11.5 x 0.8 cm silica gel coated strips (Varian Iberica SL) to which 5 µL of the labelled protein or ALD were added (30,000-40,000 cpm). For proteins 85% methanol in water was used as mobile phase. A gamma counter (Cobra II, Packard®) was used to measure free ^{125}I (R_f=1) and labelled proteins (R_f=0) as previously published (De la Riva et al., 2009). For ALD chromatography acetone or 0.9% NaCl were used as mobile phase, the chromatography performed in acetone, separates free ^{99m}Tc ($^{99m}TcO_4^-$) (R_f=1) from ALD-^{99m}Tc and hydrolyzed ^{99m}Tc (TcO_2) (R_f=0). On the other hand, when 0.9% NaCl is used as mobile phase both free ^{99m}Tc and ALD-^{99m}Tc migrate to the front (R_f=1) while hydrolyzed ^{99m}Tc does not migrate (R_f=0). These values can be used to calculate the percentage of labelled ALD applying equation 1:

$$\%(^{99m}Tc\text{-ALD}) = 100 - [\%\,^{99m}TcO_4^- + \%\,^{99m}TcO_2] \qquad \text{(eq.1)}$$

Then, to evaluate microspheres encapsulation efficiency radioactivity was measured on 3 microspheres aliquots as described for protein encapsulation efficiency in chapter 1 (section 3.1).

3.2. Preparation and characterization of electrospun meshes

3.2.1. PLGA functionalization with Alendronate

To obtain ALD-loaded electrospun fibers two acid-terminated PLGA polymers with 50:50 lactide:glycolide ratio, RG 502 (Resomer® RG502, 0.19 dL/g, Evonik) and RG 504-H (Resomer® RG504, 0.4 dL/g, Evonik), were chemically conjugated with ALD following the protocol described by Choi and coworkers (Choi & Kim, 2007). A 10% PLGA solution was prepared in 20 mL acetone to which 60 mg of N-hydroxysuccinamide (NHS, Sigma-Aldrich) and 100 mg of N, N'-dicyclohexylcarbodiimide (DCC, Sigma-Aldrich) were added and allowed to react in inert atmosphere under stirring for 24 hours at room temperature. Afterwards, the reaction mixture was filtrated through 0.45 µm (Chromafil® Xtra PET-45/25, Macherey-Nagel) to remove dicyclohexylurea, the obtained PLGA-NHS was precipitated in cold ethyl ether (Scharlau®) and

dissolved in DCM. This solution was concentrated at room temperature until drying using a rotavapor.

ALD conjugation was performed by dissolving 1.9 grams of the obtained PLGA-NHS in 19 mL of acetone: DMSO (50:50) and adding an adequate amount of ALD previously dissolved in 1 mL of water. This mixture was allowed to react at room temperature for another 24 hours. Then, the solution was concentrated by rotavapor at high vacuum and 37°C. The obtained ALD conjugated polymer (PLGA-ALD) was dissolved in the minimum amount of acetone, precipitated in ethyl ether and dissolved again in DCM to avoid free ALD. Finally, this solution was dried for 24 hours under high vacuum and the PLGA-ALD was precipitated with distilled water, filtrated through 0.45 μm and freeze-dried. To ensure adequate functionalization the obtained polymer was characterized by proton Nuclear Magnetic Resonance. ^{1}H-NMR spectra were recorded at 500 MHz (Bruker Avance 500), and chemical shifts are reported in ppm and calibrated on non-deuterated solvent residual peak. Elemental analysis was performed using a CHNS "TruSpec Micro" analyser (LECO).

3.2.2. Electrospun meshes preparation

Electrospun meshes composed by RG504-ALD: RG502-ALD: RG 855 at 1:1:1 ratio were prepared by the electrospinning method as in chapter 1 (section 3.2). For this, 375 mg of the polymer mixture was dissolved in 2.5 mL of HFIP. The electrospinning conditions were: 18G needle, flow rate of 2.75 mL/h, power supply of 7 KV, collector at a 10cm from the needle and 200 rpm. Blank meshed with the same polymer proportions and conditions were also obtained using unfunctionalized PLGAs.

Blank and ALD loaded electrospun meshes were surface treated with plasma (O_2) The plasma oxygen treatment was carried out under vacuum during 4 minutes for each side of the meshes. The generator power was at 75% of the capacity (Diener electronic, Plasma-Surface-Technology).

3.2.3. ALD-loaded and Blank meshes characterization

Meshes were characterized in terms of thickness, porosity, and fiber diameter following the methodology described in chapter 1 (section 3.2).

Here, mesh surface wettability was measured by contact angle assessments using a drop shape analyzer (DSA100; Krüss GmbH) and distilled water as the liquid media. The obtained images were analyzed with an image analyze software (ImageJ v1.52, National Institute of Health).

A proton NMR spectrum was performed on a 500 MHz equipment to determine the amount of ALD present on ALD-loaded electrospun meshes. To do so 4.41 mg of the sheet were dissolved in 0.6 mL of $CDCl_3$, and 18.4 µL of a standard solution of 1,1,2,2-tetrachloroethane ($Cl_2CHCHCl_2$) in $CDCl_3$ (33.07 mM) was added. In this way, the amount of $Cl_2CHCHCl_2$ was four times the theoretical amount of alendronate presented in the polymer sheet. The quantity of ALD was obtained by integrating the signals corresponding to 1,1,2,2-tetrachloroethane (5.96 ppm) and the alendronate signal of the protons (2.98 ppm). These measurements were performed also at different time points on ALD-loaded meshes incubated in water at 37°C to evaluate ALD release. To this end, samples were washed twice with water and freeze-dried previous to NMR characterization.

3.3. Foams preparation and characterization

3.3.1. Foam preparation

Chitosan foams including adequate drug-loaded microspheres as shown in Table 2 were obtained. Microspheres prepared under aseptic conditions as described in section in 3.1.1. 4mg were homogenously dispersed in 30 µL of a 3% chitosan solution, frozen at -20ºC and freeze-dried. Lyophilized systems were then crosslinked with 15 µL of 5% STPP, washed three times with 100 µL MilliQ water, frozen and again freeze-

dried. Afterwards, foams were stored at 4ºC until use. The porosity of the foam was calculated as described in chapter 1 (section 3.2).

Table 2. Developed cross-linked chitosan foams and their correspondent final drug amount adjusted by microsphere drug loading.

Nomenclature	Loaded molecules (dose)	Used microspheres
Control foam	-	Blank PLGA
BMP-2 foam	BMP-2 (600ng)	PLGA-BMP-2
BMP-2+ALD foam	BMP-2 (600ng) + ALD (75 µg)	PLGA/Chitosan-BMP-2+ALD
BMP-2+Low MMP-10 foam	BMP-2 (600ng) + MMP-10 (30 ng)	PLGA-BMP-2+Low MMP-10
BMP-2+High MMP-10 foam	BMP-2 (600ng) + MMP-10 (120 ng)	PLGA-BMP-2+High MMP-10

3.3.2. Foams wettability and degradation

Foam water uptake and weight loss was analyzed by incubation in ultrapure water at 37ºC under continuous stirring (25 rpm). At different time points samples were removed, weighted after discarding the excess of water and then freeze-dried to determine their mass loss.

3.3.3. In vitro drug release

Foams containing microspheres loaded with ^{125}I radiolabeled proteins or ALD were incubated in sterile MilliQ water at 37°C and 25 rpm. The amount of released proteins was quantified by measuring the radioactivity of the supernatant with a gamma counter (Cobra® II, Packard) every other day. On the other hand, the released ALD at the same time points was measured using a derivatization method as previously reported (Dolci et al., 2019). Briefly, supernatants were reacted with o-pthaldialdehyde (OPA, Sigma-Aldrich) and 2-mercaptoethanol (Sigma-Aldrich). Then the derivatization subproduct was measurement immediately using a spectrophotometer (Ultrospect 3300 pro, Biochrom) (λ= 334nm). In both

cases supernatants were removed at each time point and replaced by fresh media.

3.4. Osteoporosis mouse model

To induce the osteoporosis condition FVB mice were used. The osteoporosis was produced by a surgical procedure consisting of a dorsal incision ovariectomy (OVX) under inhaled anesthesia isoflurane (ISOFLO®, Abbott Laboratories), as described in chapter 1 (section 3.5.1.) for rats. In addition, three weeks after OVX, a 3 mg/kg dexamethasone 21-isonicotinate (DEX, Deyanil Retard, Fatro Ibérica) was administered subcutaneously every week for three months. To confirm the development of the OP condition in mice, Bone Mineral Density (BMD) at different time points (0, 15, 30, 60 and 120 days post-OVX) was analyzed using a densitometer (PIXImus, GE Lunar). To perform the test, mice were anesthetized with medetomidine (1 mg/kg/IP) and ketamine (75 mg/kg/IP). To revert the anesthesia, atipamezole (0.1 mg/kg/IP) was administrated immediately after finishing the densitometry. Complementary, animal weight and height was monitored throughout the experiment.

Additionally, histological assessments of healthy and OP mice bone tissue four months after ovariectomy were performed. Mice were euthanized and femurs were extracted, fixed in 3.7-4% p-formaldehyde (PFA, pH = 7) and decalcified in Histofix® Decalcifier (Panreac). Samples were prepared for histological analysis as previously described in chapter 1 (section 3.7).

3.5. Cell isolation and characterization

3.5..1 Osteoporotic and normal mMSCs isolation

Normal and OP murine Mesenchymal Stem Cells (mMSC or OP mMSC) were isolated from tibia and femur of 8 weeks-old FVB healthy and osteoporotic mice respectively as described previously by Soleimani and Nadri with slight modifications (Soleimani & Nadri, 2009). Mice were sacrificed by cervical dislocation and both tibias and femurs were extracted. Muscle and periosteum were dissected and isolated bones were stored in Dulbecco's phosphate buffered saline (DPBS, Lonza) and processed for mMSC extraction. Both epiphyses were ruptured and a syringe equipped with a 20G needle loaded with 10 mL of Dulbecco's Minimal Essential Medium (DMEM, Lonza) supplemented with 10% fetal bovine serum (FBS, Biowest), 2 mM L-glutamime (Sigma-Aldrich) and 1% penicillin-streptomycin (Sigma-Aldrich) was used to flush the bone marrow to elute mMSC. This process was repeated twice for each bone. Eluates were then collected and centrifuged at 2.000 rpm for 5 min, the resulting pellets were combined, resuspended in 15 mL of DPBS and centrifuged again under the same conditions. The resulting pellet was resuspended in 1.5 mL of complete DMEM, cells were seeded on a petri dish and incubated at 37°C and 5% CO_2. Cell CCM was changed every day for 72 hours, then trypsinized (Trypsin-EDTA 0.25% in HBSS free of calcium, magnesium and phenol red, Biowest) and seeded in cell culture flasks where they were allowed to grow until confluency.

3.5.2. Characterization of isolated cells

The obtained normal and OP mMSC were characterized in terms of surface markers expression by flow cytometry analysis. Cells were cultured until passage 3, trypsinized and stained with calcein AM (1 µM; Sigma-Aldrich) for 30 minutes at room temperature. Afterwards, cells were washed three times with DPBS divided into 4 tubes and incubated with the correspondent APC-labelled primary antibody for CD45, CD44 and Sca-1 or APC-labelled isotype control (ThermoFisher Scientific) for 30 minutes at 4°C. The concentration used for both control and specific

antibodies was the same 10 µg/mL. Then, cells were washed three times with DPBS and stored at 4°C until characterization. Flow cytometry was performed using the Macsquant Analyzer 10. Untreated cells were used as control.

3.6 In vitro biological performance of chitosan foams and electrospun meshes

3.6.1 Evaluation of developed foams osteogenic capacity

Alkaline phosphatase activity was used to evaluate the osteogenic and mineralization effect of the drug-loaded chitosan foams described in Table 2 on normal and OP mMSC. Experiments were performed using isolated murine MSCs. Cells were trypsinized and resuspended at high density $1x10^6$ cells/mL in CCM. Then, 20 µL of the cell suspension was added to the foams and incubated for 1.5 hours at 37°C and 5% CO_2 to increase cell attachment. Afterwards, 500 µL of complete medium was added to each well and media was changed every other day. After 7 and 21 days of culture, samples were collected in triplicate to evaluate osteogenic differentiation. Foams were washed twice with DPBS at 4°C and 500 µL of the developer solution was added an incubated at 37°C and 5% CO_2 under gentle agitation for 1.5 hours. The developer solution was a solution of tetrazolium nitro blue chloride (NBT, Roche Diagnostics) and 5-bromo-4-chloro-3-indole phosphate (BCIP, Roche Diagnostics) prepared in 0.1M Tris-HCl, 0.1M NaCl and 0.05M $MgCl_2$ (pH = 9.2-9.5). After incubation, samples were washed twice with DPBS and fixed with buffered PFA. After 30 minutes' fixation at room temperature, foams were washed twice, dehydrated, included in paraffin (Paraplast®) and cut with the microtome (5 µm thickness; Shandon Finesse 325, Thermo Fisher Scientific). Images of the obtained sections were taken in a microscope (Leica DM4000B). The percentage of cells stained positive for alkaline phosphatase activity was obtained comparing the number of positive cells against total cell numbers using an image software (ImageJ v1.52, National Institute of Health).

3.6.2. Evaluation of cell viability and adhesion to electrospun meshes

OP mMSC viability and adhesion to the plasma-treated electrospun meshes was also evaluated. Electrospun meshes were cut in disks of 8 mm diameter and placed on 48-well plates. Then, 100 µL of the cell suspension (2.5 $x10^5$ cells/mL) were added to the meshes and incubated for 1.5 hours at 37ºC and 5% CO_2 to promote cell adhesion followed by the addition of 400 µL of CCM to each well. After 24 hours of seeding, cell viability was evaluated by the XTT assay (XTT Cell Viability Kit, Cell Signaling Technology) following the manufacturer's instructions. Absorbance was measured at 445 nm using a plate reader (Biotek). Cells seeded on tissue culture treated polystyrene were used as control (100% viability).

To study cell adhesion, cells were seeded and incubated 24 hours with the meshes as described above and then fixed with PFA. To evaluate cell morphology cells were stained with Rhodamine phalloidin (Invitrogen) and 4′,6-diamidino-2-phenylindole (DAPI). Samples were washes twice with DPBS and permeabilizated with 0.1% Triton X100 in DPBS for 15 minutes. Then samples were after washed twice again with DPBS and phalloidin solution in 1% BSA was added and incubated at room temperature for 40 minutes. Afterwards, samples were washed twice with DPBS and 1µg/ml DAPI was added and incubated for 5 minutes at room temperature. Finally, samples were washed twice with DPBS, mounted with Fluromount (Invitrogen) and observed under a fluorescence microscope (Leica DM4000B, Leica Microsystems). Images were acquired using a digital camera (Leica DFC300FX). Cells per field were counted using an image analysis software (ImageJ v1.52, National Institute of Health).

3.7. In vivo experiments

3.7.1. Surgical procedure

For this study, 16-week-old FVB female mice weighing between 25-35 g were used. Mice were divided into two groups, healthy mice (non-OP group) and osteoporotic mice (OP group). After 4 months, both mice groups were subjected to a surgical procedure under inhalation anesthesia in which a 4 mm diameter critical bone defect was performed in the calvaria. Critical bone defects were made as described in chapter 1 (section 3.5.2), following a previously published protocol (Rodríguez-Évora et al., 2013). Electrospun meshes containing ALD for the BMP-2+ALD foam group (Table 3) or blank electrospun meshes for the remaining groups (Control, BMP-2 foam, BMP-2+Low MMP-10 foam and BMP-2+High MMP-10 foam; Table 3) were placed on the defect. Adequate foams were then placed above the meshes and the defect was closed placing another electrospun mesh on top of the foams with or without ALD depending on the treatment group. Finally, the wound was closed with surgical clips. Analgesia consisted of buprenorphine administered subcutaneously (0.01 mg/kg) before surgery and paracetamol (200 mg/kg) in water for 3 days after intervention. Both non-OP and OP groups were subjected to 4 different treatments (10 mice each) as shown in Table 3. An additional control group including control foam and blank electrospun mesh was added to non-OP group as control of bone formation and mineralization without any drug treatment. Two time points were tested, 6 and 12 weeks, and 5 mice were used for each time point. During all the experiment, both OP and non-OP mice were monitored for bone mass loss by densitometry (PIXImus, GE Lunar) as described in section 3.4.

Table 3. Treatment groups for the *in vivo* assessment of scaffold performance. The same treatment groups were used for control mice (non-OP group) and osteoporotic mice (OP group).

	Sandwich-like scaffolds	
Treatment Group	**Chitosan foam** 	**Electrospun mesh** 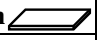
BMP	BMP-2 foam	Blank mesh
BMP+ALD	BMP-2+ALD foam	ALD-mesh
BMP+MMP-L	BMP-2+Low MMP-10 foam	Blank mesh
BMP+MMP-H	BMP-2+High MMP-10 foam	Blank mesh
		

3.7.2 In vivo drug release

To evaluate the *in vivo* protein delivery, foams loaded with radiolabeled BMP-2 (^{125}I-BMP-2) or MMP-10 (^{125}I-MMP-10) were used. The release rate was evaluated by measuring the amount of radiolabeled proteins remained in the scaffold at different time points using the non-invasive method already described in chapter 1 (section 3.5.3).

3.7.3 Histological and histomorphometric evaluation

To label the mineralization front, animals were injected with oxytetracycline-HCl (40 mg/kg, IM) and calcein blue (15 mg/kg, SC) 12 and 4 days previous to euthanasia, respectively.

To assess the *in vivo* effects of the different treatments, histological and histomorphometric assessments of the samples were performed. After tissue fixation in 10% formalin solution (pH = 7.4), undecalcified bone specimens were prepared for histological analysis as previously described (Del Rosario et al., 2015). Briefly, the samples were dehydrated in a graded series of ethanol and embedded in methyl methacrylate. Following polymerization, 10 μm thick longitudinal sections were prepared throughout the scaffold, using a sawing microtome technique (Leica SM

2500). The sections were stained with Goldner's Trichrome to identify new bone formation, or left unstained for detection of fluorochrome labels, and analyzed by light microscopy (Leica DM 4000B).

For histomorphometrical analysis, all sections per specimen were evaluated using computer-based image analysis software (Leica Q-win V3 Pro-image analysis system). The procedure was de same described in chapter 1 (section 3.7). In addition, the distance between tetracycline and calcein blue labels was measured under ultraviolet light for the calculation of mineral appositional rate (MAR). For calculation of MAR, 10 measurements at random points were made between both labeling fronts in 10 different sections along the defect in all the animals of each experimental group. The average was divided by the time elapsed between the administration of each fluorochromes, and this value was represented as the MAR.

3.8 Statistical analysis

Statistical analysis was performed with SPSS version 25 software. All experiments were run at least in triplicate. Differences between the treatment groups were analyzed by a one-way analysis of variance (ANOVA) with a Tukey multiple comparison post-test. For the *in vivo* studies different treatments at each time point (6 weeks and 12 weeks) were compared by means of a two-way ANOVA with a Tukey multiple comparison post-test. Significance was set at $p<0.05$ unless outside satated. Results are expressed as mean ± SD.

4. Results

4.1. Physicochemical performance of developed systems

4.1.1. Polymeric microspheres

Polymeric microspheres were obtained by a double emulsification method using an initial aqueous internal phase of either PVA+H_2O (PLGA microspheres) or PVA+Chitosan+H_2O (PLGA/Chitosan microspheres).

Both types of microspheres showed similar mean diameter being 69.18 ± 1.6 µm for PLGA microspheres and 65.98 ± 0.04 µm for PLGA/Chitosan microspheres with a single distribution peak. Microspheres loading efficiencies were obtained using radiolabeled proteins or ALD. PLGA microspheres showed high encapsulation efficiencies for BMP-2 (70 ± 6.8%) and MMP-10 (74.05 ± 25.9%). On the other hand, the obtained ALD encapsulation efficiency was slightly lower, 63.11 ± 11.02%.

4.1.2. Electrospun meshes

To obtain electrospun meshes incorporating ALD, the drug was covalently linked to two different PLGAs. ^{1}H NMR study (Fig. 1A-B) was performed to confirm the conjugation. The chemical shift (δ), expressed in ppm, gives information on the type of hydrogen generating the signal. When the lower molecular weight PLGA was used to link ALD, Resomer® RG 502, chemical shifts were observed at 1.57 (m, 321H), 2.98 (s, 2H), 4.54-4.98 (m, 183H) and 5.07-5.38 (m, 91H). On the other hand, when Resomer® RG 504 H was used as the polymer backbone for drug incorporation, signals at δ 1.57 (m, 352H), 2.97 (s, 2H), 4.54-4.98 (m, 246H) and 5.07-5.38 (m, 114H) were recorded. Integrating the signals obtained from PLGA (5.25-5.16 ppm) and the alendronate signal at approximately 3 ppm, the obtained percentage of polymer functionalization was 76.3% for Resomer® RG 502 and 98.8% for Resomer® RG 504. Moreover, the percentage of RG 502-ALD and RG 504-ALD polymers over the theoretical amount on the final mesh was determined in triplicate by comparing the integrals of $Cl_2CHCHCl_2$ (used as internal standard) and the alendronate signal at 3 ppm correspondent to "a", a (R-CH_2-X) proton X being the Nitrogen (N) of ALD (Fig. 1). The obtained value was 89% ± 7% indicating no loss of the linked ALD during storage and electrospinning. Therefore, the ALD dose on the meshes was 7 ng per mg of electrospun mesh. On the other hand, samples soaked for 72 hours in water did not show any ALD signal (Fig. 2) indicating the release of the drug at this time point. These effect could be more related to polymer hydrolysis than to the hydrolysis of the amide group that is formed in the conjugation of ALD with the polymer.

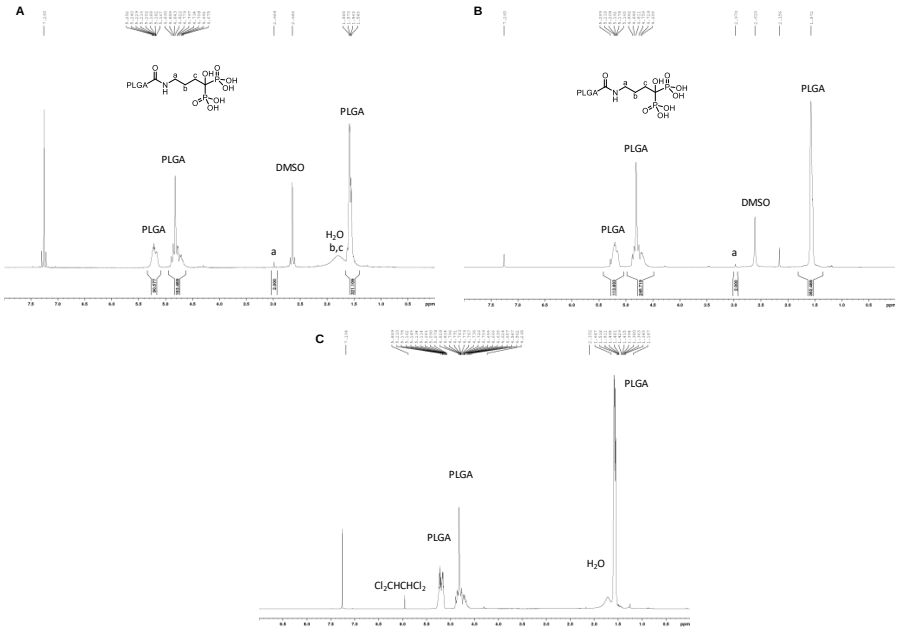

Figure 1. ^{1}H-NMR spectrum of (A) PLGA-ALD from Resomer® RG 502 H; (B) PLGA-ALD from Resomer® RG 504 H and (C) Electrospun meshes soaked 72 hours in water ($Cl_2CHCHCl_2$ was used as internal standard). The signal at 7.26 ppm corresponds to the signal from the solvent $CHCl_3$.

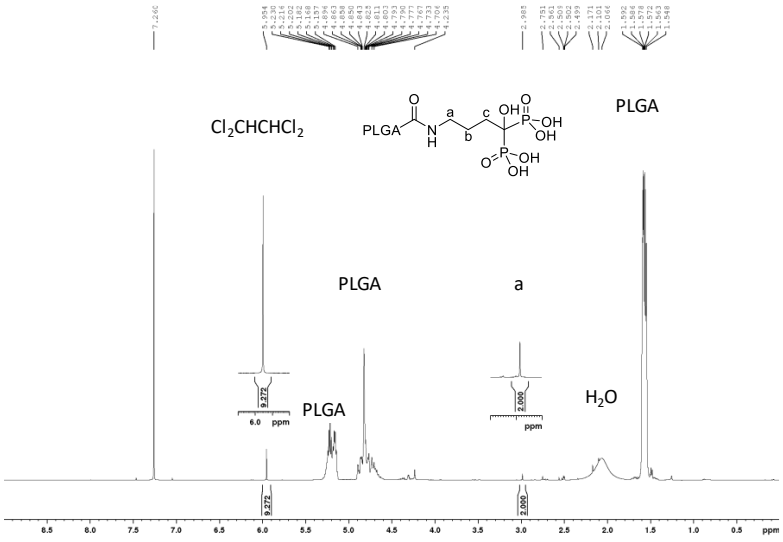

Figure 2. ^{1}H-NMR spectrum of Electrospun meshes soaked using $Cl_2CHCHCl_2$ as internal standard to quantify the amount of PLGA-ALD. The signal at 7.26 ppm corresponds to the solvent signal $CHCl_3$.

The obtained sheets were, afterwards, treated with plasma to decrease the surface hydrophobicity conferred by PLGA. Indeed, blank treated meshes showed contact angle values around 90°, the threshold for hydrophobic materials, (88.2 ± 10.7) while ALD-meshes showed a slightly higher mean contact angle of 93.43 ± 8.17. However, both types of meshes presented lower contact angle than those previously reported for non-treated PLGA meshes 114.1 ± 8.3 (María Rodríguez-Évora et al., 2014).

Furthermore, the physical properties and morphology of the meshes were characterized in terms of thickness, fiber diameter and total porosity (Fig. 3). The obtained blank and ALD-loaded fibers presented a smooth surface (Fig. 3A-B) characterized by a similar microscale fiber diameter (≈ 1.3 µm). As expected, both systems are highly porous showing a total porosity above 80%. However, the thickness of ALD meshes was significantly higher than the one for blank meshes (Table 4).

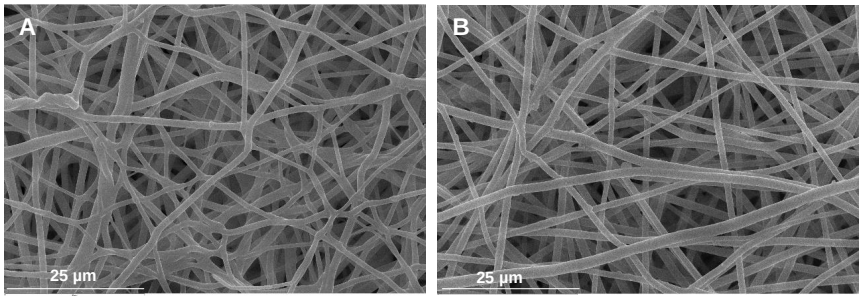

Figure 3. Scanning electron microscopy images at 1500X magnification of: (A) Blank Meshes, (B) Alendronate meshes both treated with plasma oxygen.

Table 4. Thickness, microfiber diameter and porosity of the blank and ALD linked meshes.

	Thickness (µm)	Microfiber diameter (µm)	Porosity (%)
Blank	89.79 ± 4.10	1.40 ± 0.30	82.11
ALD	103.65 ± 3.13	1.32 ± 0.28	90.92

4.1.3. Microspheres-loaded chitosan foams

Chitosan foams including adequate microspheres based on the desired scaffold composition were obtained by ionic crosslinking using a straight forward approach. The obtained foams were characterized by high porosity, 94.6 ± 1.2%, and water uptake with 366.5 ± 13.9 % of swelling after 24 hours (Fig. 4A). Moreover, the obtained foams showed high stability with a mass loss of only 10.9 ± 5.13 % after 28 days of study. Interestingly, the mass loss was stable throughout the experiment being 15.1 ± 5.7% just after 24 hours.

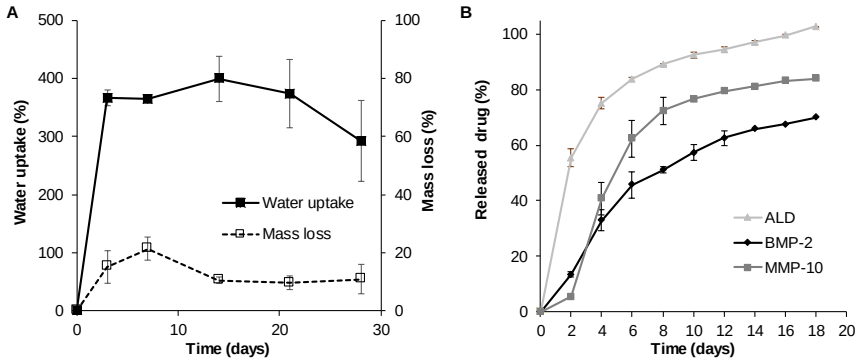

Figure 4. (A) Water uptake and mass loss and (B) drug release profiles of microsphere-loaded chitosan foams.

On the other hand, the *in vitro* release studies showed a diffusion-controlled release profile for both of the incorporated proteins reaching around 70% of protein release, 69.98 ± 2.62% for BMP-2 and 83.28 ± 4.21% for MMP-10, after 18 days of study (Fig. 4B). However, ALD showed a more pronounced burst release with 55.41 ± 3.21 % of the drug released just after two days of study followed by a sustained release rate. Despite the high burst release effect observed, the incorporation of ALD microspheres into the chitosan matrix was able to decrease the burst effect showed by plain microspheres characterized by almost all the drug released just after 2 days (94.4% ± 5.6 %) (Fig. 5).

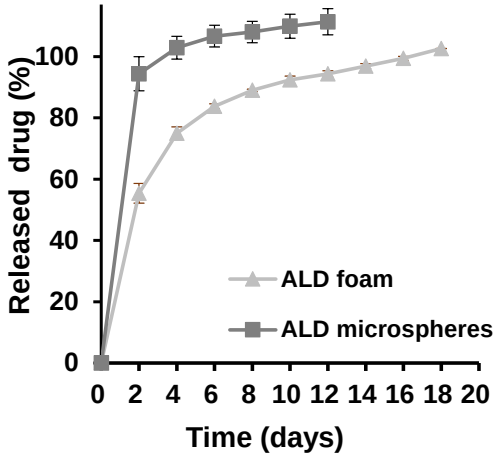

Figure 5. *In vitro* drug release profiles of ALD from microsphere-loaded chitosan foams (ALD foam) and plain microspheres (ALD microspheres).

4.2. Osteoporosis instauration

To obtain OP-like mMSC and to evaluate the *in vivo* scaffold performance in OP-like environments an osteoporotic mice model was developed. Both healthy and OP mice showed normal growth. Densiometry results (Fig. 6A) showed significantly lower BMD values for OP-mice two weeks after ovariectomy when compared to control animals ($p < 0.001$). From then, this difference was maintained during the remaining time of the experiment. Moreover, the histomorphometric assay results confirmed the OP condition (Fig. 6B). Femurs from OP mice showed significantly lower cortical bone thickness (Ct.Wi), width and number of trabeculae (Tb, Wi, Tb.N) in cancellous bone and higher separation of trabeculae (Tb. Sp) in cancellous bone.

A

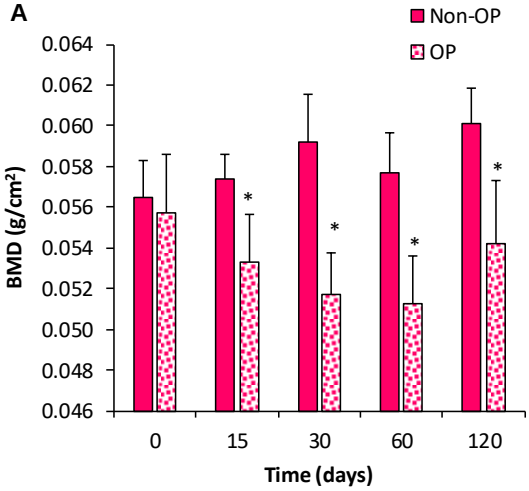

B

	Ct.Wi (µm)	Tb.Wi (µm)	Tb.Sp (µm)	Tb.N (mm)
Non-OP	171.7 ± 17.9	58.8 ± 16.7	88.3 ± 15.2	14.6 ± 3.7
OP	94.7 ± 15.7*	31.3 ± 5.4*	154.6 ± 27.2*	6.3 ± 1.6*

Figure 6. (A) Bone mineral density (BMD; g/cm^2) values for control and OP animal at 0, 15, 30, 60 and 120 days of ovariectomy. (B) Histomophometric analysis in femurs measuring thickness of the cortical bone (Ct.Wi) and width (Tb.Wi), separation (Tb.Sp) and number (Tb.N), of the trabeculae in cancellous bone. (*) denotes statistical significance differences compared to non-OP group (control) $p < 0.001$.

4.3. Characterization of OP-like mMSC and "healthy" mMSC

Cell surface markers expression was analyzed for OP-like mMSCs and control/healthy mMSC to validate the isolation procedure selected. Flow cytometry results (Fig. 7) showed the expected mMSC surface markers expression with positive expression of mMSC; stem cell antigen-1 (Sca-1) and CD44 and no expression (OP mMSC) or slight expression (non-OP mMSC) of hematopoietic markers (CD45).

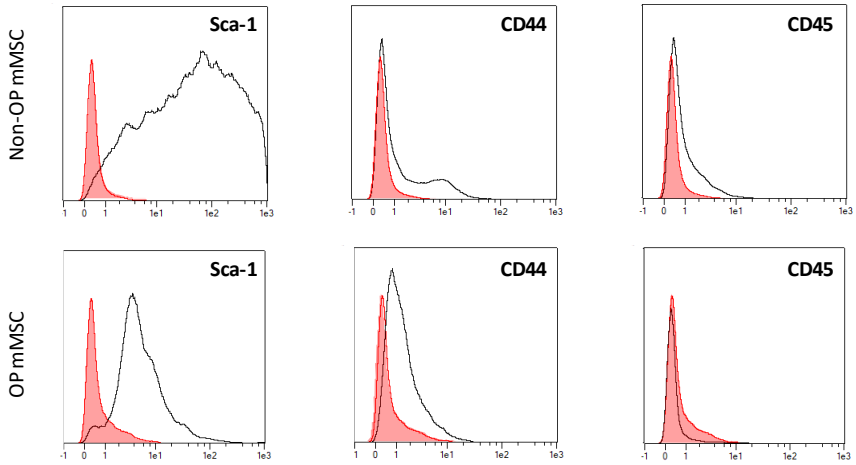

Figure 7. Cell surface markers of mouse mesenchymal stem cells extracted from healthy/control (non-OP mMSC) and osteoporotic mice (OP mMSC).

4.4. In vitro performance of chitosan foams and electrospun meshes

Alkaline Phosphatase (ALP) is a crucial enzyme on the biomineralization process increasing the local concentration of inorganic phosphate and a good predictor of neotissue mineralization (Golub & Boesze-Battaglia, 2007). Both non-OP and OP mMSCs were cultured on microsphere-loaded chitosan foams to analyze whether the presence of BMP-2 alone or combined with MMP-10 or ALD successfully promoted MSC osteogenic differentiation and mineralization in both cell populations. After 7 and 21 days ALP activity was evaluated, foams were fixed, cut and mounted on slides. The microscopic analysis showed the presence of positively stained cells (ALP + cells) in all the experimental groups at the two time points analyzed. The level of ALP activity in most cells is qualitatively high as shown by the intensity of the labelling (Fig. 8A, B), however, slight qualitative differences were observed between mMSC from normal mice (non-OP mMSC) and mMSC from OP mice, observing a higher labelling intensity in the first ones (Fig. 8A, B).

Quantification showed a significant increase in the number of non-OP mMSC ALP + cells at 7 days of culture in all the treated groups with respect to the control group, being the highest when cells were cultured on chitosan foams combining BMP-2 and ALD or BMP-2 and MMP-10 at low amount (Fig 8C). In fact, cells grown on these foams showed significantly higher ALP activity than those cultured on systems including BMP-2 alone. The same trend was observed after 21 days of culture where drug-loaded foams showed significantly higher number of ALP+ cells than blank foams. Moreover, the combination of BMP-2 with ALD or MMP-10 on the foams led to an increased ALP activity when compared to the addition of BMP-2 alone.

By contrast, this beneficial effect of the BMP-2 and ALD mixture or MMP-10 was not observed on OP mMSC ALP activity (Fig 8D). In these circumstances, the incorporation of BMP-2 to chitosan foams successfully increased the number of ALP+ cells after 7 days of culture but no additional effect was observed by its combination with ALD or MMP-10. Moreover, after 21 days of culture only the treatment combining BMP-2 and low dose of MMP-10 presented a significantly higher number of ALP+ cells compared to control foams. In general, foams seeded with OP mMSC, at 7 and 21 days post-seeding, showed a lower number of ALP+ cells per field than those seeded with non-OP mMSC. Therefore, a clear difference in mineralization potential can be observed between control and OP mMSC.

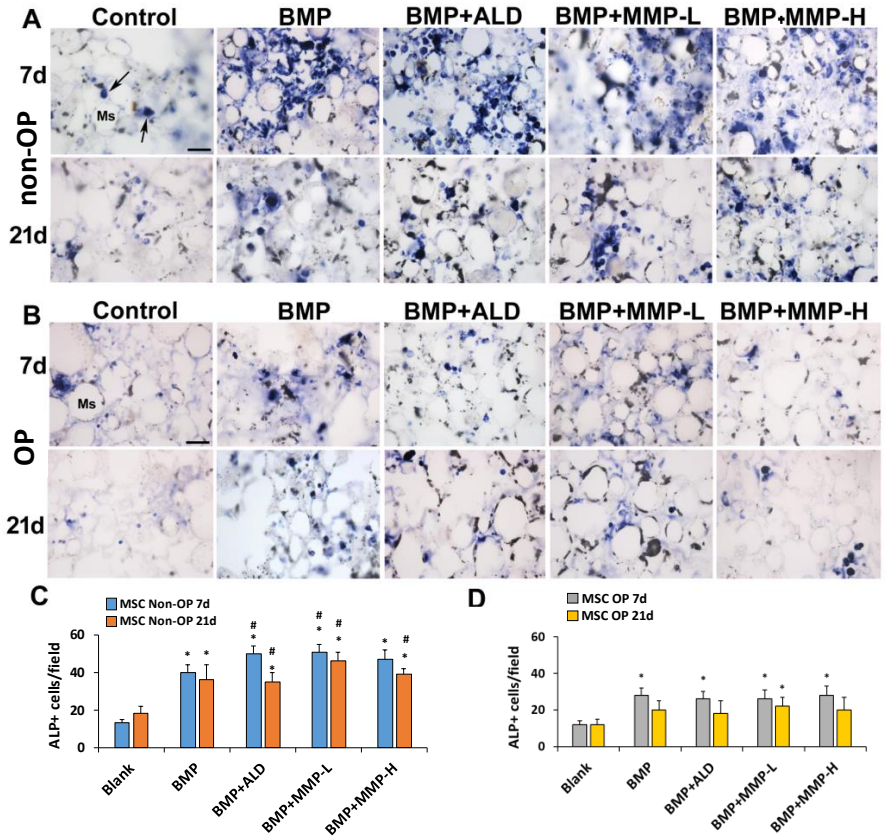

Figure 8. Panels A and B show representative images of mesenchymal stem cells from non-OP (A) and OP (B) animals cultured for 7 and 21 days and revealed for alkaline phosphatase activity. Histograms in C and D show the mean number of ALP positive cells per field at 400x magnification in non-OP and OP animals respectively. The arrows in the upper left image indicate ALP positive cells. Histograms represent mean ± SD values. (*) denotes statistical significant differences compared to Control treatment at the correspondent time point, (#) denotes statistical significant differences compared to BMP treatment at the correspondent time point. Ms: microspheres. Scale bar = 30 µm.

Moreover, OP mMSC were cultured on electrospun PLGA meshes containing or not ALD. Cell viability and attachment were evaluated to analyze the effect of ALD presence on cell behavior. Interestingly, the presence of ALD on the meshes significantly improved cell viability (Fig. 9A). Fluorescence images confirm this trend (Fig. 9B-C) showing a higher number of attached cells on ALD-linked electrospun meshes.

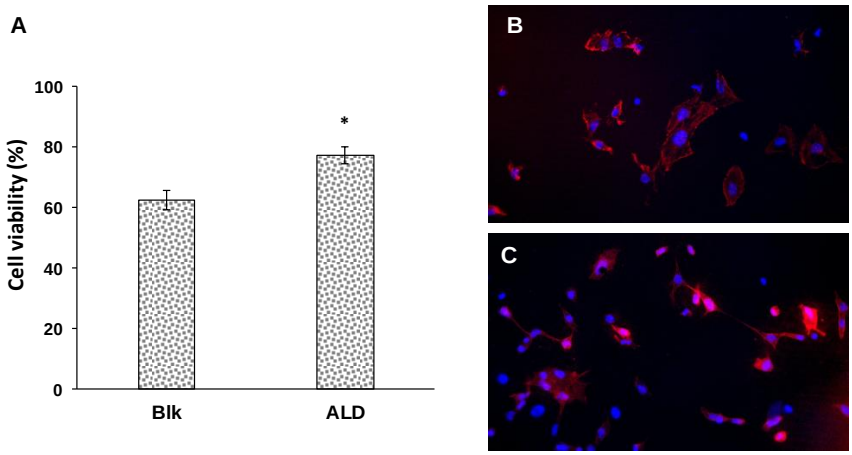

Figure 9. (A) Cell viability relative to control (Polystyrene plate) of OP mMSC cultured on plasma-treated electrospun meshes containing or not covalently linked ALD. (B) ALD-linked electrospun meshes or (C) blk electrospun meshes. Blank (blk) stands for meshes without ALD (*) denotes statistical significance differences compared to non-OP group (control) $p < 0.001$.

4.5. In vivo evaluation of sandwich-like scaffolds

4.5.1. In vivo protein drug release

The *in vivo* release of BMP-2 and MMP-10 incorporated in chitosan scaffolds showed similar profiles to those observed *in vitro* but with a slight increase on the burst effect (Fig. 10). The amount of protein released after 24 hours of implantation represented the 22.32 ± 2.68 % of the dose for BMP-2 and 25.51 ± 2.22 % of the dose for MMP-10. The release rate of both proteins fit the Higuchi model, characteristic of

release processes controlled by diffusion also explained by the high chitosan foam stability previously observed. The Higuchi constant (K_H) was 13.05 h^{-1} for BMP-2 release (R^2 = 0.99) and 11.31 h^{-1} for MMP-10 (R^2 = 0.97). Therefore, the complete dose of BMP-2 and MMP-10 would be released after 8 weeks and 11 weeks respectively indicating the achievement of a stable prolonged release.

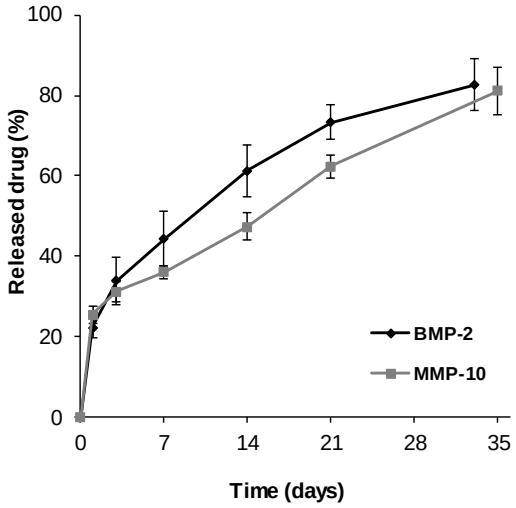

Figure 10. *In vivo* BMP-2 and MMP-10 release at different time points after implantation of the developed scaffolds on control animals. Release profiles were obtained using radiolabeled BMP-2 and MMP-10.

4.5.2. In vivo bone formation induced by sandwich-like scaffold containing BMP-2 alone or combined with ALD or MMP-10

The ability of the developed sandwich-like scaffolds to promote new bone formation and tissue mineralization was evaluated on a critical size calvarial bone defect on both normal (non-OP) and OP animals. When scaffolds were implanted on control "healthy animals" a high proportion of connective tissue surrounding the scaffold and low new bone formation restricted to the margins of the defect was observed for all experimental groups (Fig. 11A). Twelve weeks post-implantation, a significant increase

in the repair response was observed with newly formed bone at the margins of the defect and isolated ossification foci within it (Fig. 11). The histomorphometric analysis showed significantly higher repair percentages for all the treatments compared to control scaffolds (data non shown) except for the combination of BMP-2 and MMP-10 with high dose of the MMP. Both BMP and BMP+ALD treatments showed similar percentage of repair at both 6 weeks (≈ 30%) and 12 weeks (≈ 50%) post-implantation. Conversely, the combination of BMP+MMP at the two ratios tested led to a significant decrease in the percentage of repair at both time points when compared to both BMP and BMP+ALD. The combination of 120 ng MMP-10 and BMP-2 was only able to achieve a 27% of bone repair after 12 weeks of implantation (Fig. 11C).

The mineralization rate, determined by the mineralization fronts marked with calcein blue and oxytetracycline, revealed significantly lower mineral apposition rates (MAR) at six weeks post-implantation than at twelve weeks for all the experimental groups (Fig. 10D). Contrary to the results in bone repair, the combination of BMP-2 and MMP-10 led to a significant increase in mineral apposition rates compared to BMP-2 alone. In fact, when the higher dose of MMP-10 was used, 120 ng, the MAR was significantly higher to that observed for both BMP and BMP+ALD treatment groups.

Scaffold's performance was also evaluated on the developed OP mice model. In osteoporotic animals the relative proportion of connective tissue in the area of the defect was similar to that observed in normal animals (Fig. 11B). Following the same trend as for control animals the obtained percentage of repair and mineral apposition rates were significantly higher at the last time point studied (12 weeks) than at 6 weeks post-implantation (Fig. 11C-D). At this point of analysis, new bone formation was observed not only in the margins but also in larger areas of the defect. However, a shift in MMP-10 effect on tissue repair in OP animals was clearly observed when compared with control non-OP animals. In diseased animals the combination of BMP-2 and MMP-10 at either of the doses selected promoted a significant increase in tissue repair compared to BMP-2 alone and BMP+ALD (Fig. 11C). The highest

percentages of repair were observed on mice implanted with BMP+MMP-L with a value of 44% after 6 weeks of implantation and 54% after 12 weeks of implantation. On the other hand, the lowest percentages of repair were obtained with scaffolds containing plain BMP showing values of 17% after six weeks of implantation and 35% after 12 weeks.

In this case, the results of mineral apposition rate match the results above mentioned for tissue repair (Fig. 11D). The combination of BMP-2 and MMP-10 at either of the doses selected promoted a significant increase in mineral apposition rate compared to the use of scaffolds including BMP-2 alone or combined with ALD.

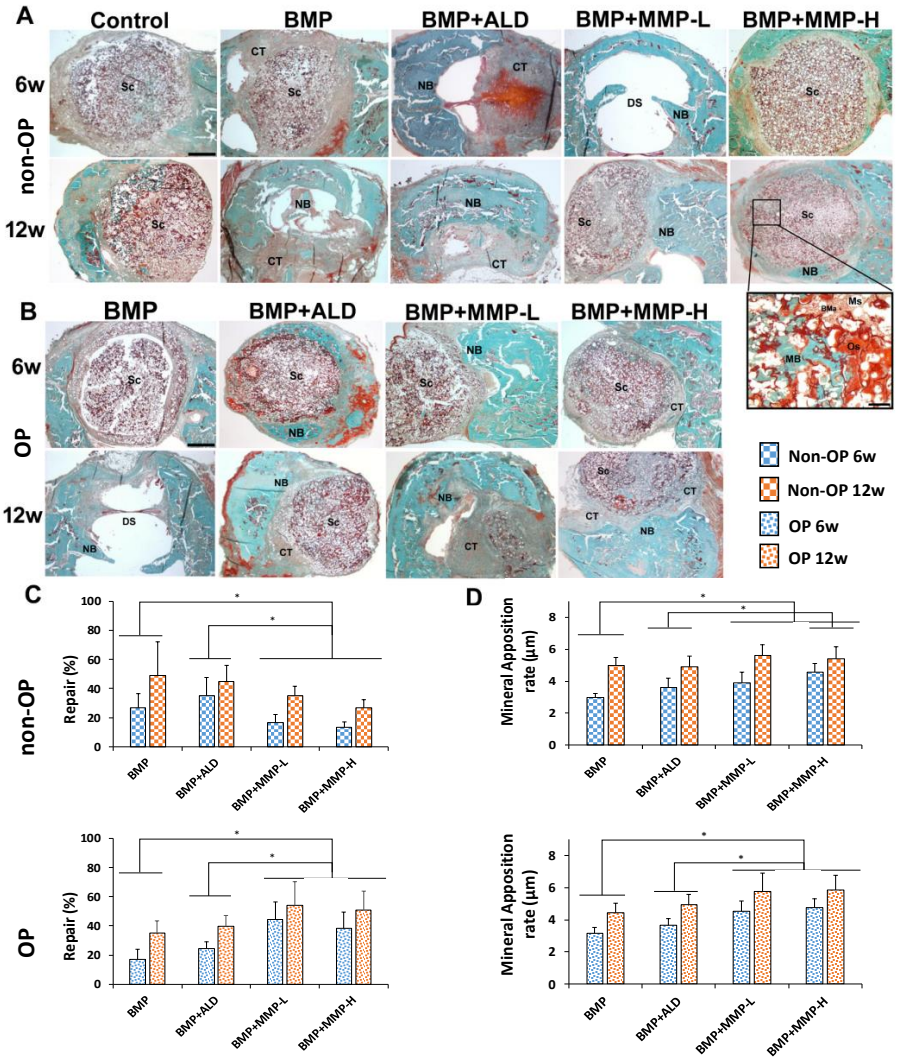

Figure 11. Representative panoramic images of the bone defect in the different experimental groups of non-OP (A) and OP (B) animals, showing the reparative response at 6 and 12 weeks post-implantation. Insert: Detail corresponding to the BMP + MMP-H group that shows active bone neoformation in the peripheral area of the scaffold. C and D. Histomorphometric analysis showing the percent of repair (C) and the mineral apposition rate (MAR) (D), six (blue) and twelve (orange) weeks post-implantation, in the different experimental groups of non-

OP (squares) and OP (points) animals. Histograms represent mean ± SD values. The identical letter/symbol on different bars indicates significant differences. BMa: Bone marrow, CT: Connective tissue, DS: Defect site, MB: Mineral bone, Ms: Microspheres, NB: New bone, Os: Osteoid, Sc: Scaffold. Scale bars: A and B: 1 mm, Inset: 80 µm. (*) denotes statistical significance differences between groups.

5. Discussion

The development of biomaterials designed for bone regeneration has been one of the main objectives in the tissue engineering field for the last decades. The strategy of these scaffolds has been mostly centered on fulfilling requirements related to scaffold mechanical performance and stem cell osteogenic induction capacities recognized as crucial to ensure the recovery of the bone function. However, not only the characteristics of the scaffold should be considered but also the quality of the regenerated bone should be taken into account, specially when scaffolds are used in pathologies characterized by an impaired bone quality. Increased bone mineral content and improved microarchitecture is directly correlated to enhanced mechanical properties and desirable for osteoporosis treatments (Faibish et al., 2006). In this study we propose to use already well-known biocompatible and biodegradable raw materials to develop sandwich-like scaffolds designed to obtain better bone quality increasing the mechanical resistance of bone. To do so, scaffolds were doped with BMP-2 alone, with already known osteogenic induction capacities, or with combinations of BMP-2 and an antiresorptive drug (ALD) or BMP-2 and metalloprotease 10 (MMP-10) at different doses.

To achieve a desirable growth factor and ALD or MMP-10 controlled release avoiding the risk of undesirable side effects derived from high concentration, therapeutic molecules were included on PLGA microspheres. The developed microspheres were characterized by high encapsulation efficiencies over 60% in all cases being even 10% higher for BMP-2 and MMP-10. The addition of chitosan in the internal phase during the synthesis of ALD-loaded PLGA microspheres aimed at increasing their drug encapsulation capacity a challenge due to the high

aqueous solubility of the drug. Indeed, the developed microspheres presented a 5 fold-increase in ALD encapsulation efficiency compared to previously reported ALD-loaded PLGA microspheres prepared following a similar double emulsification method (Deca et al., 2015). Moreover, other reports already reported lower ALD encapsulation efficiencies using a double emulsification method with levels as low as 0.2% (Nafea et al., 2007).

Microspheres were then incorporated in to chitosan networks serving as molds to obtain cross-linked foams with high water uptake capacity, porosity and remarkable stability. Chitosan is a natural polymer widely used for bone tissue engineering applications due to its several advantages as easy chemical modification and high biocompatibility (LogithKumar et al., 2016). Plain chitosan foams have been previously tested as substrates for osteoblasts attachment indicating adequate performance (Seol et al., 2004; Sukul et al., 2021). However, chitosan is commonly combined with either ceramics and/or other polymers to improve mechanical performance and confer osteoinductive capabilities (Ikono et al., 2019). The strategy used on this study proposed to include microspheres loaded with BMP-2 and MMP-10 or ALD into chitosan foams serving as therapeutic molecules' reservoir and conferring osteoinductive capabilities to the developed systems. In agreement with our hypothesis, the incorporation of the microspheres to chitosan foams led to a controlled release of the therapeutic molecules both *in vitro* and *in vivo* characterized by a diffusion-controlled profile. Moreover, the incorporation of PLGA microspheres to chitosan foams could improve the mechanical performance of the systems.

The ability of the incorporated therapeutic molecules to conferee osteoinductive capabilities to the developed foams was evaluated by culturing MSC from "healthy" and OP animals on them analyzing the alkaline phosphatase activity. The testing of the scaffold performance using both cell populations is justified by the already known alterations in differentiation and proliferation capacity of OP MSC (Paspaliaris & Kolios, 2019). Cell populations were characterized by flow cytometry showing different profiles for Sca-1 and CD44 expresion. Sca-1 deficient

mice were previously reported to undergo osteoporosis and are characterized by a decreased self-renewal of osteogenic stem cells (Bonyadi et al., 2003; Hidestrand et al., 2008; Paspaliaris & Kolios, 2019). In fact, the administration of Sca-1 + sorted MSC to osteoporotic animals was able to improve bone mineral density (Agata et al., 2019). On the other hand, similarly to Sca-1, CD44 seemed to be decreased in OP mMSC. The absence of this cell surface hyaluronan receptor has been correlated to increased osteoclastogenesis and bone loss under inflammatory environments in mice (Hayer et al., 2005). Moreover, CD44 has been described as crucial for MSC migration, a cell function reported to be decreased in OP mMSC (Sanghani-Kerai et al., 2017; Zhu et al., 2006). Altogether, the modified positive expression of Sca-1 and CD44 observed for OP mMSC (Fig. 7) could be associated to the disease instauration and the associated lower MSC migration, proliferation, and differentiation capacity (Agata et al., 2019; Bonyadi et al., 2003; Hayer et al., 2005; Hidestrand et al., 2008; Holmes et al., 2007; Paspaliaris & Kolios, 2019; Sanghani-Kerai et al., 2017; Zhu et al., 2006). Indeed, OP mMSC showed lower number of ALP+ cells than non-OP mMSC for all the evaluated treatments at both of the time points selected. Analyzing the response of both cell populations to BMP-2 alone or combined with the other therapeutic molecules clear differences were pointed out. The addition of BMP-2 significantly increased the number of ALP+ cells for both populations but while the combination of BMP-2 + ALD and BMP-2 + MMP-10 at low dose produced an even higher number of ALP+ cells for non-OP cells, no effect was observed for OP mMSC. The ability of MMP-10 to increase the number of ALP+ cells under an osteogenic environment has been already described *in vitro* on aortic valve interstitial cells (Matilla et al., 2020). This effect has been hypothesized to be mediated mainly by the PI3K/AKT cell signaling pathway, a critical signaling pathway involved in OP (Xi et al., 2015). This fact could explain the differences in cell response to MMP-10. On the other hand, in agreement with our findings for non-OP mMSC, ALD has been previously reported to promote osteogenesis and an enhancement in ALP expression on human MSC (Chan et al., 2009).

A new strategy was used to load PLGA electrospun meshes with ALD. In this case, the drug was efficiently conjugated to different PLGA polymer chains. Thus, the obtained meshes presented a drug content directly controlled by the amount of functionalized polymers used for electrospinning and not affected by storage. Plasma-treated electrospun meshes presented high porosity, microscale fiber diameter and, therefore, a high surface-area-to-volume ratio adequate characteristics to resemble natural extracellular matrix (Jun et al., 2018). Indeed, osteoporotic-like cells seeded on the developed meshes showed good attachment improved by the presence of ALD on their surface. These differences could be attributed to the acid character of un-functionalized electrospun meshes due to the carboxylic acid terminal group of not modified PLGA.

To obtain suitable scaffolds for bone regeneration the developed chitosan foams were surrounded by two electrospun meshes generating a 3D sandwich-like scaffold. To the best of our knowledge, no previous work has been devoted to combine BMP-2 and MMP-10 on microspheres embedded in a scaffold for the regeneration of critical size bone defects in OP animals. Furthermore, the results of this combination were compared to scaffolds containing BMP-2 alone or BMP-2+ALD. In our previous work, microspheres loaded with BMP-2 and MMP-10 were dispersed in a hydrogel and implanted on a critical size bone defect (Reyes et al., 2018). The regenerative effect was evaluated after 4 and 8 weeks of implantation and the ratios tested for BMP-2: MMP-10 were 20:1 and 200:1. The obtained results suggested higher percentage of bone repair and mineralization apposition rates for the higher MMP-10 dose (20:1; 30ng MMP-10) after 4 weeks of implantation (Reyes et al., 2018).

As already described above, bone formation is impaired in OP. Moreover, our previous results revealed a slow release rate of BMP-2 can be beneficial for bone regeneration promotion in OP animals. Besides, the development of solid scaffolds able to remain longer on the defect site led to better bone repair (Chapter 2). Therefore, in the present study scaffolds were designed to persist in the defect site for long time and to slowly release the therapeutic molecules. In fact, the presence of the scaffolds on the defect area was evident, at both six and twelve weeks of implantation.

Likewise, a complete infiltration of the scaffold by connective tissue was observed, with presence of cells both, between the microspheres and inside them. However, this long-term stability of the scaffolds had a negative effect on non-OP animals hindering the rapid regeneration observed on these animals and leading to lower regeneration percentages to those previously reported for BMP-2+MMP-10 (Reyes et al., 2018). This fact could also explain the *in vivo* lack of positive response in percentage of repair for the BMP+MMP and BMP+ALD treatments compared to plain BMP-2 despite the beneficial effects in ALP activity observed for these treatments *in vitro*. Moreover, the dose-dependent negative effect of MMP-10 addition on the regenerative response could be attributed to a catabolic effect aimed to degrade the scaffold. Despite the decrease observed in tissue repair, the mineralization rate for BMP+MMP treatments was significantly higher than BMP-2 confirming the positive effect of MMP-10 addition on bone mineralization.

The results obtained suggested the designed sandwich-like scaffolds match closer the requirements for bone tissue repair in OP animal. In these animals, the combination of BMP-2 and MMP-10 induced a regenerative effect and an improved mineral apposition rate when compared to scaffolds containing BMP-2 alone or BMP-2+ALD. These observations suggested the requirements to achieve a good bone regeneration in the osteoporotic population are different than those in healthy animals.

6. Conclusions

Sandwich-like scaffolds were obtained combining PLGA electrospun meshes and drug-loaded chitosan foams. Therapeutic molecules were efficiently loaded and released from microspheres embedded on the chitosan network acting *in vivo* and *in vitro* as therapeutic molecules reservoirs for the developed scaffolds. This versatile strategy for scaffold development has allowed to test the effect of BMP-2 and BMP-2 + MMP-10 or BMP-2 + ALD on osteogenic induction and bone regeneration. The obtained results point out the crucial role of the bone tissue repair activity on the treatments success. The designed BMP-2 + MMP-10 combinations

showed the desired effect of tissue repair promotion on OP animals but the opposite effect was observed on control animals.

7. References

Agata, H., Sumita, Y., Hidaka, T., Iwatake, M., Kagami, H., & Asahina, I. (2019). Intra-Bone Marrow Administration of Mesenchymal Stem/Stromal Cells Is a Promising Approach for Treating Osteoporosis. *Stem Cells International*, *2019*. https://doi.org/10.1155/2019/4214281

Bonyadi, M., Waldman, S. D., Liu, D., Aubin, J. E., Grynpas, M. D., & Stanford, W. L. (2003). Mesenchymal progenitor self-renewal deficiency leads to age-dependent osteoporosis in Sca-1/Ly-6A null mice. *Proceedings of the National Academy of Sciences*, *100*(10). https://doi.org/10.1073/pnas.1036475100

Bord, S., Horner, A., Hembry, R. ., & Compston, J. . (1998). Stromelysin-1 (MMP-3) and Stromelysin-2 (MMP-10) Expression in Developing Human Bone: Potential Roles in Skeletal Development. *Bone*, *23*(1). https://doi.org/10.1016/S8756-3282(98)00064-7

Chan, J. M., Zhang, L., Yuet, K. P., Liao, G., Rhee, J.-W., Langer, R., & Farokhzad, O. C. (2009). PLGA–lecithin–PEG core–shell nanoparticles for controlled drug delivery. *Biomaterials*, *30*(8). https://doi.org/10.1016/j.biomaterials.2008.12.013

Choi, S. W., & Kim, J. H. (2007). Design of surface-modified poly(d,l-lactide-co-glycolide) nanoparticles for targeted drug delivery to bone. *Journal of Controlled Release*, *122*(1), 24–30. https://doi.org/10.1016/j.jconrel.2007.06.003

Colnot, C., Thompson, Z., Miclau, T., Werb, Z., & Helms, J. A. (2003). Altered fracture repair in the absence of MMP9. *Development*, *130*(17). https://doi.org/10.1242/dev.00559

De la Riva, B., Nowak, C., Sánchez, E., Hernández, A., Schulz-Siegmund, M., Pec, M. K., Delgado, A., & Évora, C. (2009). VEGF-controlled release within a bone defect from alginate/chitosan/PLA-H scaffolds. *European Journal of Pharmaceutics and*

Biopharmaceutics, *73*(1), 50–58. https://doi.org/10.1016/j.ejpb.2009.04.014

Deca, A., Belu, I., Croitoru, O., Bubulică, M., Manda, C., & Neamtu, J. (2015). ormulation and In Vitro Evaluation of Alendronate Sodium/PLGA Microspheres for Applications in Bone Related Disorders. *Current Health Sciences Journal*, *41*(2), 246–250.

Del Rosario, C., Rodríguez-Évora, M., Reyes, R., Delgado, A., & Évora, C. (2015). BMP-2, PDGF-BB, and bone marrow mesenchymal cells in a macroporous β-TCP scaffold for critical-size bone defect repair in rats. *Biomedical Materials (Bristol)*, *10*(4). https://doi.org/10.1088/1748-6041/10/4/045008

Dolci, L. S., Panzavolta, S., Torricelli, P., Albertini, B., Sicuro, L., Fini, M., Bigi, A., & Passerini, N. (2019). Modulation of Alendronate release from a calcium phosphate bone cement: An in vitro osteoblast-osteoclast co-culture study. *International Journal of Pharmaceutics*, *554*, 245–255. https://doi.org/10.1016/j.ijpharm.2018.11.023

Faibish, D., Ott, S. M., & Boskey, A. L. (2006). Mineral Changes in Osteoporosis. *Clinical Orthopaedics & Related Research*, *443*. https://doi.org/10.1097/01.blo.0000200241.14684.4e

García-García, P., Reyes, R., Pérez-Herrero, E., Arnau, M. R., Évora, C., & Delgado, A. (2020). Alginate-hydrogel versus alginate-solid system. Efficacy in bone regeneration in osteoporosis. *Materials Science and Engineering C*, *115*, 111009. https://doi.org/10.1016/j.msec.2020.111009

Golub, E. E., & Boesze-Battaglia, K. (2007). The role of alkaline phosphatase in mineralization. *Current Opinion in Orthopaedics*, *18*(5). https://doi.org/10.1097/BCO.0b013e3282630851

Gundogdu, E., Ekinci, M., Ozgenc, E., Ozdemir, D. I., & Asikoglu, M. (2018). Development and Evaluation of Liquid and Solid Lipid Based Drug Delivery Systems Containing Technetium-99m-Radiolabeled Alendronate Sodium. *Current Radiopharmaceuticals*, *11*(2). https://doi.org/10.2174/1874471011666180529111914

Hayer, S., Steiner, G., Görtz, B., Reiter, E., Tohidast-Akrad, M., Amling, M., Hoffmann, O., Redlich, K., Zwerina, J., Skriner, K., Hilberg, F., Wagner, E. F., Smolen, J. S., & Schett, G. (2005). CD44 is a determinant of inflammatory bone loss. *Journal of Experimental Medicine*, *201*(6). https://doi.org/10.1084/jem.20040852

Hidestrand, M., Richards-Malcolm, S., Gurley, C. M., Nolen, G., Grimes, B., Waterstrat, A., Zant, G. V., & Peterson, C. A. (2008). Sca-1-Expressing Nonmyogenic Cells Contribute to Fibrosis in Aged Skeletal Muscle. *The Journals of Gerontology Series A: Biological Sciences and Medical Sciences*, *63*(6). https://doi.org/10.1093/gerona/63.6.566

Holmes, C., Khan, T. S., Owen, C., Ciliberti, N., Grynpas, M. D., & Stanford, W. L. (2007). Longitudinal Analysis of Mesenchymal Progenitors and Bone Quality in the Stem Cell Antigen-1-Null Osteoporotic Mouse. *Journal of Bone and Mineral Research*, *22*(9). https://doi.org/10.1359/jbmr.070604

Huntley, R., Jensen, E., Gopalakrishnan, R., & Mansky, K. C. (2019). Bone morphogenetic proteins: Their role in regulating osteoclast differentiation. *Bone Reports*, *10*. https://doi.org/10.1016/j.bonr.2019.100207

Hur, W., Park, M., Lee, J. Y., Kim, M. H., Lee, S. H., Park, C. G., Kim, S.-N., Min, H. S., Min, H. J., Chai, J. H., Lee, S. J., Kim, S., Choi, T. H., & Choy, Y. Bin. (2016). Bioabsorbable bone plates enabled with local, sustained delivery of alendronate for bone regeneration. *Journal of Controlled Release*, *222*. https://doi.org/10.1016/j.jconrel.2015.12.007

Ikono, R., Li, N., Pratama, N. H., Vibriani, A., Yuniarni, D. R., Luthfansyah, M., Bachtiar, B. M., Bachtiar, E. W., Mulia, K., Nasikin, M., Kagami, H., Li, X., Mardliyati, E., Rochman, N. T., Nagamura-Inoue, T., & Tojo, A. (2019). Enhanced bone regeneration capability of chitosan sponge coated with TiO2 nanoparticles. *Biotechnology Reports*, *24*. https://doi.org/10.1016/j.btre.2019.e00350

Jun, I., Han, H.-S., Edwards, J., & Jeon, H. (2018). Electrospun Fibrous Scaffolds for Tissue Engineering: Viewpoints on Architecture and Fabrication. *International Journal of Molecular Sciences*, *19*(3). https://doi.org/10.3390/ijms19030745

Kim, S. E., Yun, Y.-P., Shim, K.-S., Kim, H.-J., Park, K., & Song, H.-R. (2016). 3D printed alendronate-releasing poly(caprolactone) porous scaffolds enhance osteogenic differentiation and bone formation in rat tibial defects. *Biomedical Materials*, *11*(5). https://doi.org/10.1088/1748-6041/11/5/055005

Kosaki, N., Takaishi, H., Kamekura, S., Kimura, T., Okada, Y., Minqi, L., Amizuka, N., Chung, U., Nakamura, K., Kawaguchi, H., Toyama, Y., & D'Armiento, J. (2007). Impaired bone fracture healing in matrix metalloproteinase-13 deficient mice. *Biochemical and Biophysical Research Communications*, *354*(4). https://doi.org/10.1016/j.bbrc.2006.12.234

Lee, J. H., Baek, H.-R., Lee, K. M., Zheng, G. Bin, Shin, S. J., & Jin, Y. Z. (2015). The inhibitory effect of zoledronate on early-stage osteoinduction by recombinant human bone morphogenetic protein 2 in an osteoporosis model. *Growth Factors*, *33*(3). https://doi.org/10.3109/08977194.2015.1058259

Lieu, S., Hansen, E., Dedini, R., Behonick, D., Werb, Z., Miclau, T., Marcucio, R., & Colnot, C. (2011). Impaired remodeling phase of fracture repair in the absence of matrix metalloproteinase-2. *Disease Models & Mechanisms*, *4*(2). https://doi.org/10.1242/dmm.006304

Little, D. G., McDonald, M., Bransford, R., Godfrey, C. B., & Amanat, N. (2005). Manipulation of the Anabolic and Catabolic Responses With OP-1 and Zoledronic Acid in a Rat Critical Defect Model. *Journal of Bone and Mineral Research*, *20*(11). https://doi.org/10.1359/JBMR.050712

LogithKumar, R., KeshavNarayan, A., Dhivya, S., Chawla, A., Saravanan, S., & Selvamurugan, N. (2016). A review of chitosan and its derivatives in bone tissue engineering. *Carbohydrate Polymers*, *151*. https://doi.org/10.1016/j.carbpol.2016.05.049

Mao, L., Yano, M., Kawao, N., Tamura, Y., Okada, K., & Kaji, H. (2013). Role of matrix metalloproteinase-10 in the BMP-2 inducing osteoblastic differentiation. *Endocrine Journal*, *60*(12). https://doi.org/10.1507/endocrj.EJ13-0270

Mardas, N., Busetti, J., de Figueiredo, J. A. P., Mezzomo, L. A., Scarparo, R. K., & Donos, N. (2017). Guided bone regeneration in osteoporotic conditions following treatment with zoledronic acid. *Clinical Oral Implants Research*, *28*(3). https://doi.org/10.1111/clr.12810

Mathavan, N., Turunen, M. J., Guizar-Sicairos, M., Bech, M., Schaff, F., Tägil, M., & Isaksson, H. (2018). The compositional and nano-structural basis of fracture healing in healthy and osteoporotic bone. *Scientific Reports*, *8*(1). https://doi.org/10.1038/s41598-018-19296-z

Matilla, L., Roncal, C., Ibarrola, J., Arrieta, V., García-Peña, A., Fernández-Celis, A., Navarro, A., Álvarez, V., Gainza, A., Orbe, J., Cachofeiro, V., Zalba, G., Sádaba, R., Rodríguez, J. A., & López-Andrés, N. (2020). A Role for MMP-10 (Matrix Metalloproteinase-10) in Calcific Aortic Valve Stenosis. *Arteriosclerosis, Thrombosis, and Vascular Biology*, *40*(5). https://doi.org/10.1161/ATVBAHA.120.314143

Nafea, E. H., El-Massik, M. A., El-Khordagui, L. K., Marei, M. k., & Khalafallah, N. M. (2007). Alendronate PLGA microspheres with high loading efficiency for dental applications. *Journal of Microencapsulation*, *24*(6). https://doi.org/10.1080/02652040701439807

Orbe, J., Barrenetxe, J., Rodriguez, J. A., Vivien, D., Orset, C., Parks, W. C., Birkland, T. P., Serrano, R., Purroy, A., Martinez de Lizarrondo, S., Angles-Cano, E., & Páramo, J. A. (2011). Matrix Metalloproteinase-10 Effectively Reduces Infarct Size in Experimental Stroke by Enhancing Fibrinolysis via a Thrombin-Activatable Fibrinolysis Inhibitor–Mediated Mechanism. *Circulation*, *124*(25). https://doi.org/10.1161/CIRCULATIONAHA.111.047100

Paspaliaris, V., & Kolios, G. (2019). Stem cells in Osteoporosis: From Biology to New Therapeutic Approaches. *Stem Cells International*, *2019*. https://doi.org/10.1155/2019/1730978

Raina, D. B., Larsson, D., Mrkonjic, F., Isaksson, H., Kumar, A., Lidgren, L., & Tägil, M. (2018). Gelatin- hydroxyapatite- calcium sulphate based biomaterial for long term sustained delivery of bone morphogenic protein-2 and zoledronic acid for increased bone formation: In-vitro and in-vivo carrier properties. *Journal of Controlled Release*, *272*. https://doi.org/10.1016/j.jconrel.2018.01.006

Reyes, R., Rodríguez, J. A., Orbe, J., Arnau, M. R., Évora, C., & Delgado, A. (2018). Combined sustained release of BMP2 and MMP10 accelerates bone formation and mineralization of calvaria critical size defect in mice. *Drug Delivery*, *25*(1). https://doi.org/10.1080/10717544.2018.1446473

Rodríguez-Évora, M., Delgado, A., Reyes, R., Hernández-Daranas, A., Soriano, I., San Román, J., & Évora, C. (2013). Osteogenic effect of local, long versus short term BMP-2 delivery from a novel SPU–PLGA–βTCP concentric system in a critical size defect in rats. *European Journal of Pharmaceutical Sciences*, *49*(5). https://doi.org/10.1016/j.ejps.2013.06.008

Rodríguez-Évora, María, García-Pizarro, E., del Rosario, C., Pérez-López, J., Reyes, R., Delgado, A., Rodríguez-Rey, J. C., & Évora, C. (2014). Smurf1 Knocked-Down, Mesenchymal Stem Cells and BMP-2 in an Electrospun System for Bone Regeneration. *Biomacromolecules*, *15*(4). https://doi.org/10.1021/bm401854d

Sanghani-Kerai, A., Coathup, M., Samazideh, S., Kalia, P., Silvio, L. Di, Idowu, B., & Blunn, G. (2017). Osteoporosis and ageing affects the migration of stem cells and this is ameliorated by transfection with CXCR4. *Bone & Joint Research*, *6*(6). https://doi.org/10.1302/2046-3758.66.BJR-2016-0259.R1

Segredo-Morales, E., García-García, P., Reyes, R., Pérez-Herrero, E., Delgado, A., & Évora, C. (2018). Bone regeneration in osteoporosis

by delivery BMP-2 and PRGF from tetronic–alginate composite thermogel. *International Journal of Pharmaceutics*, *543*(1–2), 160–168. https://doi.org/10.1016/j.ijpharm.2018.03.034

Segredo-Morales, E., Reyes, R., Arnau, M. R., Delgado, A., & Évora, C. (2018). In situ gel-forming system for dual BMP-2 and 17β-estradiol controlled release for bone regeneration in osteoporotic rats. *Drug Delivery and Translational Research*, *8*(5), 1103–1113. https://doi.org/10.1007/s13346-018-0574-9

Seol, Y.-J., Lee, J.-Y., Park, Y.-J., Lee, Y.-M., -Ku, Y., Rhyu, I.-C., Lee, S.-J., Han, S.-B., & Chung, C.-P. (2004). Chitosan sponges as tissue engineering scaffolds for bone formation. *Biotechnology Letters*, *26*(13). https://doi.org/10.1023/B:BILE.0000032962.79531.fd

Soleimani, M., & Nadri, S. (2009). A protocol for isolation and culture of mesenchymal stem cells from mouse bone marrow. *Nature Protocols*, *4*(1). https://doi.org/10.1038/nprot.2008.221

Stickens, D., Behonick, D. J., Ortega, N., Heyer, B., Hartenstein, B., Yu, Y., Fosang, A. J., Schorpp-Kistner, M., Angel, P., & Werb, Z. (2004). Altered endochondral bone development in matrix metalloproteinase 13-deficient mice. *Development*, *131*(23). https://doi.org/10.1242/dev.01461

Sukul, M., Sahariah, P., Lauzon, H. L., Borges, J., Másson, M., Mano, J. F., Haugen, H. J., & Reseland, J. E. (2021). In vitro biological response of human osteoblasts in 3D chitosan sponges with controlled degree of deacetylation and molecular weight. *Carbohydrate Polymers*, *254*. https://doi.org/10.1016/j.carbpol.2020.117434

Toker, H., Ozdemir, H., Ozer, H., & Eren, K. (2012). A comparative evaluation of the systemic and local alendronate treatment in synthetic bone graft: a histologic and histomorphometric study in a rat calvarial defect model. *Oral Surgery, Oral Medicine, Oral Pathology and Oral Radiology*, *114*(5). https://doi.org/10.1016/j.oooo.2011.09.027

van Houdt, C. I. A., Gabbai-Armelin, P. R., Lopez-Perez, P. M., Ulrich,

D. J. O., Jansen, J. A., Renno, A. C. M., & van den Beucken, J. J. J. P. (2018). Alendronate release from calcium phosphate cement for bone regeneration in osteoporotic conditions. *Scientific Reports*, *8*(1). https://doi.org/10.1038/s41598-018-33692-5

Wang, X., Zeng, D., Weng, W., Huang, Q., Zhang, X., Wen, J., Wu, J., & Jiang, X. (2018). Alendronate delivery on amino modified mesoporous bioactive glass scaffolds to enhance bone regeneration in osteoporosis rats. *Artificial Cells, Nanomedicine, and Biotechnology*, *46*(sup2). https://doi.org/10.1080/21691401.2018.1453825

Xi, J.-C., Zang, H.-Y., Guo, L.-X., Xue, H.-B., Liu, X.-D., Bai, Y.-B., & Ma, Y.-Z. (2015). The PI3K/AKT cell signaling pathway is involved in regulation of osteoporosis. *Journal of Receptors and Signal Transduction*, *35*(6). https://doi.org/10.3109/10799893.2015.1041647

Zhu, H., Mitsuhashi, N., Klein, A., Barsky, L. W., Weinberg, K., Barr, M. L., Demetriou, A., & Wu, G. D. (2006). The Role of the Hyaluronan Receptor CD44 in Mesenchymal Stem Cell Migration in the Extracellular Matrix. *STEM CELLS*, *24*(4). https://doi.org/10.1634/stemcells.2005-0186

Discusión general

1. Discusión general

Teniendo en cuenta que en esta memoria ya se han discutido los resultados en cada uno de los capítulos correspondientes, en esta última sección se pretende discutir y comparar los resultados más destacados del trabajo en su conjunto.

El tejido óseo es un tejido del sistema esquelético especializado, heterogéneo, complejo y estructurado jerárquicamente. Su matriz extracelular consta de una fase mineral formada por hidroxiapatita (HAP), una fase orgánica compuesta por aproximadamente un 90% de colágeno tipo I, un 5% de otras proteínas, aproximadamente un 2% de lípidos en peso y agua (Faibish et al., 2006).

El hueso es un "tejido dinámico" sujeto a un continuo ciclo de "formación-destrucción", llamado remodelación. El estrecho acoplamiento de las actividades de los osteoblastos y los osteoclastos garantiza el correcto reclutamiento espacial y temporal de las células solo en el sitio a reemplazar, con el fin de mantener la estructura ósea (Rucci, 2008). Cuando se pierde el equilibrio el proceso se desacopla y las fases no se coordinan correctamente en tiempo y lugar, dando lugar a distintas patologías entre la que se destaca la osteoporosis (OP).

El proceso de remodelación ósea demuestra claramente que el hueso es un órgano regenerativo y explica la capacidad del hueso para auto-regenerarse. De hecho, la mayor evidencia de regeneración ósea es la curación de fracturas.

En la figura 1, se ilustra el proceso fisiológico que se desencadena cuando se produce una fractura y el tejido óseo reacciona para autorepararse así como la posibilidad de facilitar el proceso de regeneración o reparación ósea mediante el empleo de diferentes moléculas terapéuticas de actúan bien a nivel de promover la formación de hueso sobre osteoblastos o células madre mesenquimales o bloqueando la actividad de las células que degradan la matriz extracelular del hueso (osteoclastos) (Jakob et al., 2013).

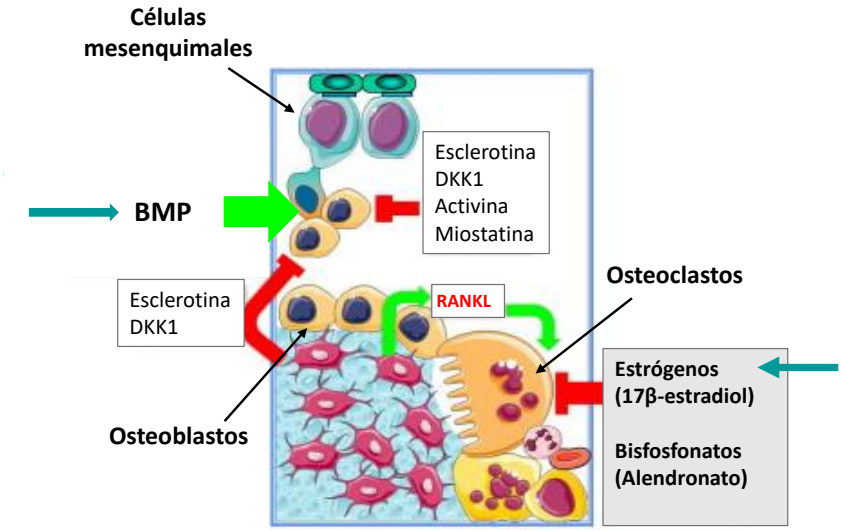

Figura 1. Representación de los principales factores que intervienen en la formación, regeneración y resorción de hueso. Las flechas verdes indican inducción y las rojas inhibición. La BMP induce la diferenciación de células mesenquimales a osteoblastos interviniendo en el proceso de remodelación y los estrógenos y bisfosfonatos actúan a nivel de la resorción ósea, disminuyendo la actividad osteoclástica. Figura adaptada de (Jakob et al., 2013).

En resumen, para el normal funcionamiento del tejido óseo y para estimular su reparación, se requiere de la presencia de células, factores de crecimiento, citoquinas y hormonas, es decir moléculas de señalización que organicen la respuesta celular y que desemboca en la diferenciación de las células mesenquimales pluripotenciales a osteoblastos (De Witte et al., 2018). Con ello se pone en evidencia el fundamento de las estrategias desarrolladas en este trabajo basadas en la utilización de MSC, BMP-2, 17β-estradiol, MMP-10, alendronato, hidroxiapatita y colágeno.

Este trabajo de investigación se inició después de que el grupo de investigación hubiera realizado una serie de estudios en animales osteoporóticos que revelaron que la implantación local de andamios, cargados con combinaciones de BMP-2 y 17β-estradiol formulados en microesferas de ácido poliláctico (PLA) o poli(láctico-co-glicólico) PLGA,

en defectos críticos de calota de rata, aumentaron la reparación ósea en ratas OP pero el hueso nuevo que rellenaba el defecto estaba menos mineralizado en comparación con los grupos sin OP (Segredo-Morales, García-García, et al., 2018; Segredo-Morales, Reyes, et al., 2018). Por tanto, las estrategias desarrolladas en el presente trabajo van principalmente dirigidas a mejorar la mineralización del hueso formado por acción de factores osteoestimulantes.

En primer lugar, cabe destacar el estudio inicial que se realiza y se detalla en el capítulo 1, relativo al establecimiento del modelo de rata OP. En los trabajos anteriores se había utilizado la combinación de ovariectomía y tratamiento con corticoides para inducir la OP, pero no se había realizado el análisis histológico para comprobar el estado de huesos de referencia como el fémur y lo que es más importante, la calota. Como comentamos, el modelo de defecto crítico en calota es muy popular para estudios de regeneración, por ello, se debe de resaltar la importancia de conocer cómo afectan los tratamientos utilizados para la inducción de la OP en el hueso que empleamos para evaluar la eficacia de nuestras estrategias. Estos resultados nos pusieron en evidencia que, efectivamente la OP inducida por la ovariectomía afecta tanto a huesos largos como a huesos planos y por tanto, es perfectamente válida para evaluar nuestros sistemas en el modelo de defecto crítico de calota de rata, sin producir un deterioro físico mayor en el animal.

Nuestra estrategia para este tipo de OP, simulación de la OP postmenopáusica, ha sido la presencia de 17β-estradiol y BMP-2 en los sistemas. El 17β-estradiol para suplir por un lado el déficit de estrógenos como consecuencia de la ovariectomía y por otro debido al importante papel que juega en la actividad de los osteoclastos. Mientras que la BMP-2 se empleó como factor involucrado en todas las etapas del proceso de regeneración de una fractura y, en el ciclo de remodelación ósea estimulando la diferenciación de las MSC a osteoblastos (Fig. 1). Estas medidas son eficaces en cuanto a regeneración, pero no alcanzan una correcta mineralización, por ello, el hidrogel de colágeno también fue enriquecido con HAP, como componentes del hueso. De hecho, los

resultados en cultivos celulares apoyaron nuestra hipótesis de que la presencia de HAP podría mejorar la mineralización.

Por otro lado, la baja solubilidad del 17β-estradiol en medios acuosos nos hizo incorporarlo en distintas formas para que se liberara a lo largo del tiempo. En las etapas iniciales podría disponerse del 17β-estradiol procedente del film o del disperso en el hidrogel mientras que a tiempos más largos sería liberado desde las microesferas. Así mismo, teniendo en cuenta que el proceso de reparación ósea en OP está retrasado hemos intentado que la liberación de las sustancias activas se prolongue más allá de las 4 semanas que había resultado útil en animales sanos (García-García et al., 2019; Segredo-Morales, García-García, et al., 2018; Segredo-Morales, Reyes, et al., 2018). Sin embargo, de acuerdo con los resultados ya comentados en el capítulo 1, no se observa una mejoría en la mineralización por ello, insistiendo un poco en la misma línea, se planteó el estudio recogido en el capítulo 2 en el que también se incorporan MSC con el objetivo de facilitar el efecto de la BMP-2 desde el inicio del proceso. Además, las microesferas de BMP-2 se elaboraron incluyendo alginato en la fase acuosa para retener la proteína y a su vez tener disponibilidad de la misma en etapas más tardías cuando se supone que el sistema estaría más poblado de células. Igualmente, nos preocupaba que el tiempo de permanencia de un hidrogel en el defecto fuera insuficiente para ejercer la función de guía para el crecimiento del tejido y, por ello, se comparó en esta segunda parte con un sistema en esponja que podría permanecer más tiempo en el lugar del defecto.

Si comparamos las liberaciones obtenidas (Fig. 2) vemos que efectivamente las estrategias aplicadas consiguen controlar la cesión de la BMP-2. Con el 17β-estradiol creemos que también podrían ser correctas las medidas aplicadas, aunque la imposibilidad de monitorizarlo *in vivo* sólo nos permite suponer que es así. Sin embargo, ni la incorporación de HAP, ni la presencia de rMSC, ni el retraso en la liberación de las sustancias activas, ni la mayor permanencia del sistema resultaron útiles para aumentar la mineralización del nuevo tejido.

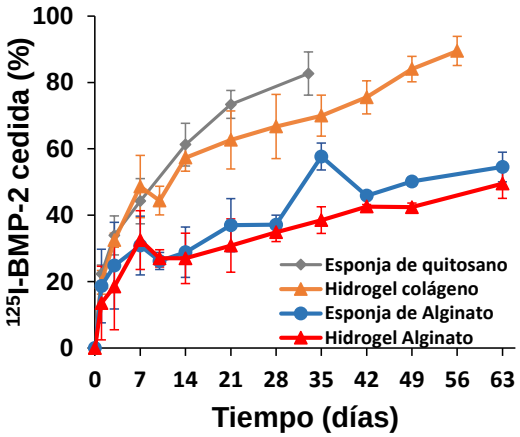

Figura 2. Cinética de liberación *in vivo* de ^{125}I-BMP-2 desde los diferentes sistemas ensayados.

La comparación de las figuras 3A y 3B, siempre con reservas porque son experimentos diferentes, nos muestra buenos resultados de regeneración en animales OP pero una incompleta mineralización. Si bien, analizando los resultados obtenidos con los hidrogeles frente a la esponja de alginato vemos que se confirma que una permanencia más prolongada del andamio en el defecto facilita la regeneración y la mejor calidad del tejido formado con un menor porcentaje de tejido adiposo y conectivo.

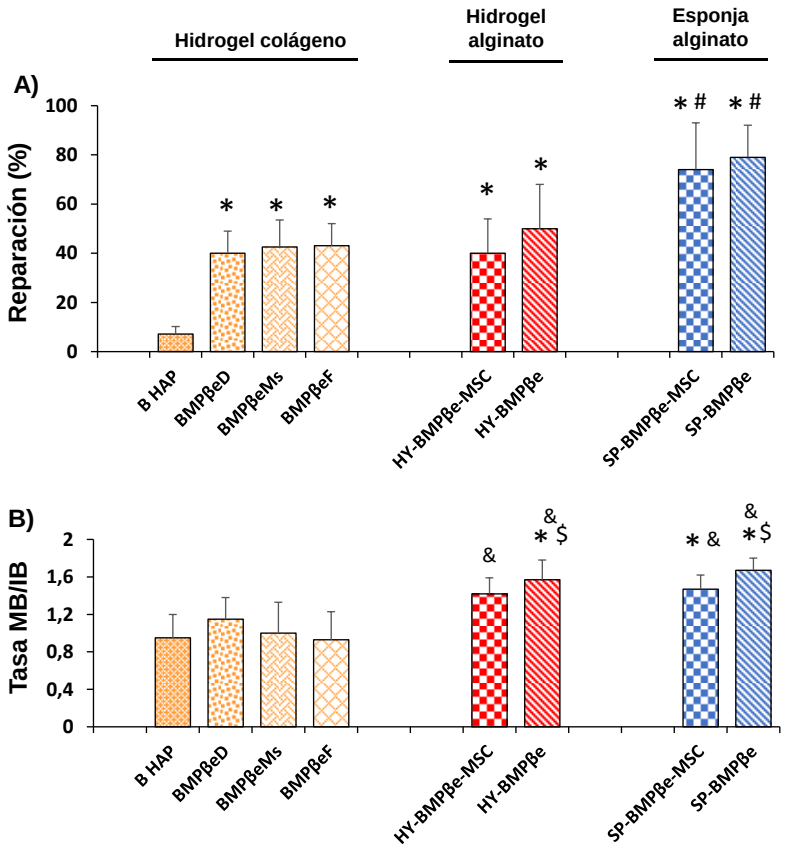

Figura 3. Representación gráfica en la que se compara el porcentaje de reparación (A) y la tasa de hueso maduro e inmaduro (MB/IB) (B) observados tras la implantación de los diferentes sistemas ensayados en calota de rata osteoporótica. (*) Indica diferencias estadísticamente significativas con el grupo B HAP, (#) indica diferencias estadísticamente significativas con BMPβeD, BMPβeMs, BMPβeF y con HY-BMPβe-MSC, ($) indica diferencias estadísticamente significativas con BMPβeMs, (&) indica diferencias estadísticamente significativas con BMPβeF.

Por último, hay que indicar que los resultados de mineralización descritos en los dos primeros capítulos se han realizados en muestras decalcificadas mediante la tinción de VOF. Esta técnica de coloración permite evaluar de

forma indirecta la mineralización del hueso y por tanto la madurez del mismo. El fundamento de dicha técnica se basa en que la deposición de hidroxiapatita en la matriz extracelular del hueso deja una impronta que permite la tinción diferencial de la misma en función del grado de mineralización, coloreándose de color azul las zonas menos mineralizadas o de mineralización más reciente (hueso inmaduro) y de color rojo oscuro a marrón las zonas más mineralizadas o de mineralización menos recientes (hueso maduro).

Por todo lo expuesto y, porque anteriormente el grupo de investigación había demostrado el efecto de la metaloproteinasa-10 (MMP-10) en la mineralización del hueso regenerado por la acción de la BMP-2, en un defecto crítico de calota en ratones sanos, en la última parte de esta memoria se decidió probar esta combinación en ratones OP (Reyes et al., 2018).

Por tanto, hemos cambiado de especie animal y por ello no hemos comparado los resultados con los anteriores. Además, en esta parte se realizó un trabajo *in vitro* en cultivos celulares exhaustivo y de acuerdo con los resultados la esponja de quitosano que se empleó tiene mayor consistencia que la esponja de alginato descrita anteriormente con el fin de facilitar su permanencia en el defecto. Así mismo, indicar que se elimina el 17β-estradiol pero se incluye en su lugar alendronato que actúa al mismo nivel que el estrógeno (Fig 1). Las microesferas elaboradas para encapsular las proteínas, BMP-2 y MMP-10 (en dos proporciones), permiten una liberación más prolongada en el tiempo que en nuestro estudio anterior (Reyes et al., 2018). Finalmente, con el fin de ser más precisos en la valoración de la mineralización del hueso formado, se inyectó azul calceína y oxitetraciclina a los animales, como marcadores de la tasa de mineralización y las muestras se analizaron sin descalcificar.

Los resultados nos confirman el efecto positivo de la combinación de MMP-10 con BMP-2, la tasa de mineralización para los tratamientos con BMP-2 + MMP-10 fue significativamente más alta que con BMP-2. Sin embargo, se observa una escasa regeneración de tejido en el defecto en comparación con los resultados expuestos en los capítulos anteriores.

Además, en el grupo de animales no-OP la regeneración en comparación con los resultados previamente publicados es significativamente menor. El conjunto de los resultados de este estudio junto con la experiencia anterior, indica que los scaffolds diseñados se ajustan más a los requisitos para la reparación del tejido óseo en animales OP que en animales sanos. En ratones OP, la combinación de BMP-2 y MMP-10 indujo un efecto regenerativo y una tasa de aposición mineral mejorada en comparación con los scaffolds que contienen BMP-2 sola o la combinación BMP-2 + ALD.

Por último, nuestros resultados en general sugieren que las necesidades para lograr una buena regeneración ósea en la población osteoporótica son diferentes a las de los animales sanos.

2. Referencias

De Witte, T.-M., Fratila-Apachitei, L. E., Zadpoor, A. A., & Peppas, N. A. (2018). Bone tissue engineering via growth factor delivery: from scaffolds to complex matrices. *Regenerative Biomaterials*, *5*(4). https://doi.org/10.1093/rb/rby013

Faibish, D., Ott, S. M., & Boskey, A. L. (2006). Mineral Changes in Osteoporosis. *Clinical Orthopaedics & Related Research*, *443*. https://doi.org/10.1097/01.blo.0000200241.14684.4e

García-García, P., Reyes, R., Segredo-Morales, E., Pérez-Herrero, E., Delgado, A., & Évora, C. (2019). PLGA-BMP-2 and PLA-17β-estradiol microspheres reinforcing a composite hydrogel for bone regeneration in osteoporosis. *Pharmaceutics*, *11*(12). https://doi.org/10.3390/pharmaceutics11120648

Jakob, F., Ebert, R., Ignatius, A., Matsushita, T., Watanabe, Y., Groll, J., & Walles, H. (2013). Bone tissue engineering in osteoporosis. *Maturitas*, *75*(2). https://doi.org/10.1016/j.maturitas.2013.03.004

Reyes, R., Rodríguez, J. A., Orbe, J., Arnau, M. R., Évora, C., & Delgado, A. (2018). Combined sustained release of BMP2 and MMP10 accelerates bone formation and mineralization of calvaria critical size defect in mice. *Drug Delivery*, *25*(1). https://doi.org/10.1080/10717544.2018.1446473

Rucci, N. (2008). Molecular biology of bone remodelling. *Clinical Cases Mineral and Bone Metabolism*, *5*(1), 49–56.

Segredo-Morales, E., García-García, P., Reyes, R., Pérez-Herrero, E., Delgado, A., & Évora, C. (2018). Bone regeneration in osteoporosis by delivery BMP-2 and PRGF from tetronic–alginate composite thermogel. *International Journal of Pharmaceutics*, *543*(1–2), 160–168. https://doi.org/10.1016/j.ijpharm.2018.03.034

Segredo-Morales, E., Reyes, R., Arnau, M. R., Delgado, A., & Évora, C. (2018). In situ gel-forming system for dual BMP-2 and 17β-estradiol controlled release for bone regeneration in osteoporotic rats. *Drug Delivery and Translational Research*, *8*(5), 1103–1113. https://doi.org/10.1007/s13346-018-0574-9

Conclusions

The conclusions of the developed work can be summarized as follows:

1- Among the osteoporosis models performed in rats, OVX and OD were characterized by alterations in calvaria and femur indicative of OP instauration. However, based on animal welfare OVX was selected in rats. Furthermore, an OP model was successfully developed and validated on mice following the OD strategy.

2- The *in vitro* release profile of 17β-estradiol depends on the release media selected and is highly conditioned by its aqueous solubility. BMP-2 release from PLGA microspheres can be tailored by modulating the microspheres composition.

3- The developed collagen-chitosan composite hydrogels were easily injectable and able to control BMP-2 release, probably due to the presence of nano-HAP. These systems induced a 40% bone regeneration in a calvaria critical defect in both non-OP and OP rats. No effect of the 17β-estradiol release profile was observed on the above-mentioned regeneration capacity.

4- In osteoporotic rats, the presence of BMP-2 and 17β-estradiol loaded solid scaffolds promoted a higher bone formation than hydrogels showing a similar release profile. This effect was associated to the residence time of the systems on the defect.

5- The incorporation of MMP-10 to scaffolds containing BMP-2 improved the mineral apposition rate of the bone regenerated in non-OP and OP mice. Moreover, the use of scaffolds containing MMP-10 and BMP-2 showing slow-release profile and high stability resulted in low regeneration capacity in non-OP animals but improved regeneration in OP animals.

6- The development of adequate systems for bone regeneration require to consider the tissue catabolic/anabolic balance to obtain biomaterials with a degradation/release behaviors suited for the existing tissue status. Among the strategies tested in this work; BMP-2, 17β-estradiol, alendronate, MMP-10 and seeding with MSC, the addition of MMP-10 to solid scaffolds was the only one able to promote suitable mineralization in OP animals.

Conclusiones

.

Annex

Ongoing experiments and future perspectives

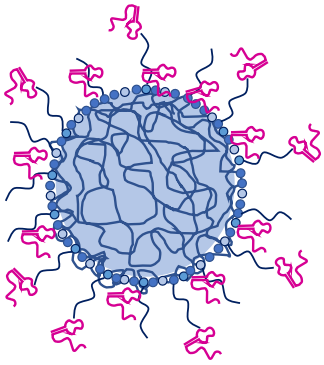

1. Introduction

As previously discussed, the new bone formed using the developed strategies in Chapters 1, 2 and 3 can be further improve. To enhance the quality of the regenerated bone a new approach was designed based on the use of hybrid nanoparticles (NPs) loaded with GapmeRs. To do this, I performed an international period at University of Oporto devoted to learn how to prepare NPs through microfluidic methods, their characterization and optimization. The use of gene therapy strategies devoted to control osteoblast activity and bone homeostasis have successfully increased osteogenesis *in vitro* in osteoporotic-derived mesenchymal stem cells and promoted mature bone formation in an *in vivo* model of osteoporosis (OP) (García-García et al., 2019).

Gene silencing has emerged as a promising tool for treating complex diseases such as cancer or systemic metabolic disorders as OP (Lundin et al., 2015). Despite the huge potential of synthetic oligonucleotides as gene silencing molecules, their efficient administration remains a challenge to beat due to their low stability, small cell internalization and lack of specificity (Juliano, 2016). Among synthetic oligonucleotides, GapmeRs are antisense oligonucleotides comprised of a synthetic single strand containing a central block of DNA nucleotides flanked by locked nucleic acids on each side. This structure provides several advantages as increased stability and decreased size when compared to other synthetic oligonucleotides (Abewe et al., 2020). Nanoparticulated systems allow for the incorporation of several therapeutic molecules on their structure that, owing to their surface modification abilities, can be specifically released to the target cells (Machado Cruz et al., 2019).

The main techniques to produce PLGA-based NPs are emulsion-based methods or nanoprecipitation. Recently, the microfluidic-based fabrication of NPs has been introduced. Microfluidic-based technology allows the manipulation of fluids within micro-scale channels that assures laminar flow patterns (Chiesa et al., 2018; Liu et al., 2018), offering a

controlled, homogenous and mild environment for NPs generation without turbulence. All these lead to numerous advantages over the conventional methods, such us batch-to-batch reproducibility, easy scale-up, high yield production, low reagent volumes, increased mass and heat transfer and narrow particle size distributions (Liu et al., 2018; Martins et al., 2018). A good mixing pattern is the main requirement in microfluidics-based technology. Mixing is produced by a molecular diffusion process because of the small mixing path and high contact surface involved (Liu et al., 2018). Regarding NPs preparation by nanoprecipitation using microfluidic methods they allow a rapid exchange between the solvent (partially water miscible organic solvent) and the non-solvent (aqueous phase) by diffusion throughout the interface between phases. This approach avoids the undesired NPs aggregation and decreases the average particle size and polydispersity index (PdI), since the nucleation happens first when the diffusion of the solvent starts instead of being a second step as is the case for conventional methods (Liu et al., 2018; Xu et al., 2017).

The physicochemical characteristics and composition of nanoparticles (NPs) condition both their *in vivo* and *in vitro* performance. Therefore, the development of nanomaterials with tailorable characteristics based on the selected application is a crucial step in the formulation development (Patra et al., 2018). However, the establishment of the formulation characteristics (composition, formulation procedures, concentrations…) responsible for the final formulation properties is complex. The nanosize nature of NPs makes these systems highly sensitive to any minimal change during formulation leading to unexpected formulation properties (Rouco et al., 2018). In order to obtain robust and reproducible formulations is crucial to understand the effect of the different components on the formulation characteristics. Moreover, NPs surface characteristics have been recognized as critical factors conditioning nanoparticle-cell interactions and proteins recognition (Godara et al., 2020). However, NPs surface electric charge should also be considered as it conditions nanoparticles bioavailability, absorption and cell uptake (Du et al., 2018). The entrance of NPs into the cells is an important step to

ensure therapeutic efficacy when designing formulations aimed at intracellular delivery, usually the case for antisense oligonucleotides delivery systems. Recently, the effect of cell status as cell cycle position and cell type on NPs endocytosis has been pointed out (Rees et al., 2019).

Hybrid lipid-polymer NPs are composed by a polymeric core surrounded by a lipid shell. They have numerous advantages combining the favorable characteristics of polymeric and lipid nanoparticles. Therefore, they possess high stability and physical integrity due to the polymeric core, and ease of functionalization, high stability in general circulation and cell uptake due to the lipid shell (Mukherjee et al., 2019). These characteristics make hybrid nanoparticles a promising next generation of drug delivery platforms. In hits sense, Zhu and coworkers (Zhu et al., 2017) proposed the preparation of self-assembled PEG-lipid-polymer hybrid NPs of different composition by a modified nanoprecipitation method to entrap siRNA with an EE of 50-60 % in PLGA-lipid PEG.

2. Objectives

The main objective of this work is to develop hybrid nanosystems able to incorporate GapmeRs suitable for intramedullary administration to improve the maturation of the induced bone formation in a critical bone defect. To obtain tailor made nanoparticles with the desired properties to target bone marrow MSC we initially aimed at understanding the effect of the shell lipid composition on nanoparticles physicochemical properties. NPs were prepared by two methods: conventional nanoprecipitation and microfluidic-based nanoprecipitation. On a next step, we evaluated the GapmeRs loading efficiency of the developed hybrid NPs.

3. Materials and methods

3.1. GapmeR condensation using protamine

The ability of the cationic protein protamine to interact with GapmeR and promote its complexation was evaluated using three different oligonucleotide:protein weight ratios (1:2, 1:1 and 1:0,5). GapmeRs were

allowed to interact with the protein for 40 minutes at room temperature. Samples were then loaded on 15 % acrylamide gels and electrophoresis was performed for 45 min. The migration of the GapmeR was visualized by ethidium bromide staining.

3.2. Hybrid nanoparticles preparation

3.2.1. Conventional nanoprecipitation method

Lipid-polymer hybrid nanoparticles were prepared by a modified single-step nanoprecipitation method. Briefly, poly (lactide.coglycolide acid) (PLGA, Resomer® RG 502 H, Mw: 7,000-17,000, Evonik Industries) or PLGA+DOTAP (1,2-dioleoyl 1.3-trimethylammonium-propane, Sigma-Aldrich) at the desired concentrations depicted in Table 1 were dissolved in acetone (1mL) then, 50µL of an aqueous solution of protamine or protamine+GapmeR were added and mixed. Immediately, this mixture was poured on an aqueous solution (4% ethanol in water; 10mL) containing the required amount of DSPE-PEG_{2000} (Nanosoft Polymers) with or without lecithin (L-α-phosphatidylcholine, Avanti Polar Lipids) (Table 1). Lecithin was previously dissolved on the aqueous phase by heating the solution to 65 °C. To obtain GapmeR loaded nanoparticles the oligonucleotide was condensed with the protamine at a oligonucleotide:protamine 1:2 weight ratio for 40 minutes before their addition. The GapmeR was custom designed and synthesized by Integrated DNA Technologies.

3.2.2. Microfluidic-based nanoprecipitation

Hybrid nanoparticles were prepared by a nanoprecipitation method using two different micromixer chips (A: Part N° 3000158, B: Part N° 3200401, Dolomite microfluidics). The used settings are shown in Figure 1. Aqueous and organic phases were prepared as described above for the conventional method using the amounts described in Table 2. In this case, two different organic solvents were tested acetone (ACT) and acetonitrile (ACN). When protamine was used on the NPs (M3) 50 µL of the solution at 0.9mg/mL were added to the organic phase and mixed. Both phases

were filtered using 0.45 µm filters in order to remove potential precipitates before their loading on the syringe. Afterwards, the aqueous phase was introduced in the selected micromixer chip at a flow rate of 1 mL/min, by means of a syringe pump (KD scientific, model 569), until a total aqueous phase volume of 6 mL per formulation was achieved. Simultaneously, the organic phase was also introduced in the micromixer chip using a Mitos-Duo-XS-Pump (Dolomite microfluidics) at a flow rate of 200 µL/min, until a total organic phase volume of 1 mL per formulation was achieved.

Nanoparticle suspensions were collected during the formulation process in a beaker and kept under constant stirring until the remaining organic solvent was completely evaporated.

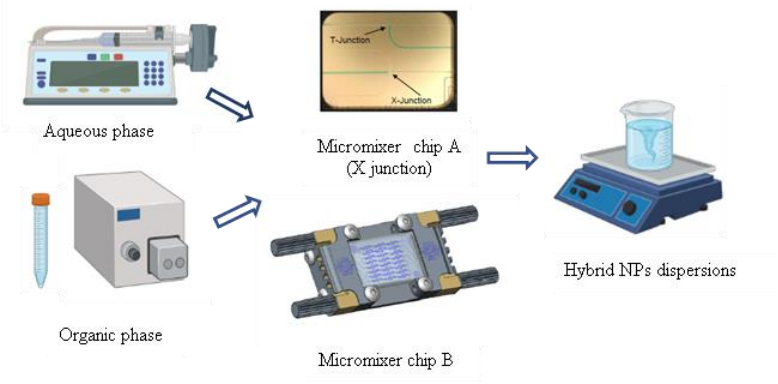

Figure 1. Schematic representation of the microfluidic system employed.

3.3. Physicochemical characterization of hybrid nanoparticles

The physicochemical properties of the nanoparticles were characterized in terms of average diameter, polydispersity index (PdI) and Zeta-potential (ζ-potential) on a Zetasizer Nano-ZS (Malvern Instruments). Samples were adequately diluted in ultrapure Milli-Q water and sonicated for one minute on a water bath before characterization (P Selecta). All measurements were performed in triplicate for each sample.

3.4. Encapsulation efficiency of hybrid nanoparticles

To analyze the encapsulation efficiency of NPs, fluorescently labelled GapmeRs were used (IDT Technologies). Formulations were prepared as described above and NPs suspensions were filtered through 10 KDa MWCO (Millipore Amicon) filters. Non-encapsulated oligonucleotide was quantified on the filtrate by measuring the fluorescence on a plate reader (Biotek). Oligonucleotide concentration was assessed by means of the correspondent calibration curve. The physicochemical properties of GapmeR-loaded NPs were also analyzed as described above.

4. Results

4.1. Protamine complexation of the selected GapmeR

Figure 2 shows the migration of GapmeRs alone (denoted as 1:0) or complexed with variable amounts of protamine. The addition of protamine to the oligonucleotide solution indeed promoted its complexation with the protein avoiding GapmeR migration. Moreover, while the GapmeR:Protamine ratio 1:0.5 led to some free oligonucleotide, an increase in the protein amount (1:1 and 1:2 ratios) completely blocked oligonucleotide migration indicating its successful complexation with protamine. Therefore the selected ratio used for further experiments was 1:2 GapmeR:Protamine.

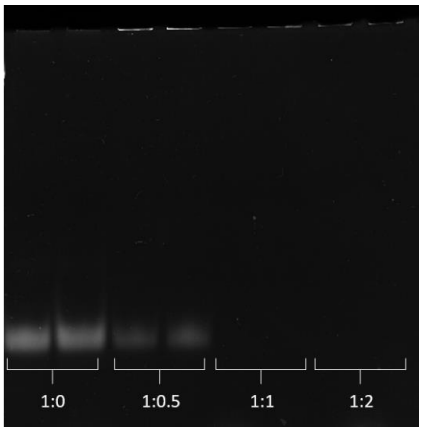

Figure 2. Gel electrophoresis of GapmeR alone (1:0) or GapmeR:Protamine complexes at 1:0.5, 1:1 and 1:2 weight rations in a 15 % acrylamide gel.

4.2. Analysis of composition-properties relationship of NPs obtained by the conventional nanoprecipitation method

Hybrid nanoparticles with suitable physicochemical properties were successfully obtained by a modified single-step nanoprecipitation method without the need of synthetic surfactants. The physicochemical characteristics of the developed formulations are shown in Table 1. As indicated below, the core components were kept constant for all the formulations (PLGA 5mg/batch and protamine 45 µg/batch) while the lipid components of the shell were combined of variable proportions. The amount of DOTAP tested varied from 0 to 0.5 mg, DSPE-PEG_{2000} was used in variable amounts from 0 to 1.45 mg and soy lecithin was studied using proportions from 0 to 2 mg. Further compositions were tested but discarded due to high size (> 200 nm) and/or PdI (> 0.20). All the selected formulations presented adequate size ranging from 137.6 to 179.77 nm with low standard deviation. The PdI values of the analyzed formulations was between 0.08 and 0.19 also with low standard deviation. As expected, ζ-potential values were highly variable, obtaining formulations from -34.30 to +51.7 mV with different standard deviation depending on the composition.

Table 1. Shell composition and physicochemical characteristics of the analyzed formulations prepared by nanoprecipitation using the conventional method. Core components were kept constant (PLGA 5mg/batch and protamine 45 µg/batch).

	DOTAP	DSPE-PEG_{2000}	Lecithin	**Size (nm)**		**PdI**		**ζ-potential**	
	mg	mg	mg	Mean	SD	Mean	SD	Mean	SD
C1	-	-	2.00	179.77	3.76	0.18	0.03	38.97	3.24
C2	-	-	1.20	171.75	5.87	0.13	0.04	-6.33	28.57
C3	-	0.43	0.60	150.77	0.78	0.11	0.01	-34.30	1.85
C4	-	0.85	0.60	178.47	2.48	0.09	0.02	-24.47	2.91
C5	-	1.45	0.55	161.50	0.36	0.19	0.02	-25.57	2.06
C6	-	1.10	0.4	170.34	20.81	0.12	0.01	-20.68	5.70
C7	0.10	-	0.30	176.45	11.29	0.08	0.01	28.72	9.64
C8	0.10	-	0.40	176.22	0.12	0.12	0.04	32.23	2.12
C9	0.20	-	0.30	178.07	2.42	0.10	0.04	51.07	2.58
C10	0.20	-	0.40	184.02	5.49	0.08	0.01	44.72	0.64
C11	0.20	0.43	0.30	167.77	0.91	0.10	0.004	35.33	3.20
C12	0.20	0.43	0.40	163.56	9.66	0.13	0.06	13.87	8.86
C13	0.20	0.43	0.60	173.57	5.81	0.10	0.03	14.33	0.23
C14	0.20	1.10	0.20	168.85	21.96	0.08	0.01	0,30	11,46
C15	0.40	-	-	167.40	0.72	0.06	0.002	49.43	1.31
C16	0.40	0.55	-	153.93	1.79	0.10	0.004	39.55	0.64
C17	0.40	0.43	-	165.03	0.45	0.10	0.02	44.37	2.75
C18	0.40	0.85	-	144.97	1.40	0.10	0.01	28.07	1.40
C19	0.40	0.85	0.60	166.10	4.37	0.16	0.06	19.80	0.50
C20	0.4	1.10	-	162.90	14.97	0.09	0.01	25,08	6.89
C21	0.50	0.90	0.10	145.37	0.49	0.11	0.01	35.30	0.89

Based on the results obtained the surface charge of the nanoparticles can be tailored by controlling the amount of DOTAP on the lipid shell.

4.3. Analysis of the composition-properties relationship by microfluidic nanoprecipitation method

In order to select the most suitable solvent for the preparation of lipid-polymer hybrid NPs by microfluidic-based nanoprecipitation, two blank formulations (without including protamine) of identical composition, were prepared using either acetone (ACT; M1) or acetonitrile (ACN; M2) as organic solvents. As shown in Table 2, hybrid nanoparticles exhibiting a low particle size, a narrow size distribution, along with a negative surface charge were obtained in both cases. As for the conventional nanoprecipitation method further compositions were tested but discarded due to high size and/or PdI. Among the adequate formulations M2 exhibited superior properties in terms of particle size and size distribution. Furthermore, while in the case of M1 a PLGA precipitate was formed in the micromixer channels during the formulation process, in F2 this precipitate was not noticeable, and therefore, acetonitrile was selected as organic solvent to continue with further assays.

Starting from the basis of M2 and grounded on the effect of surface modification DOTAP addition this lipid was added to the organic phase to modulate surface charge. In addition, due to the absence of a PLGA precipitate with the use of acetonitrile as organic solvent, the polymer concentration was increased in order to improve NPs loading capacity. In this case, a different micromixer (chip B) was selected to prepare this last formulation. This micromixer type is known to lead to NPs exhibiting lower particle sizes and distributions due to the presence of several mixing points, but it is also more sensitive to polymer precipitation in the microchannels, and therefore could not be employed in the previous step.

In this way, as can be derived from Table 2, hybrid nanoparticles exhibiting suitable particle sizes together with highly narrow particle size distributions were obtained (M3). Moreover, a slight decrease in zeta potential values related to the presence of DOTAP was observed

regarding the previous formulations consistent with the effect observed after DOTAP addition on conventional nanoprecipitation.

Table 2. NPs composition and physicochemical characteristics of the analyzed formulations prepared by microfluidic-based nanoprecipitation. *Denotes the formulation including protamine.

	PLGA	DOTAP	Solvent	DSPE-PEG_{2000}	Lecithin	Chip	**Size (nm)**		**PdI**		**ζ-potential**	
	mg	mg		mg	mg		Mean	SD	Mean	SD	Mean	SD
M1	1.25	-	ACT	0.330	0.096	A	126.87	2.41	0.27	0.00	-29.97	0.46
M2	1.25	-	ACN	0.330	0.096	A	103.83	3.11	0.23	0.03	-37.37	1.39
M3*	2.5	0.15	ACN	0.330	0.096	B	151.87	3.02	0.16	0.01	-24.43	4.48

4.4. Encapsulation efficiency of lipid-polymer hybrid NPs

The capacity of some of the developed NPs to incorporate oligonucleotides was determined. Three compositions were selected based on their variable surface charge C6, C14 and C20. All nanoparticles showed high GapmeR encapsulation efficiency with no significant differences between the samples being of 83.27 ± 1.14 % for C6, 84.55 ± 0.41 % for C14 and 84.47 ± 0.52 % for C20. Moreover, while no effect of GapmeR incorporation was observed on NPs size, the NPs surface charge was modified on a composition-dependent manner. NPs presenting almost neutral surface charge (C14) significantly decreased their ζ-potential with the incorporation of GapmeR reaching a value of -20.83 ± 0.94.

5. Discussion

Lipid-polymer hybrid nanoparticles were obtained without requiring the use of surfactants, other than soy lecithin, showing a monodisperse distribution with an adequate diameter by both of the methods used. Remarkably, the formulations we prepared following our developed protocols presented similar size or even lower than those reported by other authors for hybrid PLGA nanoparticles using similar methodology (Ling et al., 2010; Yue et al., 2011). Surfactants are commonly included in nanoparticulated systems during the formulation step to control the

formation, morphology, and surface properties of NPs (Wang et al., 2005). Moreover, their use as stabilizers to avoid particle aggregation is a common practice for both metallic and polymeric NPs (Kennedy et al., 2018; Khan et al., 2019). However, the presence of synthetic surfactants on NPs surface hinders their interaction with the surrounding components while conditioning cell binding and target recognition (Khan et al., 2019). Furthermore, synthetic surfactants are highly toxic and compromise the cytocompatibility of the final formulations. In this context, natural surfactants as lecithins have been proposed as alternatives in NPs formulation due to their high biocompatibility and amphiphilicity, presenting great emulsifying properties (Vater et al., 2019). Therefore, the NPs designed in this work presented adequate characteristics evading the drawbacks of synthetic surfactants.

NPs with variable composition (C6, C14 and C20) were loaded with nucleic acids (GapmeRs) by their incorporation in the polymeric core. Oligonucleotides were condensed with the cationic protein (protamine) showing adequate complexation (Figure 2). This approach led to high encapsulation efficiencies for all the formulations tested. Hybrid nanoparticles have been already tested as gene delivery systems. However, these NPs were superficially loaded with oligonucleotides based on a surface charge-dependent mechanism through electrostatic complexation (Dave et al., 2019). This strategy entangles the risk of nucleic acid desorption during storage or administration and higher exposure to nucleases in the extracellular space (Roberts et al., 2020; Yang et al., 2019). On the other hand, the method followed on this work, unlike superficial ionic loading, allowed to reach an adequate oligonucleotide incorporation independent of NPs surface charge.

6. Conclusion

The results obtained in this study proved the conventional nanoprecipitation technique is adequate to obtain lipid-polymer NPs with adequate encapsulation capacity and physicochemical properties for the intended purpose. According to the bibliography consulted, microfluidics allows to obtain a production of NPs with less difference between batches

and with a more homogeneous and narrow distribution size than conventional strategies. However, our experimental data do not show a clear difference between NPs obtained by both methods but clearly points out to the need of changing the solvent to adapt to the microfluidic synthesis method. Therefore, according to the results obtained so far, we still need to optimize the conditions to obtain NPs with improved properties using microfluidic-based nanoprecipitation.

7. References

Abewe, H., Deshmukh, S., Mukim, A., & Beliakova-Bethell, N. (2020). Use of GapmeRs for gene expression knockdowns in human primary resting CD4+ T cells. *Journal of Immunological Methods*, *476*. https://doi.org/10.1016/j.jim.2019.112674

Chiesa, E., Dorati, R., Modena, T., Conti, B., & Genta, I. (2018). Multivariate analysis for the optimization of microfluidics-assisted nanoprecipitation method intended for the loading of small hydrophilic drugs into PLGA nanoparticles. *International Journal of Pharmaceutics*, *536*(1). https://doi.org/10.1016/j.ijpharm.2017.11.044

Dave, V., Tak, K., Sohgaura, A., Gupta, A., Sadhu, V., & Reddy, K. R. (2019). Lipid-polymer hybrid nanoparticles: Synthesis strategies and biomedical applications. *Journal of Microbiological Methods*, *160*. https://doi.org/10.1016/j.mimet.2019.03.017

Du, X.-J., Wang, J.-L., Iqbal, S., Li, H.-J., Cao, Z.-T., Wang, Y.-C., Du, J.-Z., & Wang, J. (2018). The effect of surface charge on oral absorption of polymeric nanoparticles. *Biomaterials Science*, *6*(3). https://doi.org/10.1039/C7BM01096F

García-García, P., Ruiz, M., Reyes, R., Delgado, A., Évora, C., Riancho, J. A., Rodríguez-Rey, J. C., & Pérez-Campo, F. M. (2019). *Smurf1* Silencing Using a LNA-ASOs/Lipid Nanoparticle System to Promote Bone Regeneration. *STEM CELLS Translational Medicine*, *8*(12). https://doi.org/10.1002/sctm.19-0145

Godara, S., Lather, V., Kirthanashri, S. V., Awasthi, R., & Pandita, D.

(2020). Lipid-PLGA hybrid nanoparticles of paclitaxel: Preparation, characterization, in vitro and in vivo evaluation. *Materials Science and Engineering: C*, *109*. https://doi.org/10.1016/j.msec.2019.110576

Juliano, R. L. (2016). The delivery of therapeutic oligonucleotides. *Nucleic Acids Research*, *44*(14). https://doi.org/10.1093/nar/gkw236

Kennedy, P. J., Perreira, I., Ferreira, D., Nestor, M., Oliveira, C., Granja, P. L., & Sarmento, B. (2018). Impact of surfactants on the target recognition of Fab-conjugated PLGA nanoparticles. *European Journal of Pharmaceutics and Biopharmaceutics*, *127*. https://doi.org/10.1016/j.ejpb.2018.03.005

Khan, R., Inam, M., Khan, S., Jiménez, A., Park, D., & Yeom, I. (2019). The Influence of Ionic and Nonionic Surfactants on the Colloidal Stability and Removal of CuO Nanoparticles from Water by Chemical Coagulation. *International Journal of Environmental Research and Public Health*, *16*(7). https://doi.org/10.3390/ijerph16071260

Ling, G., Zhang, P., Zhang, W., Sun, J., Meng, X., Qin, Y., Deng, Y., & He, Z. (2010). Development of novel self-assembled DS-PLGA hybrid nanoparticles for improving oral bioavailability of vincristine sulfate by P-gp inhibition. *Journal of Controlled Release*, *148*(2). https://doi.org/10.1016/j.jconrel.2010.08.010

Liu, D., Zhang, H., Fontana, F., Hirvonen, J. T., & Santos, H. A. (2018). Current developments and applications of microfluidic technology toward clinical translation of nanomedicines. *Advanced Drug Delivery Reviews*, *128*. https://doi.org/10.1016/j.addr.2017.08.003

Lundin, K. E., Gissberg, O., & Smith, C. I. E. (2015). Oligonucleotide Therapies: The Past and the Present. *Human Gene Therapy*, *26*(8). https://doi.org/10.1089/hum.2015.070

Machado Cruz, R., Santos-Martinez, M. J., & Tajber, L. (2019). Impact of polyethylene glycol polymers on the physicochemical properties and mucoadhesivity of itraconazole nanoparticles. *European Journal of Pharmaceutics and Biopharmaceutics*, *144*.

https://doi.org/10.1016/j.ejpb.2019.09.004

Martins, J. P., Torrieri, G., & Santos, H. A. (2018). The importance of microfluidics for the preparation of nanoparticles as advanced drug delivery systems. In *Expert Opinion on Drug Delivery* (Vol. 15, Issue 5, pp. 469–479). Taylor and Francis Ltd. https://doi.org/10.1080/17425247.2018.1446936

Mukherjee, A., Waters, A. K., Kalyan, P., Achrol, A. S., Kesari, S., & Yenugonda, V. M. (2019). Lipids-polymer hybrid nanoparticles as a next-generation drug delivery platform: state of the art, emerging technologies, and perspectives</p>. *International Journal of Nanomedicine*, *Volume 14*. https://doi.org/10.2147/IJN.S198353

Patra, J. K., Das, G., Fraceto, L. F., Campos, E. V. R., Rodriguez-Torres, M. del P., Acosta-Torres, L. S., Diaz-Torres, L. A., Grillo, R., Swamy, M. K., Sharma, S., Habtemariam, S., & Shin, H.-S. (2018). Nano based drug delivery systems: recent developments and future prospects. *Journal of Nanobiotechnology*, *16*(1). https://doi.org/10.1186/s12951-018-0392-8

Rees, P., Wills, J. W., Brown, M. R., Barnes, C. M., & Summers, H. D. (2019). The origin of heterogeneous nanoparticle uptake by cells. *Nature Communications*, *10*(1). https://doi.org/10.1038/s41467-019-10112-4

Roberts, T. C., Langer, R., & Wood, M. J. A. (2020). Advances in oligonucleotide drug delivery. *Nature Reviews Drug Discovery*, *19*(10). https://doi.org/10.1038/s41573-020-0075-7

Rouco, H., Diaz-Rodriguez, P., Rama-Molinos, S., Remuñán-López, C., & Landin, M. (2018). Delimiting the knowledge space and the design space of nanostructured lipid carriers through Artificial Intelligence tools. *International Journal of Pharmaceutics*, *553*(1–2). https://doi.org/10.1016/j.ijpharm.2018.10.058

Vater, C., Adamovic, A., Ruttensteiner, L., Steiner, K., Tajpara, P., Klang, V., Elbe-Bürger, A., Wirth, M., & Valenta, C. (2019). Cytotoxicity of lecithin-based nanoemulsions on human skin cells and ex vivo skin permeation: Comparison to conventional surfactant

types. *International Journal of Pharmaceutics*, *566*. https://doi.org/10.1016/j.ijpharm.2019.05.078

Wang, W., Gu, B., & Liang, L. (2005). Effect of Surfactants on the Formation, Morphology, and Surface Property of Synthesized SiO_2 Nanoparticles. *Journal of Dispersion Science and Technology*, *25*(5). https://doi.org/10.1081/DIS-200027309

Xu, J., Zhang, S., Machado, A., Lecommandoux, S., Sandre, O., Gu, F., & Colin, A. (2017). Controllable Microfluidic Production of Drug-Loaded PLGA Nanoparticles Using Partially Water-Miscible Mixed Solvent Microdroplets as a Precursor. *Scientific Reports*, *7*(1). https://doi.org/10.1038/s41598-017-05184-5

Yang, Z., Qian, Y., Yang, F., Chen, C., Tang, X., & Jin, J. (2019). Investigating Adsorption/Desorption of DNA on ZIF-8 Surface by Fluorescently Labeled Oligonucleotides. *Langmuir*, *35*(49). https://doi.org/10.1021/acs.langmuir.9b02692

Yue, Z.-G., Wei, W., Lv, P.-P., Yue, H., Wang, L.-Y., Su, Z.-G., & Ma, G.-H. (2011). Surface Charge Affects Cellular Uptake and Intracellular Trafficking of Chitosan-Based Nanoparticles. *Biomacromolecules*, *12*(7). https://doi.org/10.1021/bm101482r

Zhu, X., Tao, W., Liu, D., Wu, J., Guo, Z., Ji, X., Bharwani, Z., Zhao, L., Zhao, X., Farokhzad, O. C., & Shi, J. (2017). Surface de-PEGylation controls nanoparticle-mediated siRNA delivery in vitro and in vivo. *Theranostics*, *7*(7), 1990–2002. https://doi.org/10.7150/thno.18136

Published papers

Regenerative Biomaterials, 2019, 149–162
doi: 10.1093/rb/rbz018
Advance Access Publication Date: 10 May 2019
Research Article

New injectable two-step forming hydrogel for delivery of bioactive substances in tissue regeneration

Edgar Pérez-Herrero [1,2,†], Patricia García-García[1,†], Jaime Gómez-Morales[3], Matias Llabrés[1,4], Araceli Delgado [1,2] and Carmen Évora [1,2,*]

[1]Department of Chemical Engineering and Pharmaceutical Technology, University of La Laguna, La Laguna 38200, Tenerife, Spain; [2]Institute of Biomedical Technologies (ITB), Center for Biomedical Research of the Canary Islands (CIBICAN), University of La Laguna, La Laguna 38071, Tenerife, Spain; [3]Laboratory of Crystallographic Studies, Andalusian Earth Sciences Institute, Spanish Research Council—University of Granada, Armilla, Granada 18100, Spain; [4]Institute of Tropical Diseases and Healthcare of the Canary Islands, University of La Laguna, La Laguna 38203, Tenerife, Spain

*Correspondence address. Department of Chemical Engineering and Pharmaceutical Technology, University of La Laguna, La Laguna 38200, Tenerife, Spain. E-mail: cevora@ull.es
†These authors have contributed equally in this work.

Received 20 December 2018; revised 6 March 2019; accepted on 21 March 2019

Abstract

A hydrogel based on chitosan, collagen, hydroxypropyl-γ-cyclodextrin and polyethylene glycol was developed and characterized. The incorporation of nano-hydroxyapatite and pre-encapsulated hydrophobic/hydrophilic model drugs diminished the porosity of hydrogel from 81.62 ± 2.25% to 69.98 ± 3.07%. Interactions between components of hydrogel, demonstrated by FTIR spectroscopy and rheology, generated a network that was able to trap bioactive components and delay the burst delivery. The thixotropic behavior of hydrogel provided adaptability to facilitate its implantation in a minimally invasive way. Release profiles from microspheres included or not in hydrogel revealed a two-phase behavior with a burst- and a controlled-release period. The same release rate for microspheres included or not in the hydrogel in the controlled-release period demonstrated that mass transfer process was controlled by internal diffusion. Effective diffusion coefficients, D_{eff}, that describe internal diffusion inside microspheres, and mass transfer coefficients, h, i.e. the contribution of hydrogel to mass transfer, were determined using 'genetic algorithms', obtaining values between $2.64 \cdot 10^{-15}$ and $6.67 \cdot 10^{-15}$ m^2/s for D_{eff} and $8.50 \cdot 10^{-10}$ to $3.04 \cdot 10^{-9}$ m/s for h. The proposed model fits experimental data, obtaining an R^2-value ranged between 95.41 and 98.87%. *In vitro* culture of mesenchymal stem cells in hydrogel showed no manifestations of intolerance or toxicity, observing an intense proliferation of the cells after 7 days, being most of the scaffold surface occupied by living cells.

Keywords: hydrogel; collagen–cyclodextrin–chitosan; rheology; mass transfer; estradiol; FITC-dextran

Introduction

Hydrogels are three-dimensional hydrophilic polymeric networks, which are able to absorb and retain large quantities of water, solvents or biological fluids in the free space of their structure without being dissolved in the same media. They can be generated through physical crosslinking by weak cohesive forces, like ionic or hydrogen bonds and π–π or van der Waals interactions, or chemical crosslinking by stable covalent forces that improve the mechanical properties

of the hydrogel. However, the toxicity derived from the use of crosslinking agents, like glutaraldehyde, and the possibility of irreversible broken bonds that can fracture the structure, are some of the drawbacks of the chemical crosslinking [1–3]. The high permeability and porosity of hydrogels facilitates, not only integration in the majority of tissues, but also incorporation by the cells, and their biocompatibility and biodegradation avoid surgery to remove polymer after treatment [2, 3]. Moreover, their similarity to the extracellular matrix or tissues, low interfacial tension between gel and solvents, and minimal irritation after application due to their water content and soft nature [2, 3] have made hydrogels the ideal candidates for biomedical and pharmaceutical applications, such as implants and sutures, wound dressings, controlled drug delivery, diagnostic imaging, medical and biological sensors or microfluidics [3, 4]. In this regard, *'in situ'* two-step forming injectable hydrogels have attracted the attention of scientific community since they can be implanted without surgery directly by injection in the treatment site, where the crosslinker agent forms stable scaffolds. Rheology of this type of hydrogels provides adaptability to the shape of the area to be treated, an easy '*in vivo*' implantation in a minimally invasive way and capacity to incorporate bioactive substances and/or cells.

A long list of biodegradable natural or synthetic polymers has been used to prepare hydrogels. Natural polymers include polysaccharide-based polymers (chitosan, alginate, cellulose, dextran, gellan or guar gum, cyclodextrins and hyaluronic acid) and protein-based polymers (gelatin, collagen, albumin, fibrin or heparin). Although they are abundant in nature and can be part of biological events, such as signaling or cell adhesion, they do not have good mechanical properties and tunable degradation by themselves and can lead to possible immunogenic responses [4, 5]. In particular, polysaccharide-based hydrogels offer interesting options to enclose molecules since they can be easily formed by mild conditions methods, like ionic gelation or complexation in aqueous environments at room temperature, avoiding the use of organic solvents and high shear homogenization or ultrasonication. In fact, chitosan, a cationic natural linear polymer derived from chitin and composed of D-glucosamine and *N*-acetyl-D-glucosamine units, gels by interaction with polyanions, like the negatively charged and nontoxic tripolyphosphate (TPP) [6]. Chitosan-based hydrogels have been used as injectable platforms in controlled drug delivery and tissue engineering applications [5]. Moreover, chitosan can be mixed with the protein-based polymer collagen since both solutions are miscible and chitosan does not denature collagen [7]. The strategy of adding collagen to hydrogel formulation brings advantages like enhanced mechanical strength, biocompatibility and biodegradability, and a more efficient cellular growth [4]. Although collagen can form gels by natural means, the resulting mechanical strength is weak, being necessary the use of crosslinking agents. For example, glutaraldehyde or formaldehyde have demonstrated effectiveness in creating crosslinking structures in collagen but limit their application in biomedical systems because of their cytotoxicity [3, 8]. Another option to crosslink collagen is the use of water-soluble carbodiimides, although they are not usable when the enclosed bioactive substances are proteins because they react with them [3]. Riboflavin combined with ultraviolet-A light has been widely used in clinic to reinforce the collagen structure of the cornea in the treatment of keratoconus [9, 10]. Therefore, this seems to be a good strategy to induce crosslinking of collagen and increase its mechanical strength without compromising cell viability. Moreover, the addition of cyclodextrins, a cyclic oligosaccharide composed of six to eight glucopyranose units, can lead to the formation of inclusion complexes with certain polymer regions. The toxicity of these compounds decreases with increasing number of glucopyranose units, thus, gamma cyclodextrins are less toxic than alpha or beta ones [11]. Synthetic polymers, like poly(DL-lactide-co-glycolide) (PLGA), poly(DL-lactide) (PLA), poly(vinyl alcohol) (PVA), poly(acrylic acid) (PAA), polyethylene glycol (PEG), can enhance and control the mechanical strength and degradation rates of hydrogels. Still, they do not provide the optimal environment for cell inclusion and tissue regeneration, so, a combination of both types of polymers, natural and synthetic, must be used for the biomedical application of hydrogels [5, 12, 13]. Moreover, the incorporation of inorganic components into the hydrogel structure, such as hydroxyapatite (HAp) i.e. part of the bone matrix, have been used in hard tissue repair to reinforce the mechanical properties of the hydrogel [14]. In this regard, nanosized HAp (nano-HAp) should be used to promote their degradation by osteoblastic enzymes, like the alkaline phosphatase, and form new tissue by osteoblasts, being this size the optimum for enhanced cell adhesion and proliferation [14].

Bioactive substances can be released from hydrogels by either degradation of polymer or diffusion through the pores of their structure, or by a combination of both. Release profiles in these systems typically reveal a two-phase behavior, a burst step followed by a slow controlled release period. Because of burst may cause high concentrations of bioactive substances in the application site and consequently loss of these drugs, more complex systems are required to reduce such burst profiles, maintaining the total delivery values in longer periods.

In this work, an innovative hydrogel based on biocompatible and biodegradable polymers, such as, chitosan, collagen, hydroxypropyl-γ-cyclodextrin (HP-γ-CD) and PEG, has been designed, developed and characterized in terms of porosity, rheology and mass transfer studies. The hydrogel was injectable, adaptable to treatment sites with diverse dimensions and shapes, easily crosslinked by means of TPP and blue light and presented adequate characteristic for good cell adhesion, viability and proliferation. Moreover, 17-β-estradiol or rhodamine-B-isothiocyanate-dextran (RITC-dextran), as low molecular weight hydrophobic or high molecular weight hydrophilic model drugs, respectively, were encapsulated in PLGA/PLA microspheres and included in the hydrogel, together with the nano-HAp for further use in bone regeneration.

Materials and methods

Materials

PLGA Resomer® RG504 (acid-terminated, lactide:glycolide 50:50, M_w 38–54 kDa) and RG858S (ester-terminated, lactide:glycolide 85:15, M_w 190–240 kDa) and PLA Resomer® RG203-S (ester-terminated, M_w 18–28 kDa) were acquired from Boehringer-Ingelheim (Germany). HP-γ-CD (CAVASOL® W8 HP) was obtained from Wacker (Germany). Ultrapure chitosan Protasan™ UP-CL-213 (86% deacetylation, viscosity 150 mPa·s at 1 wt. % aqueous solution) and ultrapure alginate Pronova™ UP MVG were purchased from NovaMatrix (Norway). Bovine collagen, type I, was purchased from CellSystems Biotechnologie Vertrieb GmbH (Germany). Calcium chloride dihydrate (Bioxtra, ≥99% pure), sodium citrate tribasic dihydrate (ACS reagent, ≥99% pure), disodium hydrogen phosphate (ACS reagent, ≥99% pure), sodium carbonate monohydrate (ACS reagent, 99.5% pure), hydrochloric acid (ACS reagent, 37 wt. % in H_2O), 17β-estradiol, dichloromethane (puriss ≥99, 0% pure), PVA (Mw 30–70 kDa, 87–90% hydrolyzed), riboflavin (≥98% pure), PEG 400 (for synthesis), RITC-dextran (average M_w 70 kDa) and TPP (practical grade, 90–95% pure) were provided

from Sigma Aldrich (St. Louis, MO, USA). All solutions were prepared with ultrapure water (0.22 µS, 25°C, Milli-Q, Millipore). High glucose DMEM and penicillin/streptomycin were acquired to HyClone (Utah, USA) and PAA laboratories (Pashing, Austria), respectively. Fetal bovine serum (South America Origin) and L-glutamine were provided from Biowest (France). Calcein-AM and *p*-formaldehyde were purchased from Fluka Analytical (USA) and Panreac (Spain), respectively.

Microspheres preparation

RITC-dextran-loaded PLGA microspheres were prepared, as previously described [15], by double emulsion solvent evaporation method (water/oil/water). Briefly, a first emulsion was formed by mixing (vortex) 200 µl of a solution of 14.4 mg/ml of RITC-dextran (2880 µg) in 0.2% w/v PVA with 1 ml of DCM containing 150 mg of PLGA [RG504: RG858S (4:1)]. Then, this first emulsion was poured into 10 ml of 0.2% w/v PVA under vortex, forming the second emulsion that was added over 100 ml of 0.1% w/v PVA under magnetic stirring. This preparation was then left for 1 h under mild agitation to evaporate the solvent. Microspheres were collected by filtration, lyophilized and stored at 4°C until required. Blank microspheres were prepared with the same method but using as aqueous phase 200 µl of a solution of 0.2% w/v PVA without RITC-dextran.

17-β-Estradiol-loaded PLA/PLGA microspheres were prepared by simple emulsion solvent evaporation method (oil/water). Briefly, 0.6 ml of an organic phase DCM: MeOH (83:17) containing 200 mg of polymer PLA/PLGA [RG-203S: RG858S (4:1)] and 4 mg of 17-β-estradiol were mixed by vortex with 4 ml of 1% w/v PVA to form an emulsion that was poured into 96 ml of 0.16% w/v PVA under magnetic stirring. Then, the formulation was left 1 h under mild agitation to allow the evaporation of the solvent. Microspheres were collected by filtration, lyophilized and stored at 4°C until use. Blank microspheres were synthetized using the same method but removing 17-β-estradiol from the organic phase.

Carbonated apatite nanoparticles preparation (nano-hydroxyapatite)

Citrate-coated carbonated apatite nanoparticles were prepared by the thermal decomplexing of metastable solution containing Ca^{2+}–citrate complexes in the presence of phosphate and carbonate ions at pH = 8.5 [16, 17]. Powders were synthesized as follows: 50 ml of a solution (a) of composition 0.06 M Na_2HPO_4 + 0.1 M Na_2CO_3 was poured into 50 ml of a solution (b) of composition 0.1 M $CaCl_2$ + 0.2 M Na_3(cit) at 4°C. Then, pH was adjusted to 8.5 with diluted HCl. The mixed solution was introduced into a bottle sealed with a screw cap, immediately submerged in a water bath at 80°C and then moved to an oven with circulated forced air at the same temperature. The experiments lasted 96 h. Upon completion, the precipitates were washed with ultrapure water by six consecutive cycles of centrifugation to remove unreacted species or salts. Afterward they were freeze-dried overnight. Theoretical reaction yielding carbonated apatite nanoparticles can be represented by:

$$5\mathrm{Ca(cit)}^- + 3\mathrm{HPO_4}^- + (x+y)\ \mathrm{CO_3}^{2-} + \mathrm{OH}^- \rightarrow \mathrm{Ca_5(OH)_{1-x}(CO_3)_x(PO_4)_{3-y}(CO_3)_y} + 5\mathrm{cit}^{3-} + 3\mathrm{H}^+ + x\mathrm{OH}^-$$

Hydrogel preparation

A 10 mg/ml type I collagen solution in a cold solution of acetic acid 0.043 M, a 0.43 g/ml aqueous solution of HP-γ-CD with riboflavin (5 mg/ml) and a 20 mg/ml solution of chitosan in water were prepared. In addition, pure PEG 400 (density: 1.128 g/ml) was used. Hydrogel was prepared by mixing with vortex the enough quantity of all the previous components to obtain the following final concentrations, 5.3 mg/ml of collagen, 33.8 mg/ml of HP-γ-CD (0.4 mg/ml of riboflavin), 5.3 mg/ml of chitosan and 148.4 mg/ml of PEG 400. Afterward, this hydrogel was crosslinked with 25 µl of 5% w/v TPP sterile aqueous solution per 50 µl of hydrogel under blue visible light (468 nm, quartz-tungsten halogen Hilux UltraPlus, Benlioglu Dental Inc.). In addition, hydrogels with microspheres and nano-HAp were prepared by adding 14 mg of blank or 17-β-estradiol-loaded PLA/PLGA microspheres, 5 mg of blank or RIBD-dextran-loaded PLGA microspheres and 5 mg of nano-HAp per 50 µl of hydrogel, simulating the therapeutic doses of 17-β-estradiol and osteogenic proteins, such as BMP-2, in 50 µl of hydrogel.

Characterization of microspheres, nano-HAp and hydrogels

Size and morphology of microspheres were determined by laser diffractometry (Mastersizer 2000, Malvern Instruments) and scanning electron microscopy (SEM, Jeol JSM-6300), respectively.

Size and morphology of nano-HAp were performed by transmission electron microscopy (TEM) with a Carl Zeiss Libra 120. The composition analysis of the carbonated apatite nanoparticles were carried out by X-ray diffraction (XRD) and Fourier transform infrared (FTIR) spectroscopy. XRD data were collected by using a Bruker D8 Advance Vario diffractometer with Bragg–Brentano parafocusing geometry. FTIR spectrum of the sample was recorded in transmittance mode with a Perkin-Elmer Spectrum One FTIR spectrometer within the wavenumber range from 4000 to 400 cm^{-1} at a resolution of 4 cm^{-1}, using a pellet that was prepared by mixing ~1 mg of sample with 100 mg of anhydrous KBr and then pressed with a hydraulic pump into 13 mm diameter discs.

Porosity of hydrogels, with and without microspheres and nano-HAp, was calculated from the true density (helium pycnometer, Micromeritics AccuPyc 1330) and the apparent density of the freeze-dried hydrogels prepared in a graduated cylindrical mold. To avoid collapse processes during freeze-drying, the hydrogel was maintained in a mold and quickly frozen with liquid nitrogen before being exposed to a high-vacuum lyophilization process. The existence of true pores was verified by means of SEM.

Viscoelastic and thixotropic behaviors of hydrogel were obtained with a Bohlin CVOD 100 rheometer at 37°C by means of a Peltier system, using cone-plate and parallel geometries with a diameter for the fixed lower plate of 60 mm and a gap between the fixed and rotating part of 1 mm. The evolution of viscosity with shear rate (from 0.071 to 30 s^{-1}) was acquired by cone-plate geometry (diameter of cone 40 mm, angle 4°). The evolution of elastic (G') and viscous moduli (G'') with frequency (from 0.128 to 4.015 Hz) was acquired by a parallel plate geometry (diameter of rotating upper plate 20 mm) at a constant shear stress of 0.2387 Pa. Note that for the viscoelastic characterization, the final crosslinking step with blue light and 5% w/w TPP was not used and only blank microspheres were used.

Analysis of the functional groups of the components of the hydrogel were determined by FTIR spectroscopy with a Bruker IFS 66/S, in transmittance mode, within the wavenumber range from 4000 to 400 cm^{-1} at a resolution of 4 cm^{-1}, using the attenuated total reflectance accessory that permit to examine samples in the solid state.

In vitro release profiles and encapsulation efficiencies of 17-β-estradiol and RITC-dextran from microspheres and microspheres-

loaded hydrogels were determined at 37°C and 120 rpm (orbital agitator) with a spectrophotometer (Ultrospec 3300 'pro', Amersham Biosciences) at 280 or 555 nm, respectively. Precisely, 26 mg of 17-β-estradiol-loaded PLA/PLGA microspheres (382 µg), included or not into 100 µl of hydrogel were placed in a vessel with 4 ml of release medium. Simultaneously, 70 mg of RITC-dextran-loaded PLGA microspheres (1071 µg) included or not into 200 µl of hydrogel were placed in a vessel with 2.5 ml of release medium. The release media consisted of 0.9% NaCl solution, which was mixed with methanol in a ratio 60:40 to increase the solubility of the hydrophobic drug and then assess the sink condition, or ultrapure water. Two methods of sampling were used, 500 µl of media was collected at different time points and then either returned to the vessel (batch) or removed and replaced with fresh medium (semi-continuous).

All the experiments performed to characterize the microspheres and the hydrogel were performed in the SEGAI (Servicio General de Apoyo a la Investigación) of the Universidad de La Laguna.

Cell culture

Cell isolation

All animal experiments were performed according to the EC directive 2010/63/EU on Care and Use of Animals in Experimental Procedures. Furthermore, animal experiments were approved by the committee for animal studies of Universidad de La Laguna. Mesenchymal stem cells from femur bone marrow of 6 weeks-old male Sprague Dawley rats (rMSC) were obtained by centrifugal isolation as previously described by Dobson *et al.* [18]. Briefly, the cells were resuspended in high glucose DMEM supplemented with 10% fetal bovine serum, 1% penicillin/streptomycin and 2 mM L-glutamine stable (complete culture medium, CCM). They were seeded in flasks of 75 cm^2 and incubated at 37°C and 5% CO_2. Every 2–3 days the culture medium was changed until ~80% of confluence.

Culture of rMSC in the hydrogel and cell viability

Aliquots of 300 µl of crosslinked collagen gel were placed into a 48-well plate. Then, 50 000 cells in 20 µl of CCM were added to each well and incubated at 37°C and 5% CO_2 for 1.5 h for cell adhesion. The homogeneous cell distribution was confirmed by light microscopy. Afterward, 500 µl of CCM were added to each well, and the plates were incubated during 7 days and the medium changed every 3 days.

The seeded cell viability was tested with calcein-AM. After 1, 5 h and 1, 3 and 7 days of culture, 3 wells of each time were washed (3 times) with Hank's balanced salt solution (HBSS 1×). Then 500 µl of 1 µM calcein-AM in HBSS solution were added and incubated at 37°C and 5% CO_2 under soft agitation for 30 min. Then, calcein was removed and cells were fixed with a solution of 3.7–4% *p*-formaldehyde buffered to pH = 7.0 during 30 min. After this, formaldehyde was removed, and the wells were washed 3 times with HBSS 1×. Immediately after this, viable cells were visualized using a fluorescence inverted microscope (EVOS FL, Life Technology, Invitrogen).

Results and discussion

Nano-HAp characterization

The nanoparticles displayed plate-shape morphologies with average length (L = 40.0 ± 5.0 nm) and width (W = 9.5 ± 1.2 nm) (TEM).

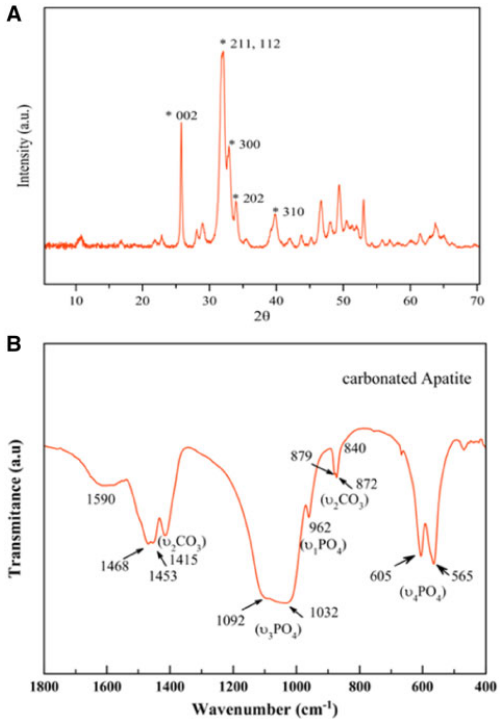

Figure 1. (A) XRD pattern of carbonated apatite prepared by thermal decomplexing of Ca/citrate/phosphate/carbonated solutions at pH = 8.5 at 80°C. (B) FTIR spectrum in transmittance mode of carbonated apatite prepared by thermal decomplexing of Ca/citrate/phosphate/carbonated solutions at pH = 8.5 at 80°C

The XRD pattern of the sample is reported on Fig. 1A and correspond to the apatite phase (PDF 01-1008), with peaks at 2θ = 25.87° corresponding to the (002) plane, the triplet at 31.77°, 32.19° and 32.90° (planes (211), (112) and (300)) respectively, the reflections at 33.9° and 39.81° (planes (202) and 310)) and other minor peaks in the 2θ range from 40° to 55°. The absence of octacalcium phosphate (OCP) is witnessed by the absence of the main reflection at 4.74°, plane (100), (OCP, PDF 44-0778).

Figure 1B shows the FTIR spectrum of the sample in 400–1800 cm^{-1} region. The main band at 1000–1100 cm^{-1} corresponds to the asymmetric stretching mode of PO_4^{3-} groups (υ_3 PO_4). The shoulder at ~965 cm^{-1} is ascribed to the symmetric stretching (υ_1 PO_4) while less intense bands at ~608 and 565 cm^{-1} are due to the (υ_4 PO_4) bending mode of PO_4^{3-} groups [17, 19]. The presence of carbonate (CO_3^{2-}) bands is attested by vibrational signatures due to the υ_3CO_3 mode, with maxima around ~1415 and 1473 cm^{-1}, and the υ_2 CO_3 mode with a peak around 873 cm^{-1}. Detailed analysis of the υ_2CO_3 region shows the signals at ~879 and 872 cm^{-1} corresponding to A-type and B-type carbonate substitutions, with carbonate ions replacing respectively OH^- and PO_4^{3-} lattice ions. Beside apatitic vibrational contributions, a band at ~1590 cm^{-1} is also noticed on all samples, which can be ascribed to the antisymmetric stretching frequencies of the carboxylate groups of the citrate. Bands at ~2930 cm^{-1} (not shown) and ~840 cm^{-1} (shoulder) are assignable to υCH_2 and δCOO modes of the citrate ions [20], respectively.

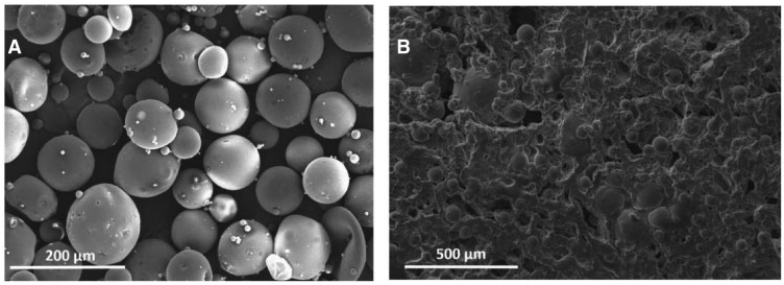

Figure 2. (A) SEM image of lyophilized PLGA microspheres. (B) SEM image showing the internal structure of hydrogel

The presence of carbonate substituting –OH and PO_4^{3-} lattice ions in the crystal structure as well as of a citrate layer coating the surface of the nano-HAp crystals is also a characteristic feature of the bone apatite. In bone, the apatite component is poorly crystalline and also displays a plate-like morphology and is doped with carbonate [21]. Recently, Hu *et al.* [22] have revealed that citrate, which accounts for about 5.5 wt % of total organic matrix of bone, is found strongly bound to the surface of the apatite nanoparticles. The use of carbonate and citrate in the mother solutions is thus, a straightforward nature inspired strategy to prepare bonelike apatites to be used in combination with the new hydrogels for the tissue regeneration.

Microspheres and collagen based-hydrogel characteristics

The mean diameters in volume of the RITC-dextran-loaded PLGA microspheres and β-estradiol-loaded PLA/PLGA microspheres were 99.70 ± 5.00 µm and 119.14 ± 0.25 µm, respectively. Both PLGA and PLA/PLGA microparticles were generated using PVA which is adsorbed in the surface of the particle and protect them from agglomeration. Shakesheff *et al.* [23] indicated that part of PVA molecules remain in the surface of the particles after consecutive washing and cannot be removed since PVA forms a stable network with PLGA. Figure 2A shows a SEM image of the generated PLGA microspheres. The encapsulation efficiency of RITC-dextran and β-estradiol in the microspheres was 80.1 ± 7.4% and 74.8 ± 5.2%, respectively. The high porosity of dry hydrogel, 81.62 ± 2.25%, was decreased up to 69.98 ± 3.07% when microspheres and nano-HAp were incorporated. Figure 2B shows a SEM image of the porous internal structure of the hydrogel after the incorporation of microspheres.

PLGA and PLA/PLGA microspheres were generated without the use of a porogen to avoid a rapid release of the model drugs. Oh *et al.* [24] showed a decrease in encapsulation efficiency and a large increase in the release rate of budesonide when ammonium bicarbonate (porogen) was included to generate PLGA microspheres. As can be seen in the SEM image (Fig. 2A), the surface of microspheres is solid and flat and no pores can be seen. Zhang *et al.* [25] reported the synthesis of porous and non-porous PLGA microspheres by the simple emulsion solvent evaporation method. In the absence of a porogen, no pores were found in the resultant particles that had a smooth surface; however, by using 2-methylpentane in the oil phase as porogen, porous particles were generated. In the case of the technique of double emulsion solvent evaporation, several authors have demonstrated the generation of porous PLGA microspheres by the addition of ammonium bicarbonate [24, 26] or phosphate buffered saline [27] in the first aqueous phase. In the absence of a porogen, these authors did not found pores in the particles that showed a smooth surface.

In the other hand, citrate-coated carbonated apatite nanoparticles prepared by thermal decomplexing are non-porous and tend to aggregate with time in mesoporous materials with a mean pore diameter in the range between 100 and 200 A [16].

The inclusion of non-porous microparticles and mesoporous nano-HAp to the highly porous hydrogel will lead to a reduction in their porosity. In fact, Wang *et al.* [26] showed the reduction of porosity of sintered scaffolds by the inclusion of non-porous PLGA microspheres (from 87.50 ± 5.23% for scaffolds including porous particles generated with a 1:10 porogen–polymer ratio to 43.2 ± 9.39% for scaffolds including non-porous particles).

Viscoelastic behavior and interactions of compounds on hydrogel

The incorporation of cyclodextrin, chitosan and PEG to the initial collagen solution (10 mg/ml) (COL) did not add additional viscosity, but generated consecutive dilutions as can be seen in Fig. 3, where viscosity versus shear rate at 37°C is represented. As expected, the incorporation of microspheres and nano-hydroxyapatite produced an increase in the viscosity values (Fig. 3, top right box).

Collagen, as many other polymers with long chains, has a non-Newtonian pseudoplastic behavior, i.e. viscosity decreases as the shear rate increases, being this process reversible when the stress is removed. In particular, collagen solutions have thixotropic properties, taking some time to recover the initial viscosity values after stress have been removed since the rearrangement of its structure is a time-dependent process. In Fig. 3, the values of viscosity after the application (forward curve) and removal (backward curve) of stress did not match, mainly for the collagen solution (COL) and the complete gel with spheres (COL+CD+CS+PEG + spheres). The forward and backward curves did not overlap, being the area between both (or hysteresis loop) an indication of the magnitude of the thixotropic behavior that permit the implantation of hydrogel in a minimally invasive way and facilitate the adaptation to the shape of the area to be treated, before being crosslinked 'in-situ' by means of blue light and TPP.

The different interactions between the components of the hydrogel: collagen, cyclodextrin, chitosan and PEG, generate a gel network i.e. able to trap the bioactive components, i.e. the pre-encapsulated bioactive substances and nano-hydroxyapatite.

Collagen is a protein with a special and atypical combination of amino acids, being glycine (Gly), proline (Pro) and hydroxyproline (Hyp) the most repeated units that are responsible of the

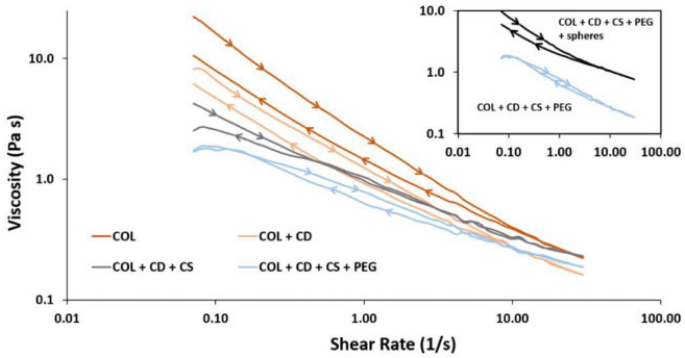

Figure 3. Variation of viscosity of collagen solution (10 mg/ml), before (COL) and after cyclodextrin (COL+CD), chitosan (COL+CD+CS) and PEG (COL+CD+CS+PEG) incorporation, with shear rate at 37°C. The upper box shows the viscosity versus shear rate of the complete gel, before (COL+CD+CS+PEG) and after the incorporation of microspheres and nano-hydroxyapatite (COL+CD+CS+PEG + spheres)

triple-helical structure. Glycine, the dominant unit in collagen, facilitates the formation and stabilization of collagen structure by internal hydrogen bonding. This amino acid can be mostly part of the sequences, Gly–Pro–X or Gly–X–Hyp, where X can be any other amino acid with different functional groups, like carboxyl and amino groups, in the outside part of the helix that are available for reaction with other molecules [28, 29]. At the very end of both sides of collagen molecules, there are terminal carboxyl and amino groups that are not incorporated in the triple-helix and are part of two non-helical domains (telopeptides) that are available for reaction with other molecules [30]. The existence of hydrophobic residues within the telopeptides region may allow their incorporation to the hydrophobic cavities of cyclodextrins, compromising the crosslinking process in collagen and the subsequent fibrillogenesis and aggregation processes [30]. In fact, cyclodextrin is a fundamental component in the hydrogel by allowing the incorporation of hydrophobic compounds, like the β-estradiol, directly in the gel without the need to pre-encapsulate them in spheres. Moreover, cyclodextrin can reinforce the collagen matrix by means of hydrogen bonds between the multiple hydroxyl groups of cyclodextrin and the terminal and/or side hydroxyl, amino, amide or carboxyl groups of collagen. Figure 4A and B represents the variation of viscosity with the shear rate and the elastic and viscous modulus with the frequency, respectively, for a collagen solution (COL) and a mixture of collagen and cyclodextrin (COL+CD). These figures demonstrated the above-mentioned interactions between collagen and cyclodextrin. In this regard, the incorporation of cyclodextrin to the collagen solution increases the viscosity values (Fig. 4A) and the solid behavior of collagen (both modulus increase, although the elastic to a greater extent, staying above in both cases) (Fig. 4B). Note that the same mass ratio of the complete gel and the same collagen concentration was maintained to avoid the dilution effect that was commented above (Fig. 3).

The existence of hydrogen bonds between cyclodextrin and collagen is observed in Fig. 5A, from the comparison of the fingerprint region of the FT-IR spectra (from 1700 to 500 cm^{-1}) of collagen solution and collagen/cyclodextrin mixture. The collagen spectra shows the typical bands at 1627 cm^{-1} (amide I: C = O stretching) and 1546 cm^{-1} (amide II: N–H deformation and C–N stretching). The incorporation of cyclodextrin to collagen produces a shift in the amide I band to higher wave numbers (1658 cm^{-1}) and a great decrease in the intensity of the amide II band (1546 cm^{-1}) in comparison with the amide I band that may suggest the formation of new hydrogen bonds between peptide carbonyl groups in collagen and hydroxyl groups in cyclodextrin. Note that the amide II band is not present in the cyclodextrin spectra. The appearance of the band at 1014 cm^{-1} is due to the C–O vibrations because of the contribution of ether and hydroxyl groups of cyclodextrin molecules to the mixture as can be seen in the cyclodextrin spectra of Fig. 5A.

Chitosan was added to the collagen–cyclodextrin mixture to harden the hydrogel by crosslinking with TPP. Hydroxyl and amino groups in chitosan are able to form hydrogen bonds with side groups or carboxyl and amino end groups of collagen. Ionic interactions between the positively charged amino groups in chitosan and the negatively charged carboxyl end groups in the telopeptide areas of collagen are also possible [31]. Because of these interactions, chitosan may be rolled around triple-helix of collagen, forming a complex with an increased viscosity compared to the collagen–cyclodextrin mixture. This behavior can be seen in the evolution of viscosity with shear rate of collagen–cyclodextrin (COL+CD) and collagen–cyclodextrin–chitosan (COL+CD+CS) mixtures (Fig. 4C). Moreover, the incorporation of chitosan (COL+CD+CS) increase the elastic behavior of the collagen–cyclodextrin mixture (COL+CD) since the difference between elastic and viscous modulus becomes bigger (Fig. 4D). Note that the comparison between COL+CD and COL+CD+CS was performed at the same conditions as Fig. 4A and B.

The incorporation of chitosan to the collagen/cyclodextrin mixture did not produce major changes in the fingerprint region of the IR-spectra (Fig. 5B), showing the amide I band at 1658 cm^{-1}, the amide II band of much lower intensity at 1546 cm^{-1} and the C–O band at 1014 cm^{-1}. This absence of changes in the IR-spectra indicates the predominance of the ionic interactions between the cationic amino groups in chitosan and the anionic carboxylic end groups in collagen against the hydrogen bonds between both molecules.

Chitosan spectra in the fingerprint region (Fig. 5B) showed mainly the amide I band at 1623 cm^{-1} and the C–O stretching at 1050 cm^{-1}. This spectra also shows a band at 1515 cm^{-1} that may be due to the N–H bending of primary amines, since its greater intensity with respect to the amide I band do not match with the amide II band, which is not present in this spectra.

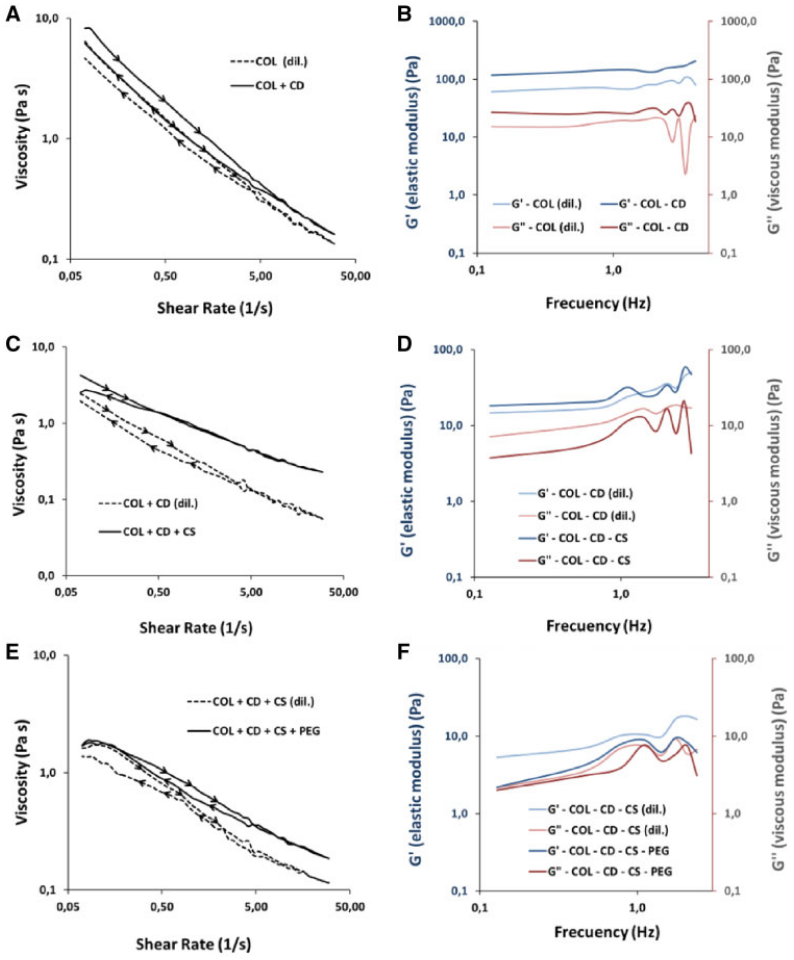

Figure 4. Evolution of the viscoelastic behavior of collagen with the incorporation of cyclodextrin, chitosan and PEG. Variation of (A) viscosity with shear rate and (B) elastic and viscous moduli with frequency in collagen (COL) versus a mixture of collagen and cyclodextrin (COL+CD) with a mass ratio equal to that in the final gel, maintaining the collagen concentration in both samples (COL) and (COL+CD). Variation of (C) viscosity with shear rate and (D) elastic and viscous moduli with frequency in collagen–cyclodextrin mixture (COL+CD) versus a collagen–cyclodextrin–chitosan mixture (COL+CD+CS) with a mass ratio equal to that in the final gel, maintaining the collagen and cyclodextrin concentration in both samples (COL+CD) and (COL+CD+CS). Variation of (E) viscosity with shear rate and (F) elastic and viscous moduli with frequency in collagen–cyclodextrin–chitosan mixture (COL+CD+CS) versus the complete gel (COL+CD+CS+PEG) with a mass ratio equal to that in the final gel, maintaining the collagen, cyclodextrin and chitosan concentrations in both samples (COL+CD+CS) and (COL+CD+CS+PEG)

The last component to be incorporated to hydrogel was PEG that may produce the molecular crowding of collagen, forming aligned fibrils. However, minor reversible interactions between collagen and PEG by hydrogen bonding and ionic interactions may be also possible [32, 33]. These facts may be supported by the increase on viscosity in all the range of shear rate (Fig. 4E), when PEG is included to the collagen–cyclodextrin–chitosan mixture. At low frequencies, the big difference between the elastic and viscous modulus of the collagen–cyclodextrin–chitosan mixture is decreased when the PEG is incorporated, as shown in Fig. 4F. This behavior may be caused by an approach to a Newtonian behavior because of the great dilution of the final mixture, but, despite this, the hydrogel remains elastic in the complete gel since the elastic module is above the viscous module in all the frequency range. Note that comparison between COL+CD+CS and COL+CD+CS+PEG were generated at the same conditions as Fig. 4A and B. Although it is well known the formation of inclusion complexes (polyrotaxanes) between alpha-cyclodextrin and PEG [34, 35], the utilization of beta or gamma cyclodextrin as an alternative of alpha-cyclodextrin avoid the formation of polyrotaxane structures [36].

PEG 400 IR-spectra in the fingerprint region (Fig. 5C) shows the C–H bands at 1457 and 1350 cm^{-1}, the C–O bands corresponding to alcohol at 1292 and 1245 cm^{-1}, and the C–O–C of ether at 1099 cm^{-1}. The incorporation of PEG 400 to the hydrogel did not alter the previously commented IR-spectra of collagen/cyclodextrin/chitosan mixture, beyond the superimposition of both spectra. Only

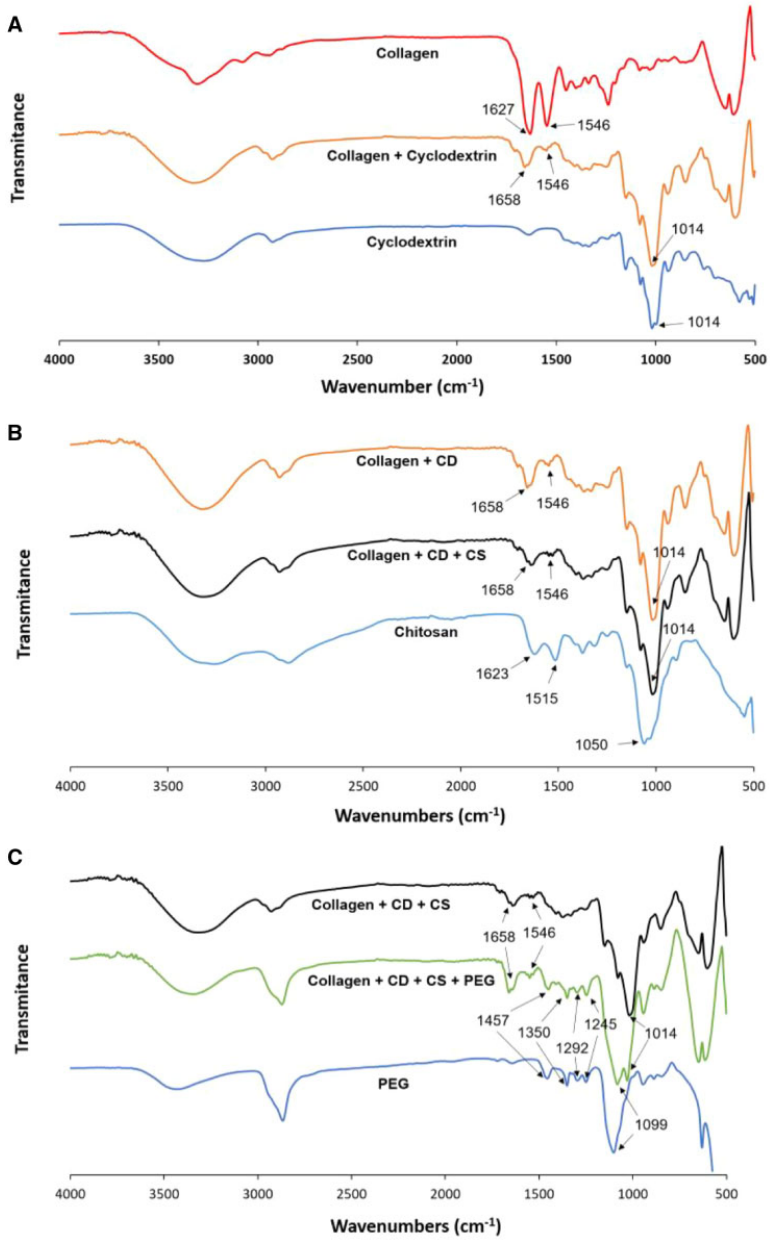

Figure 5. FT-IR spectra in transmittance mode for (A) collagen, cyclodextrin and the mixture of both; (B) chitosan, collagen/cyclodextrin and collagen/cyclodextrin/chitosan mixtures; (C) PEG, collagen/cyclodextrin/chitosan and collagen/cyclodextrin/chitosan/PEG mixtures

a small increase in the difference between the intensities of the amide I and amide II peaks (Fig. 5C) can be observed. This small change may indicate a higher probability of occurrence of hydrogen bindings and ionic interactions between collagen and PEG over the molecular crowding of collagen.

In vitro release profiles

In vitro release profiles of β-estradiol (Fig. 6) or RITC-dextran (Fig. 7) from the microsphere-loaded hydrogel reveal a two-phase behavior with a burst and a controlled release period. By comparing these results with the respective profiles of microspheres, it is

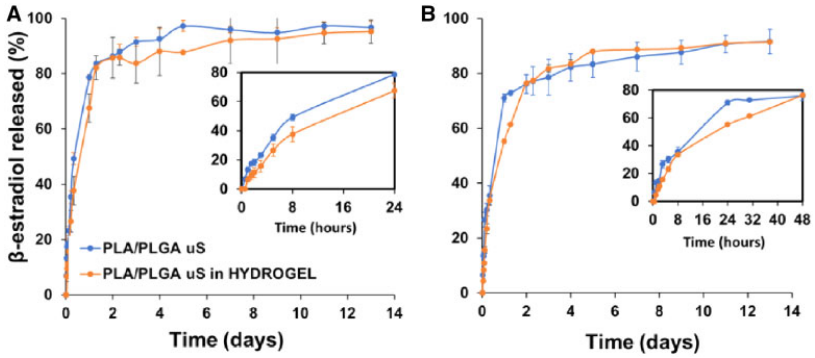

Figure 6. *In vitro* release profile of β-estradiol from microspheres and microspheres-loaded hydrogel. In the upper right part of the figure is shown a magnification of the first hours. (A) Semi-continuous sampling method; (B) batch sampling method

possible to conclude that burst release was reduced (see enlargement of Fig. 6 or 7) because of the different interactions between the components of the hydrogel previously mentioned and the crosslinking process that entrap the bioactive substances. Burst release for β-estradiol is accentuated during the first 24 h, while for RITC-dextran is moderate the first 2–3 days, being the damping effect of the hydrogel much more visible in the case of the latter. The controlled release period is produced the following 15 days or 3 weeks for β-estradiol or RITC-dextran, respectively. The fact that this period occurs at the same rate for the microspheres included or not in the hydrogel may indicate that the release process is mainly controlled by internal diffusion within microspheres. However, depending on the sampling method, the final released fraction varies. When media is returned after the measurement (Fig. 6B or 7B), the drug is accumulated continuously and the total drug released before the process stops will be less than in the case of removing the sample after the measurement (Fig. 6A or 7A). This is because in the latter case, the media is renewed continuously and the concentration gradient between the spheres and the media is increased each sampling time, which forces the remaining drug to be released from the spheres until the concentration inside them is at equilibrium with the media.

Experiments were carried out under sink conditions for both, hydrophobic and hydrophilic model drugs. Thus, β-estradiol was almost completely released from the spheres, i.e. 97 or 92% for the semi-continuous or batch sampling methods, respectively (Fig. 6), being able to assure that there was not crystallization inside the particles. However, not all the RITC-dextran molecules diffuse out and the final released fraction was in the range between 29 and 47% for all the experiments with this molecule (Fig. 7). These data are in accordance with the literature [37–39] and may be due to electrostatic interactions between the negatively charged deprotonated carboxyl groups of PLGA and the positively charged amine groups of rhodamine from the RITC-dextran at pH values between 6 and 7 [40]. The complete release of this model drug can be achieved at acidic pH values of 4–5 [40]. Note that the slower release rate of RITC-dextran with respect to the data from literature is due to the high molecular weight of dextran.

Mass transfer studies for hydrophobic and hydrophilic drugs

The mass transfer process that occurs from polymeric microspheres, as isolated systems or included in porous hydrogels, to the media in body cavities with low clearance rates was simulated using two model compounds, 17-β-estradiol and RITC-dextran, which mimic low molecular weight hydrophobic and high molecular weight hydrophilic drugs, respectively.

Some systems based on natural polymers, like alginate or chitosan, with short release times [41–43] behave as concentrated systems, i.e. uniform drug concentration within microspheres. Then, diffusional resistance inside the microspheres is negligible compared to the liquid boundary layer resistance i.e. the rate-limiting step, being able to describe the simplified release process by means of the mass transfer coefficient, h [41, 42]. However, based on the experimental *in vitro* profiles mentioned above, a distributed system must be assumed, where the concentration gradient inside the microspheres is rate limiting. Thus, the release process is mainly described by means of the diffusion process inside the spheres and therefore by the effective diffusion coefficient, D_{eff} [44, 45].

Diffusion process from the spherical microparticles is governed by Fick's second law of diffusion in radial coordinates [44], according to the Equation (1):

$$\frac{\partial C}{\partial t} = D_{\text{eff}}\left(\frac{\partial^2 C}{\partial r^2} + \frac{2}{r}\frac{\partial C}{\partial r}\right) \text{ for } 0 < r < R, \tag{1}$$

where C is the concentration of the drug, D_{eff} is the effective diffusion coefficient, t is the time, r is the radial coordinate and R is the radius of the microparticles.

Equation (1) is solved with the surface boundary condition of no accumulation described by Equation (2), which assumes that the mass flow rate of the drug i.e. released to the media is equal to the mass flow rate of the drug that reach the surface of the spheres by diffusion [44, 45]:

$$-D_{\text{eff}}\left(\frac{\partial C}{\partial r}\right) = h\left(C_{S,sf} - C_{0,\infty}\right) \text{ for } r = R, \tag{2}$$

where $C_{S,sf}$ is the drug concentration inside the spheres, but in the surface; $C_{0,\infty}$ is the drug concentration in equilibrium with the liquid; D_{eff} is the effective diffusion coefficient; r is the radial coordinate; R is the radius of the microparticles and h is the mass transfer coefficient in the boundary layer.

Resolution of Equation (1) with Equation (2) for a spherical geometry, considering a homogeneous distribution of the drug inside the spheres at the beginning of the process, i.e. $C(r) = C_0$ *at* $t = 0$, for $0 < r < R$ (monolithic system), leads to Equation (3). This expression

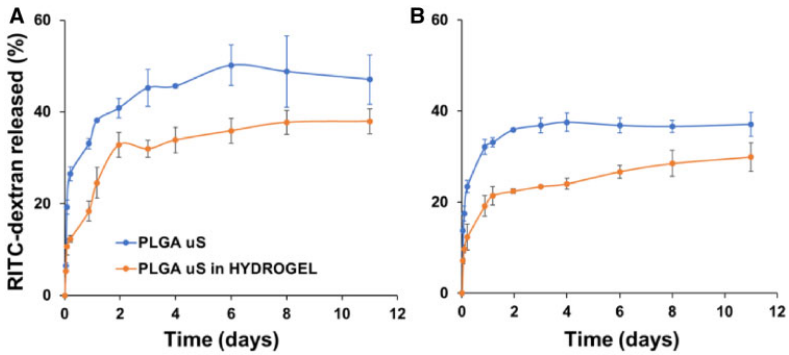

Figure 7. *In vitro* and *in vivo* release profiles of RITC-dextran from microspheres and microspheres-loaded hydrogel. (A) Semi-continuous sampling method; (B) batch sampling method

permits the calculation of the fraction of the cumulative amount of drug leaving the microspheres as a function of time [44, 45]. Note that, C_0 is the initial drug concentration inside the spheres, and perfect sink conditions during all the experiments were assured.

$$\frac{M_t}{M_\infty} = 1 - \sum_{n=1}^{\infty} \frac{6\ L^2}{\beta_n{}^2\ (\beta_n{}^2 + L^2 - L)} \exp\left(-\frac{\beta_n{}^2}{R^2}\ D_{\text{eff}}\ t\right), \qquad (3)$$

where M_t and M_∞ are the total mass of drug released to the media at time t and at the final of the process, respectively. M_∞ can be obtained from the concentration of the drug inside the spheres at the beginning of the process ($t = 0$) i.e. the value obtained by dissolution of the spheres. The β_ns are the infinite roots (eigenvalues) of the Equation (4):

$$\beta_n \cot\beta_n + L - 1 = 0. \qquad (4)$$

L is the dimensionless mass transfer Biot number, described by the Equation (5):

$$L = \frac{h\ R}{D_{\text{eff}}}\ . \qquad (5)$$

For L below 0.01, the drug concentration within microspheres is uniform, so the liquid boundary layer surrounding the spheres is rate limiting and the spheres behaves as a concentrated system; while for L above 10 the spheres acts as a distributed system, being the resistance inside the polymer matrix of the spheres rate limiting.

For large values of L, the roots of Equation (4) are multiple of the number *pi* and Equation (3) can be simplified in Equation (6) i.e. a simplified solution of Fick's second law of diffusion:

$$\frac{M_t}{M_\infty} = 1 - \frac{6}{\pi^2} \sum_{n=1}^{\infty} \frac{1}{n^2} \exp\left(-\frac{n^2\ \pi^2}{R^2}\ D_{\text{eff}}\ t\right). \qquad (6)$$

Since microspheres in all cases are assumed as distributed systems, they must contribute in the same way to the global mass transport process, whether or not they are included in the hydrogel. Thus, the latter can be considered as part of the boundary layer between the spheres and the media. Equations (3–6) describe the complete mass transfer process, permitting to determine not only the effective diffusion coefficient in the polymer matrix of the spheres, D_{eff}, but also the mass transfer coefficient in the boundary layer, h, to which the hydrogel contributes to a greater extent.

Table 1 shows, for each sampling method, batch and semi-continuous, the values of D_{eff} that describe the internal diffusion of 17-β-estradiol and RITC-dextran inside microspheres and are in the range of $2.64{\cdot}10^{-15}$ to $6.67{\cdot}10^{-15}$ m^2/s. The contribution of hydrogel to the mass transfer process throughout the values of h, which are in the range of $8.50{\cdot}10^{-10}$ to $3.04{\cdot}10^{-9}$ m^2/s, are also shown in Table 1. The behavior of both model drugs was similar in the system regardless of the sampling method and no tendency was detected.

To obtain D_{eff} and h, deviations between experimental released fractions, M/M_∞, from microspheres included or not in hydrogels and the predicted M/M_∞ according to Equations (3–6) were minimized. This was made for each model drug and sampling method with 'genetic algorithms', already implemented in 'R software' (R Foundation for Statistical Computing, version 3.5.1., 2018, Vienna) [46, 47], because of the ill-conditioned nature of diffusion equation. The 'residual sum of squares (RSS)' values obtained were between $4.44{\cdot}10^{-4}$ and $2.27{\cdot}10^{-3}$ and the R^2-values were ranged between 95.41 and 98.87%. The mathematical form of diffusion models is an infinite series of terms itself nonlinear, making difficult the use of the classical methods to fit nonlinear models. The RSS allows identifying two common problems: multiple minima and strong nonlinear profiles, which can result in a relative minimum, not the absolute one. Note that predicted M/M_∞ was obtained using Equation (6) for microspheres and Equations (3–5) for microspheres included in hydrogels. The value of D_{eff} was the same for microspheres, whether they were included or not in the hydrogel, for each condition. The hydrogel contributed to the mass transfer process with h, as part of the boundary layer. The location of the predicted D_{eff} and h within the RSS level curves, obtained for a great variety of values of both coefficients (Fig. 8), and the comparison (Fig. 9) of the experimental released fractions, M/M_∞, (points) versus the simulated ones (lines) demonstrate that the proposed model fits the experimental data for both model drugs.

In vitro cell culture in hydrogels

The hydrogel presented adequate characteristics for a good cell adhesion, viability and proliferation. The green fluorescent intensity produced by the living cells was increased over the time (Fig. 10). At 1.5 h a few cells were observed on the surface of the scaffold. The cell proliferation increased and after 7 days, most of the scaffold was occupied by living cells.

Table 1. Effective diffusion coefficient, D_e (m^2/s), and mass transfer coefficient, h (m/s), values for 17-β-estradiol and RITC-dextran according to Equations (3–6)

Sampling method	D_e (m^2/s)		h (m/s)		R^2 (%)/RSS values	
	β-Estradiol	RITC-dextran	β-Estradiol	RITC-dextran	β-Estradiol	RITC-dextran
Batch	$2.9281 \cdot 10^{-15}$	$6.6716 \cdot 10^{-15}$	$8.5030 \cdot 10^{-10}$	$3.0350 \cdot 10^{-9}$	$98.87/1.2857 \cdot 10^{-3}$	$95.41/4.4388 \cdot 10^{-4}$
Semi-continuous	$3.9852 \cdot 10^{-15}$	$2.6409 \cdot 10^{-15}$	$9.2152 \cdot 10^{-10}$	$1.2050 \cdot 10^{-9}$	$98.29/2.2671 \cdot 10^{-3}$	$95.72/8.6032 \cdot 10^{-4}$

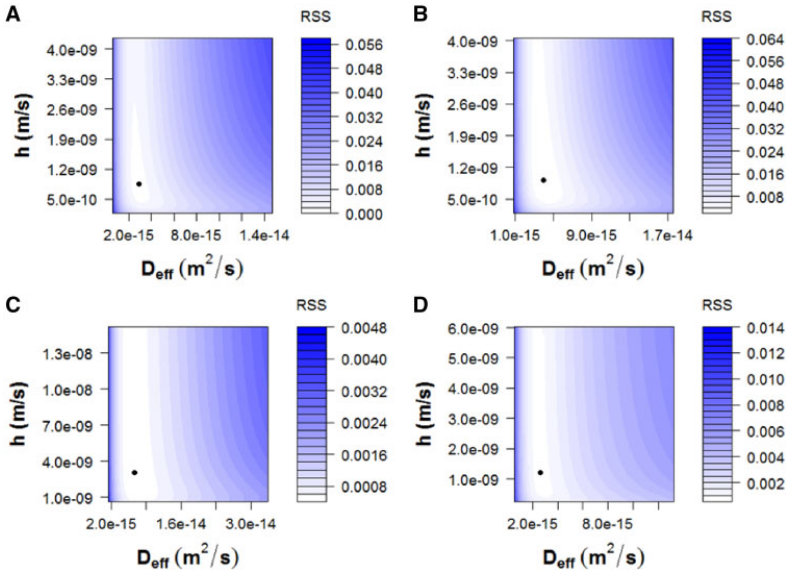

Figure 8. Location of the predicted D_{eff} and h within the residual sum of squares (RSS) level curves. (A) 17-β-Estradiol, batch sampling method; (B) 17-β-estradiol, semi-continuous sampling method; (C) RITC-dextran, batch sampling method; (D) RITC-dextran, semi-continuous sampling method

Conclusions

An innovative thixotropic hydrogel based on chitosan, collagen, HP-γ-CD and PEG has been developed. In order to target its use in bone regeneration, the hydrogel incorporated nano-hydroxyapatite and microspheres loaded with hydrophobic or hydrophilic model drugs (17-β-estradiol or RITC-dextran) that slightly diminished the porosity of hydrogel to 69.98 ± 3.07%.

The changes in the FT-IR spectra, the increase of viscosity and the intensification of the solid behavior of collagen with the incorporation of cyclodextrin suggested the incorporation of the residues of the telopeptide region of collagen inside the cavities of cyclodextrins and the formation of new hydrogen bonds between both molecules. In a similar way, the rheological parameters indicated the formation of hydrogen bonds between chitosan and collagen; however, the FTIR spectroscopy suggested the predominance of ionic interactions over the hydrogen bonds between both molecules. The increase on viscosity, the maintenance of the elastic behavior and the lack of variation in FT-IR spectra when PEG was incorporated to the rest of components, suggested the existence of ionic interactions between collagen and PEG. The interactions between components together with the rheological behavior of hydrogel explain the formation of a gel network that allows to trap the bioactive components and facilitate the adaptation and injection of the hydrogel to diverse treatment sites.

In vitro release profiles of pre-encapsulated model drugs showed a two-phase behavior with a burst release period that was damped by hydrogel and a controlled release period with a similar rate whether they are included or not in hydrogel, which indicated a mass transfer process controlled by internal diffusion within microspheres. Thus, a distributed system was assumed to model mass transfer process of drugs from polymeric microspheres, as isolated systems or included in porous hydrogels, to the media in body cavities with low clearance rates. The calculated effective diffusion coefficients, D_{eff}, that describe the internal diffusion of the model drugs inside the microspheres, and the mass transfer coefficients, h, i.e. the contribution of hydrogel to the mass transfer process, as part of the boundary layer, did not show any tendency regardless of the sampling method or the model drug used.

The *in vitro* culture of rMSC in hydrogel showed no signs of intolerance or toxicity, observing an intense proliferation of the cells after 7 days, being most of the scaffold surface occupied by living cells.

Since mass transfer process is controlled by the internal diffusion within microspheres, in order to obtain an optimal release profile, an improvement in the structure of the microspheres would be necessary. To do that, new combinations of polymers to form their matrix or different type of coatings should be tested. Moreover, as long

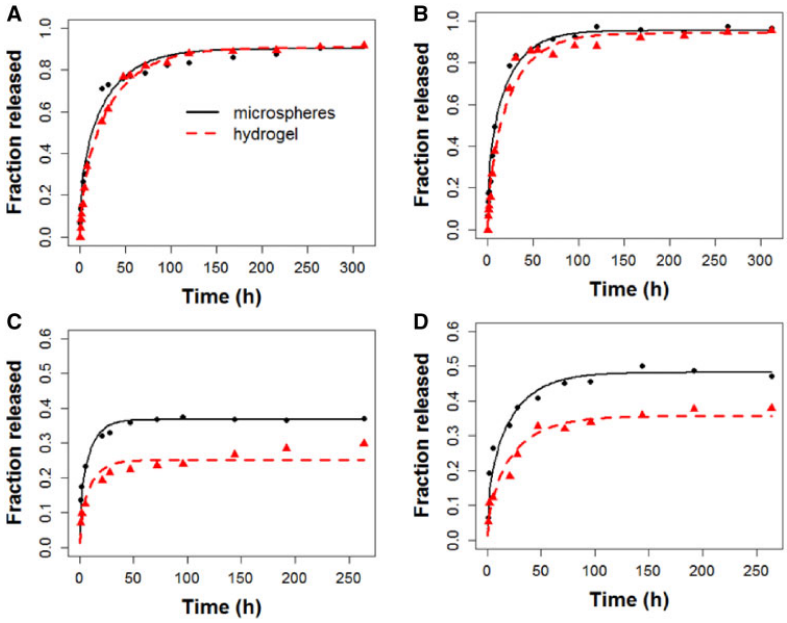

Figure 9. Comparison of the experimental released fractions, M/M_∞ (points) versus the simulated ones (lines) for: (A) 17-β-estradiol, batch sampling method; (B) 17-β-estradiol, semi-continuous sampling method; (C) RITC-dextran, batch sampling method; (D) RITC-dextran, semi-continuous sampling method

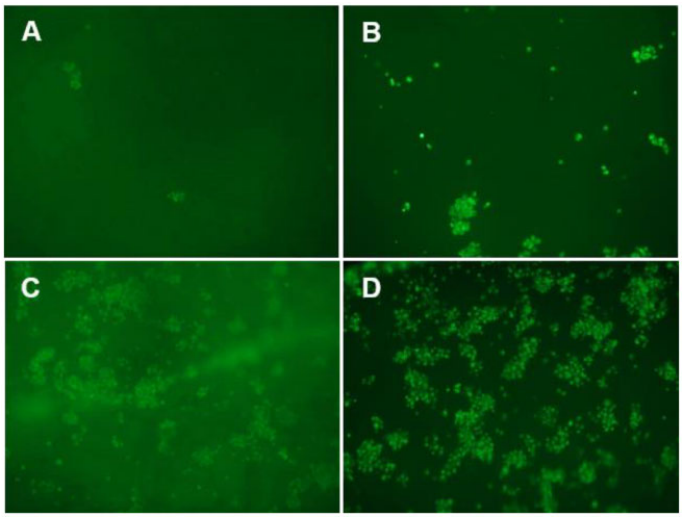

Figure 10. rMSC seeded on the hydrogel scaffold. Representative photomicrographs (10×) of cell viability by calcein-AM staining after (A) 1.5 h (time for cellular adhesion); (B) 1 day; (C) 3 days and (D) 7 days of incubation in complete culture medium at 37°C and 5% CO_2

as the hydrogel continues to be a good support for bioactive substances and presents good cell adhesion, viability and proliferation properties, a greater contribution of the hydrogel in the mass transfer process would be desirable.

Acknowledgements

The authors would like to thank Dr Alberto Fernández-Medarde (Instituto de Biología Molecular y Celular del Cáncer, Centro de Investigación del Cáncer, CSIC-USAL) for proofreading the article. Moreover, the help and the advice

in the interpretation on FTIR spectra given by Dr Jose Adrián Gavin (Organic Chemistry Department, ULL) and Dr Antonio Manuel Hernández-Daranas (Instituto de Productos Naturales y Agrobiología, CSIC) is appreciated.

Funding

This work was supported by the Ministry of Science and Technology, Spain (MAT2014-55657-R).

References

1. Peppas NA, Bures P, Leobandung W *et al*. Hydrogels in pharmaceutical formulations. *Eur J Pharm Biopharm* 2000;**50**:27–46.
2. Hoffman AS. Hydrogels for biomedical applications. *Adv Drug Deliv Rev* 2002;**54**:3–12.
3. Vermonden T, Censi R, Hennink WE. Hydrogels for protein delivery. *Chem Rev* 2012;**112**:2853–88.
4. Peppas NA, Hilt JZ, Khademhosseini A *et al*. Hydrogels in biology and medicine: from molecular principles to bionanotechnology. *Adv Mater* 2006;**18**:1345–60.
5. Li Y, Rodrigues J, Tomás H. Injectable and biodegradable hydrogels: gelation, biodegradation and biomedical applications. *Chem Soc Rev* 2012; **41**:2193–221.
6. Calvo P, Remuñán-López C, Vila-Jato JL *et al*. Novel hydrophilic chitosan-polyethylene oxide nanoparticles as protein carriers. *J Appl Polym Sci* 1997;**63**:125–32.
7. Salomé Machado AA, Martins VCA, Plepis A. Thermal and rheological behavior of collagen. Chitosan blends. *J Therm Anal Calorim* 2002;**67**: 491–8.
8. Borde B, Grunert P, Hartl R *et al*. Injectable, high-density collagen gels for annulus fibrosus repair: an in vitro rat tail model. *J Biomed Mater Res A* 2015;**103**:2571–81.
9. Wollensak G, Spoerl E, Seiler T. Riboflavin/ultraviolet-a-induced collagen crosslinking for the treatment of keratoconus. *Am J Ophthalmol* 2003; **135**:620–7.
10. Hashemi H, Seyedian MA, Miraftab M *et al*. Corneal collagen cross-linking with riboflavin and ultraviolet A irradiation for keratoconus: long-term results. *Ophthalmology* 2013;**120**:1515–20.
11. Segredo-Morales, E, Martin-Pastor M, Salas A *et al*. Mobility of water and polymer species and rheological properties of supramolecular poly-pseudorotaxane gels suitable for bone regeneration. *Bioconjug Chem* 2018;**29**:503–16.
12. Lin C-C, Anseth KS. PEG hydrogels for the controlled release of biomolecules in regenerative medicine. *Pharm Res* 2009;**26**:631–43.
13. Kim JK, Kim HJ, Chung J-Y *et al*. Natural and synthetic biomaterials for controlled drug delivery. *Arch Pharm Res* 2014;**37**:60–8.
14. Diaz-Gomez L, García-González CA, Wang J *et al*. Biodegradable PCL/fibroin/hydroxyapatite porous scaffolds prepared by supercritical foaming for bone regeneration. *Int J Pharm* 2017;**527**:115–25.
15. Hernández A, Sánchez E, Soriano I *et al*. Material-related effects of BMP-2 delivery systems on bone regeneration. *Acta Biomater* 2012;**8**: 781–91.
16. López-Macipe A, Gómez-Morales J, Rodríguez-Clemente R. Nanosized hydroxyapatite precipitation from homogeneous calcium/citrate/phosphate solutions using microwave and conventional heating. *Adv Mater* 1998;**10**:49–53.
17. Delgado-López JM, Iafisco M, Rodríguez I *et al*. Crystallization of bioinspired citrate-functionalized nanoapatite with tailored carbonate content. *Acta Biomater* 2012;**8**:3491–9.
18. Dobson KR, Reading L, Haberey M *et al*. Centrifugal isolation of bone marrow from bone: an improved method for the recovery and quantitation of bone marrow osteoprogenitor cells from rat tibiae and femurae. *Calcif Tissue Int* 1999;**65**:411–3.
19. Gómez-Morales J, Verdugo-Escamilla C, Fernández-Penas R *et al*. Luminescent biomimetic citrate-coated europium-doped carbonated apatite nanoparticles for use in bioimaging: physico-chemistry and cytocompatibility. *RSC Adv* 2018;**8**:2385–97.
20. Socrates G. *Infrared and Raman Characteristic Group Frequencies: Tables and Charts*. Chichester: Wiley, 2004.
21. Gómez–Morales J, Iafisco M, Delgado-López JM *et al*. Progress on the preparation of nanocrystalline apatites and surface characterization: overview of fundamental and applied aspects. *Prog Cryst Growth Charact Mater* 2013;**59**:1–46.
22. Hu YY, Rawal A, Schmidt-Rohr K. Strongly bound citrate stabilizes the apatite nanocrystals in bone. *Proc Natl Acad Sci USA* 2010;**107**: 22425–9.
23. Shakesheff KM, Evora C, Soriano I *et al*. The adsorption of poly(vinyl alcohol) to biodegradable microparticles studied by X-ray photoelectron spectroscopy (XPS). *J Colloid Interface Sci* 1997;**185**: 538–47.
24. Oh YJ, Lee J, Seo JY *et al*. Preparation of budesonide-loaded porous PLGA microparticles and their therapeutic efficacy in a murine asthma model. *J Control Release* 2011;**150**:56–62.
25. Zhang T, Zhang Q, Chen J *et al*. The controllable preparation of porous PLGA microspheres by the oil/water emulsion method and its application in 3D culture of ovarian cancer cells. *Colloids Surf A Physicochem Eng Asp* 2014;**452**:115–24.
26. Wang Y, Shi X, Ren L *et al*. Porous poly (lactic-co-glycolide) microsphere sintered scaffolds for tissue repair applications. *Mater Sci Eng C* 2009;**29**:2502–7.
27. Qutachi O, Vetsch JR, Gill D *et al*. Injectable and porous PLGA microspheres that form highly porous scaffolds at body temperature. *Acta Biomater* 2014;**10**:5090–8.
28. Szpak P. Fish bone chemistry and ultrastructure: implications for taphonomy and stable isotope analysis. *J Archaeol Sci* 2011;**38**:3358–72.
29. Shoulders MD, Raines RT. Collagen structure and stability. *Annu Rev Biochem* 2009;**78**:929–58.
30. Friess W. Collagen—biomaterial for drug delivery. *Eur J Pharm Biopharm* 1998;**45**:113–36.
31. Sionkowska A, Wisniewski M, Skopinska J *et al*. Molecular interactions in collagen and chitosan blends. *Biomaterials* 2004;**25**:795–801.
32. Peak CW, Nagar S, Watts RD *et al*. Robust and degradable hydrogels from poly(ethylene glycol) and semi-interpenetrating collagen. *Macromolecules* 2014;**47**:6408–17.
33. Saeidi N, Karmelek KP, Paten JA *et al*. Molecular crowding of collagen: a pathway to produce highly-organized collagenous structures. *Biomaterials* 2012;**33**:7366–74.
34. Harada A, Kamachi M. Complex formation between poly(ethylene glycol) and α-cyclodextrin. *Macromolecules* 1990;**23**:2821–3.
35. Wang J, Williamson GS, Yang H. Branched polyrotaxane hydrogels consisting of alpha-cyclodextrin and low-molecular-weight four-arm polyethylene glycol and the utility of their thixotropic property for controlled drug release. *Colloid Surf B* 2018;**165**:144–9.
36. Ceccato M, Lo Nostro P, Baglioni P. α-cyclodextrin/polyethylene glycol polyrotaxane: a study of the threading process. *Langmuir* 1997;**13**:2436–9.
37. Jonderian A, Maalouf R. Formulation and in vitro interaction of rhodamine-B loaded PLGA nanoparticles with cardiac myocytes. *Front Pharmacol* 2016;**7**:458.
38. Cartiera MS, Johnson KM, Rajendran V *et al*. The uptake and intracellular fate of PLGA nanoparticles in epithelial cells. *Biomaterials* 2009;**30**: 2790–8.
39. Abulateefeh SR, Spain SG, Thurecht KJ *et al*. Enhanced uptake of nanoparticle drug carriers via a thermoresponsive shell enhances cytotoxicity in a cancer cell line. *Biomater Sci* 2013;**1**:434–42.
40. Betancourt T, Shah K, Brannon-Peppas L. Rhodamine-loaded poly(lactic-co-glycolic acid) nanoparticles for investigation of in vitro interactions with breast cancer cells. *J Mater Sci Mater Med* 2009;**20**:387–95.
41. Lewińska D, Rosiński S, Hunkeler D *et al*. Mass transfer coefficient in characterization of gel beads and microcapsules. *J Memb Sci* 2002;**209**: 533–40.

42. Patra S, Bal DK, Ganguly S. Diffusion in and around alginate and chitosan films with embedded sub-millimeter voids. *Mater Sci Eng C* 2016;**59**: 61–9.
43. Rosiński S, Lewińska D, Wójcik M *et al*. Mass transfer characteristics of poly-lysine, poly-ornithine and poly-methylene-co-guanidine membrane coated alginate microcapsules. *J Memb Sci* 2005;**254**:249–57.
44. Crank J. *The Mathematics of Diffusion*. Oxford: Clarendon Press, 1975.
45. Siepmann J, Elkharraz K, Siepmann F *et al*. How autocatalysis accelerates drug release from PLGA-based microparticles: a quantitative treatment. *Biomacromolecules* 2005;**6**:2312–9.
46. Scrucca L. GA: a package for genetic algorithms in R. *J Stat Softw* 2013; **53**:37.
47. Scrucca L. On some extensions to GA package: hybrid optimisation, parallelisation and islands evolution. *R J* 2017;**9**:187–206.

pharmaceutics

MDPI

Article

PLGA-BMP-2 and PLA-17β-Estradiol Microspheres Reinforcing a Composite Hydrogel for Bone Regeneration in Osteoporosis

Patricia García-García [1], Ricardo Reyes [2,3], Elisabet Segredo-Morales [1], Edgar Pérez-Herrero [1,2], Araceli Delgado [1,2,*] and Carmen Évora [1,2,*]

1 Department of Chemical Engineering and Pharmaceutical Technology, University of La Laguna, 38206 La Laguna, Spain; patg0991@gmail.com (P.G.-G); esegredm@ull.edu.es (E.S.-M.); eperezhe@ull.edu.es (E.P.-H.)
2 Institute of Biomedical Technologies (ITB), University of La Laguna, 38206 La Laguna, Spain; rreyesro@ull.edu.es
3 Department of Biochemistry, Microbiology, Cell Biology and Genetics, University of La Laguna, 38206 La Laguna, Spain
* Correspondence: adelgado@ull.edu.es (A.D.); cevora@ull.edu.es (C.É.)

Received: 23 October 2019; Accepted: 29 November 2019; Published: 3 December 2019

Abstract: The controlled release of active substances—bone morphogenetic protein 2 (BMP-2) and 17β-estradiol—is one of the main aspects to be taken into account to successfully regenerate a tissue defect. In this study, BMP-2- and 17β-estradiol-loaded microspheres were combined in a sandwich-like system formed by a hydrogel core composed of chitosan (CHT) collagen, 2-hidroxipropil γ-ciclodextrin (HP-γ-CD), nanoparticles of hydroxyapatite (nano-HAP), and an electrospun mesh shell prepared with two external electrospinning films for the regeneration of a critical bone defect in osteoporotic rats. Microspheres were made with poly-lactide-*co*-glycolide (PLGA) to encapsulate BMP-2, whereas the different formulations of 17β-estradiol were prepared with poly-lactic acid (PLA) and PLGA. The in vitro and in vivo BMP-2 delivered from the system fitted a biphasic profile. Although the in vivo burst effect was higher than in vitro the second phases (lasted up to 6 weeks) were parallel, the release rate ranged between 55 and 70 ng/day. The in vitro release kinetics of the 17β-estradiol dissolved in the polymeric matrix of the microspheres depended on the partition coefficient. The 17β-estradiol was slowly released from the core system using an aqueous release medium (D_{eff} = 5.58·10^{-16} ± 9.81·10^{-17}m^{2}s^{-1}) and very fast in MeOH-water (50:50). The hydrogel core system was injectable, and approximately 83% of the loaded dose is uniformly discharged through a 20G needle. The system placed in the defect was easily adapted to the defect shape and after 12 weeks approximately 50% of the defect was refilled by new tissue. None differences were observed between the osteoporotic and non-osteoporotic groups. Despite the role of 17β-estradiol on the bone remodeling process, the obtained results in this study suggest that the observed regeneration was only due to the controlled rate released of BMP-2 from the PLGA microspheres.

Keywords: BMP-2-microspheres; hydrogel system; 17-βestradiol release; bone regeneration; osteoporosis; poly-lactide-*co*-glycolide; polylactic acid

1. Introduction

Regeneration of bone critical defects is still a challenge in the orthopedic field. Local treatment with bone morphogenetic protein (BMP-2) incorporated in different biomaterial scaffolds has demonstrated to be efficient to induce new bone formation for critical bone defect in several animal models. Nowadays, collagen sponges loaded with recombinant BMP-2 are clinically available as bone graft substitutes

for the treatment of nonunion and critical-sized bone defects. Although BMP-2 is a potent osteogenic agent, a controlled release profile is required for safety and efficacy. Thus, the scaffold to fill the bone defect should not only be designed to act as support and guide for tissue growth, but also to control the release rate of active substances. Although many materials and structures have been proposed to construct these scaffolds, the control of the release rate has not always been taken into account. In fact, in some cases the protein is incorporated in the material by incubation and, unless a material-protein interaction occurs, a burst release at an early period would be expected. Consequently, a high dose of BMP-2 would be in blood circulation, leading to a high risk of side effects and, at the same time, a significant loss of the protein in the site of action. In addition, some authors showed that BMPs in these cases might also stimulate bone resorption due to the high dose of BMP-2 associated to uncontrolled release [1]. To minimize the osteoclastic effect of BMPs, some authors proposed the addition of an anti-catabolic agent. The most frequently studied combination has been BMP-2 with bisphosphonates as anti-resorption agents such as alendronate [2,3] and zolendronate [4]. The results indicated good bone regeneration with improved bone quality and mineralization in different localizations compared to BMP-2 alone [5,6].

Among the several natural polymeric scaffolds prepared for bone regeneration, chitosan is a biomaterial frequently used for this purpose. In a recent extensive review [7] based on chitosan (CHT) applied in bone tissue regeneration, different advantageous aspects were showed and discussed such as biocompatibility, capacity for BMPs sustained release, improvement of cell proliferation, and increase of in vitro and in vivo differentiation and mineralization. However, bone graft materials to simulate bone structure, e.g., collagen, the major ECM of bone tissue, and hydroxyapatite (HAP), a mineral component of the bone, have also been widely studied [6,8–14].

Although the aforementioned studies indicated positive results, the mentioned strategies applied in osteoporosis (OP) conditions have not always been effective [15]. According to recent reports, the prolonged subcutaneous administration of alendronate and the low level of estrogen in OP alters the evolution of calvarial bone repair due to estrogen, Transforming Growth Factor beta 1 (TGF-β1), and α-estrogen receptor (α-ER) interaction [16]. Menopausal women are the population most affected by this disease due to estrogen deficiency. Previous reports revealed that local implantation of scaffolds loaded with combinations of BMP-2 and 17β-estradiol formulated in microspheres of polylactic acid (PLA) or PLGA, in rat calvaria critical defects increased the bone repair in OP rats, but the new bone that refilled the defect was less mineralized compared to non-OP groups [17,18].

As some biomaterials may promote bone regeneration, controlled release of the active substances is required for efficient and safe bone regeneration [19,20]. In this study, we propose a loaded BMP-2 and 17β-estradiol sandwich-like system, comprising two polymeric external films and a core of a biocomposite hydrogel containing microspheres, to provide sustained release of active substances. The core system composed of CHT, collagen, HAP nanoparticles (nano-HAP), polyethylene glycol (PEG-400) and 2-Hidroxipropil γ-Ciclodextrin HP-γ-CD was previously characterized in terms of composition, rheological behavior and mass-transfer using RITC-dextran as macromolecule model and 17β-estradiol in microspheres [21]. In the present study, we aim to study the influence of the release rate of 17β-estradiol on the osteogenic effect induced by BMP-2 released from PLGA microspheres within core system after sandwich-like system implantation in a OP rats critical size defect. Therefore, 17β-estradiol was incorporated into the system in 3 forms: free and dispersed in the core, encapsulated in microspheres prepared with a mixture of PLA and PLGA dispersed within the hydrogel and lastly encapsulated in the PLGA films shell prepared by electrospinning technique.

2. Materials and Method

2.1. Materials

PLGA 75:25 (Resomer® RG755-S), PLGA 50:50 (Resomer® RG504), PLGA 85:15 (Resomer® RG858-S), and PLA (Resomer® RG203-S) were supplied by Evonic Industries (Darmstadt, Germany). Chitosan

(Protasan® UP-CL-213) was purchased from NovaMatrix (Sandvika, Norway). 2-Hidroxipropil γ-Ciclodextrin (CAVASOL® W8 HP), was supplied by Wacker Chemical (Burghausen, Germany). The bovine collagen type I was purchased from CellSystems Biotechnologie (Vertrieb GmbH, Germany). Riboflavin (RB), Poly(ethylene glycol) 400, Poly(vinyl alcohol) (PVA, Mw 33–70 kDa; 87–90% hydrolyzed), 17β-estradiol, and all the other reagents were purchased from Sigma-Aldrich, (St. Louis, MO, USA). The recombinant human bone morphogenetic protein 2 (BMP-2) was bought from Biomedal Life Sciences (Sevilla, Spain). Citrate-coated carbonated apatite nanoparticles (nano-HAP) were kindly donated (Jaime Gómez-Morales, PhD, Laboratory of Crystallographic Studies, CSIC, Granada, Spain).

2.2. Microspheres Preparation and Characterization

The BMP-2 microspheres were prepared by the double emulsion method (w/o/w) previously described [22]. Briefly, 200 μL of an aqueous solution (0.2% PVA) of BMP-2 (260 μg) was emulsified with 1 mL of a PLGA mixture (150 mg) of RG504 and RG858 [4:1] in methylene chloride (DCM) by vortexing 1 min (position 10, Genie® Industries 2, Sciencies Industries Inc. USA). Then, this emulsion was poured into 10 mL of 0.2% PVA solution vortexed 15 s, then poured into 100 mL of 0.1% PVA and kept under magnetic stirring for 1 h for solvent evaporation.

The 17β-estradiol microspheres were prepared by a modified solvent evaporation method previously described [17]. Briefly a mixture of 17β-estradiol (4 mg), PLA-S RG203-S (160 mg) and PLGA RG858 (40 mg) dissolved in 0.6 mL of DCM:Methanol (DCM:MeOH) (80:20) was emulsified with 4 mL of 1% PVA aqueous solution by vortexing 1 min (position 10), and then added to 100 mL of 0.16% PVA solution, under magnetic stirring for organic solvent evaporation (1 h).

Both type of microspheres were collected by filtration (Pall Corporation, pore size 45 μm, Sigma-Aldrich, USA), lyophilized, and stored at 4 °C until use.

Microspheres were characterized in terms of size (Mastersizer 2000, Malver Instruments, Malvern, UK) and morphology (SEM, Jeol JSM-6300, Tokyo, Japan). To determine the BMP-2 encapsulation efficiency and to carry out the BMP-2 release assays, some batches were prepared with ^{125}IBMP-2. The BMP-2 was labeled with ^{125}INa (Perkin-Elmer) by the iodogen method [23]. The content of 17β-estradiol in the microspheres was determined spectrophotometrically at λ = 280 nm previous dissolution in a mix of DCM:MeOH (80:20).

To determine the solubility of 17β-estradiol in the polymer matrix of the microspheres, differential scanning calorimetry (DSC 025, TA Instruments, New Castle, DE, USA) was performed. 17β-estradiol and lyophilized microspheres were analyzed after drying in an oven at 37 °C overnight. In addition, samples of polymer blends (RG 203-S and RG 858, 4:1) and samples of the polymer blend with excess 17β-estradiol (8.5%) were dissolved in DCM:MeOH (80:20) and maintained in a hood for 24 h. Then, samples were placed 48 h more in a vacuum desiccator to complete the evaporation of the organic solvent. The analysis of all samples was performed with the same thermal program in two thermal cycles under a nitrogen atmosphere (50 mL/min). In the first cycle, temperature was increased to 40 °C (10 °C/min) and then cooled to −20 °C (5 °C/min) to avoid possible water interference. Once the samples were stabilized, they underwent a final heating cycle from −20 °C to 270 °C (10 °C/min).

2.3. Fabrication and Characterization of the Film

The film was fabricated by a previously described electrospinning method [24]. Briefly, 7 mg of 17β-estradiol and 300 mg of a mixture of PLGAs, RG755-S and RG858 [4:1] were dissolved in 2 mL of hexafluoroisopropanol (Sigma-Aldrich, Steinheim, Germany) and electrospun at 7kV; flow rate of 3.0 mL/h and 10 cm of distance from the collector.

The film quality was checked in terms of porosity, thickness and fiber diameter using helium pycnometer (AccuPyc 1330, Micromeritics, Norcross, GA, USA), stereo microscopy (Leica M205C, Leica Las, v3 sofware), and SEM (Jeol, JSM-6300, Tokyo, Japan), respectively.

2.4. Core System Preparation and Characterization

To prepare the core system, approximately 20 mg of microspheres were dispersed in 50 µL of the hydrogel composed by a mixture of collagen type I (5 mg/mL), HP-γ-CD (34 mg/mL), RB (0.4 mg/mL), CHT (5 mg/mL), PEG-400 (150 mg/mL), and 5 mg of nano-HAP. Then, the hydrogel was cross-linked with 5% *w*/*w* TPP sterile aqueous solution (0.5 µL/µL of hydrogel) and visible light blue at 468 nm (Dental device) for 3 min [21]. The dose of BMP-2 was 6 µg in microspheres and the total 17β-estradiol dose was 200 µg in three different forms: electrospun films, microspheres, or dispersed into the gel.

The quality of the core system was checked according to its rheological characteristics and porosity previously described [21]. In addition, water uptake and mass loss assays were carried out by incubation of aliquots of 300 µL of the core system in 5 mL of sterile MilliQ water (37 °C) under orbital agitation (25 rpm). At specific times, six samples were withdrawn, we then removed excess water, weighed, and freeze-dried the samples. Then, three samples were visualized by SEM (Jeol JSM-6300) to see the evolution of the internal structure after incubation. The other three samples were used to record the dried weight and calculate the percentage of mass loss and water uptake, applying Equations (1) and (2), respectively, where W_0 is the initial weight of the sample and W_w and W_d are the weights of the wet and dried sample, respectively, at the different times tested.

$$Mass\ loss(\%) = \frac{(W_0 - W_d)}{W_0} \times 100 \quad (1)$$

$$Water\ uptake(\%) = \frac{(W_w - W_d)}{W_d} \times 100 \quad (2)$$

To test the syringeability of the core system two syringes of 1 mL were loaded with a suspension of microspheres of 17β-estradiol in the hydrogel, up to 0.5 mL. Then, 4 doses of 50 µL each were unloaded from both syringes assayed for fluidity through a 20G needle and dose uniformity. For this, the discharged samples were lyophilized, and the 17β-estradiol content evaluated by spectrophotometry at 280 nm, after dissolution in DCM: MeOH (80:20).

2.5. In Vitro Release Assays

BMP-2 in vitro release assays were carried out by incubating an amount of ^{125}I-BMP-2 microspheres and an amount of core system with the same amount of ^{125}I-BMP-2 microspheres in sterile MilliQ water at 37 °C and 25 rpm. The amount of BMP-2 released was calculated by measuring the radioactivity of supernatant samples with a gamma counter (Cobra® II, Packard).

The in vitro release of 17β-estradiol from the different formulations (dispersed in the core system, microspheres, microspheres incorporated to the core system, and electrospun films) was carried out at 37 °C and 25 rpm using two release media: an aqueous solution of sodium lauryl sulfate (SLS) 1% [25] and MeOH:water (50:50) [26,27]. The released 17β-estradiol was measured in the supernatant using the spectrophotometric method. The effective diffusion coefficient, D_{eff} in the matrix of the microspheres and the mass transfer coefficient of the drug in the boundary layer h, were calculated according to the non-steady-state Fick law, as previously described in detail [21]. Whether or not the released fraction of 17β-estradiol from the microspheres dispersed in the core system was analyzed, and Equations (3)–(6) were applied for D_{eff} and h calculation.

$$\frac{M_t}{M_\infty} = 1 - \sum_{n=1}^{\infty} \frac{6\,L^2}{\beta_n^2\left(\beta_n^2 + L^2 - L\right)} exp\left(-\frac{\beta_n^2}{R^2}\,D_{eff}\,t\right) \quad (3)$$

where M_t and M_∞ are the total mass of drug released to the media at time t and at the end of the experiment, respectively. The β_ns are the infinite roots (eigenvalues) of the Equation (4):

$$\beta_n \cot\beta_n + L - 1 = 0 \quad (4)$$

L is the dimensionless mass transfer Biot number Equation (5):

$$L = \frac{h\,R}{D_{eff}} \tag{5}$$

For large values of L, the roots of Equation (4) are multiples of the number *pi* and Equation (3) can be simplified in the Equation (6), that is, a simplified solution of non-steady-state Fick law:

$$\frac{M_t}{M_\infty} = 1 - \frac{6}{\pi^2}\sum_{n=1}^{\infty}\frac{1}{n^2}exp\left(-\frac{n^2\,\pi^2}{R^2}\,D_{eff}\,t\right) \tag{6}$$

As stated previously, to minimize the residual sum of squares, "genetic algorithms" already implanted in R software (R Foundation for Statistical Computing, version 3.6.1., 2019, Vienna, Austria) were used [21].

2.6. Animal Experiments

All animal experiments were carried out in conformity with the European Directive (2010/63UE) on Care and Use in Experimental Procedures. Furthermore, the animal protocols were approved on 5 November 2014 by the Ethics Committee for Animal Cares of the University of La Laguna (CEIBA) with identification code CEIBA2014-0128. All surgical procedures were made under aseptic conditions.

2.6.1. Animal Models

Forty female adult Sprague-Dawley rats approximately 12 weeks old, weighing 200–250 g, were divided in 4 groups of 10 each. The experimental osteoporosis was induced in 3 groups by three different protocols, OVX, chronic administration of DEX and OD. The forth group was the sham, non-osteoporotic control group (non-OP). The bilateral ovariectomy was carried out under isoflurane anesthesia, via dorsal approach to the animals of OVX and OD groups. Analgesia consisted in buprenorphine administered subcutaneously (0.05 mg/kg) before surgery and paracetamol (70 mg/100 mL) in the water, for 3 days post-surgery. The DEX group received 0.3 mg/kg body weight of dexamethasone-21-isonicotinate (Deyanil retard, Fatro Ibérica, Barcelona, Spain) administered subcutaneously once ievery two weeks [28] up to the time of euthanasia. Then, two weeks after the ovariectomy, the rats of group OD were chronically treated with DEX as the DEX group. The 40 rats were sacrificed after 12 weeks and the calvaria and femurs were extracted to be histologically analyzed. The results of these analyzes were used to evaluate the 3 protocols tested to induce OP.

2.6.2. Animals Groups

Fifty female Sprague-Dawley rats (12 weeks old), weighing 200–250 g, were divided into 2 groups of 25 each: OP and non-OP. The rats of the OP group were ovariectomized and the rats of the non-OP group underwent similar surgery but the ovaries were not resected. Twelve weeks post-surgery, 8 mm critical size cranial defects were created surgically with a trephine burr in the rats under isoflurane and the systems were placed into the defects [20]. Analgesia treatment was administrated.

Female rats were divided into 5 groups of 10 rats each—5 OP and 5 non-OP—and the applied regenerative treatment is reflected in Table 1. The implantation of the systems was carried out following a two steps procedure. First, a layer of film (bottom film), previously soaked in the blood produced during the surgery, was placed in the defect then 50 µL of the hydrogel mixed with the microspheres and partially cross-linked with UV light, was discharged. Second, the hydrogel was completely cross-linked by dripping 25 µL of sodium tripolyphosphate (TPP) forming the core system, after 5 min, a second layer of film (soaked in blood) was placed on the top, like a sandwich, and the wound was then closed.

Table 1. Experimental groups to evaluate regenerative efficiency.

Group Designations	Treatment
Blank I (B)	System loaded with blank microspheres and blank films
Blank II (B-HAP)	System loaded with blank microspheres and 5 mg of nano-HAP and blank films
BMP+EF	System loaded with 6 μg of BMP-2 in microspheres and 200 μg of 17β-estradiol in the 2 films
BMP+EMs	System loaded with 6 μg of BMP-2 in microspheres and 200 μg of 17β-estradiol in microspheres, blank films
BMP+ED	System loaded with 6 μg of BMP-2 and 200 μg of 17β-estradiol dispersed, blank films

2.6.3. ^{125}I-BMP-2 in Vivo Release Assay

The BMP-2 release kinetics was monitored periodically by measuring the remaining ^{125}I-BMP-2 at the rat calvarial defect site (n = 5) using an external probe-type gamma counter (Captus ®, Capintec Inc., Ramsey, NJ, USA), as previously described and validated [29].

2.7. Rat Mesenchymal Stem Cells (rMSCs) Osteogenic Differentiation

The rMSCs were obtained by centrifugal isolation as previously described [30] from the bone marrow of the femur of OVX female Sprague-Dawley rats. Briefly, the cells were resuspended in high glucose DMEM (HyClone® Utah) supplemented with 10% fetal bovine serum (Biowest, South America Origin), 1% penicillin–streptomycin (PAA, Pasching, Austria), and 2 mM L-Glutamine stable (Biowest, France) (Complete Culture Medium, CCM). Then, cells were cultured in flasks of 75 cm^2 and subcultured by incubating at 37°C and 5% CO_2. The culture medium was changed every 2–3 days.

To test the osteogenic differentiation, 50,000 cells (passage 2) in 20 μL of CCM were added over aliquots of 300 μL of the core system (hydrogel with microspheres) with and without nano-HAP and incubated at 37 °C and 5% CO_2 for 1.5 h for cell adhesion. The homogeneous cell distribution was checked by light microscopy. Afterwards, 500 μL of CCM were added to each well, after 3 days incubation the medium was changed to CCM supplemented with 10 mM β-glycerol phosphate, 10^{-7} M dexamethasone and 50 μM ascorbate-2-phosphate. At 7, 14, and 21 days of culture, three wells of each time point were washed (2 times) with Hank's balanced salt solution (HBSS 1x) and cooled at 4 °C. Then, 500 μL of 0.1 M buffer Tris-HCl, 0.1M NaCl, and 0.05 M $MgCl_2$ (pH = 9.2–9.5) containing Nitro blue tetrazolium chloride (NBT, Roche Diagnostics, Mannheim, Germany) and 5-Bromo-4-chloro-3-indolyl phosphate (BCIP, Roche Diagnostics, Mannheim, Germany) were added and incubated at 37 °C and 5% CO_2 under soft agitation for 1.5 h. Then, the NBT/BCIP was removed and the cells were fixed with a solution of 3.7–4% p-formaldehyde buffered to pH = 7.0 (Panreac®, Barcelona, Spain) during 30 min. After this, the formaldehyde was removed, and the wells were washed 3 times with HBBS 1x. Immediately after this, cells were visualized by stereo microscopy (Leica M205C, Leica Las, v3 software). In addition, samples were dehydrated in a graded series of ethanol before being embedded in Paraplast® and microtome (Shandon Finesse 325, Thermo Fisher Scientific, Madrid, Spain) sections were observed by light microscopy (LEICA DM 4000B, Barcelona, Spain).

2.8. Histology, Immunohistochemical, and Histomorphometrically Evaluation

First, to check the osteoporotic-like condition, 12 weeks after the 12 rats undergone the different protocols were sacrificed and the femurs and calvaria were analyzed. The femurs and calvaria were fixed (4% paraformaldehyde solution), decalcified in Histofix® Decalcifier (Panreac, Barcelona, Spain) and prepared for histological analysis as previously described [20,22].

Bone morphology was analyzed by hematoxylin–erythrosin staining. The histomorphometric analyze was carried out in femurs by measuring the following parameters; thickness of the cortical

bone (Ct.Wi) and number (Tb.N), width (Tb.Wi) and separation (Tb.Sp) of the trabeculae in cancellous bone. In the calvaria bone, the histomorphometric analysis was carried out by measuring the following parameters, cortical bone thickness (CBT) and intercortical space thickness (IST) occupied by trabecular bone in transversal sections of calvaria.

To determine the capacity of the bone active substances, so as to regenerate the critical size defect practiced in the calvaria of the rats, samples of the 10 groups of 5 rats each were examined.

Samples were processed as previously described [22]. New bone formation was identified by hematoxylin–erythrosin staining. Bone mineralization was assessed with VOF trichrome stain, in which red and brown staining indicates advanced mineralization, whereas less mineralized, newly formed bone stains blue [31]. Sections were analyzed by light microscopy (LEICA DM 4000B, Barcelona, Spain). Computer-based image analysis software (Leica Q-win V3 Pro-Image Analysis System, Barcelona, Spain) was used to evaluate all sections. A region of interest (ROI) within the defect (50 mm^2) for quantitative evaluation of new bone formation was defined. New bone formation was expressed as a percentage of repair with respect to the original defect area within the ROI. From the total bone repair, the areas of mature bone (MB) and immature bone (IB) were determined, and the MB/IB ratio for each experimental group as well as between non-osteoporotic and osteoporotic-like animals was calculated.

For immunohistochemical analysis, sections were deparaffined and rehydrated in Tris-buffered saline (TBS) (pH 7.4, 0.01 M Trizma base, 0.04 M Tris hydrochloride, 0.15 M NaCl), which was used for all further incubations and rinse steps. Sections were incubated in citrate buffer (pH 6) at 90 °C for antigen retrieval, followed by incubation in 0.3% hydrogen peroxide in TBS buffer for 20 min. After a rinse step, sections were blocked with 2% FBS in TBS–0.2% Triton X-100 (blocking buffer). The indirect immunohistochemical procedure was carried out by incubating the sections with osteocalcin (OCN) polyclonal antiserum (1/100) (Millipore, Barcelona, Spain) in blocking buffer overnight at 4 °C. Sections were rinsed three times, then incubated with biotin-SP-conjugated donkey anti-rabbit F(ab) fragment (1/200) (Millipore, Barcelona, Spain) in blocking buffer for 1 h followed, after another rinse step, by incubation in peroxidase-conjugated streptavidin (1/300) (Millipore, Barcelona, Spain) for 1 h. Peroxidase activity was revealed in Tris–HCl buffer (0.05 M, pH 7.6) containing 0.05% of 3,3′-diaminobenzidine tetrahydrochloride (Sigma, Poole, UK) and 0.004% hydrogen peroxide. Reaction specificity was confirmed by replacing the specific antiserum with normal serum or by pre-adsorption of the specific antiserum with the corresponding antigen.

OCN staining was evaluated using computer-based image analysis software (ImageJ, NIH, Bethesda, MD, USA). OCN staining was measured by applying a fixed threshold to select for positive staining within the ROI. Positive pixel areas were divided by the total surface size (mm^2) of the ROI. Values were normalized to those measured from blank scaffolds and are reported as relative staining intensities.

Statistical analysis was performed with SPSS.25 software. We compared the distinct treatments by means of a one-way analysis of variance (ANOVA) with a Tukey multiple comparison post-test. Significance was set at $p < 0.05$. Results are expressed as means ± SD.

3. Results

3.1. Sandwich-Like System Characterization

The characteristics of the microspheres, electrospun film, and core system are shown in Table 2.

Table 2. Characteristics of the component of the sandwich-like system. Microspheres: size and encapsulation efficiency. Electrospun film: thickness and porosity of the film and average diameter of the fibers). Core system: porosity freshly prepared and lyophilized and water uptake and mass loss after incubation in MilliQ water, 37 °C, and 25 rpm.

Microspheres	**Size (μm)**			**E.E. (%)**
17β-estradiol	101.4 (10% < 29.73, 90% < 198.31)			83.5 ± 1.84
BMP-2	112.1 (105 < 60.3, 905 < 174.8)			71 ± 7
Film	Thickness (μm)	Fiber diameter (μm)		Porosity (%)
	63.4 ± 4.3	1.2 ± 0.26		71.9 ± 0.41
Core system (Hydrogel + microspheres)	Porosity (%)	Incubation time	Water uptake (%)	Mass loss (%)
	72	7 days	135.9 ± 2.6	18.85 ± 7
		28 days	138.9 ± 11.0	29.19 ± 4.88

SEM image of the microspheres is shown in Figure 1A and the differential scanning calorimetry thermograms of the 17β-estradiol microspheres components are plotted in Figure 2. The glass transition temperature (Tg) of the mixture of polymers RG 203-S and RG 858 [4:1] was located at 52–58 °C, in the temperature range of the PLA (RG203-S) and PLGA (RG858). The DSC analysis of pure 17β-estradiol showed three endothermic peaks (Figure 2A), the first two at 118.1 °C and 174.4 °C, previously attributed to the partial and complete loss of hydrogen-bound water and reticular water, respectively. The third at 179.4 °C corresponds to the melting point [32]. This last peak, characteristic of the crystalline structure of 17β-estradiol, was not detected in the spectrum of the polymers and 17β-estradiol blend or in the thermogram of the microspheres (Figure 2B). These results indicated that 17β-estradiol was dissolved in the polymer by at least 8.5%.

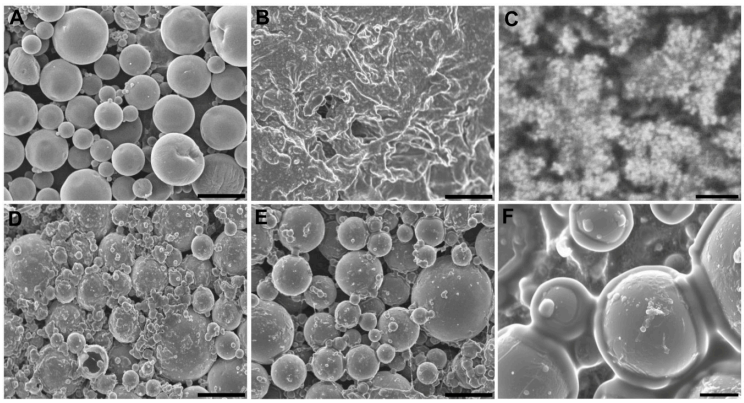

Figure 1. SEM images (**A**) microspheres, (**B**) hydrogel, (**C**) hydrogel high magnification detail, (**D**) core system freshly prepared, (**E**) internal structure of the core system after 4 weeks incubation in water at 37 °C and 25 rpm, and (**F**) high magnification detail of Figure 1E. Scale bars: (**A**–**E**) 100 μm, (**C**) 1 μm, (**F**) 20 μm.

The integrity of the system was assayed throughout the 4-week test duration. The SEM images of the internal structure of the hydrogel (Figure 1B,C), the freshly prepared core system (Figure 1D), and after 4 weeks incubation showed that the microspheres were homogeneously dispersed in the hydrogel and are trapped in the core system during incubation (Figure 1E,F). The core system absorbed a significant amount of water during the first days of incubation which was maintained over time.

Contrarily, the system lost little mass: less than 20% during the first week and approximately 35% after 4 weeks (Table 2). In addition, the core system flew well through the 20 G needle and the average dose discharged was 83.5 ± 6% of the loaded dose.

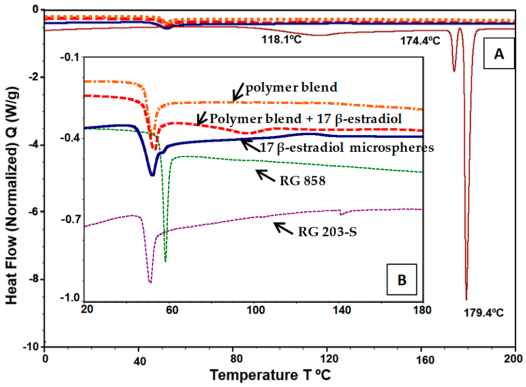

Figure 2. Differential scanning calorimetry thermograms. (**A**) Curve of pure 17β-estradiol. (**B**) Curves of PLA (RG203-S); PLGA (RG858), polymer blend (RG203-S:RG858, [4:1]), and polymer blend with 8.5% of 17β-estradiol, previously dissolved in DCM:MeOH (80:20) and the curve of the microspheres of 17β-estradiol (**B**).

3.2. Osteogenic Differentiation

The alkaline phosphatase positive (ALP+) cell count, in the hydrogels pre-seeded with rMSCs and cultured in the osteogenic differentiation culture medium, showed a discrete and progressive increase in the number of cells between 7 and 21 days of culture in the hydrogels without and with nano-HAP; the number being significantly higher in those containing nano-HAP (Figure 3). Likewise, qualitatively, the cells presented, in the scaffolds with nano-HAP, greater intensity of color, suggesting greater ALP activity (Figure 3) than without nano-HAP.

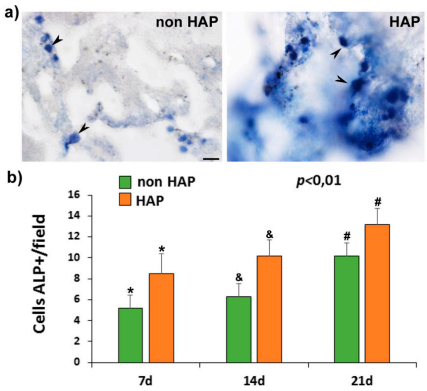

Figure 3. Alkaline phosphatase (ALP) activity in rMSCs cultures. (**a**) Representative images from hydrogels 20 days after cultured showing the AP-positive (ALP+) cells' morphology (arrowheads) in hydrogel without (non-HAP) and with nanohydroxyapatite (HAP). (**b**) Graphic showing the number of APL+ cells/ microscopic field at different time points of analyses (7, 14, and 21 days) after culture in each system. Scale bar = 20 μm. The identical symbol on different bars indicates significant differences.

3.3. Release Profiles of ^{125}I-BMP-2 and 17β-Estradiol.

Although the hydrogel provoked a strong reduction of the burst effect, the in vitro release of BMP-2 from the microspheres and from the core system showed a biphasic profile. During the first 24 h, approximately 7% of the protein was release from the core system versus 27% from the microspheres directly dispersed in the medium. Afterward, the release rate was kept in the range of 60 to 55 ng/day (Figure 4). The in vivo release profile was also biphasic, with a first phase that lasted up to 7 days whereas approximately 50% of the protein released. Then, the release rate was reduced to 70 ng/day, which is slightly higher than the in vitro rate.

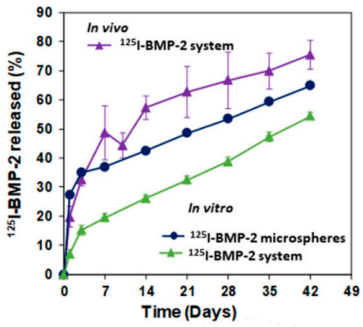

Figure 4. BMP-2 release assays. In vivo release profile of ^{125}I-BMP-2 from PLGA-microspheres in the system after implantation in the rat calvaria defect (n = 5). In vitro release of ^{125}I-BMP-2 (incubation in water at 37 °C and 25 rpm) from PLGA-microspheres and from the PLGA microspheres dispersed in the system.

The in vitro release rate of 17β-estradiol in the aqueous medium depended on the formulation (Figure 5B); 100% and 70% of the 17β-estradiol dispersed in the hydrogel and in the electrospun film were detected in the medium after 4 weeks incubation, respectively. The release profile was characterized by a high burst effect; approximately half of the dose was released during the first day. By contrast, the 17β-estradiol release rate was extremely slow from the microspheres alone and from the microspheres included in the hydrogel (core system). Both release profiles were similar: less than 20% was delivered in 4 weeks. However, in the MeOH: water (50:50) medium there were not differences in the transfer profiles. The presence of MeOH modifies the solubility of 17β-estradiol, showing a strong burst effect that varied in a range between 70 and 85% in the first 24 h (Figure 5A).

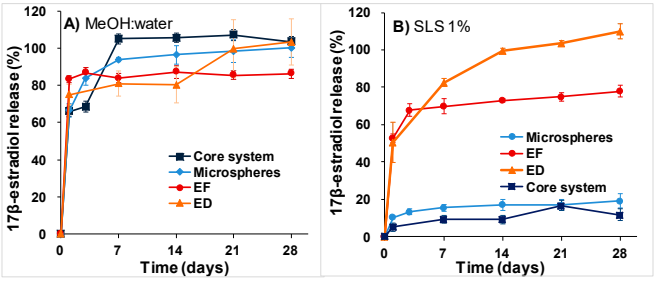

Figure 5. In vitro 17-β-estradiol release profiles in different release media at 37 °C and 25 rpm. (**A**) In MeOH:water (50:50). (**B**) In aqueous solution of SLS 1%. (ED) 17β-estradiol dispersed in the core system; (EF) 17β-estradiol in the electrospinned film; (microspheres) 17β-estradiol pre-encapsulated in microspheres and (core system) 17β-estradiol microspheres in the hydrogel.

The estimated values of D_{eff} and h for 17β-estradiol release in the different media are showed in Table 3. Although the value of D_{eff} of 17β-estradiol in SLS was significantly lower compared to the MeOH:water (50:50), there were not differences for h regardless of the release media used. h is the contribution of hydrogel, as part of the boundary layer, to the whole mass transfer process, and the value of this coefficient should not change by varying the release media. The values of R^2 (Table 3), together with the comparison of experimental and predicted values of the released fractions shows a good fit of the data to the proposed model for both release media.

Table 3. Estimated values of effective diffusion coefficient (D_{eff}) and mass transfer coefficient (h) for 17β-estradiol release in different media applying Equations (3)–(6).

Release Media	D_{eff} (m²/s)	h (m/s)	R^2 (%) Value
MeOH:water (50:50)	$2.28{\cdot}10^{-15} \pm 5.00{\cdot}10^{-17}$	$7.56{\cdot}10^{-10} \pm 2.89{\cdot}10^{-10}$	95.47 ± 0.07
SLS 1%	$5.58{\cdot}10^{-16} \pm 9.81{\cdot}10^{-17}$	$4.01{\cdot}10^{-10} \pm 4.94{\cdot}10^{-10}$	92.49 ± 2.71

3.4. Histology, Immunohistochemical, and Histomorphometrically Evaluation

3.4.1. Osteoporotic Model

The osteoporotic model was assessed in both long bone (femur) and flat bone (calvaria). The histological analysis of calvaria showed evident changes in the structure and microarchitecture of the bone among the different experimental groups. Although the non-OP animals showed a normal bone structure in cortical bone (CB) and trabecular bone (TB), in the intercortical space (ICS), for the different OP models (DEX, OVX, and OD (Figure 6a), it was observed a progressive decrease in cortical bone thickness (CBT) and an increase in the intercortical space thickness (IST), being the group OD the one that presented greater alteration of the tissue bone structure (Figure 6b).

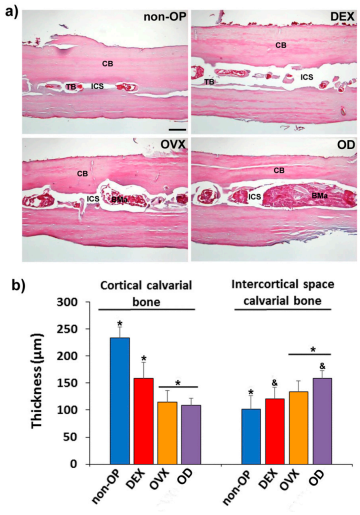

Figure 6. Validation of the OP model in calvarial bone. (**a**) Representative images in transversal section of calvaria in non-osteoporotic animals (non-OP) and in each of the different experimental models of osteoporosis tested showing the bone structure in each one. (**b**) Histomorphometric analysis of the cortical bone thickness and intercortical space thickness evaluated in calvaria in the different models of osteoporosis. CB: cortical bone; BMa: bone marrow; ICS: intercortical space; TB: trabecular bone. Scale bar = 100 µm. The identical symbol on different bars indicates significant differences.

The histological analysis of the femurs showed evident changes in the structure and microarchitecture of the bone among the different experimental groups. Although the non-OP animals showed a normal bone structure, in the different OP models (DEX, OVX and OD), structural changes were observed, both at the level of cortical and cancellous bone, showing a less compact bone and with a more porous structure (Figure 7a). The histomorphometric analysis revealed differences in the parameters measured in cancellous bone (Tb.N, Tb.Wi., and Tb.Sp.), with a significant reduction in all of them, in OVX and OD compared to the non-OP and DEX animals (Figure 7b–d). The cortical bone thickness (Ct.Wi.), although it showed a slight reduction in the groups (OVX and OD) with respect to the non-OP and DEX groups, was not significant (Figure 7e).

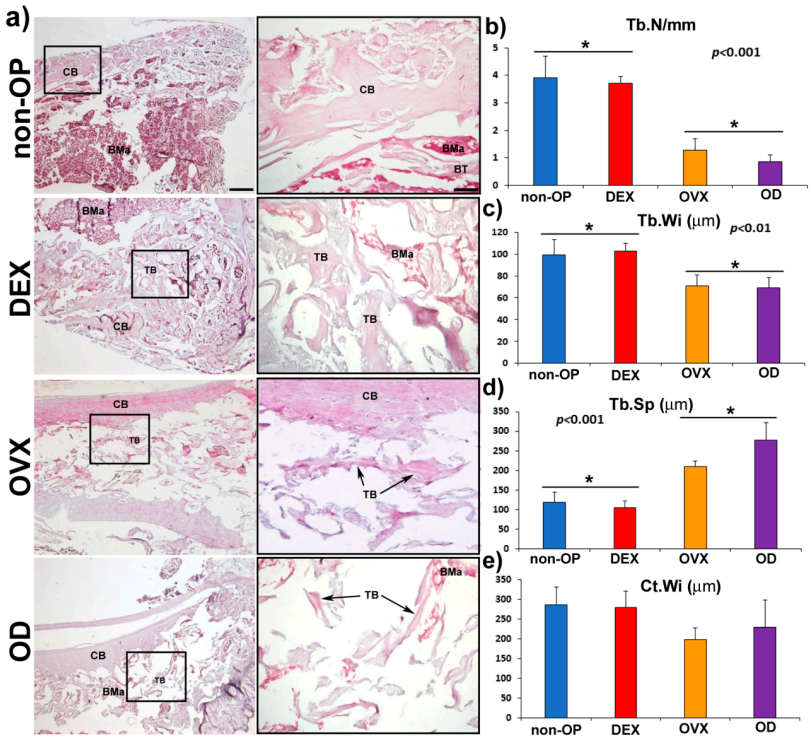

Figure 7. Validation of the OP model in long bone (femur). (**a**) The left column shows representative panoramic images in longitudinal section of rat femur in non-osteoporotic animals (non-OP) and in each of the different experimental models of osteoporosis tested. The right column shows high magnification images of the distal portion of the femur, showing differences in the microarchitecture of the bone in the different models. The column on the left shows detail of the boxed areas in which the structural characteristics of the compact and trabecular bone can be observed in each of the models. Histomorphometric analysis of the different parameters evaluated in femur in the different models of osteoporosis (**b**), Tb. N (mm), (**c**) Tb. Wi (μm), (**d**) Tb. Sp. (μm), and (**e**) Ct. Wi (μm). CB: cortical bone; TB: Trabecular bone; BMa: bone marrow. Scale bars: Left column 250 μm. Right column 50 μm. The identical symbol on different bars indicates significant differences.

3.4.2. Calvarial Critical Size Defect

The histological analysis at the level of the calvarial defect showed a few new bone formations in the blank groups (B and B HAP), being limited to the margins of the defect in both, non-OP, and OP groups (Figure 8a). The groups implanted with BMP-2 + 17β-estradiol in the three different formulations showed a greater area of newly formed bone in the defect area, not only in the margins, but also in inner zone of the defect (Figure 8a). The newly formed bone in the different experimental groups of non-OP and OP animals showed a normal morphology and VOF staining, revealing significant areas of mineralization, slightly higher in the groups of non-OP animals (Figure 8a).

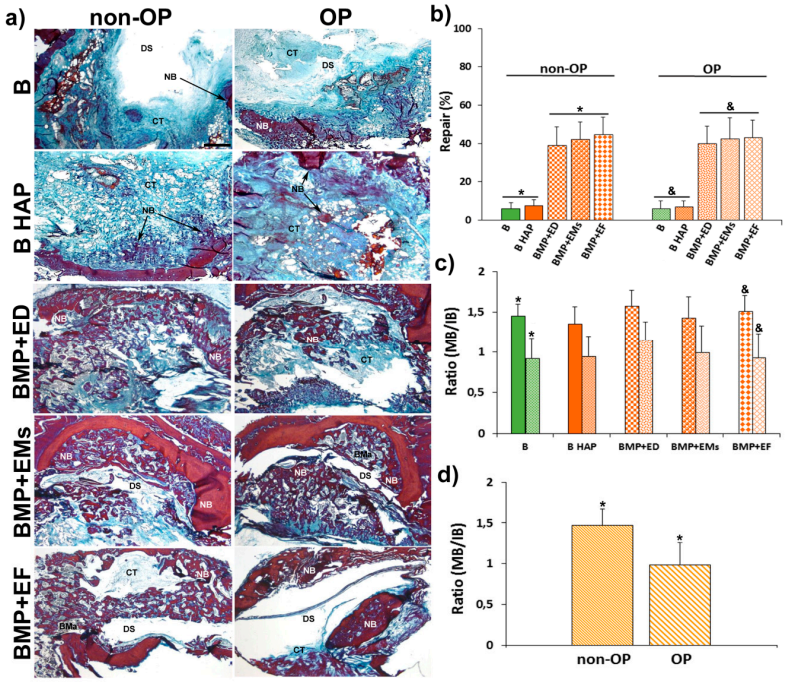

Figure 8. Repair process in calvarial defect. (**a**) Representative images in horizontal section of calvarial critical size defects in non-OP and OP rats showing the repair response at the defect level in the different experimental groups 12 weeks post-implantation. (**b**) Histomorphometrical analysis comparing of the degrees of repair (%) among the different experimental groups in non-OP and OP rats 12 weeks post-implantation. (**c**) Histomorphometric analysis showing the ratio between mature bone and immature bone (MB/IB) among the different experimental groups (**d**) and between non-OP and OP rats, estimated using VOF staining. Bars represent means ± SD (n = 4). The identical letter on different bars indicates significant differences. BMa: bone marrow; CT: connective tissue; NB: newly formed bone; DS: defect site. Scale bar = 1 mm. The identical symbol on different bars indicates significant differences.

The histomorphometric analysis showed little repair response in the blanks groups (B and B HAP) of non-OP and OP animals, with repair percent between 6 and 8%. The groups implanted with BMP-2 + 17β-estradiol in the three different formulations, on the contrary, showed a significantly higher repair response of 38–45%, with no differences being observed between non- OP and OP animals (Figure 8b).

The histomorphometric analysis of mature and immature bone showed a higher quantity of mature bone, and therefore with a greater degree of mineralization, in the experimental groups of

non-OP with respect to OP animals. The ratio between mature and immature bone (MB/IB) showed individually higher values in all non-OP with respect to OP groups as well as on the whole, with values of 1.47 in non-OP animals and 0.99 in OP (Figure 8c,d).

The immunohistochemical analysis of osteocalcin (OCN), a marker of late osteogenesis and mineralization, showed a low immunoreaction in the blank groups (B and B HAP) in both non-OP and OP animals, with no differences between them (Figure 9a). In the groups implanted with BMP-2 + 17β-estradiol in the three different formulations, the immunoreaction was higher and more intense with respect to the blank groups, in this case being slightly higher in the non-OP animals (Figure 9a).

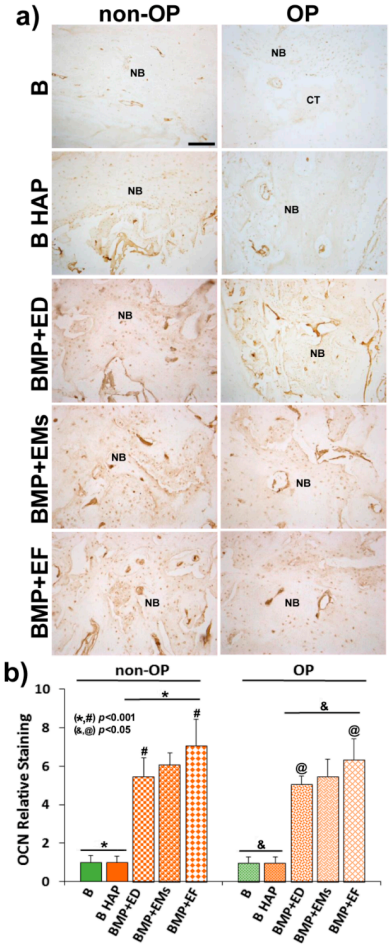

Figure 9. OCN relative expression. (**a**) Representative images in horizontal section of calvarial critical size defects in non-OP and OP rats showing OCN immunoreactivity in the different experimental groups 12 weeks post-implantation. (**b**) Histomorphometric analysis showing the relative staining values for OCN-ir. Bars represent means ± SD (n = 4). The identical letter on different bars indicates significant differences. CT: connective tissue; NB: newly formed bone. Scale bar = 100 μm. The identical symbol on different bars indicates significant differences.

The histomorphometric analysis confirmed the histological data, showing slightly higher relative staining values in the BMP-2 +17β-estradiol groups in non-OP animals (Figure 9b).

4. Discussion

In the present study, a BMP-2-17β-estradiol hydrogel system, with porosity of approximately 72%, was evaluated for regeneration of a critical size defect in rat calvaria. Although the system had already been characterized in terms of rheological behavior, porosity, interactions between components, mass transfer parameters, and cell viability, here the good injectability of the system was showed, and its characterization has been completed by testing the water uptake and mass loss as well as differentiation studies in cultures of osteoporotic rMSCs. In vitro release profiles of 17β-estradiol in two media and the in vitro and in vivo release profile of BMP-2 were also analyzed.

The osteogenic differentiation of osteoporotic rMSCs seeded on the system was assessed in order to test the effect of the incorporation of the nano-HAP on the cell behavior. The results showed greater ALP activity and a greater number of differentiated cells in the systems with nano-HAP. Therefore, nano-HAP systems were subsequently used in the in vivo experiments.

First, a histological evaluation of the femur and calvaria of rats suffering the three treatments for osteoporosis induction was carried out. OP is a systemic bone disease characterized by the increase of bone porosity, loss of bone mass and changes in the microstructure of the skeletal. Consequently, the OP population has an increased risk of fracture.

Despite the high number of OP studies and the several publications dedicated to tissue repair in non-OP specimens, very few reports devoted to bone defect regeneration in OP have been published. As OP might be primary post-menopausal or secondary, due to corticoid chronic administration, three animal models were used for OP induction: OVX, chronic glucocorticoid treatment, and the combination of both. In previous reports, a combination OD rat model was used. However, the high deterioration observed in the animals, the risk of induced additional disorders on the skeletal and the fact that bone loss reverses after corticoid stop [33] justify the bone histological study of the different treatment, in order to simplify the model and improve animal welfare. In general, OP condition is established through the analysis of long bones and lumbar spine but few data of the effect on the calvaria of the animals used as OP models are available [34]. Most of the publications on the regeneration of calvaria critical size defect in OP animals do not report the effects of OP in the calvaria [35,36]. In the present study, the data comparing the response of the femurs and calvarias to the three treatments revealed that the effect of OVX was similar to OD combination, consequently the fabricated system was tested in OVX rats.

As some authors have observed a delay in bone consolidation of OVX rats [37] and as this combination of BMP-2 and 17β-estradiol, formulated in microspheres, when applied to a critical calvaria defect, improved bone healing in OP rats, but the new bone was less mineralized [17,18], we tried to prolong the release of active substances to cover this delay. The drugs were incorporated to the hydrogel system pre-encapsulated in microspheres for prolonged controlled release. To reduce the release rate of the active substances the microspheres were prepared with a mixture of polymers, 25% of the RG 858 was incorporated to the RG 504 for BMP-2 microspheres as well as to the RG203-S for 17β-estradiol microspheres. RG 858 is a PLGA 85:15, of high molecular weight with a degradation rate lower than that of RG 504 and RG203-S. The BMP-2 release profiles showed a two-phase behavior with a weak burst effect that coincides with the period in which the system loses mass and uptakes a high amount of water. However, the burst effect of BMP-2 that can be seen from the microspheres was damped by the hydrogel, probably due to the interaction of the protein with the chemical groups of the HAP [6,13]. Afterwards, the second phases were practically parallel, which indicated a mass transfer process controlled by the access of water inside the microspheres, dissolution and diffusion of the protein throughout the porous of the polymeric matrix.

The release profile of 17β-estradiol as liposoluble drug in a MeOH:water (60:40) release medium was previously characterized [21]. By contrast, here two release media were used, MeOH:water (50:50)

and an aqueous solution of SLS, because we suspected that the solvent affected the release rate of the lipophilic substance. In fact, the release of 17β-estradiol in MeOH:water was fast regardless of the formulations. However, the in vitro release of 17β-estradiol was formulation-dependent when an aqueous medium was used; a high decrease of the release rate of the drug from the microspheres was observed. As DSC results indicated, 17β-estradiol formed a solid solution in the microspheres, which indicates that the release process takes place by molecular diffusion of 17β-estradiol within the microspheres, governed by the partition coefficient, and consequently the aqueous medium dissolved it very slowly. In addition, the higher estimated values of D_{eff} in the MeOH:water compared with the aqueous medium, confirmed the dependency on the release media. The calorimetric analysis of the electrospun sheet was not carried out because the amount of 17β-estradiol would have had to be increased to be detected and its characteristics would have been modified. Although 17β-estradiol is expected to also be dissolved in the polymer of the film, the large specific surface area that microfibers expose to the medium causes the drug to release rapidly. Similarly, 17β-estradiol dispersed in the hydrogel was very little retained. Obviously, neither media are physiological, but it seems more correct to use an aqueous medium to predict release in vivo. Although, with reservations, one would also expect a slightly faster release rate in vivo as the biological components present in the tissue could accelerate the drug release from the system.

Despite the beneficial role of the nano-HAP controlling the BMP-2 burst effect as well as its positive effect on the proliferation and osteogenic differentiation of rMSC, which justifies the use of nano-HAP in the system, the reparative effect of the blank scaffolds with and without nano-HAP was not enough to be considered useful. Unlike that observed in this study, other authors showed better bone repair in different bone defects practiced in osteoporotic goats implanted with a system of type I collagen containing nano-HAP than without [38]. By contrast, another study [6] found, as in the present study, that the use of nano-HAP and calcium sulfate bone substitute scaffolds in rat critical calvaria defect showed no effect on repair and mineralization at 8 and 12 weeks with respect to the empty defect. In both studies, the systems were loaded with BMP-2 combined with 17β-estradiol or zolendronic acid [6] that might abolish the effect of the HAP observed in vitro.

Although previously our group reported [17,18] a better result in bone regeneration of OP animals combining BMP-2 and 17β-estradiol, in this study, the repair effect observed has been similar to that observed in non-OP groups. The three combinations of BMP-2 with 17β-estradiol in each of the three formulations used showed the same effect at 12 weeks. However, the ratios of mature and immature bone in normal and osteoporotic animals showed significant differences, indicating that the quality of the repaired bone, at least after 12 weeks, was better in normal animals.

Although these results coincide with previous work, in the present study it seems that the mineralization of the bone formed slightly improved in the OP animals. The difference in the relative osteocalcin expression was not statistically significant. These results might suggest that a longer release of BMP-2 together with the composition of the system, presence of collagen and nanoHAP favor the mineralization process. In any case, it would be necessary in future to conduct studies aimed at discerning the role of each of these components in the process. However, we have not been able to reproduce the positive effect of 17β-estradiol combined with BMP-2 in a hydrogel composed of Pluronic, Tetronic and, cyclodextrin, with other scaffolds of different composition [18]. In addition, according to the present study, the fact that the different release profiles of 17β-estradiol had no effect on the repair of the defect indicates that 17β-estradiol, when applied locally, and regardless of the release rate (available dose) and of the obvious role that it plays on bone remodeling, does not justify its inclusion as active substance in the repair of bone defects neither in normal animals nor in osteoporotic ones. Therefore, new strategies and alternative drugs are currently being designed trying to accelerate mineralization of new bone in OP groups.

5. Conclusions

The prepared hydrogel system resulted to be easily injectable and solidified fast due to crosslinking of collagen and chitosan chains. The system helps control the burst effect of BMP-2 pre-encapsulated in PLGA microspheres, probably due to the nano-HAP. Release of 17β-estradiol from PLA-PLGA microspheres was more complex and is governed by the partition coefficient of the drug which is in solid dissolution in the microspheres. The system was biocompatible both in vivo and in vitro. However, the regenerative effect detected in the critical bone defect of both OP and non -OP rats was mainly due to the osteogenic effect of BMP-2 released in a controlled rate for 6 weeks. A delay in the mineralization of the new bone which fills the defect in OP animals was observed. 17β-estradiol released from different formulations and included in the system does not improve bone repair.

Author Contributions: Conceptualization, E.P.-H., A.D., and C.É.; methodology, E.P.-H., A.D., C.É., R.R., E.S.-M., P.G.-G; validation, R.R.; formal analysis, E.P.-H., A.D., C.É., R.R., P.G.-G.; investigation, E.P.-H., A.D., C.É., R.R. and P.G.-G.; resources, A.D. and C.É.; writing—original draft preparation, R.R., A.D., and C.É.; writing—review and editing, A.D. and C.É.; supervision, A.D. and C.É.; funding acquisition, A.D. and C.E. All authors have made a substantial contribution to the work.

Funding: This research and the APC was funded by Ministry of Science and Technology (MAT2014-55657-R).

Conflicts of Interest: The authors declare no conflicts of interest.

References

1. Murphy, C.M.; Schindeler, A.; Gleeson, J.P.; Yu, N.Y.; Cantrill, L.C.; Mikulec, K.; Peacock, L.; O'Brien, F.J.; Little, D.G. A collagen–hydroxyapatite scaffold allows for binding and co-delivery of recombinant bone morphogenetic proteins and bisphosphonates. *Acta Biomater.* **2014**, *10*, 2250–2258. [CrossRef] [PubMed]
2. Cho, T.H.; Kim, I.S.; Lee, B.; Park, S.N.; Ko, J.H.; Hwang, S.J. Early and Market Enhancement of New Bone Quality by alendronate-Loaded Collagen Sponge Combined with Bone Morphogenetic Protein-2 at High Dose: A Long-Term Study in Calvarial Defects in Rat Model. *Tissue Eng. Part A* **2017**, *23*, 1343–1360. [CrossRef] [PubMed]
3. Kim, H.C.; Son, J.M.; Kim, C.J.; Yoon, S.Y.; Kim, I.R.; Park, B.S.; Shin, S.H. Effect of bisphosphonate and recombinant human bone morphogenetic protein 2 on bone healing of rat calvarial defects. *Maxillofac. Plast. Reconstr. Surg.* **2015**, *37*, 16. [CrossRef] [PubMed]
4. Horstmann, P.F.; Raina, D.B.; Isaksson, H.; Hettwer, W.; Lidgren, L.; Petersen, M.M.; Tägil, M. Composite Biomaterial as a Carrier for Bone-Active Substances for Metaphyseal Tibial Bone Defect Reconstruction in Rats. *Tissue Eng. Part A* **2017**, *23*, 1403–1412. [CrossRef]
5. Raina, D.B.; Isaksson, H.; Teotia, A.K.; Lidgren, L.; Tägil, M.; Kumar, A. Biocomposite macroporous cryogels as potential carrier scaffolds for bone active agents augmenting bone regeneration. *J. Control Release* **2016**, *10*, 365–378. [CrossRef]
6. Teotia, A.K.; Raina, D.B.; Singh, C.; Sinha, N.; Isaksson, H.; Tägil, M.; Lidgren, L.; Kumar, A. Nano-Hydroxyapatite Bone Substitute Functionalized with Bone Active molecules for Enhanced Cranial Bone Regeneration. *Appl. Mater. Interfaces* **2017**, *1*, 6816–6828. [CrossRef]
7. Venkatesan, J.; Anil, S.; Kim, S.K.; Shim, M.S. Chitosan as a vehicle for growth factor delivery: Various preparations and their applications in bone tissue regeneration. *Int. J. Biol. Macromol.* **2017**, *104*, 1383–1397. [CrossRef]
8. Ma, X.; He, Z.; Han, F.; Zhong, Z.; Chen, L.; Li, B. Preparation of collagen/hydroxyapatite/alendronate hybrid hydrogels as potential scaffolds for bone regeneration. *Colloids Surf. B Biointerfaces* **2016**, *1*, 81–87. [CrossRef]
9. Cholas, R.; Kunjalukkal Padmanabhan, S.; Gervaso, F.; Udayan, G.; Monaco, G.; Sannino, A.; Licciulli, A. Scaffolds for bone regeneration made of hydroxyapatite microspheres in a collagen matrix. *Mater. Sci. Eng. C Mater. Biol. Appl.* **2016**, *63*, 499–505. [CrossRef]
10. Zhang, P.; Hong, Z.; Yu, T.; Chen, X.; Jing, X. In vivo mineralization and osteogenesis of nanocomposite scaffold f poly(lactide-co-glycolide) and hydroxyapatite surface-grafted wit poly(L-lactide). *Biomaterials* **2009**, *30*, 58–70. [CrossRef]

11. Zhang, B.; Zhang, P.B.; Wang, Z.L.; Lyu, Z.W.; Wu, H. Tissue-engineered composite scaffold of poly(lactide-co-glycolide) and hydroxyapatite nanoparticles seeded with autologous mesenchymal stem cells for bone regeneration. *J. Zhejiang Univ. Sci. B* **2017**, *18*, 963–976. [CrossRef] [PubMed]
12. Gupta, V.; Lyne, D.V.; Barragan, M.; Berkland, C.J.; Detamora, M.S. Microsphere-Based Scaffolds Encapsulating Tricalcium Phosphate and Hydroxyapatite for Bone Regeneration. *J. Mater. Sci. Mater. Med.* **2016**, *27*, 121. [CrossRef] [PubMed]
13. Quinlan, E.; López-Noriega, A.; Thompson, E.; Kelly, H.M.; Cryan, S.A.; O'Brien, F.J. Development of collagen-hydroxyapatite scaffolds incorporating PLGA and alginate microparticles for the controlled delivery of rhBMP-2 for bone tissue engineering. *J. Control. Release* **2015**, *28*, 71–79. [CrossRef] [PubMed]
14. Wang, X.; Wu, X.; Xing, H.; Zhang, G.; Shi, Q.; E, L.; Liu, N.; Yang, T.; Wang, D.; Qi, F.; et al. Porous Nanohydroxyapatite/Collagen Scaffolds Loading Insulin PLGA Particles for Restoration of Critical Size Bone Defect. *ACS Appl. Mater. Interfaces* **2017**, *5*, 11380–11391. [CrossRef] [PubMed]
15. Segredo-Morales, E.; García-García, P.; Évora, C.; Delgado, A. BMP delivery systems for bone regeneration: Healthy vs osteoporotic population. Review. *J. Drug Deliv. Sci. Tec.* **2017**, *42*, 107–118. [CrossRef]
16. Giovanini, A.F.; de Sousa Passoni, G.N.; Göhringer, I.; Deliberador, T.M.; Zielak, J.C.; Storrer, C.L.M.; Costa-Casagrande, T.A.; Scariot, R. Prolonged use of alendronate alters the biology of cranial repair in estrogen-deficients rats' associated simultaneous immunohistochemical expression of TGF-β1 + α-ER+, and BMPR1B. *Clin. Oral Investig.* **2018**, *22*, 1959–1971. [CrossRef]
17. Segredo-Morales, E.; Reyes, R.; Arnau, M.R.; Delgado, A.; Évora, C. In situ gel-forming system for dual BMP-2 and 1717β-estradiol controlled release for bone regeneration in osteoporotic rats. *Drug Deliv. Transl. Res.* **2018**, *8*, 1103–1113. [CrossRef]
18. Segredo-Morales, E.; García-García, P.; Reyes, R.; Pérez-Herrero, E.; Delgado, A.; Évora, C. Bone regeneration in osteoporosis by delivery BMP-2 and PRGF from tetronic-alginate composite thermogel. *Int. J. Pharm.* **2018**, *30*, 160–168. [CrossRef]
19. Seo, B.B.; Koh, J.T.; Song, S.C. Tuning physical properties and BMP-2 release rates injectable hydrogel systems for an optimal bone regeneration effect. *Biomaterials* **2017**, *122*, 91–104. [CrossRef]
20. Rodríguez-Évora, M.; Delgado, A.; Reyes, R.; Hernández-Daranas, A.; Soriano, I.; San Román, J.; Évora, C. Osteogenic effect of local, long versus short term BMP-2 delivery from a novel SPU-PLGA-βTCP concentric system in a critical size defect in rats. *Eur. J. Pharm. Sci.* **2013**, *16*, 873–884. [CrossRef]
21. Pérez-Herrero, E.; García-García, P.; Gómez-Morales, J.; Llabrés, M.; Delgado, A.; Évora, C. New injectable two-step forming hydrogel for delivery of bioactive substances in tissue regeneration. *Regen. Biomater.* **2019**, *6*, 149–162. [CrossRef] [PubMed]
22. Hernández, A.; Reyes, R.; Sánchez, E.; Rodríguez-Évora, M.; Delgado, A.; Évora, C. In vivo osteogenic response to different ratios of BMP-2 and VEGF released from a biodegradable porous system. *J. Biomed. Mater. Res.* **2012**, *100*, 2382–2391. [CrossRef] [PubMed]
23. Fraker, P.J.; Speck, J.C. Proteion and cell membrane iodinations with a spraringly soluble chloroamide, 1,3,4,6-tetrachloro-3a,6a-diphenylglycoluril. *Biochem. Biophys. Res. Commum.* **1978**, *80*, 849–857. [CrossRef]
24. García-García, P.; Reyes, R.; Pérez-Herrero, E.; Arnau, M.R.; Évora, C.; Delgado, A. Alginate-hydrogel versus alginate-solid system. Efficacy in bone regeneration in osteoporosis. *Eur. J. Pharm. Biopharm.*. Manuscript submitted.
25. *Pharmaceutical Compounding–Estradiol Tablets*; The United States Pharmacopeial Convention: Baltimore, MD, USA, 2014.
26. Birnbaum, D.T.; Kosmala, J.D.; Henthorn, D.B.; Brannon-Peppas, L. Controlled release of b-estradiol from PLAGA microparticles:The effect of organic phase solvent on encapsulation and release. *J. Control Release* **2000**, *65*, 375–387. [CrossRef]
27. Zaghloul, A.A. *β*-Estradiol biodegradable microspheres: Effect of formulation parameters on encapsulation efficiency and in vitro release. *Pharmazie* **2006**, *61*, 775–779.
28. Govindarajan, P.; Khassawna, T.; Kampschulte, M.; Bócker, W.; Huerter, B.; Dúrselen, L.; Faulenbach, M.; Heiss, C. Implications of combined ovariectomy and glucocorticoid (dexamethasone) treatment on mineral, microarchitectural, biomechanical and matrix properties of rat bone. *Int. J. Exp. Pathol.* **2013**, *94*, 387–398. [CrossRef]

29. Delgado, J.; Évora, C.; Sánchez, E.; Baro, M.; Delgado, A. Validation of a method for non-invasive in vivo measurement of growth factor release from a local delivery system in bone. *J. Control Release* **2006**, *114*, 223–229. [CrossRef]
30. Dobson, K.R.; Reading, L.; Haberey, M.; Marine, X.; Scutt, A. Centrifugal isolation of bone marrow from bone: An improved method for the recovery and quantitation of bone marrow osteoprogenitor cells from rat tibiae and femurae. *Celcif. Tissue Int.* **1999**, *65*, 411–413. [CrossRef]
31. Martínez-Sanz, E.; Ossipov, D.A.; Hilborn, J.; Larsson, S.; Jonsson, K.B.; Varghese, O.P. Bone reservoir: Injectable hyaluronic acid hydrogel for minimal invasive bone Augmentation. *J. Control Release* **2011**, *152*, 230–240. [CrossRef]
32. Turek, A.; Olakowska, E.; Borecka, A.; Janeczek, H.; Sobota, M.; Jaworska, J.; Kacmarczyk, B.; Jarzabek, B.; Gruchlik, A.; Libera, M.; et al. Shape-Memory Terpolymer Rods with 17-17β-estradiol for the Treatment of Neurodegenerative Diseases: An In Vitro and In Vivo Study. *Pharm. Res.* **2016**, *33*, 2967–2978. [CrossRef] [PubMed]
33. Zhang, Z.; Ren, H.; Shen, G.; Qiu, T.; Liang, D.; Yang, Z.; Yao, Z.; Tang, J.; Jiang, X.; Wei, Q. Animal models for glucocorticoid-induced postmenopausal osteoporosis: An updated review. *Biomed. Pharmacother.* **2016**, *84*, 438–446. [CrossRef] [PubMed]
34. Calciolari, E.; Mardas, N.; Dereka, X.; Kostomitsopoulos, N.; Petrie, A.; Donos, N. The effect of experimental osteoporosis on bone regeneration: Part 1, histology findings. *Clin. Oral. Impl.* **2017**, *28*, 101–110. [CrossRef] [PubMed]
35. Durão, S.F.; Gomes, P.S.; Colaço, B.J.; Silva, J.C.; Fonseca, H.M.; Duarte, J.R.; Felino, A.C.; Fernandes, M.H. The biomaterial-mediated healing of critical size bone defects in the ovariectomized rat. *Osteoporos Int.* **2014**, *25*, 1535–1545.
36. Engler-Pinto, A.; Siéssere, S.; Calefi, A.; Oliveira, L.; Ervolino, E.; Souza, S.; Furlaneto, F.; Messora, M.R. Effects of leukocyte- and platelet-rich fibrin associated or not with bovine bone graft on the healing of bone defects in rats with osteoporosis induced by ovariectomy. *Clin. Oral Impl. Res.* **2019**, *30*, 962–976. [CrossRef]
37. Cortet, B. Bone repair in osteoporosic bone: Postmenopausal and cortione-induced osteoporosis. *Osteoporos Int.* **2011**, *22*, 2007–2010. [CrossRef]
38. Alt, V.; Cheung, W.H.; Chow, S.K.; Thormann, U.; Cheung, E.N.; Lips, K.S.; Shenettler, R.; Leung, K.S. Bone formation and degradation behavior of nanocrystalline hydroxyapatite with or without collagen-type 1 in osteoporotic bone defects—An experimental study in osteoporotic goats. *Injury* **2016**, *47*, 58–65. [CrossRef]

Materials Science & Engineering C 115 (2020) 111009

Contents lists available at ScienceDirect

Materials Science & Engineering C

journal homepage: www.elsevier.com/locate/msec

Alginate-hydrogel versus alginate-solid system. Efficacy in bone regeneration in osteoporosis

Patricia García-García[a], Ricardo Reyes[b,d], Edgar Pérez-Herrero[a,d], María Rosa Arnau[c,d], Carmen Évora[a,d,*], Araceli Delgado[a,d,*]

[a] Department of Chemical Engineering and Pharmaceutical Technology, Universidad de La Laguna, 38200 La Laguna, Spain
[b] Department of Biochemistry, Microbiology, Cell Biology and Genetics, Universidad de La Laguna, 38200 La Laguna, Spain
[c] Servicio de Estabulario, Universidad de La Laguna, 38200 La Laguna, Spain
[d] Institute of Biomedical Technologies (ITB), Center for Biomedical Research of the Canary Islands (CIBICAN), Universidad de La Laguna, 38200 La Laguna, Spain

ARTICLE INFO

Keywords:
Scaffold
BMP-2
β-Estradiol
Osteoporosis
Bone regeneration
Mesenchymal stem cells

ABSTRACT

In the present study, two different PLGA-Alginate scaffolds, a hydrogel (HY) and a solid sponge (SS), were developed for β-estradiol and BMP-2 sustained delivery for bone regeneration in osteoporosis. β-Estradiol and BMP-2 were encapsulated in PLGA and PLGA-Alginate microspheres respectively. Scaffolds were characterized in vitro in terms of porosity, water uptake, release rate and HY rheological properties. BMP-2 release profiles were also analysed in vivo. The bone regeneration induced by both HY and SS was evaluated using a critical-sized bone defect in an osteoporotic (OP) rat model. Compared to HY, SS presented 30% higher porosity, more than double water absorption capacity and almost negligible mass loss compared to the 40% of HY. Both systems were flexible and fit well the defect shape, however, HY has the advantage of being injectable. Despite both delivery systems had similar composition and release profile, bone repair was around 30% higher with SS than with HY, possibly due to its longer residence time at the defect site. The incorporation of mesenchymal stem cells obtained from OP rats did not result in any improvement or synergistic effect on bone repair.

1. Introduction

The regeneration of the bone mass lost by several causes such as trauma, infections or surgery requires the contribution of three key elements: scaffolds, cells and growth factors [1–3]. Scaffolds are porous structures able to adapt to the bone defect acting as support and guide for cell proliferation and differentiation with the help of signalling molecules [4,5]. Therefore, scaffolds must also act as reservoirs for growth factors involved in the cascade of cellular events that leads to bone formation.

Clearly, the best bone graft is autologous bone, however, several well-known disadvantages (invasive surgery, limited availability and damage in the donor bone) have led to the search for alternative approaches [6]. The type of biomaterials used to develop scaffolds for bone regeneration during the last decades is very wide. Taking into account the scaffolds active role in bone regeneration as artificial extracellular matrix, different biodegradable and/or osteointegrable materials of diverse nature (phosphates, bio-glass, natural and synthetic polymers) have been used to construct 3D-scaffolds. The design of these scaffolds is based on fulfilling several characteristics to facilitate tissue ingrowth, such as biocompatibility, porous structure with interconnected pores, permeability for blood perfusion, nutrients supply, cell adhesion and differentiation [7]. Hydrogels suit these characteristics, thus the development and preparation of biodegradable hydrogels for bone tissue engineering applications is currently of great interest [8,9]. In addition, scaffold bioactivity is required to successfully tackle critical size bone defect regeneration. One strategy to "activate" scaffolds is their loading with growth factors such as bone morphogenetic proteins (BMPs). Particularly, BMP-2, which is involved in most of the processes required for bone formation [1,6]. In fact, due to its osteogenic capacity rhBMP-2 is already marketed incorporated in a collagen scaffold to locally treat some bone injuries [10]. The benefits of rhBMP-2 have been already proven nevertheless, the risk of adverse effects associated with the high dose required in the clinic and the inability of the carrier to retain the protein in the defect, make necessary the development of scaffolds with controlled release capacity for greater efficacy and safety [10]. Injectability and adaptability to the bone defect shape are among the most characteristic advantages of hydrogels [8,9]. However, their weak mechanical properties and short residence time in the defect could be a disadvantage depending on the

* Corresponding authors at: Department of Chemical Engineering and Pharmaceutical Technology, Universidad de La Laguna, 38200 La Laguna, Spain.
E-mail addresses: cevora@ull.edu.es (C. Évora), adelgado@ull.edu.es (A. Delgado).

https://doi.org/10.1016/j.msec.2020.111009
Received 22 November 2019; Received in revised form 1 April 2020; Accepted 21 April 2020
Available online 23 April 2020

type of bone lesion to be treated. Finally, their incapacity to regulate growth factors release has led to the development of different strategies to control drug release rate by increasing the drug binding to the hydrogel matrix [11–13] or combining hydrogels with sustained release platforms [12–14]. We previously reported hydrogels composed of poloxamine alone or combined with alginate or cyclodextrin containing microspheres of different composition to control BMP-2 release. These systems were tested in osteoporotic (OP) and non-OP rats, not observing significant differences in bone repair between both groups [15–18]. However, the mineralization in OP groups was notably inferior to that of non-OP groups [17,18]. Given that all bone repair processes are impaired and bone healing time is delayed in OP [19–22], to overcome the low mineralization observed in our previous study we hypothesized a longer residence time of the scaffold in the defect and a longer release of BMP-2 in OP is required.

In this study, a new alginate hydrogel system, crosslinked in two steps and loaded with β-estradiol and BMP-2 within microspheres was developed. Microspheres were elaborated from a combination of alginate and polylactide-*co*-glycolide (PLGA) with different lactide to glycolide ratio and molecular weight (Mw). The hydrogel system was compared with a solid sponge system with the same composition. The goal is to keep similar some of the physical and chemical properties for both systems such as composition, hydrophilicity/hydrophobicity, water uptake, swelling behaviour and porosity and BMP-2 and β-estradiol release rates. The main expected difference between both systems is the scaffold residence time in the critical size calvarial defect. Therefore, two β-estradiol-BMP-2-Alginate-PLGA systems, hydrogel (HY) and solid sponge (SS), were developed and in vitro characterized. The induced bone regeneration by both systems was compared in a critical size defect in OP rats alone or seeded with OP mesenchymal stem cells (MSCs).

2. Materials and methods

2.1. Materials

The polylactide-*co*-glycolide 75:25 (PLGA 75:25, Resomer® RG 755 S) and 85:15 (PLGA 85:15, Resomer® RG 858 S) and the sodium alginate (Protasan® UP MVG) were supplied by Evonic Industries (Darmstadt, Germany) and Novamatrix (Biopolymer Systems, Sandvika, Norway) respectively. 17-β-estradiol and recombinant human bone morphogenetic protein 2 (rhBMP-2) were purchase from Sigma-Aldrich (USA) and Biomedal Life Sciences (Sevilla, Spain) respectively. rhBMP-2 was reconstituted at 1 mg/mL in 20 mM acetic acid and 0.1% bovine serum albumin (BSA, Sigma-Aldrich, St. Louis, USA). Poly(vinyl alcohol) (PVA, Mw 33,000-70,000; 87–90% hydrolysed) was from Sigma-Aldrich, (St. Louis, USA) and $CaCl_2$ from Merck (Darmstadt, Germany).

2.2. Microsphere preparation and characterization

The alginate-PLGA microspheres of BMP-2 were prepared by modifying a previously described double emulsion (w/o/w) method [23,24]. Briefly, an aqueous solution of 500 μL of rhBMP-2 (500 μg), 100 μL of 15% polyvinyl alcohol (PVA) and 300 μL of 6% sodium alginate (*w/v*) was emulsified with 2 mL of a mixture of PLGA 75:25 and PLGA 85:15 (4:1) methylene chloride solution (125 mg/mL, DCM) by vortexing (position 10, Genie® Industries 2, Sciencies Industries Inc. USA) for 1 min. Then, 5.2 mL of an aqueous solution of 2.5 mL of PVA (10% *w/v*), 2.5 mL of NaCl (10% w/v) and 200 μL of $CaCl_2$ (0.5 M) was poured over the first emulsion and vortexed for 30 s (position 10). Finally, the organic solvent was evaporated in 100 mL of 0.25 M $CaCl_2$ aqueous solution under constant magnetic stirring for 1.5 h.

The microspheres of β-estradiol were prepared by the solvent evaporation method. Briefly a mixture of β-estradiol (6 mg), PLGA 75:25 (160 mg) and PLGA 85:15 (40 mg) dissolved in 0.6 mL methanol:DCM (20:80) solution was emulsified with 4 mL of 1% PVA aqueous solution by vortexing for 1 min (position 10), poured into 100 mL of PVA (0.15%) aqueous solution and left under magnetic stirring for 1 h [17,18].

Both types of microspheres were collected by filtration (Supor®-450, 0.45 μm, 47 mm filters, Pall Corporation, Sigma-Aldrich, USA), lyophilized and conserved at 4 °C until use.

Some batches were prepared with ^{125}I-BMP-2 as a tracer to determine rhBMP-2 encapsulation efficiency and release assays. BMP-2 was labelled with ^{125}INa (Perkin-Elmer) by the iodogen method [25], as described [16]. The content of β-estradiol in the microspheres was determined spectrophotometrically at λ = 280 nm, previous dissolution in a mix of MeOH:DCM (20:80).

Microspheres size distribution was determined by laser diffractometry using a Mastersizer 2000 (Malvern Instruments, Malvern, UK) and the morphology was observed by scanning electron microscopy (SEM, Jeol JSM-6300, Tokio, Japan).

2.3. Fabrication and characterization of electrospinning film

The polymer film was fabricated by electrospinning a solution of PLGA 75:25 and PLGA 85:15 at a ratio 4:1 and β-estradiol. Briefly, 7 mg of β-estradiol, 240 mg of PLGA 75:25 and 60 mg of PLGA 85:15 dissolved in 2 mL of hexafluoroisopropanol (Sigma-Aldrich, USA) were loaded into a Luer-lock syringe (Norm-Ject) with an 18-gauge needle attached to a syringe pump (Harvard Apparatus, MA, USA). The electrospinning process was carried out at a flow rate of 3 mL/h under 10 kV power supply and the collector rotating at 200 rpm located at 10 cm from the needle.

The film quality and fiber diameter were analysed using SEM (Jeol, JSM-6300) images and the film thickness was measured by stereo microscopy (Leica M205C, Leica Las, v 3 software).

The porosity was calculated using Eq. (1), where ρ_{app} and ρ_{real} are the apparent and real densities of the film, respectively,

$$\text{Porosity}\ (\%) = \left(\frac{\rho_{real} - \rho_{app}}{\rho_{real}}\right) \times 100 \quad (1)$$

The real density was measured in a helium pycnometer (AccuPyc 1330, Micromeritics, USA). While the real density was calculated by dividing the mass by the geometric volume of the film (length × width × height).

Water uptake and mass loss assays were carried out by samples (3 × 3 cm) incubation in water (37 °C) under orbital agitation (25 rpm). At specific times, three samples were withdrawn, the excess of water removed, weighted and freeze-dried to record the dry weight. The percentages of mass loss and water uptake were calculated applying Eqs. (2) and (3), respectively. Where W_o was the initial weight of the sample, W_w and W_d were the weights of the wet and dried sample respectively, at the different times tested.

$$\text{Mass loss}\ (\%) = \frac{(W_0 - W_d)}{W_0} \times 100 \quad (2)$$

$$\text{Water uptake}\ (\%) = \frac{(W_w - W_d)}{W_d} \times 100 \quad (3)$$

2.4. Systems preparation and characterization

2.4.1. Solid system

To prepare the alginate solid sponge system 15 mg of microspheres were dispersed in 100 μL of 2% alginate aqueous solution and freeze-dried. The alginate was then cross-linked by incubation with 100 μL of 1% $CaCl_2$ during 3 min and washed with 100 μL of sterile MilliQ water three times and freeze-dried. All the systems were stored at 4 °C until use.

2.4.2. Hydrogel system

To prepare the alginate hydrogel system 4.5% *w*/w sodium alginate sterile aqueous solution was partially cross-linked by sufficient quantity of a 1% w/w $CaCl_2$ sterile aqueous solution to give final concentrations of 4% w/w of sodium alginate and 0.12% w/w of $CaCl_2$. Then, 15 mg of microspheres were dispersed in the partially cross-linked hydrogel (PC-HY). Afterward, it was cross-linked with 5% w/w $CaCl_2$ sterile aqueous solution (0.7 μL/μL of hydrogel).

The systems were characterized in terms of porosity, water uptake and mass loss, as previously described for the polymer film (Eqs. (1), (2) and (3)). Morphology and structural characteristics were observed by SEM (Jeol JSM-6300). For hydrogel characterization, the system was prepared in a graduated cylindrical mold and freeze-dried.

In addition, rheological characteristics of the PC-HY, freshly prepared with and without microspheres, and after 4 h at rest (PC-HY + 4 h), were obtained with a Bohlin CVOD 100 rheometer at 20 °C and 37 °C by means of a Peltier system, using cone-plate and parallel geometries with a diameter of the fixed lower plate of 60 mm and a gap between the fixed and rotating part of 1 mm. The evolution of viscosity with shear rate (from 0.071 to 30 s^{-1}) was acquired by a cone-plate geometry (diameter of cone 40 mm, angle 4°). The evolution of elastic (G′) and viscous moduli (G″) with frequency (0.128 a 6.93 Hz) was acquired by a parallel plate geometry (diameter of rotating upper plate 20 mm) at a constant shear stress of 0.2387 Pa.

The systems to be implanted were prepared under aseptic conditions and all contained 6 μg of BMP-2 in microspheres. In addition, the solid sponge systems were loaded with 300 μg of β-estradiol in microspheres (SS-BMPβe). However, in the hydrogel system the dose of β-estradiol was divided, 240 μg in microspheres dispersed in the hydrogel and placed in between two electrospun films containing 60 μg of β-estradiol forming an alginate hydrogel sandwich system (HY-BMPβe). Both systems, solid sponge and hydrogel, seeded with MSCs obtained from osteoporotic rats, SS-BMPβe-MSC and HY-BMPβe-MSC, were also implanted.

2.5. In vitro release assay

The rhBMP-2 in vitro release assays were carried out by incubating (37 °C, 25 rpm orbital stirring) each system in sterile water (Milli-Q). The amount of the ^{125}I-BMP-2 released was calculated by measuring the radioactivity of supernatant samples (Cobra® II, Packard).

The in vitro release assays of β-estradiol from free microspheres, microspheres in the HY, microspheres in the SS and samples of the electrospun films were carried out in three release media (37 °C, 25 rpm orbital stirring), dimethyl sulfoxide (DMSO, Acofarma, Barcelona, Spain):H_2O (40:60), MeOH:H_2O (50:50) and sodium lauryl sulphate (SLS, Sigma-Aldrich, St. Louis, USA) in water (1% *w*/*v*).

2.6. Cells

Bone marrow rat MSCs were obtained as described [26] from femur and tibiae bone marrow of 18 weeks-old female Sprague-Dawley rats ovariectomized (OVX) 12 weeks before. Briefly, whole bone marrow was pooled and resuspended in Dulbecco's Minimal Essential Medium (DMEM) with 4.5 g/L glucose, supplemented with 20% fetal bovine serum, 50 UI/mL penicillin, 50 μg/mL streptomycin, and 200 mM stabilized L-glutamine, seeded on cell culture plastic, and incubated at 37 °C and 5% CO_2. After 3 days, non-adhered cells were removed and fresh medium was added. Confluent cells were detached and frozen. Stock frozen MSCs were thawed, precultured for 3–4 d, and trypsin-detached for scaffold loading. The SS-BMPβe-MSC and HY-BMPβe-MSC systems were loaded with 5×10^5 MSCs in passage 2 suspension (60 μL) approximately 20 min before implantation.

The 60 μL of the MSCs suspension were dropped on the solid sponge or mixed with the microspheres in the hydrogel system. In previous in vitro studies it was demonstrated that both the materials used and the type of scaffolds are biocompatible with MSCs, allowing their adhesion and viability [27,28].

2.7. Animals experiments

All animal experiments were carried out in conformity with the European Directive (2010/63UE) on Care and Use of Animals in Experimental Procedures. Furthermore, the animal protocols (CEIBA2014-0128) were approved by the ethics committee for animal care of the University of La Laguna. Animals were supplied by the Central Animal House of the University of La Laguna.

2.7.1. Surgical procedures

30 female Sprague-Dawley rats, weighing 250–300 g, were used in this study. Surgery was made under aseptic conditions. The experimental osteoporosis was induced by bilateral ovariectomy (OVX) under isoflurane anaesthesia, via dorsal approach. Three months post-OVX, critical size (8 mm, ∅) calvarial defects were created surgically with a trephine burr in the rats under isoflurane and the systems were placed into the defects, as previously described [29]. Analgesia consisted in buprenorphine administered subcutaneously (0.05 mg/kg) before surgery and paracetamol (70 mg/100 mL) in the water for 3 days post-surgery.

2.7.2. Animal groups

The 30 female rats pre-OVX were dividing in 6 groups of 5 rats each. 2 groups of 5 OP rats each were implanted with SS-^{125}I-BMPβe and HY-^{125}I-BMPβe to determine the ^{125}I-BMP-2 release kinetics. After 6 weeks the rats were sacrificed.

The other four groups were used to evaluate bone regeneration induced by a combination of BMP-2 and β-estradiol with and without MSCs in the two systems. 2 groups were implanted with the solid systems: SS-BMPβe (6 μg BMP-2 + 300 μg β-estradiol) and SS-BMPβe-MSC (6 μg BMP-2 + 300 μg β-estradiol + 5×10^5 MSCs) and 2 groups were implanted with the hydrogel system, HY-BMPβe and HY-BMPβe-MSC. The animals were sacrificed at 12 weeks post-implantation, and defect enclosing segments were resected from the calvaria.

2.7.3. ^{125}I-BMP-2 release assay

In vivo ^{125}I-BMP-2 release assay was carried out with a non-invasive method as previously described and validated [30]. This method permitted periodic assessment of the remaining ^{125}I-BMP-2 at the defect site using an external probe-type gamma counter (Captus®, Capintec Inc.). Briefly, at each sampling time point, five 1-min readings were taken at the ^{125}I emission peak (27 keV) and the mean accepted as the remaining radioactivity. The initial measure (time = 0) was considered the administered dose (100%). After 6 weeks, when no measurable levels of radioactivity remained, the rats (5 rats per group) were sacrificed.

2.8. Histology and histomorphometrical evaluation

The samples were fixed (10% formalin solution) and decalcified in Histofix® Decalcifier (Panreac) and prepared for histological analysis, as previously described [31]. New bone formation and the presence of adipose and connective tissue were identified by hematoxylin-erythrosin staining, based on their different morphological characteristics. The degree of new bone mineralization was assessed with VOF trichrome stain, in which red staining indicates advanced mineralization, whereas less mineralized, newly formed bone stains blue [32]. Sections were analysed by light microscopy (LEICA DM 4000B). Computer based image analysis software (LeicaQ-win V3 Pro-image analysis system, Barcelona, Spain) was used to evaluate histomorphometrically all sections per specimen. A region of interest (ROI) for quantitative evaluation of new bone formation and adipose and connective tissue presence, was defined as the area of the tissue within the defect. The ROI

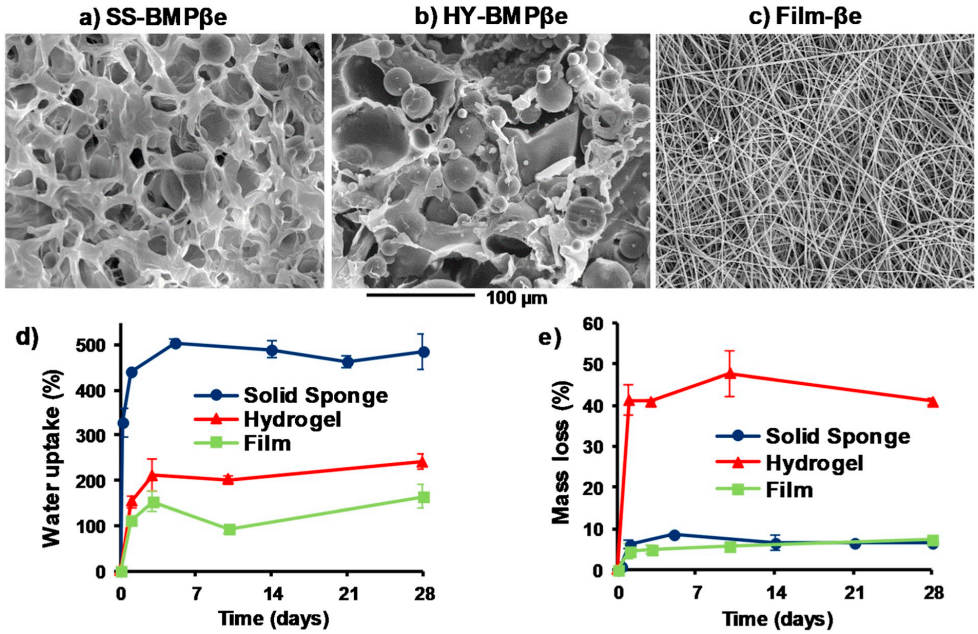

Fig. 1. Scanning electron microscope images of alginate solid sponge (a) and cross-linked hydrogel (b) containing BMP-2 and β-estradiol microspheres as well as the PLGA electrospinning film (c) containing β-estradiol. Water uptake (d) and mass loss (e) of the above systems during incubation in water at 37 °C under orbital agitation (25 rpm).

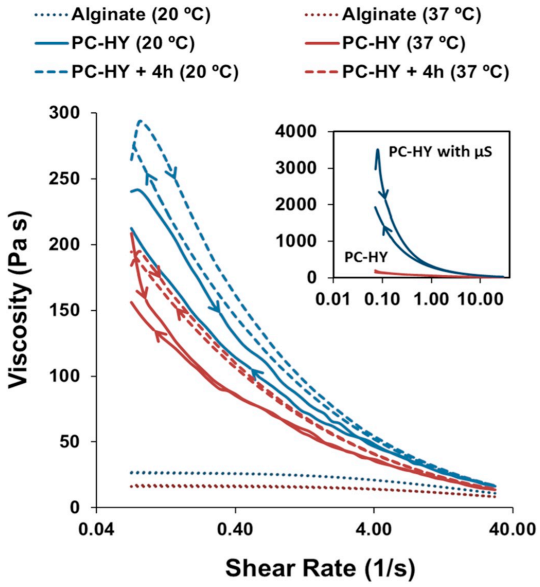

Fig. 2. Evolution of the viscosity with shear rate at 20 °C and 37 °C, of pure alginate aqueous solution (4% *w*/w) and partially cross-linked hydrogel (4% w/w alginate and 0.12% w/w of $CaCl_2$) freshly prepared (PC-HY) and after 4 h at rest (PC-HY + 4 h). In the upper right part of the figure is shown the change in viscosity of the PC-HY with the inclusion of microspheres. The curve direction (forward and backward) is indicated by arrows.

consisted of a circular region of 50 mm^2, the center of which coincided with that of the defect site. New bone formation was expressed as a percentage of repair, applying the equation,

$$\%\text{repair} = \frac{\text{new bone area}}{\text{original defect area within the ROI}} \times 100$$

Similarly, the percentage of adipose or connective tissue was obtained from the ratio between the area occupied by each specific tissue and the area of the original defect.

Statistical analyses were performed using SPSS 18.0 software. One-way analysis of variance (ANOVA) and a Tukey multiple comparison post-test were used to compare the overall performance of the different groups. Results are expressed as mean ± standard deviation. Significance was set at $p < 0.05$.

3. Results

3.1. Scaffolds characterization

The mean volume diameters of the microspheres of alginate-PLGA containing BMP-2 and PLGA microspheres with β-estradiol were 64.0 µm (10% < 14.8 µm; 90% < 111.6 µm) and 171.4 µm (10% < 46.2 µm; 90% < 286.0 µm) respectively. The encapsulation efficiency was 71% and 99% for the BMP-2 and β-estradiol, respectively.

Scaffolds were prepared by dispersing a mixture of the above microspheres in an alginate aqueous solution from which a final presentation of solid sponge or hydrogel was set. The SS scaffold presented a higher porosity (89.4 ± 1.8%) than the freeze-dried HY system (63 ± 2.2%) (Fig. 1 a, b). For in vivo administration the HY was assembled between two electrospun membranes (Fig. 1 c). The characteristics of the film were: 63.4 ± 4.3 µm of thickness, microfiber diameter of 1.2 ± 0.26 µm and 71.4 ± 4.1% of porosity (Fig. 1 c).

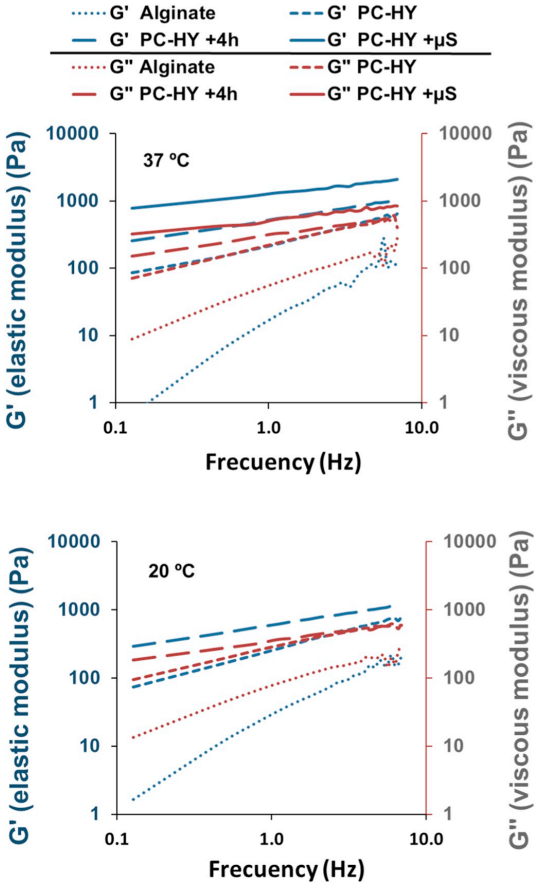

Fig. 3. Viscoelastic behaviour at 20 °C and 37 °C, of pure alginate aqueous solution (4% w/w) and partially cross-linked hydrogel (4% w/w alginate and 0.12% w/w of $CaCl_2$) freshly prepared (PC-HY) and after 4 h at rest (PC-HY + 4 h). Behaviour of PC-HY with the inclusion of microspheres (PC-HY + µS) at 37 °C is also shown.

The incubation of the systems in water at 37 °C, showed that most of the water uptake (Fig. 1 d) and mass loss (Fig. 1 e) occurred during the first days but in a different ratio depending on the system. The SS water uptake was more than double (500%) of that showed by the HY (200%) or the film (150%). On the other hand, the HY suffered a very important mass loss (40%) compared with that detected in the other two systems (6%).

3.2. Viscoelastic behaviour of hydrogel

Viscoelastic behaviour of partially cross-linked alginate hydrogel freshly prepared (PC-HY) as well as after 4 h at rest or containing microspheres were analysed.

All the samples evaluated showed a progressive viscosity decrease with the shear rate (Fig. 2), characteristic of a pseudo-plastic material. However, the viscosity curves with the increase (forward curve) and decrease (backward curve) of the shear rate in the freshly prepared PC-HY and after 4 h at rest, do not overlap, which reveals a thixotropic behaviour that was more evident at 20 °C than at 37 °C, according to a smaller hysteresis loop area recorded at this latter temperature. The area of the hysteresis loop characterizes the energy associated with the sol-gel transition and the time for the material reorganization, hence the greater the area, the longer the time for recover its initial state after of stress [33]. The 4% *w*/w aqueous solution of alginate showed no thixotropic behaviour (Fig. 2).

The viscosity values of the freshly prepared PC-HY and after 4 h at rest or containing microspheres, were markedly superior to those of the alginate solution (4% *w*/w), especially at low shear rates (Fig. 2). In all the analysed samples, the viscosity was lower at 37 °C than at 20 °C. (Fig. 2).

For the different samples, the evolution of elastic (G′) and viscous moduli (G″) with the frequency (Fig. 3) confirms the above results. The highest G′ and G″ values were found in the PC-HY containing microspheres, followed by PC-HY after 4 h at rest and freshly prepared, the lowest values being obtained with the alginate aqueous solution (4% *w*/w). The alginate solution (4% w/w) showed a viscous behaviour, as indicated by G″ values being higher than those of G′ throughout the studied frequency range, while in PC-HY systems an evolution towards more elastic behaviour was observed. Thus, the freshly prepared PC-HY presented similar values of both G′ and G″ moduli, after 4 h at rest those values had separated resulting in an elastic module higher than the viscous module. The inclusion of the microspheres further increases this difference between the elastic and the viscous moduli due to a greater predominance of solid-like behaviour in the system.

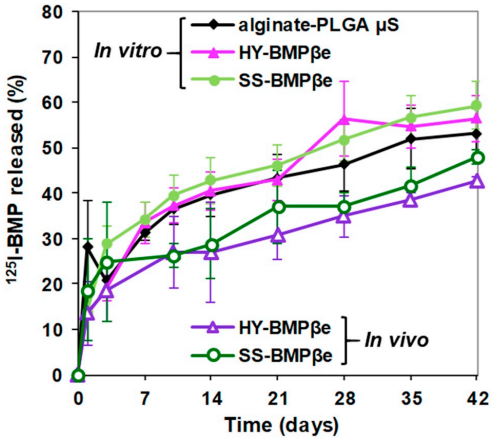

Fig. 4. BMP-2 in vitro and in vivo release assays. Release profile of ^{125}I-BMP-2 from alginate-PLGA microspheres alone and included in the hydrogel (HY-BMPβe) and solid sponge (SS-BMPβe) systems in water at 37 °C (n = 3) and after implantation in the rat calvarial defect (n = 5).

3.3. ^{125}I-BMP-2 and β-estradiol release profiles

The in vivo release profiles of BMP-2 from SS-^{125}I-BMP and HY-^{125}I-BMP were similar, during the first 24 h approximately 20% of the dose, equivalent to 1,2 µg of the BMP-2, was released (Fig. 4). At 6 weeks, the percentage of BMP-2 released was about 43–48%. However, the in vitro ^{125}I-BMP-2 release profiles were faster than in vivo. Around 15–20% was released in the first day reaching the 57–60% released at 6 weeks. A similar in vitro release profile (Fig. 4) was obtained from the microspheres alone dispersed in the medium, which indicates that the release profile of BMP-2 from both systems, SS and HY, is governed by the microspheres.

The β-estradiol release profiles were similar in the different media used although the percentages delivered were higher (87–100%) in MeOH:water, than in the more polar media, DMSO or SLS in water, (14–25% from microspheres and 67–78% from the film) (Fig. 5).

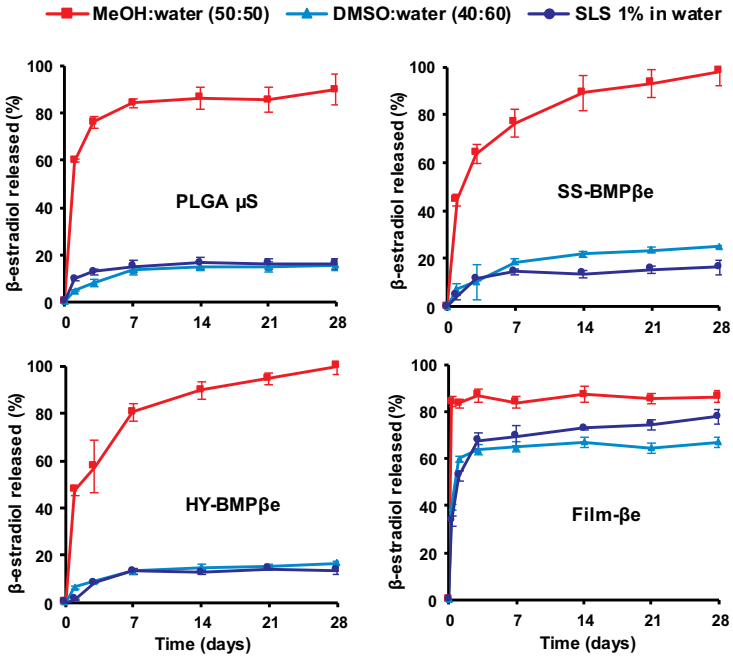

Fig. 5. Release profiles of β-estradiol from PLGA microspheres alone (PLGA μS) and included in the solid sponge (SS-BMPβe) or hydrogel (HY-BMPβe) systems as well as from the electrospinning film, at 37 °C, in three different release media: methanol:-water (50:50), dimethyl sulfoxide:water (40:60) and sodium lauryl sulphate 1% in water. (n = 3).

Therefore, the β-estradiol released was medium dependent. Regardless of medium used, β-estradiol was released faster from the films (Fig. 5 d) than from the SS and HY scaffolds (Fig. 5 b, c) being, in these last two cases, quite similar to that obtained from microspheres alone (Fig. 5 a). Thus, in MeOH:water, 84% was released in the first day from the film with no further release in the next 4 weeks while, from SS or HY, around 46% was released in the first day, reaching approximately 80% in a week and finally, almost 100% in 4 weeks. Compared with the microspheres, the β-estradiol release rate was slightly reduced during the first days by the incorporation in the SS or the HY.

3.4. Histological and histomorphometrical evaluation

Visual inspection of the SS and HY systems 12 weeks post-implantation, showed a different degree of filling of the defect, being higher in the groups implanted with the SS scaffold.

The macroscopic analysis of the calvaria showed that in groups implanted with the SS, the defect appeared completely filled with a tissue of homogeneous aspect similar to the adjacent normal bone (Fig. 6 a). This was observed both in the groups treated with BMPβe and in those treated with BMPβe + MSCs. The histological analysis confirmed the new bone formation. In all these experimental groups, the repair was observed not only in the margins but also inside the defect (Fig. 6 c, e). However, a more detailed analysis showed that the repaired bone presented a somewhat fragmented appearance, with areas of bone surrounded by connective tissue and the presence of adipose tissue between both of them (Fig. 6 g).

In the animals implanted with the HY, the macroscopic analysis of the calvaria allowed to observe clearly the morphology of the defect, filled with a tissue of semi-transparent hyaline appearance (Fig. 6 b). The histological analysis confirmed these results, the new bone formation in these animals being lower than that observed with the SS scaffold (Fig. 6 d, f). The repair in this case was mainly limited to the margins of the defect (Fig. 6 d, f). The repaired bone also showed a fragmented appearance, with a higher abundance of adipose tissue and numerous spaces of variable size that were sometimes occupied by what appeared to be remains of scaffold material (Fig. 6 h, i).

The qualitative histological results were confirmed by histomorphometrical analysis of the samples. A higher percentage of repair, between 74% in the group treated with BMPβe + MSC and 79% in that with BMPβe alone, was found in the animals implanted with the SS compared with those implanted with the HY, which ranged between 40% for the group treated with BMPβe + MSC and 50% in the group with BMPβe alone (Fig. 7 a). In fact, significant differences were found between the implanted systems, SS and HY, although no differences were observed between the applied treatments, with or without MSCs. On the other hand, in all animal groups, the proportion of mature bone, with a high degree of mineralization, was greater than the immature bone, independently of the treatment and the implanted system (Fig. 7 b). The mature bone to the immature bone ratios ranged between 1.42 and 1.67, the animals implanted with the HY presenting the lower values. Nevertheless, the statistical analysis of the data did not show significant differences neither between treatments nor between the implanted system type (Fig. 7 b).

The analysis of adipose and connective tissues in the area of the defect, revealed the existence of slightly higher amounts of adipose (22% and 17% with HY and SS respectively) than of connective tissue (18% and 10% with HY and SS respectively), being the percentages of both tissues higher with the HY systems than with the SS systems. Consequently, the ratio of adipose or connective tissue to bone present in the defect area (Fig. 7 c) were significantly higher in the HY implanted systems compared with the SS systems for both tissues. Differences due to the treatment with BMPβe or BMPβe + MSC were not found in any case.

4. Discussion

The present study evaluates the permanence time effect of BMP-2

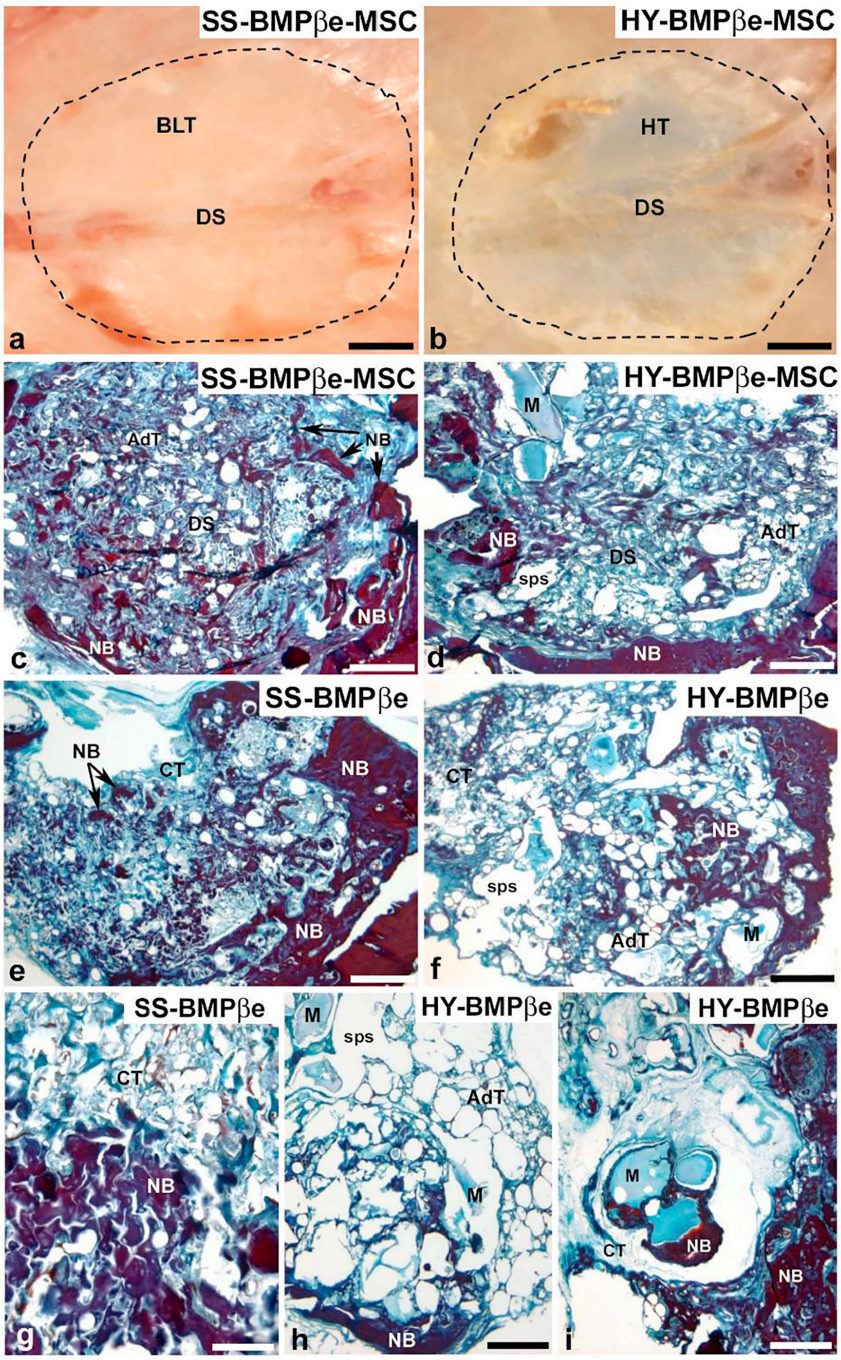

(caption on next page)

Fig. 6. Histological evaluation of the implanted systems, alginate solid sponge (SS) or in situ alginate cross-linked hydrogel (HY), containing BMP-2 and β-estradiol (BMPβe) with and without mesenchymal stem cells (MSCs) in a calvarial defect of OP rats. (a, b) macroscopic images of the defect area (dashed line) showing the extent and appearance of the repaired tissue; (c–f) microscopic images in horizontal section showing the repaired tissue (newly formed bone), as well as the presence of connective and adipose tissue in the defect area; (g, h) details at higher magnification showing the morphological characteristics of the repaired tissue with both implanted systems; (i) detail in the group HY-BMPβe showing rests of the alginate hydrogel surrounded by newly formed bone in the defect area. AdT: adipose tissue; BLT: bone like tissue; CT: connective tissue; DS: defect site; HT: hyaline tissue; M: Material; NB. New bone; sps: spaces. Scale bars = a–f: 2 mm; g: 250 μm; h: 500 μm; i: 350 μm.

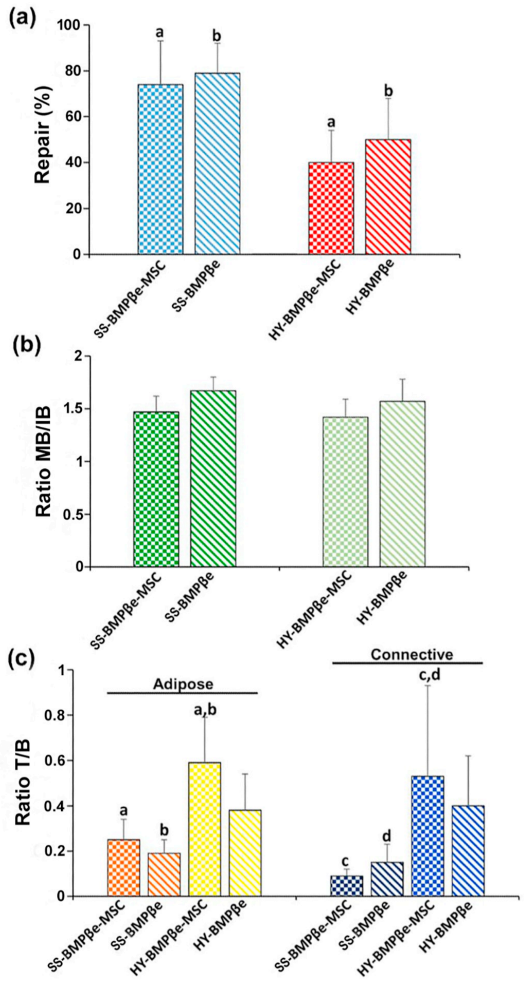

Fig. 7. Histomorphometrical evaluation of the implanted systems: (a) Degree of bone repair (%); (b) the ratio of mature bone/immature bone (MB/IB) estimated using VOF staining and (c) the ratios of adipose or connective tissue/bone (T/B) in the different experimental groups. Bars represent means ± SD ($n = 3$), $p < 0.05$. The identical letter on different bars indicates significant differences.

and β-estradiol systems with and without MSCs, in an OP rats critical size bone defect regeneration. Since bone regeneration is slower in OP animals than in non-OP, the system permanency in the defect and the maintenance of local therapeutic concentrations of BMP-2 and β-estradiol may play an important role in tissue regeneration. The material osteointegration and/or degradation rate should ideally match the bone formation rate. Therefore, the preparation of two BMP-2-β-estradiol PLGA-alginate systems, a solid sponge and a hydrogel, with the same composition, were suitable to test our hypothesis. Both systems exhibited high porosity and great water uptake capacity, these characteristics facilitate the free diffusion of oxygen and nutrients including endogenous growth factors and other cytokines providing an optimum environment for bone tissue ingrowth. Furthermore, the release profiles of both drugs from the two systems were similar as the release rate was controlled by the microspheres. In comparison with the sponge, the hydrogel had better characteristics for minimally invasive administration. Immediately after the addition of a small amount of cross-linker, the alginate solution increases its viscosity forming a dense polymer network with thixotropic behaviour, especially at 20 °C. Therefore, the viscosity of the material decreases when subjected to a certain mechanical stress, and gradually recovers at rest. This behaviour allows for the injection of highly viscous materials, even at room temperatures, and facilitate their adaptation to the target site. The incorporation of microspheres to the hydrogel increased the viscosity by 10 times while maintaining its thixotropic behaviour. To ensure formulations remain at the defect for a sufficient time, both hydrogel and sponge were placed between two electrospun polymer sheets loaded with β-estradiol forming a sandwich system. Despite of this, the hydrogel mass loss was greater than that of the sponge, hence its defect permanence time would be shorter. This characteristic probably prevents the hydrogel formulation from remaining long enough on the defect to guide tissue growth as reflected by the in vivo repair results.

Although the hydrogel formulation has the advantage of being easily injectable, sponges were also flexible and adapted perfectly to the defect edge. The histological analysis clearly showed the efficiency of the sponge system to promote bone regeneration with approximately 75% of defect regeneration against the approximately 50% reached for the hydrogel. In addition, the architecture of the repaired tissue was different, the newly formed tissue in the defects treated with the hydrogel presented a more disorganized structure with large hollow spaces, probably due to the rapid and large hydrogel mass loss observed in vitro. Additionally, a greater presence of adipose tissue, typical of osteoporosis, was found, evidencing a lower quality of the repaired tissue in this group. On the other hand, the implantation of sponges led to a more compact tissue, with a lower presence of connective tissue, probably as a consequence of the higher percentage of regeneration achieved, as this tissue plays an important role guiding and regulating the repair process at the initial steps of bone formation [34,35].

As we already reported, hydrogels of variable composition loaded with BMP-2 and β-estradiol within microsphere showed similar bone regeneration rate on calvarial defects in OP and non-OP rats. However, the mineralization process was tremendously reduced in OP rats [17,18]. For this reason, two new strategies were incorporated in the present work: the addition of MSCs and the microspheres composition modification to reduce the BMP-2 release rate. The use of polymers characterized by a relatively slow degradation rate and the incorporation of alginate in the internal aqueous phase of the microspheres was reflected in an extension of the BMP-2 release time. After 6 weeks approximately 46% of the BMP-2 dose was released in vivo. For β-estradiol, the unavailability of the radiotracer labelled molecule (that allows one to monitor the in vivo release kinetics) together with its low aqueous solubility makes difficult to predict its release profile from the implanted system. However, it is reasonable to expect the in vivo

release rate to be similar or even higher to that observed in vitro in DMSO or SLS solutions due to the continuous blood flow, which will increase as new tissue refills the defect. In any case, probably a very slow in vivo release would take place, which would be supplemented by the rapid release of the drug incorporated in the electrospun polymer sheets due to the large specific surface area of the fibers.

Unfortunately, none of the tools applied accelerated the mineralization of the formed bone. No differences were observed in the mineralization degree with either of the scaffolds with or without MSCs. The addition of MSCs to the systems pre-loaded with BMP-2 did not improve neither the regeneration rate nor the mineralization of the new bone tissue. The osteogenic effect of MSCs and BMP-2 is widely documented in the literature in different animal models. Furthermore, the synergistic effect of the combination of these two elements has been demonstrated in a calvarial defect [36–45] which is the animal model used in this study. The different animal models, composition and architecture of scaffolds, and the BMP-2 doses used by some authors together with the lack of literature (PubMed database) referred to the MSCs and BMP-2 combination efficacy for bone regeneration in osteoporosis, hinders direct comparison of our data with previous works. To the best of our knowledge, this is the first time that the combination of BMP-2 and osteoporotic MSCs has been assayed in an osteoporotic rat critical defect. The molecular alterations of osteoporotic MSCs are reflected on a proliferative capacity decrease [46], production of type I collagen-deficient matrix and a tendency to adipogenic differentiation [47] leading to significant deficiencies in self-repair and an impaired differentiation. Despite of this, the in vitro osteogenic response of osteoporotic MSCs after BMP-2 stimulation has been described [48]. Therefore, future studies are required to optimize the MSCs loading and their combination with BMP-2 to reduce the protein dose while maintaining the regenerative capacity of the system and improving the mineralization of the newly formed tissue.

5. Conclusion

In this work, two physically different PLGA-alginate scaffolds, SS and HY, have been successfully elaborated presenting the same BMP-2 and β-estradiol release rate. Both systems promoted bone regeneration in a critical size calvarial defect in OP rats, although SS showed a significantly higher percentage of bone formation. Moreover, SS promoted the formation of bone with better quality, in terms of lower proportion of adipose and connective tissue. Since the active substances release rate was similar, this difference in bone regeneration can be related to the shorter permanence time of HY in the defect and highlights the importance of the scaffold's physical configuration to optimize the effect of the sustained delivery of active molecules. Finally, the incorporation of osteoporotic MSCs in the scaffolds did not improve the bone regeneration process in any case.

Declaration of competing interest

The authors declare no conflict of interest.

Acknowledgments

This work was supported by the Ministry of Economy and Competitiveness, Spain (MAT2014-55657-R).

References

[1] H. Begam, S.K. Nandi, B. Kundu, A. Chanda, Strategies for delivering bone morphogenetic protein for bone healing, Mater. Sci. Eng. C. 70 (2017) 856–869, https://doi.org/10.1016/j.msec.2016.09.074.
[2] H.C. Fayaz, P.V. Giannoudis, M.S. Vrahas, R.M. Smith, C. Moran, H.C. Pape, C. Krettek, J.B. Jupiter, The role of stem cells in fracture healing and nonunion, Int. Orthop. 35 (2011) 1587–1597, https://doi.org/10.1007/s00264-011-1338-z.
[3] A. Nauth, B. Ristevski, R. Li, E.H. Schemitsch, Growth factors and bone regeneration: how much bone can we expect? Injury 42 (6) (2011) 574–579 (doi: 1016/j.injury.2011.03.034).
[4] D.W. Hutmacher, Scaffolds in tissue engineering bone and cartilage, Biomaterials. 21 (24) (2000) 2529–2543, https://doi.org/10.1016/s0142-9612(00)00121-6.
[5] G. Chen, N. Kawazoe, Porous scaffolds for regeneration of cartilage, bone and osteochondral tissue, Adv. Exp. Med. Biol. 1058 (2018) 171–191, https://doi.org/10.1007/978-3-319-76711-6_8.
[6] T.N. Vo, F.K. Kasper, A.G. Mikos, Strategies for controlled delivery of growth factors and cells for bone regeneration, Adv. Drug Deliv. Rev. 64 (12) (2012) 1292–1309, https://doi.org/10.1016/j.addr.2012.01.016.
[7] M.A. Velasco, C.A. Narváez-Tovar, D.A. Garzón-Alvarado, Design, materials and mechanobiology of biodegradable scaffolds for bone tissue engineering, Biomed. Res. Int. 2015 (2015) 729076, https://doi.org/10.1155/2015/729076.
[8] A.S. Hoffman, Hydrogels for biomedical applications, Adv. Drug Deliv. Rev. 64 (2012) 18–23, https://doi.org/10.1016/j.addr.2012.09.010.
[9] N.A. Peppas, J.Z. Hilt, A. Khademhosseini, R. Langer, Hydrogels in biology and medicine: from molecular principles to bionanotechnology, Adv. Mater. 18 (11) (2006) 1345–1360, https://doi.org/10.1002/adma.200501612.
[10] I.E. Bialy, W. Jiskoot, M.R. Nejadnik, Formulation, delivery and stability of bone morphogenetic proteins for effective bone regeneration, Pharm. Res. 34 (6) (2017) 1152–1170, https://doi.org/10.1007/s11095-017-2147-x.
[11] V. Agrawal, M. Sinha, A review on carrier systems for bone morphogenetic protein-2, J. Biomed. Mater. Res. Part B 105 (2016) 904–925, https://doi.org/10.1002/jbm.b.33599.
[12] P.J. Kondiah, Y.E. Choonara, P.P.D. Kondiah, T. Marimuthu, P. Kumar, L.C. du Toit, V. Pillay, A review of injectable polymeric hydrogel systems for application in bone tissue engineering, Molecules 21 (2016) E1580, , https://doi.org/10.3390/molecules21111580.
[13] M. Moreno, M.H. Amaral, J.M. Lobo, A.C. Silva, Scaffolds for bone regeneration: state of the art, Curr. Pharm. Des. 22 (2016) 2726–2736, https://doi.org/10.2174/1381612822666160203114902.
[14] R. Dorati, A. DeTrizio, T. Modena, B. Conti, F. Benazzo, G. Gastaldi, I. Genta, Biodegradable scaffolds for bone regeneration combined with drug-delivery systems in osteomyelitis therapy, Pharmaceuticals 10 (2017) E96, , https://doi.org/10.3390/ph10040096.
[15] M. Rodríguez-Évora, R. Reyes, C. Alvarez-Lorenzo, A. Concheiro, A. Delgado, C. Évora, Bone regeneration induced by an in situ gel-forming poloxamine, bone morphogenetic protein-2 system, J. Biomed. Nanotechnol. 10 (2014) 1–11, https://doi.org/10.1166/jbn.2014.1801.
[16] C. del Rosario, M. Rodríguez-Évora, R. Reyes, S. Simões, A. Concheiro, C. Évora, C. Alvarez-Lorenzo, A. Delgado, Bone critical defect repair with poloxamine-cyclodextrin supramolecular gels, Int. J. Pharm. 495 (2015) 463–473, https://doi.org/10.1016/j.ijpharm.2015.09.003.
[17] E. Segredo-Morales, R. Reyes, M.R. Arnau, A. Delgado, C. Évora, In situ gel-forming system for dual BMP-2 and 17β-estradiol controlled release for bone regeneration in osteoporotic rats, Drug Deliv. Transl. Res. 8 (2018) 1103–1113, https://doi.org/10.1007/s13346-018-0574-9.
[18] E. Segredo-Morales, P. García-García, R. Reyes, E. Pérez-Herrero, A. Delgado, C. Évora, Bone regeneration in osteoporosis by delivery BMP-2 and PRGF from tetronic–alginate composite thermogel, Int. J. Pharm. 543 (2018) 160–168, https://doi.org/10.1016/j.ijpharm.2018.03.034.
[19] T. Kubo, T. Shiga, J. Hashimoto, M. Yoshioka, H. Honjo, M. Urabe, I. Kitajima, I. Semba, Y. Hirasawa, Osteoporosis influences the late period of fracture healing in a rat model prepared by ovariectomy and low calcium diet, J. Steroid Biochem. Mol. Biol. 68 (1999) 197–202, https://doi.org/10.1016/S0960-0760(99)00032-1.
[20] H. Namkung-Matthai, R. Appleyard, J. Jansen, J. Hao Lin, S. Maastricht, M. Swain, R.S. Mason, G.A. Murrell, A.D. Diwan, T. Diamond, Osteoporosis influences the early period of fracture healing in a rat osteoporotic model, Bone 28 (2001) 80–86, https://doi.org/10.1016/S8756-3282(00)00414-2.
[21] R. Oliver, Y. Yu, G. Yee, A. Low, A. Diwan, W. Walsh, Poor histological healing of a femoral fracture following 12 months of oestrogen deficiency in rats, Osteoporos. Int. 24 (2013) 2581–2589, https://doi.org/10.1007/s00198-013-2345-2.
[22] W.H. Cheung, T. Miclau, S.K. Chow, F.F. Yang, V. Alt, Fracture healing in osteoporotic bone, Injury Int. J. Care Injured 47 (S2) (2016) 21–26, https://doi.org/10.1016/S0020-1383(16)47004-X.
[23] G. Gainza, J.J. Aguirre, J.L. Pedraz, R.M. Hernández, M. Igartua, rhEGF-loaded PLGA-alginate microspheres enhance the healing of full-thickness excisional wounds in diabetised Wistar rats, Eur. J. Pharm. Sci. 50 (2013) 243–252, https://doi.org/10.1016/j.ejps.2013.07.003.
[24] P. Zhai, X.B. Chenb, D.J. Schreyer, PLGA/alginate composite microspheres for hydrophilic protein delivery, Mater. Sci. Eng. C Mater. Biol. Appl. 56 (2015) 251–259, https://doi.org/10.1016/j.msec.2015.06.015.
[25] P.J. Fraker, J.C. Speck Jr., Protein and cell membrane iodinations with a sparingly soluble chloroamide, 1,3,4,6-tetrachloro-3a,6a-diphrenylglycoluril, Biochem. Biophys. Res. Commun. 80 (1978) 849–857, https://doi.org/10.1016/0006-291x(78)91322-0.
[26] K.R. Dobson, L. Reading, M. Haberey, X. Marine, A. Scutt, Centrifugal isolation of bone marrow from bone: an improved method for the recovery and quantitation of bone marrow osteoprogenitor cells from rat tibiae and femurae, Calcif. Tissue Int. 65 (1999) 411–413, https://doi.org/10.1007/s002239900723.
[27] R. Reyes, M.K. Pec, E. Sánchez, C. del Rosario, A. Delgado, C. Évora, Comparative, osteochondral defect repair: stem cells versus chondrocytes versus bone morphogenetic protein-2, solely or in combination, Eur. Cell. Mater. 25 (2013) 351–365, https://doi.org/10.22203/eCM.v025a25.
[28] R. Vayas, R. Reyes, M.R. Arnau, C. Évora, A. Delgado, Injectable scaffold for bone marrow stem cells and bone morphogenetic protein-2 to repair cartilage, Cartilage

(2019) 1–14, https://doi.org/10.1177/1947603519841682.
[29] M. Rodríguez-Évora, A. Delgado, R. Reyes, A. Hernández-Daranas, I. Soriano, J. San Román, C. Évora, Osteogenic effect of local, long versus short term BMP-2 delivery from a novel SPU-PLGA-βTCP concentric system in a critical size defect in rats, Eur. J. Pharm. Sci. 49 (2013) 873–884, https://doi.org/10.1016/j.ejps.2013.06.008.
[30] J.J. Delgado, C. Evora, E. Sánchez, M. Baro, A. Delgado, Validation of a method for non-invasive in vivo measurement of growth factor release from a local delivery system in bone, J. Control. Release 114 (2006) 223–229, https://doi.org/10.1016/j.jconrel.2006.05.026.
[31] A. Hernández, E. Sánchez, I. Soriano, R. Reyes, A. Delgado, C. Évora, Material-related effects of BMP-2 delivery systems on bone regeneration, Acta Biomater. 8 (2012) 781–791, https://doi.org/10.1016/j.actbio.2011.10.008.
[32] E. Martinez-Sanz, D.A. Ossipov, J. Hilborn, S. Larsson, K.B. Jonsson, O.P. Varghese, Bone reservoir: injectable hyaluronic acid hydrogel for minimal invasive bone augmentation, J. Control. Release 152 (2011) 232–240, https://doi.org/10.1016/j.jconrel.2011.02.003.
[33] R. Barbucci, D. Pasqui, R. Favaloro, G. Panariello, Thixotropic hydrogel from chemically cross-linked guar gum: synthesis, characterization and rheological behaviour, Carbohydr. Res. 343 (2008) 3058–3065, https://doi.org/10.1016/j.carres.2008.08.029.
[34] J.M. Reinke, H. Sorg, Wound repair and regeneration, Eur. Surg. Res. 49 (2012) 35–43, https://doi.org/10.1159/000339613.
[35] E.S. Chermnykh, E.V. Kiseleva, O.S. Rogovaya, A.L. Rippa, A.V. Vasiliev, E.A. Vorotelyak, Tissue-engineered biological dressing accelerates skin wound healing in mice via formation of provisional connective tissue, Histol. Histopathol. 33 (2018) 1189–1199, https://doi.org/10.14670/HH-18-006.
[36] S.J. Stephan, S.S. Tholpady, B. Gross, C.E. Petrie-Aronin, E.A. Botchway, L.S. Nair, R.C. Ogle, S.S. Park, Inyectable tissue-engineered bone repair of a rat calvarial defect, Laryngoscope. 120 (2010) 895–901, https://doi.org/10.1002/lary.20624.
[37] X. He, Y. Liu, X. Yuan, L. Lu, Enhanced healing of rat calvarial defects with MSCs loaded on BMP-2 releasing chitosan/alginate/hidroxyapatite scaffolds, PLoS One 9 (2014) e104061, , https://doi.org/10.1371/journal.pone.0104061.
[38] C. del Rosario, M. Rodríguez-Évora, R. Reyes, A. Delgado, C. Évora, BMP-2, PDGF-BB, and bone marrow mesenchymal cells in a macroporous β-TCP scaffold for critical-size bone defect repair in rats, Biomed. Mater. 10 (2015) 045008, , https://doi.org/10.1088/1748-6041/10/4/045008.
[39] B.S. Kim, M.K. Choi, J.H. Yoon, J. Lee, Evaluation of bone regeneration with biphasic calcium phosphate substitute implanted with bone morphogenetic protein 2 and mesenchymal stem cells in a rabbit calvarial defect model, Oral Surg. Oral Med. Oral Pathol. Oral Radiol. 120 (1) (2015) 2–9, https://doi.org/10.1016/j.oooo.2015.02.017.
[40] S. Eap, L. Keller, J. Schiavi, O. Huck, L. Jacomine, F. Fioretti, C. Gauthier, V. Sebastian, P. Schwinté, N. Benkirane-Jessel, A living thick nanofibrous implant bifunctionalized wht active growth factor and stem cells for bone regeneration, Int. J. Nanomedicine 10 (2015) 1061–1075, https://doi.org/10.2147/IJN.S72670.
[41] S.S. Ho, N.L. Vollmer, M.I. Refaat, O. Jeon, E. Alsber, M.A. Lee, J.K. Leach, Bone morphogenetic protein-2 promotes human mesenchymal stem cell survival and resultant bone formation when entrapped in photocrosslinked alginate hydrogels, Adv. Healthc. Mater. 5 (2016) 2501–2509, https://doi.org/10.1002/adhm.201600461.
[42] R. Aquino-Martínezx, N. Artigas, B. Gámez, J.L. Rosa, F. Ventura, Extracellular calcium promotes bone formation from bone marrow mesenchymal stem cells by amplifying the effects of BMP-2 on SMAD signalling, PLoS One 12 (2017) e0178158, , https://doi.org/10.1371/journal.pone.0178158.
[43] R. Zhang, X. Li, Y. Liu, X. Gao, T. Zhu, L. Lu, Acceleration of bone regeneration in critical-size defect using BMP-9-loaded nHA/Coll/MWCNTs scaffolds seeded with bone marrow mesenchymal stem cells, Biomed. Res. Int. 2019 (2019) 7343957, , https://doi.org/10.1155/2019/7343957.
[44] X. Li, R. Zhang, X. Tan, B. Li, Y. Liu, X. Wang, Synthesis and evaluation of BMMSC-seeded BMP-6/nHAG/GMS scaffolds for bone regeneration, Int. J. Med. Sci. 16 (2019) 1007–1017, https://doi.org/10.7150/ijms.31966.
[45] Y. Kong, Y. Zhao, D. Li, H. Shen, M. Yan, Dual delivery of encapsulated BM-MSCs and BMP-2 improves osteogenic differentiation and new bone formation, J. Biomed. Mater. Res. A 107 (2019) 2282–2295, https://doi.org/10.1002/jbm.a.36737.
[46] E. Tsiridis, N. Upadhyay, P. Giannoudis, Molecular aspects of fracture healing: which are the important molecules? Injury 38 (2007) S11–S25, https://doi.org/10.1016/j.injury.2007.02.006.
[47] J.P. Rodríguez, L. Montecinos, S. Ríos, P. Reyes, J. Martínez, Mesenchymal stem cells from osteoporotic patients produce a type I collagen-deficient extracellular matrix favoring adipogenic differentiation, J. Cell. Biochem. 79 (2000) 557–565, https://doi.org/10.1002/1097-4644(20001215)79:4<557::AID-JCB40>3.0.CO;2-H.
[48] W.C. Prall, F. Haasters, J. Heggebö, H. Polzer, C. Schwarz, C. Gassner, S. Grote, D. Anz, M. Jäger, W. Mutschler, M. Schieker, Mesenchymal stem cells from osteoporotic patients feature impaired signal transduction but sustained osteoinduction in response to BMP-2 stimulation, Biochem. Biophys. Res. Commun. 440 (2013) 617–622, https://doi.org/10.1016/j.bbrc.2013.09.114.

pharmaceutics

MDPI

Article

The Bone Regeneration Capacity of BMP-2 + MMP-10 Loaded Scaffolds Depends on the Tissue Status

Patricia Garcia-Garcia [1,2], Ricardo Reyes [2,3], José Antonio Rodriguez [4,5], Tomas Martín [6,7], Carmen Evora [1,2], Patricia Díaz-Rodríguez [1,2,*] and Araceli Delgado [1,2,*]

1 Department of Chemical Engineering and Pharmaceutical Technology, Universidad de La Laguna, 38206 La Laguna, Spain; pgarciag@ull.edu.es (P.G.-G.); cevora@ull.edu.es (C.E.)
2 Institute of Biomedical Technologies (ITB), Universidad de La Laguna, 38320 La Laguna, Spain; rreyesro@ull.edu.es
3 Department of Biochemistry, Microbiology, Cell Biology and Genetics, Universidad de La Laguna, 38200 La Laguna, Spain
4 Laboratory of Atherothrombosis, CIMA, Universidad de Navarra, Instituto de Investigación Sanitaria de Navarra (IdisNA), 31009 Pamplona, Spain; josean@unav.es
5 Centro de Investigación Biomédica en Red en Enfermedades Cardiovasculares (CIBERCV), Instituto de Salud Carlos III, 28029 Madrid, Spain
6 Instituto de Productos Naturales y Agrobiología, CSIC, Francisco Sánchez 3, 38206 La Laguna, Spain; tmartin@ipna.csic.es
7 Instituto Universitario de Bio-Orgánica Antonio González, Universidad de La Laguna, Francisco Sánchez 2, 38206 La Laguna, Spain
* Correspondence: patricia.diaz.rodriguez@usc.es (P.D.-R.); adelgado@ull.edu.es (A.D.); Tel.: +34-922318507 (A.D.)

Citation: Garcia-Garcia, P.; Reyes, R.; Rodriguez, J.A.; Martín, T.; Evora, C.; Díaz-Rodríguez, P.; Delgado, A. The Bone Regeneration Capacity of BMP-2 + MMP-10 Loaded Scaffolds Depends on the Tissue Status. *Pharmaceutics* **2021**, *13*, 979. https://doi.org/10.3390/pharmaceutics13070979

Academic Editor: Hyuk Sang Yoo

Received: 1 June 2021
Accepted: 25 June 2021
Published: 29 June 2021

Abstract: Biomaterials-mediated bone formation in osteoporosis (OP) is challenging as it requires tissue growth promotion and adequate mineralization. Based on our previous findings, the development of scaffolds combining bone morphogenetic protein 2 (BMP-2) and matrix metalloproteinase 10 (MMP-10) shows promise for OP management. To test our hypothesis, scaffolds containing BMP-2 + MMP-10 at variable ratios or BMP-2 + Alendronate (ALD) were prepared. Systems were characterized and tested in vitro on healthy and OP mesenchymal stem cells and in vivo bone formation was studied on healthy and OP animals. Therapeutic molecules were efficiently encapsulated into PLGA microspheres and embedded into chitosan foams. The use of PLGA (poly(lactic-co-glycolic acid)) microspheres as therapeutic molecule reservoirs allowed them to achieve an in vitro and in vivo controlled release. A beneficial effect on the alkaline phosphatase activity of non-OP cells was observed for both combinations when compared with BMP-2 alone. This effect was not detected on OP cells where all treatments promoted a similar increase in ALP activity compared with control. The in vivo results indicated a positive effect of the BMP-2 + MMP-10 combination at both of the doses tested on tissue repair for OP mice while it had the opposite effect on non-OP animals. This fact can be explained by the scaffold's slow-release rate and degradation that could be beneficial for delayed bone regeneration conditions but had the reverse effect on healthy animals. Therefore, the development of adequate scaffolds for bone regeneration requires consideration of the tissue catabolic/anabolic balance to obtain biomaterials with degradation/release behaviors suited for the existing tissue status.

Keywords: BMP-2; MMP-10; osteoporotic bone; microspheres; mesenchymal stem cells

1. Introduction

Bone tissue is under continuous remodeling throughout our lifetime. However, its regeneration capacity is limited by defects size, blood perfusion, age, and metabolic disorders [1]. Craniofacial bone defects or craniofacial congenital malformations generally require surgery and defects to be refilled with natural or synthetic biomaterials to promote

bone healing. Often scaffolds are not enough to induce osteogenesis, and the contribution of other key elements such as progenitor cells or signaling molecules are required to ensure clinical success. In addition, the defects size and the comorbidity with other diseases altering bone tissue metabolism, compromise complete bone healing. Specifically, osteoporosis (OP) is characterized by an imbalance between the processes of bone formation and resorption and, consequently, by a delay in bone defects regeneration [2].

Bone morphogenetic proteins (BMPs) are a well-known growth factors family with osteo- and chondroinductive properties. Particularly, recombinant human BMP-2 (rhBMP-2) has shown a strong osteoinductive effect when incorporated in local delivery carriers placed in the injury site [3]. Postmenopausal osteoporosis is related to multiple factors, emphasizing the decreased levels of estrogens. These molecules play a key role in bone cell metabolism through estrogen receptor α (ERα). Estrogens inhibit osteoclastic bone resorption via increasing osteoclast apoptosis, reducing osteoblastic production of the receptor activator of nuclear factor kB ligand (RANKL) and increasing osteoprotegerin production [4]. Hence, in our previous works, scaffolds loaded with combinations of BMP-2 and 17β-estradiol formulated in microspheres were tested in an osteoporotic rat calvarial critical defect. Experimental results showed the new bone formed in OP rats was less mineralized than in non-OP rats [5–7]. On the other hand, bisphosphonates are routinely used drugs for OP treatment. These antiosteoclastic agents systemically administrated or integrated into scaffolds of different nature have been reported to support bone defects regeneration in both OP and non-OP animals [8–12]. Yet some authors stated no bisphosphonates effect in the regeneration of calvarial bone defects [13].

Moreover, BMPs have been combined with different bisphosphonates to reduce the excessive osteoclastogenesis that they induce as a consequence of their strong osteogenesis [14]. This combination formulated in local release systems generally causes a remarkable improvement in the bone defect regeneration induced by BMP-2 [15,16]. However, very few publications are devoted to studying the effect of this combination in osteoporotic animals. In fact, only two reports were found describing the effect of an IV or subcutaneous zoledronate single dose on the regeneration of a calvarial defect or a mid-diaphyseal open femoral fracture treated with a local release of BMP-2 or BMP-7, respectively [17,18].

The outcomes of both studies were different, the combination of a BMP-2 embedded collagen carrier with IV zoledronate initially had a negative effect in bone quantity and quality induced by rhBMP-2. Although this undesirable effect disappeared at long term assessments, the combination did not exceed the regeneration capacity of BMP-2 alone [17]. Conversely, the local implantation of BMP-7 incorporated in a collagen putty combined with zolendronate injected subcutaneously suggested that the hypothesis that osteoporosis is a disease that delays or hinders bone regeneration is incorrect [18]. However, the aforementioned studies are complicated to compare as defect models because the experimental designs and the BMPs used were different.

Lastly, matrix metalloproteinases (MMPs) are enzymes that play pivotal roles in tissue remodeling, by degrading a wide variety of matrix or nonmatrix substrates. MMPs expression, detected in osteoblasts and osteoclasts, has been shown to be required for bone homeostasis and proper fracture healing. In fact, altered cartilage remodeling and vascularization leading to impaired fracture repair has been reported in murine models with genetic deficiency in MMP9 [19] or MMP13 [20,21], while delayed bone remodeling has been observed in MMP2-KO mice [22]. Among them, MMP-10 has been shown to be expressed in osteoblasts and chondrocytes during bone formation in humans [23]. Interestingly, this MMP can enhance the in vitro osteoblastic differentiation of myoblastic cells induced by BMP-2 [24]. Moreover, we have recently demonstrated that MMP-10 is overexpressed in calcified human aortic valves (AVs) and active MMP-10 promotes calcification of valvular interstitial cells isolated from human AVs through Akt phosphorylation [25]. Furthermore, we have also shown that MMP-10 accelerates bone repair by enhancing BMP-2-promoted bone healing and improving the mineralization rate in a murine model of a calvaria critical size defect [26].

Therefore, the aim of this study is to further analyze the in vitro and in vivo MMP-10 pro-mineralization effect when combined with BMP-2 on a 3D scaffold. To accomplish this, different MMP-10 doses were tested. Moreover, the MMP-10+BMP-2 activity was compared with scaffolds incorporating alendronate, a bisphosphonate, and BMP-2. Both proteins and bisphosphonate were formulated on microspheres and embedded on a crosslinked chitosan foam. The obtained foams were then surrounded by electrospun meshes loaded or not with alendronate to form the final scaffold with a sandwich-like structure. The in vitro promotion of ALP activity and in vivo mineralization using a critical size calvarial defect was assessed in both healthy and osteoporotic mice.

2. Materials and Methods

2.1. Microspheres Preparation and Characterization

2.1.1. Microsphere Preparation

Different drug-loaded PLGA (poly(lactic-co-glycolic acid)) microspheres were designed for the experiment and prepared following different protocols (Table 1). PLGA microspheres loaded with BMP-2 and MMP-10 were prepared by a double emulsion method ($w/o/w$). For this purpose, a combination of two ester terminated PLGAs with variable molecular weight and lactide:glycolide ratio were selected. To obtain loaded microspheres 35 µg of BMP-2 (ED50: 0.74 µg/µL; GenScript, Piscataway, NJ, USA) and 2.1 µg or 8.5 µg rhMMP-10 (obtained equally to [27]) as described in Table 1 were dissolved in 200 µL of 0.8% PVA (MW: 30,000–70,000; Sigma-Aldrich, St. Louis, MO, USA). This aqueous phase was added to 1 mL of oil phase formed by the PLGA 75:25 (Resomer® RG755, 0.54 dL/g, Evonik, Darmstadt, Germany) and 85:15 (Resomer® RG858, 1.5 dL/g, Evonik) mixture used at 9 to 1 ratio at 150 mg/mL in DCM and homogenized for 1 min by vortex. Then, 3 mL of a second aqueous solution prepared with 2.5% PVA was added to the first emulsion and homogenized for one minute. Finally, the solvent was evaporated by pouring the obtained microspheres in 100 mL of PVA at 0.1% for one hour under continuous stirring.

Table 1. Developed PLGA microspheres and drug amounts used per batch.

Microspheres Type	BMP-2 (µg)	ALD (µg)	MMP-10 (µg)
Blank PLGA	-	-	-
PLGA-BMP-2	35 µg	-	-
PLGA/Chitosan-BMP-2 + ALD	35 µg	75 µg	-
PLGA-BMP-2 + Low MMP-10	35 µg	-	2.1 µg
PLGA-BMP-2 + High MMP-10	35 µg	-	8.5 µg

Alendronate (ALD; Sigma-Aldrich) microspheres were prepared by a double emulsion method as described above with slight modifications. An internal aqueous phase (450 µL) was prepared containing PVA at 0.8%, chitosan (CHT, 150mPa.s, Protasan® UP-CL-213, Sandvika, Norway) at 1%, and 75 µg ALD. The oil phase prepared as described above was added to this aqueous phase and homogenized for one minute. The second aqueous phase was added as described and the solvent was evaporated by pouring the microspheres in 100 mL of 0.1% PVA and 2.5% of Pentabasic sodium tripolyphosphate (STPP; Sigma-Aldrich) for one hour under continuous stirring.

The obtained microspheres were washed with double-distilled water, filtered through a 0.45 µm pore size filter (Pall Corporation, Sigma-Aldrich), freeze-dried, and stored at 4 °C until use. Microspheres were characterized in terms of size and size distribution by light diffraction using a Mastersizer (Mastersized 2000, Malvern Instruments, Malvern, UK) and the morphology was evaluated by scanning electron microscopy (SEM; JSM-6300, Jeol, Tokio, Japan) after silver coating.

2.1.2. Microspheres Loading Efficiency

Protein loading efficiencies were evaluated using radiolabeled BMP-2 (125I-BMP-2) or MMP-10 (125I-MMP-10). Proteins were labeled following the Iodogen method [28] as previously described [29]. Briefly, in 50 µg Iodogen coated tubes (Pierce® Pre-coated Iodination Tube, Thermo Scientific, Rockford, IL, USA) 50 µL of the protein solution (1 mg/mL) was mixed with 10 µL of 125INa (≈1 mCi) (Perkin-Elmer, Waltham, MA, USA) and taken to a final volume of 150 µL with Phosphate Buffer Saline (PBS, 0.5M pH 7). This mixture was kept at room temperature for 15 min under continuous stirring (120 rpm), then, 50 µL of a saturated tyrosine solution in PBS was added to remove any unreacted 125I. Labelled proteins were purified using ZebaTM Spin Desalting Column (Thermo Scientific).

ALD loading efficiency was evaluated on microspheres loaded with 99 mTechnetium radiolabeled ALD. Drug labelling was performed as described by Gundogdu and coworkers [30]. In Brief, 5 mg of ALD was mixed with 1 mg of ascorbic acid and 0.5 mg of tin chloride dihydrate ($SnCl_2$ $2H_2O$) and kept under inert atmosphere. Afterwards, 0.5 mL of ultrapure water was added (MilliQ, Darmstadt, Germany). Once dissolved, 100 µL of generator eluate (0.5–1 mCi) was added and the solution was stirred (120 rpm) at room temperature for 15 min.

Labelling yields and stability were evaluated by instant thin layer chromatography (iTLC) using 11.5 × 0.8 cm silica gel coated strips (Varian Iberica SL) to which 5 µL of the labelled protein or ALD were added (30,000–40,000 cpm). For proteins, 85% methanol in water was used as mobile phase. A gamma counter (Cobra II, Packard®, Downers Grove, IL, USA) was used to measure free 125I (Rf = 1) and labelled proteins (Rf = 0) as previously published [31]. For ALD chromatography, acetone or 0.9% NaCl were used as mobile phase. The chromatography performed in acetone separated free 99mTc (99mTcO4-) (Rf = 1) from ALD-99mTc and hydrolyzed 99mTc (TcO_2) (Rf = 0). On the other hand, when 0.9% NaCl is used as mobile phase both free 99mTc and ALD-99mTc migrate to the front (Rf = 1) while hydrolyzed 99mTc does not migrate (Rf = 0). These values can be used to calculate the percentage of labelled ALD as follows:

$$\%(^{99m}\text{Tc-ALD}) = 100 - [\%\ ^{99m}TcO_4^- + \%\ ^{99m}TcO_2] \quad (1)$$

To evaluate the encapsulation efficiency of the microspheres, radioactivity was measured on the microspheres aliquots using a gamma counter (Cobra II, Packard®®) and compared with total protein reactivity.

2.2. Preparation and Characterization of Electrospun Meshes

2.2.1. PLGA Functionalization with ALENDRONATE

To obtain ALD-loaded electrospun fibers, two acid-terminated PLGA polymers with 50:50 lactide:glycolide ratio, Resomer® RG502 (0.19 dL/g, Evonik), and Resomer® RG504 (0.4 dL/g Evonik) were chemically conjugated with ALD following the protocol described by Choi and coworkers (Choi et al., 2007). A 10% PLGA solution was prepared in 20 mL acetone to which 60 mg of N-hydroxysuccinamide (NHS, Sigma-Aldrich) and 100 mg of N, N′-dicyclohexylcarbodiimide (DCC, Sigma-Aldrich) were added and allowed to react in inert atmosphere under stirring for 24 h at room temperature. Afterwards, the reaction mixture was filtrated through 0.45 µm (Chromafil® Xtra PET-45/25, Macherey-Nagel, Lake Forest, CA, USA) to remove dicyclohexylurea and the obtained PLGA-NHS was precipitated in cold ethyl ether (Scharlau®, Barcelona, Spain) and dissolved in DCM. This solution was concentrated at room temperature until drying using a rotavapor.

ALD conjugation was performed by dissolving 1.9 g of the obtained PLGA-NHS in 19 mL of Acetone:DMSO (50:50) and adding an adequate amount of ALD previously dissolved in 1 mL of water. This mixture was allowed to react at room temperature for another 24 h. Then, the solution was concentrated by rotavapor at high vacuum and 37 °C. The obtained ALD conjugated polymer (PLGA-ALD) was dissolved in the minimum amount of acetone, precipitated in ethyl ether and dissolved again in DCM to avoid free

ALD. Finally, this solution was dried for 24 h under high vacuum and the PLGA-ALD was precipitated with distilled water, filtrated through 0.45 µm, and freeze-dried. To ensure adequate functionalization, the obtained polymer was characterized by proton nuclear magnetic resonance. ^{1}H-NMR spectra were recorded at 500 MHz (Bruker Avance 500, Billerica, MA, USA), and chemical shifts were reported in ppm and calibrated on non-deuterated solvent residual peak. Elemental analysis was performed using a CHNS TruSpec Micro analyzer (LECO, St. Joseph, MI, USA).

2.2.2. Electrospun Meshes Preparation

Electrospun meshes composed by RG504-ALD: RG502-ALD: RG 855 at 1:1:1 ratio were prepared. The polymers mixture (375 mg) was dissolved in 2.5 mL of Hexafluoroisopropanol (HFIP, Sigma-Aldrich) and loaded into a syringe equipped with a 18G needle. This solution was ejected at a continuous flow of 2.75 mL/h using a syringe pump (Harvard Apparatus ®, Holliston, MA, USA) under an electric field of 7 KV. Fibers were collected on a cylindrical metal collector that rotates at 200 rpm located at a 10 cm distance from the syringe. The process took place at room temperature and 65% of relative humidity. Blank meshes with the same polymers proportions and conditions were also obtained using unfunctionalized PLGAs. Blank and ALD loaded electrospun meshes were surface treated with plasma (O_2). The plasma oxygen treatment was carried out under vacuum during 4 min for each side of the meshes. The generator power was at 75% of the capacity (Diener electronic, Plasma-Surface-Technology, Ebhausen, Germany).

2.2.3. ALD-Loaded and Blank Meshes Characterization

Meshes were characterized in terms of thickness, porosity, contact angle, and fiber diameter. Mean fiber diameter was obtained measuring 50 fibers for each sample after silver coating using scanning electron microscopy images (SEM, JSM 6300, JEOL) at a 1500 magnification by an image analysis software (ImageJ v1.52, National Institute of Health, Madison, WI, USA). Mesh thickness was obtained using stereomicroscope images (Leica M205 C, LAS, v3 software, Leica, Wetzlar, Germany).

Real mesh density was obtained by helium pycnometry (Micromeritics, AccuPyc 1330, Norcross, GA, USA) while apparent density was calculated from the weight and volume values. Volume was obtained from the length, width, and thickness as described in Equation (2). Mesh total porosity was calculated using real density and apparent density values as shown in Equation (3).

$$Apparent\ density = \frac{weight}{(lenght \cdot width \cdot thickness)} \quad (2)$$

$$Porosity\ (\%) = \frac{real\ density - apparent\ density}{real\ density} \cdot 100 \quad (3)$$

Mesh surface wettability was measured by contact angle assessments using a drop shape analyzer (DSA100; Krüss GmbH, Hamburg, Germany) and distilled water as the liquid media. The obtained images were analyzed with an image analyze software (ImageJ v1.52, National Institute of Health).

A proton NMR spectrum was performed on a 500 MHz equipment to determine the amount of ALD present on ALD-loaded electrospun meshes. To do so, 4.41 mg of the sheet were dissolved in 0.6 mL of $CDCl_3$, and 18.4 µL of a standard solution of 1,1,2,2-tetrachloroethane ($Cl_2CHCHCl_2$) in $CDCl_3$ (33.07 mM) was added. In this way, the amount of $Cl_2CHCHCl_2$ was four times the theoretical amount of alendronate presented in the polymer sheet. The quantity of ALD was obtained by integrating the signals corresponding to 1,1,2,2-tetrachloroethane (5.96 ppm) and the alendronate signal of the protons (2.98 ppm). These measurements were performed also at different time points on ALD-loaded meshes incubated in water at 37 °C to evaluate ALD release. To this end, samples were washed twice with water and freeze-dried previous to NMR characterization.

2.3. Foams Preparation and Characterization

2.3.1. Foam Preparation

Chitosan foams including adequate drug-loaded microspheres as shown in Table 2 were obtained. 4 mg of microspheres prepared under aseptic conditions as described in Section 2.1.1 were homogenously dispersed in 30 µL of a 3% chitosan solution, frozen at −20 °C and freeze-dried. Lyophilized systems were then crosslinked with 15 µL of 5% STPP, washed three times with 100 µL MilliQ water, frozen, and again freeze-dried. Afterwards, foams were stored at 4 °C until use. The porosity of the foam was calculated as described for electrospun meshes.

Table 2. Developed cross-linked chitosan foams and their correspondent final drug amount adjusted by microsphere drug loading.

Nomenclature	Loaded Molecules (Dose)	Used Microspheres
Control foam	-	Blank PLGA
BMP-2 foam	BMP-2 (600 ng)	PLGA-BMP-2
BMP-2 + ALD foam	BMP-2 (600 ng) + ALD (75 µg)	PLGA/Chitosan-BMP-2 + ALD
BMP-2 + Low MMP-10 foam	BMP-2 (600 ng) + MMP-10 (30 ng)	PLGA-BMP-2 + Low MMP-10
BMP-2 + High MMP-10 foam	BMP-2 (600 ng) + MMP-10 (120 ng)	PLGA-BMP-2 + High MMP-10

2.3.2. Foams Wettability and Degradation

Foam water uptake and weight loss was analyzed by incubation in ultrapure water at 37 °C under continuous stirring (25 rpm). At different time points samples were removed, weighted after discarding the excess water and then freeze-dried to determine their mass loss.

2.3.3. In Vitro Drug Release

Foams containing microspheres loaded with ^{125}I radiolabeled proteins or ALD were incubated in sterile MilliQ water at 37 °C and 25 rpm. The amount of the released proteins was quantified by measuring the radioactivity of the supernatant with a gamma counter (Cobra® II, Packard, Downers Gove, IL, USA) every other day. The released ALD, at the same time points, was measured using a derivatization method as previously reported [32]. Briefly, supernatants were reacted with o-pthaldialdehyde (OPA, Sigma-Aldrich) and 2-mercaptoethanol (Sigma-Aldrich). Then, the derivatization subproduct was measurement immediately using a spectrophotometer (Ultrospect 3300pro, Biochrom, Cambridge, England) (λ = 334 nm). In both cases, supernatants were removed at each time point and replaced by fresh media.

2.4. Osteoporosis Animal Model

Animal experiments were performed according to the European Union legislation on Care and Use of Animals in Experimental Procedures (2010/63/UE) and after approval by the Ethic Committee for animal care of the University of La Laguna (CEIBA 2014-0128, 5 November 2014).

The osteoporosis mice model was obtained by a surgical procedure consisting of a dorsal incision ovariectomy (OVX) under inhaled anesthesia (isofluorane, ISOFLO®, Abbott Laboratories, Valencia, Spain) on 16-week-old FVB mice. FVB mice were selected because other mice strains did not show signs of OP by densitometry. In addition, three weeks after ovariectomy, a 3 mg/kg dexamethasone 21-isonicotinate ((DEX) Deyanil Retard, Fatro Ibérica, Barcelona, Spain) was administered subcutaneously every week for three months. To confirm the development of the OP condition, bone mineral density (BMD) of the whole animal at different time points (0, 15, 30, 60 and 120 days post-OVX) was analyzed using a densitometer (PIXImus, GE Lunar, Madison, WI, USA). To perform the test, animals were anesthetized with medetomidine (1 mg/kg/IP) and ketamine (75 mg/kg/IP). To revert the

anesthesia, atipamezole (0.1 mg/kg/IP) was administrated immediately after finishing the densitometry. Animal weight and height was monitored throughout the experiment.

Additionally, histological assessments of healthy and osteoporotic mice bone tissue four months after ovariectomy were performed. Mice were euthanized and femurs were extracted, fixed in 3.7–4% p-formaldehyde (PFA, pH 7) and decalcified in Histofix® (Panreac, Barcelona, Spain). Samples were prepared for histological analysis as previously described [33].

2.5. Cell Isolation and Characterization

2.5.1. Osteoporotic and Normal mMSCs Isolation

Normal and OP murine Mesenchymal Stem Cells (mMSC or OP mMSC) were isolated from tibia and femur of 8-week-old FVB healthy and osteoporotic mice, respectively, as previously described by Soleimani and Nadri with slight modifications [34]. Mice were sacrificed by cervical dislocation and both tibias and femurs were extracted. Muscle and periosteum were dissected and isolated bones were stored in Dulbecco's phosphate-buffered saline (DPBS, Lonza, Merelbeke, Belgium) and processed for mMSC extraction. Both epiphyses were ruptured and a syringe equipped with a 20 G needle loaded with 10 mL of Dulbecco's minimal essential medium (DMEM, Lonza) supplemented with 10% fetal bovine serum (FBS, Biowest, Riverside, CA, USA), 2 mM L-glutamime (Sigma-Aldrich), and 1% penicillin-streptomycin (Sigma-Aldrich) was used to flush the bone marrow to elute mMSC. This process was repeated twice for each bone. Eluates were then collected and centrifuged at 2000 rpm for 5 min, and the resulting pellets were combined, resuspended in 15 mL of DPBS, and centrifuged again under the same conditions. The resulting pellet was resuspended in 1.5 mL of complete DMEM and cells were seeded on a petri dish and incubated at 37 °C and 5% CO_2. Cell culture media was changed every day for 72 h, then trypsinized (Trypsin-EDTA 0.25% in HBSS free of calcium, magnesium, and phenol red, Biowest) and seeded in cell culture flasks where they were allowed to grow until confluency.

2.5.2. Characterization of Isolated Cells

The obtained normal and OP mMSC were characterized in terms of surface markers expression by flow cytometry analysis. Cells were cultured until passage 3, then trypsinized and stained with calcein AM (1 µM; Sigma-Aldrich) for 30 min at room temperature. Afterwards, cells were washed three times with DPBS divided into 4 tubes and incubated with the correspondent APC-labelled primary antibody for CD45, CD44, and Sca-1 or APC-labelled isotype control (ThermoFisher Scientific) for 30 min at 4 °C. The concentration used for both control and specific antibodies was the same 10 µg/mL. Then, cells were washed three times with DPBS and stored at 4 °C until characterization. Flow cytometry was performed using the Macsquant Analyzer 10. Untreated cells were used as control.

2.6. In Vitro Biological Performance of Chitosan Foams and Electrospun Meshes

2.6.1. Evaluation of Developed Foams Osteogenic Capacity

Alkaline phosphatase activity was used to evaluate the osteogenic and mineralization effect of the drug-loaded chitosan foams described in Table 2 on normal and OP mMSC. Experiments were performed using isolated murine MSCs. Cells were trypsinized and resuspended at high density 1×10^6 cells/mL in complete media. Then, 20 µL of the cell suspension was added to the foams and incubated for 1.5 h at 37 °C and 5% CO_2 to increase cell attachment. Afterwards, 500 µL of complete medium was added to each well and media was changed every other day. After 7 and 21 days of culture, samples were collected in triplicate to evaluate osteogenic differentiation. Foams were washed twice with DPBS at 4 °C and 500 µL of the developer solution was added and incubated at 37 °C and 5% CO_2 under gentle agitation for 1.5 h. The developed solution was a solution of tetrazolium nitro blue chloride (NBT, Roche Diagnostics, Mannheim, Germany) and 5-bromo-4-chloro-3-indole phosphate (BCIP, Roche Diagnostics) prepared in 0.1 M Tris-HCl, 0.1 M NaCl,

and 0.05 M MgCl2 (pH = 9.2–9.5). After incubation, samples were washed twice with DPBS and fixed with buffered PFA. After 30 min fixation at room temperature, foams were washed twice, dehydrated, included in paraffin (Paraplast®, Barcelona, Spain) and cut with the microtome (5 µm thickness; Shandon Finesse 325, Thermo Fisher Scientific). Images of the obtained sections were taken in a microscope (Leica DM4000B, Barcelona, Spain). The percentage of cells stained positive for alkaline phosphatase activity was obtained comparing the number of positive cells against total cell numbers using an image software (ImageJ v1.52, National Institute of Health).

2.6.2. Evaluation of Cell Viability and Adhesion to Electrospun Meshes

OP mMSC viability and adhesion to the plasma-treated electrospun meshes was evaluated. Electrospun meshes were cut in disks of 8 mm diameter and placed on 48-well plates. Then, 100 µL of the cell suspension (2.5 × 105 cells/mL) was added to the meshes and incubated for 1.5 h at 37 °C and 5% CO_2 to promote cell adhesion followed by the addition of 400 µL of complete media to each well. After 24 h of seeding, cell viability was evaluated by the XTT assay (XTT Cell Viability Kit, Cell Signaling Technology, Indianapolis, IN, USA) following the manufacturer's instructions. Absorbance was measured at 445 nm using a plate reader (Biotek, Winooski, VT, USA). Cells seeded on tissue culture treated polystyrene were used as control (100% viability).

To study cell adhesion, cells were seeded and incubated for 24 h with the meshes as described above and then fixed with PFA. To evaluate cell morphology, cells were stained with rhodamine phalloidin (Invitrogen, Eugene, OR, USA) and DAPI. Samples were washed twice with DPBS and permeabilizated with 0.1% Triton X100 in DPBS for 15 min. Then, samples were washed twice again with DPBS and phalloidin solution; 1% BSA was added and then incubated at room temperature for 40 min. Afterwards, samples were washed twice with DPBS and 1 µg/mL DAPI was added and incubated for 5 min at room temperature. Finally, samples were washed twice with DPBS, mounted with Fluromount (Invitrogen) and observed under a fluorescence microscope (Leica DM4000B, Leica Microsystems, Barcelona, Spain). Images were acquired using a digital camera (Leica DFC300FX). Cells per field were counted using an image analysis software (ImageJ v1.52, National Institute of Health).

2.7. In Vivo Experiments

2.7.1. Surgical Procedure

For this study, 16-week-old FVB female mice weighing between 25–35 g were used. Mice were divided into two groups: healthy mice (non-OP group) and osteoporotic mice (OP group) as described in Supplementary Figure S1. After 4 months, both mice groups were subjected to a surgical procedure under inhalation anesthesia in which a 4 mm diameter critical bone defect was performed in the calvaria. Prior to the surgical intervention, the animal's head hair was shaved and povidone iodine was applied, a sagittal incision was made along the skull, and the skin was displaced to leave the skull exposed. Critical bone defects were made following a previously published protocol [35]. Electrospun meshes containing ALD for the BMP-2+ALD foam group (Table 3) or blank electrospun meshes for the remaining groups (Control, BMP-2 foam, BMP-2 + Low MMP-10 foam and BMP-2 + High MMP-10 foam; Table 3) were placed on the defect. Adequate foams were then placed above the meshes and the defect was closed placing another electrospun mesh with or without ALD, depending on the treatment group, on top of the foams. Finally, the wound was closed with surgical staples. Analgesia consisted of buprenorphine administered subcutaneously (0.01 mg/kg) before surgery and paracetamol (200 mg/kg) in water for 3 days after intervention. Both non-OP and OP groups were subjected to 4 different treatments (10 mice each) as shown in Table 3. An additional control group (10 mice) including control foam and blank electrospun mesh was added to the non-OP group as control of bone formation and mineralization without any drug treatment. Therefore, the experiment was performed using 90 mice: 50 non-OP and 40 OP. Two time points were

tested, 6 and 12 weeks, and 5 mice were used for each time point. Animals were euthanized by CO_2 inhalation. During all the experiments, both OP and non-OP mice were monitored for bone mass loss by densitometry (PIXImus, GE Lunar) as described in Section 2.4.

Table 3. Treatment groups for the in vivo assessment of scaffold performance. The same treatment groups were used for control mice (non-OP group) and osteoporotic mice (OP group).

	Sandwich-Like Scaffolds	
Treatment Group	**Chitosan Foam**	**Electrospun Mesh**
BMP	BMP-2 foam	Blank mesh
BMP + ALD	BMP-2 + ALD foam	ALD-mesh
BMP + MMP-L	BMP-2 + Low MMP-10 foam	Blank mesh
BMP + MMP-H	BMP-2 + High MMP-10 foam	Blank mesh

2.7.2. In Vivo Drug Release

To evaluate the in vivo protein delivery, foams loaded with radiolabeled BMP-2 (125I-BMP-2) or MMP-10 (125I-MMP-10) were used. The release rate was evaluated by measuring the amount of radiolabeled proteins remaining in the scaffold at different time points using a non-invasive method. The signal was compared with the one obtained immediately after implantation as previously described [35,36]. The radioactivity was measured using a probe-type gamma counter (Captus®, Nuclear Iberica, Ramsey, NJ, USA) coupled to a 3.2 × 2 cm collimator. Mice were immobilized and 3 measurements (27KV, 1 min) were performed. The average of the measurements carried out just after implantation was considered as the administered dose and the release percentage was obtained as the difference between the administered radioactivity and the remaining radioactivity at each time point, all of which was corrected by the tracer disintegration factor, in this case 125I (t1/2 = 60 days).

Moreover, for MMP-10 release experiments, an extra group consisting of plain MMP-10 microspheres (no foam and no mesh) was added. In this group, 7 µL of 15% Pluronic PF127 was added to ensure microspheres stay at the defect site [26].

2.7.3. Histological and Histomorphometric Evaluation

To label the mineralization front, animals were injected with oxytetracycline-HCl (40 mg/kg, IM) and calcein blue (15 mg/kg, SC) 12 and 4 days previous to euthanasia, respectively.

To assess the in vivo effects of the different treatments, histological and histomorphometric assessments of the samples were performed. After tissue fixation in 10% formalin solution (pH 7.4), undecalcified bone specimens were prepared for histological analysis as previously described [37]. The sections were stained with Goldner's trichrome to identify new bone formation, or left unstained for detection of fluorochrome labels, and analyzed by light microscopy (LEICA DM 4000B, Barcelona, Spain).

For histomorphometrical analysis, all sections per specimen were evaluated using computer-based image analysis software (Leica Q-win V3 Pro-image analysis system, Barcelona, Spain). We defined a region of interest (ROI) consisting of a circular area of 12.5 mm^2, the center of which coincided with that of the defect site. This region covered the entire defect surface and was limited by the host bone. Within this ROI, newly formed bone was distinguished from scaffold material through structure and color differences. New bone formation was expressed as a percentage of repair in relation to the total area of the defect. The distance between tetracycline and calcein blue labels was measured under ultraviolet light for the calculation of mineral appositional rate (MAR).

2.8. Statistical Analysis

Statistical analysis was performed with SPSS version 25 software. All experiments were run at least in triplicate. Differences between the treatment groups were analyzed by a one-way analysis of variance (ANOVA) with a Tukey multiple comparison post-test. For the in vivo studies, different treatments at each time point (6 weeks and 12 weeks) were compared by means of a two-way ANOVA with a Tukey multiple comparison post-test. Significance was set at $p < 0.05$. Results are expressed as mean ± SD.

3. Results

3.1. Physicochemical Performance of Developed Systems

3.1.1. Polymeric Microspheres

Polymeric microspheres were obtained by a double emulsification method using an initial aqueous internal phase of either PVA+H2O (PLGA microspheres) or PVA+Chitosan+ H2O (PLGA/Chitosan microspheres). Both types of microspheres showed similar mean diameter being 69.18 ± 1.6 µm for PLGA microspheres and 65.98 ± 0.04 µm for PLGA/ Chitosan microspheres with a single distribution peak. Microspheres' loading efficiencies were obtained using radiolabeled proteins or ALD. PLGA microspheres showed high encapsulation efficiencies for BMP-2 (70 ± 6.8%) and MMP-10 (74.05 ± 25.9%). On the other hand, the obtained alendronate encapsulation efficiency was slightly lower, 63.11 ± 11.02%.

3.1.2. Electrospun Meshes

To obtain electrospun meshes incorporating ALD, the drug was covalently linked to two different PLGAs. 1H NMR study (Supplementary Figure S2A,B) was performed to confirm the conjugation. The chemical shift (δ), expressed in ppm, gives information on the type of hydrogen generating the signal. When the lower molecular weight PLGA was used to link ALD, Resomer® RG 502, chemical shifts were observed at 1.57 (m, 321 H), 2.98 (s, 2 H), 4.54–4.98 (m, 183 H) and 5.07–5.38 (m, 91 H). On the other hand, when Resomer® RG 504 H was used as the polymer backbone for drug incorporation signals at δ 1.57 (m, 352 H), 2.97 (s, 2 H), 4.54–4.98 (m, 246 H) and 5.07–5.38 (m, 114 H) were recorded. Integrating the signals obtained from PLGA (5.25–5.16 ppm) and the alendronate signal at approximately 3 ppm, the obtained percentage of polymer functionalization was 76.3% for Resomer® RG 502 and 98.8% for Resomer® RG 504. Moreover, the percentage of RG 502-ALD and RG 504-ALD polymers over the theoretical amount on the final mesh was determined in triplicate by comparing the integrals of $Cl_2CHCHCl_2$ (used as internal standard) and the alendronate signal at 3 ppm correspondent to "a", a (R-CH2-X) proton X being the Nitrogen (N) of ALD (Figure 1). The obtained value was 89 ± 7% indicating no loss of the linked ALD during storage and electrospinning. Therefore, the ALD dose on the meshes was 7 ng per mg of electrospun mesh. On the other hand, samples soaked for 72 h in water did not show any ALD signal (Supplementary Figure S2C) indicating the release of the drug at this time point. These effects could be more related to polymer hydrolysis than to the hydrolysis of the amide group that is formed in the conjugation of ALD with the polymer.

The obtained sheets were afterwards treated with plasma to decrease the surface hydrophobicity conferred by PLGA. Indeed, blank-treated meshes showed contact angle values around 90°, the hydrophobic materials threshold, (88.2 ± 10.7) while ALD-meshes showed a slightly higher mean contact angle of 93.43 ± 8.17. However, both types of meshes presented lower contact angles than those previously reported for non-treated PLGA meshes 114.1 ± 8.3 [38].

Furthermore, the physical properties and morphology of the meshes were characterized in terms of thickness, fiber diameter, and total porosity (Figure 2). The obtained blank and ALD-electrospun fibers presented a smooth surface (Figure 2A,B) characterized by a similar microscale fiber diameter (≈1.3 µm). As expected, both systems are highly porous showing a total porosity above 80%. However, the thickness of ALD meshes was significantly higher than the one for blank meshes (Figure 2C).

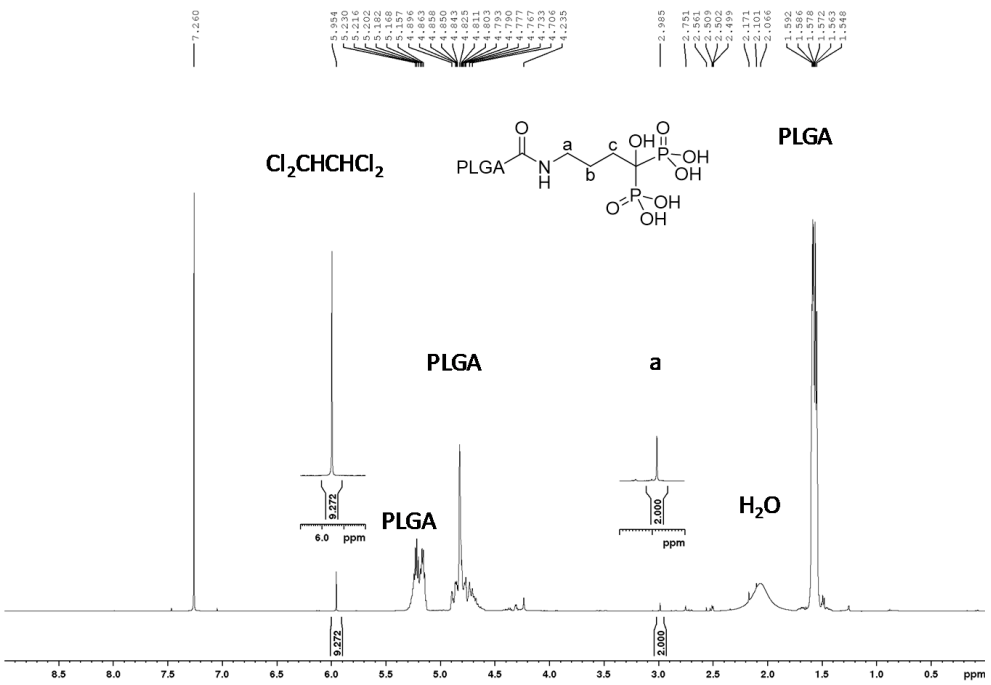

Figure 1. 1H-NMR spectrum of electrospun meshes soaked using Cl2CHCHCl2 as internal standard to quantify the amount of PLGA-ALD. The signal at 7.26 ppm corresponds to the solvent signal CHCl3.

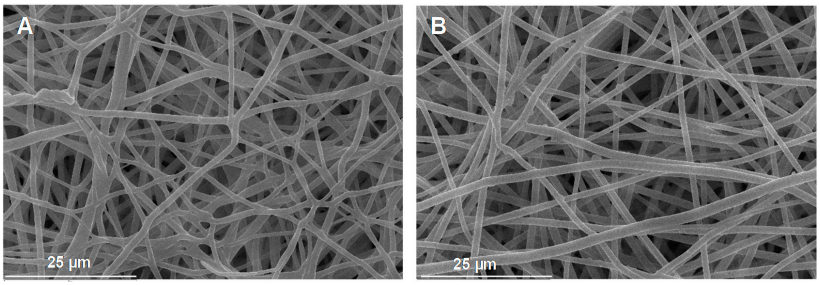

C

	Thickness (µm)	Microfiber diameter (µm)	Porosity (%)
Blank	89.79 ± 4.10	1.40 ± 0.30	82.11
ALD	103.65 ± 3.13	1.32 ± 0.28	90.92

Figure 2. Scanning electron microscopy images at 1500× magnification of: (**A**) blank meshes (without ALD) and (**B**) alendronate meshes both treated with plasma oxygen. (**C**) Thickness, microfiber diameter, and porosity of the blank and ALD linked meshes.

3.1.3. Microsphere-Loaded Chitosan Foams

Chitosan foams including adequate microspheres based on the desired scaffold composition were obtained by ionic crosslinking using a straightforward approach. The obtained foams were characterized by high porosity, 94.6 ± 1.2%, and water uptake with 366.5 ± 13.9% of swelling after 24 h (Figure 3A). Moreover, the obtained foams showed high stability with a mass loss of only 10.9 ± 5.13% after 28 days of study. Interestingly, the mass loss was stable throughout the experiment being 15.1 ± 5.7% just after 24 h.

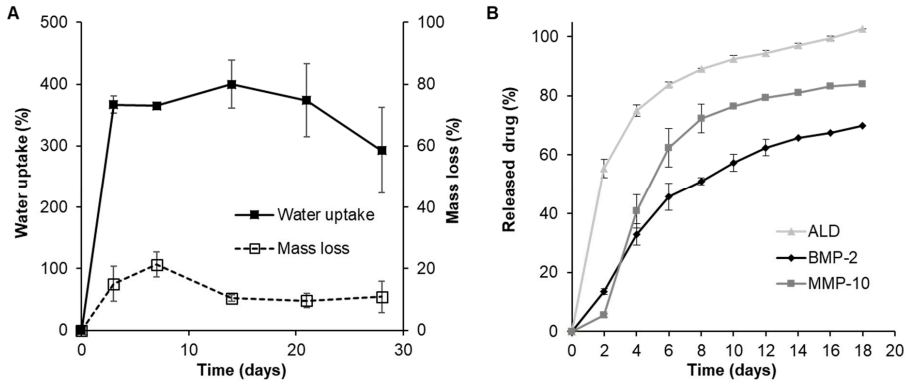

Figure 3. (**A**) Water uptake and mass loss and (**B**) drug release profiles of microsphere-loaded chitosan foams.

On the other hand, the in vitro release studies showed a diffusion-controlled release profile for both of the incorporated proteins reaching around 70% of protein release, 69.98 ± 2.62% for BMP-2 and 83.28 ± 4.21% for MMP-10, after 18 days of study (Figure 3B). However, ALD showed a more pronounced burst release with 55.41 ± 3.21% of the drug released just after two days of study followed by a sustained release rate. Despite the high burst release effect observed, the incorporation of ALD microspheres into the chitosan matrix was able to decrease the burst effect showed by plain microspheres characterized by almost all the drug released just after 2 days (94.4 ± 5.6%) (Supplementary Figure S3).

3.2. Osteoporosis Instauration

To obtain OP-like mMSC and to evaluate the in vivo scaffold performance in OP-like environments, an osteoporotic mice model was developed. Both healthy and OP mice showed normal growth. Densiometry results (Figure 4A) showed significantly lower bone mineral density values for OP-mice two weeks after ovariectomy when compared with control animals (p-value < 0.001). From then, this difference was maintained during the remaining time of the experiment. Moreover, the histomorphometric assay results confirm the OP condition (Figure 4B). Femurs from OP mice showed significantly lower cortical bone thickness, width and number of trabeculae in cancellous bone, and higher separation of trabeculae in cancellous bone.

3.3. Characterization of OP-Like mMSC and "Healthy" mMSC

Cell surface markers expression was analyzed for OP-like mMSCs and control/healthy mMSC to validate the isolation procedure selected. Flow cytometry results (Figure 5) showed the expected mMSC surface markers expression with positive expression of mMSC identifiers markers; stem cell antigen-1 (Sca-1) and CD44 and no expression (OP mMSC) or slight expression (non-OP mMSC) of hematopoietic markers (CD45).

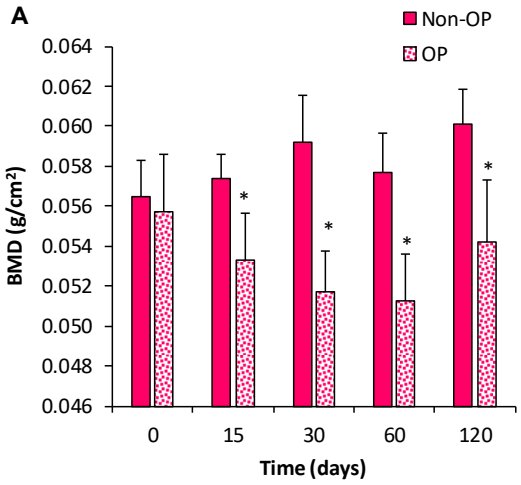

B

	Ct.Wi (µm)	Tb.Wi (µm)	Tb.Sp (µm)	Tb.N (mm)
Non-OP	171.7 ± 17.9	58.8 ± 16.7	88.3 ± 15.2	14.6 ± 3.7
OP	94.7 ± 15.7*	31.3 ± 5.4*	154.6 ± 27.2*	6.3 ± 1.6*

Figure 4. (**A**) Bone mineral density (BMD; g/cm^2) values for control and OP animals at 0, 15, 30, 60, and 120 days of ovariectomy. (**B**) Histomophometric analysis in femurs measuring cortical bone width (Ct.Wi) and, in cancellous bone, trabeculae width (Tb.Wi), trabeculae separation (Tb.Sp), and trabeculae number (Tb.N). (*) denotes statistical significance differences compared with non-OP group (control) $p < 0.001$.

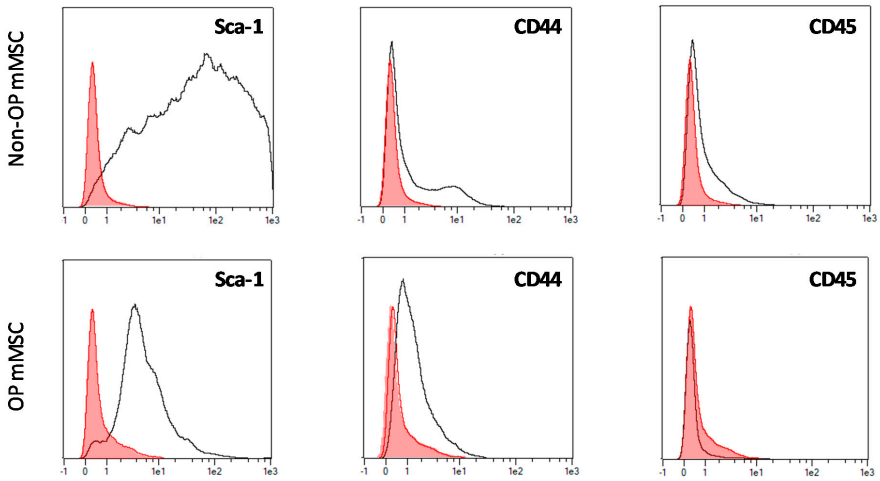

Figure 5. Cell surface markers of mouse mesenchymal stem cells extracted from healthy/control (non-OP mMSC) and osteoporotic mice (OP mMSC).

3.4. In Vitro Performance of Chitosan Foams and Electrospun Meshes

Alkaline Phosphatase (ALP) is a crucial enzyme on the biomineralization process increasing the local concentration of inorganic phosphate and a good predictor of neotissue mineralization [39]. Both non-OP and OP mMSCs were cultured on microsphere-loaded chitosan foams to analyze whether the presence of BMP-2 alone, or combined with MMP-10 or ALD, successfully promoted MSC osteogenic differentiation and mineralization in both cell populations. After 7 and 21 days, ALP activity was evaluated and foams were fixed, cut, and mounted on slides. The microscopic analysis showed the presence of positively stained cells (ALP + cells) in all the experimental groups at the two time points were analyzed. The level of ALP activity in most cells is qualitatively high as shown by the intensity of the labelling (Figure 6A,B); however, slight qualitative differences were observed between mMSC from normal mice (non-OP mMSC) and mMSC from OP mice, observing a higher labelling intensity in the first ones (Figure 6A,B).

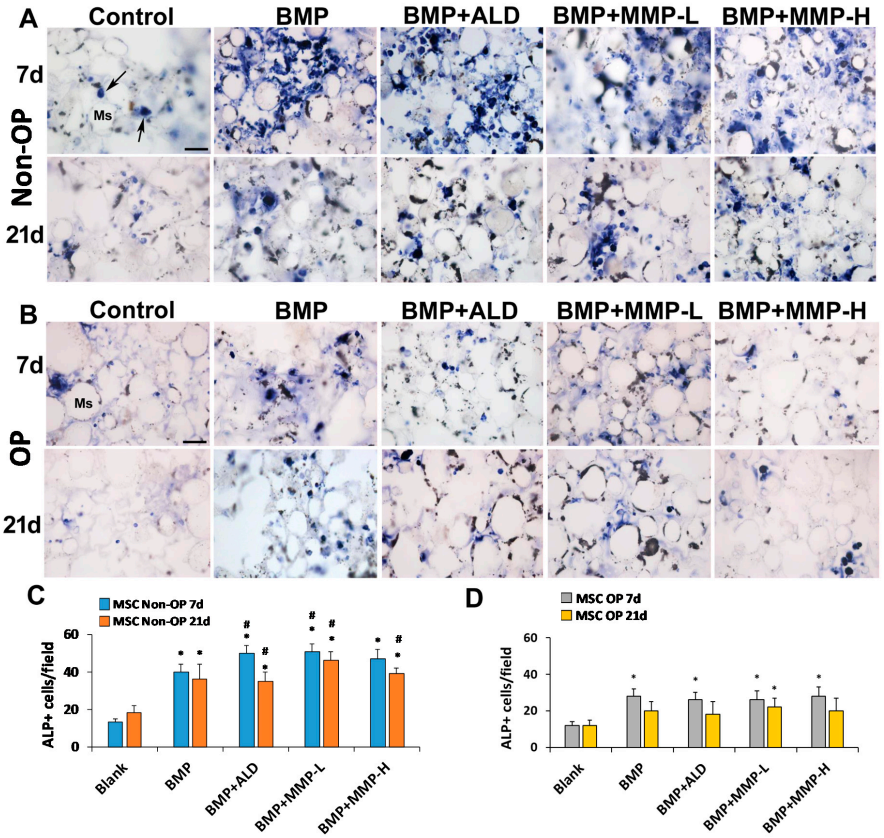

Figure 6. Panels (**A**,**B**) show representative images of mesenchymal stem cells from non-OP (**A**) and OP (**B**) animals cultured for 7 and 21 days and revealed for alkaline phosphatase activity. Histograms in (**C**,**D**) show the mean number of ALP positive cells per field at 400× magnification in non-OP and OP animals, respectively. The arrows in the upper left image indicate ALP-positive cells. Histograms represent mean ±SD values. (*) denotes statistical significant differences compared with control treatment at the corresponding time point. (#) denotes statistical significant differences compared with BMP treatment at the corresponding time point. Ms: microspheres. Scale bar = 30 μm.

Quantification showed a significant increase in the number of non-OP mMSC ALP + cells at 7 days of culture in all the treated groups with respect to the control group, which was highest when cells were cultured on chitosan foams combining BMP-2 and ALD and BMP-2 and MMP-10 at low amounts (Figure 6C). In fact, cells grown on these foams showed significantly higher ALP activity than those cultured on systems including BMP-2 alone. The same trend was observed after 21 days of culture where drug-loaded foams showed significantly higher number of ALP + cells than blank foams. Moreover, the combination of BMP-2 with ALD or MMP-10 on the foams led to an increased ALP activity when compared with the addition of BMP-2 alone.

On the other hand, this beneficial effect of the mixture of BMP-2 and ALD or MMP-10 was not observed on OP mMSC ALP activity (Figure 6D). In these circumstances, the incorporation of BMP-2 to chitosan foams successfully increased the number of ALP + cells after 7 days of culture but no additional effect was observed by its combination with ALD or MMP-10. Moreover, after 21 days of culture, only the treatment combining BMP-2 and low dose of MMP-10 presented a significantly higher number of ALP+ cells compared with control foams. In general, foams seeded with OP mMSC, at 7 and 21 days post-seeding, showed a lower number of ALP+ cells per field than those seeded with non-OP mMSC. Therefore, a clear difference in mineralization potential can be observed between the control and OP mMSC.

Moreover, OP mMSC were cultured on electrospun PLGA meshes containing ALD or not. Cell viability and attachment were evaluated to analyze the effect of ALD presence on cell behavior. Interestingly, the presence of ALD on the meshes significantly improved cell viability (Figure 7A). Fluorescence images confirmed this trend (Figure 7B,C), showing a higher number of attached cells on ALD-linked electrospun meshes.

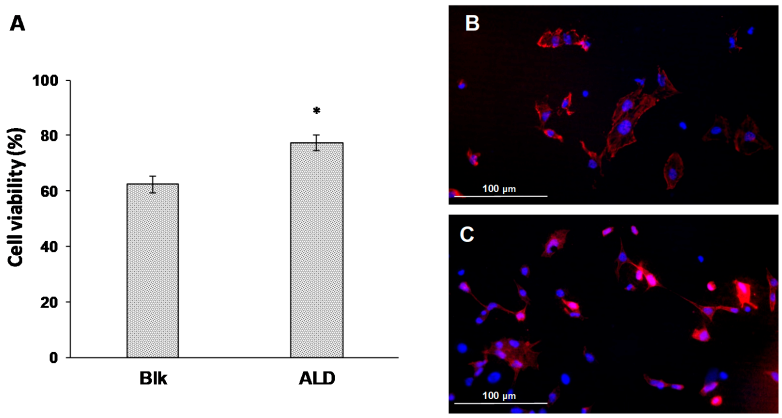

Figure 7. (**A**) Cell viability relative to control (polystyrene plate) of OP mMSC cultured on plasma-treated electrospun meshes containing covalently linked ALD or not and cell morphology of OP mMSC cultured on (**B**) ALD-linked electrospun meshes or (**C**) blk electrospun meshes. Blank (blk) stands for meshes without ALD. (*) denotes statistical significance differences compared with non-OP group (control) $p < 0.001$.

3.5. In Vivo Evaluation of Sandwich-Like Scaffolds

3.5.1. In Vivo Protein Drug Release

The in vivo release of BMP-2 and MMP-10 incorporated in chitosan scaffolds showed similar profiles to those observed in vitro but with a slight increase on the burst effect (Figure 8). The amount of protein released after 24 h of implantation represented the 22.32 ± 2.68% of the dose for BMP-2 and 25.51 ± 2.22% of the dose for MMP-10. The release rate of both proteins fit the Higuchi model, characteristic of release processes

controlled by diffusion also explained by the high chitosan foam stability previously observed. The Higuchi constant (KH) was 13.05 for BMP-2 release (R^2 = 0.99) and 11.31 for MMP-10 (R^2 = 0.97). Therefore, the complete dose of BMP-2 and MMP-10 would be released after 8 weeks and 11 weeks, respectively, indicating the achievement of a stable prolonged release.

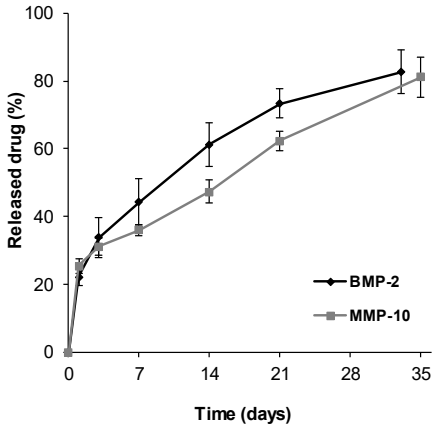

Figure 8. In vivo BMP-2 and MMP-10 release at different time points after implantation of the developed scaffolds on control animals. Release profiles were obtained using radiolabeled BMP-2 and MMP-10.

3.5.2. In Vivo Bone Formation Induced by Sandwich-Like Scaffold Containing BMP-2 Alone or Combined with ALD or MMP-10

The ability of the developed sandwich-like scaffolds to promote new bone formation and tissue mineralization was evaluated on a critical size calvarial bone defect on both normal (non-OP) and OP animals. When scaffolds were implanted on control "healthy animals" a high proportion of connective tissue surrounding the scaffold and low new bone formation restricted to the margins of the defect was observed for all experimental groups (Figure 9A). Twelve weeks post-implantation, a significant increase in the repair response was observed with newly formed bone at the margins of the defect and isolated ossification foci within it (Figure 9). The histomorphometric analysis showed significantly higher repair percentages for all the treatments compared with control scaffolds (data not shown) except for the combination of BMP-2 and MMP-10 with a high dose of the MMP. Both BMP and BMP + ALD treatments showed similar percentages of repair at both 6 weeks (≈30%) and 12 weeks (≈50%) post-implantation. Conversely, the combination of BMP+MMP at the two concentrations tested led to a significant decrease in the percentage of repair at both time points when compared with both BMP and BMP +ALD. The combination of 120 ng MMP-10 and BMP-2 was only able to achieve 27% of bone repair after 12 weeks of implantation (Figure 9C).

The mineralization rate, determined by the mineralization fronts marked with calcein blue and oxytetracycline, revealed significantly lower mineral apposition rates (MAR) at six weeks post-implantation than at twelve weeks for all the experimental groups (Figure 9D). Contrary to the results in bone repair, the combination of BMP-2 and MMP-10 led to a significant increase in mineral apposition rates compared with BMP-2 alone. In fact, when the higher dose of MMP-10 was used, 120 ng, the mineral apposition rate was significantly higher to that observed for both BMP and BMP + ALD treatment groups.

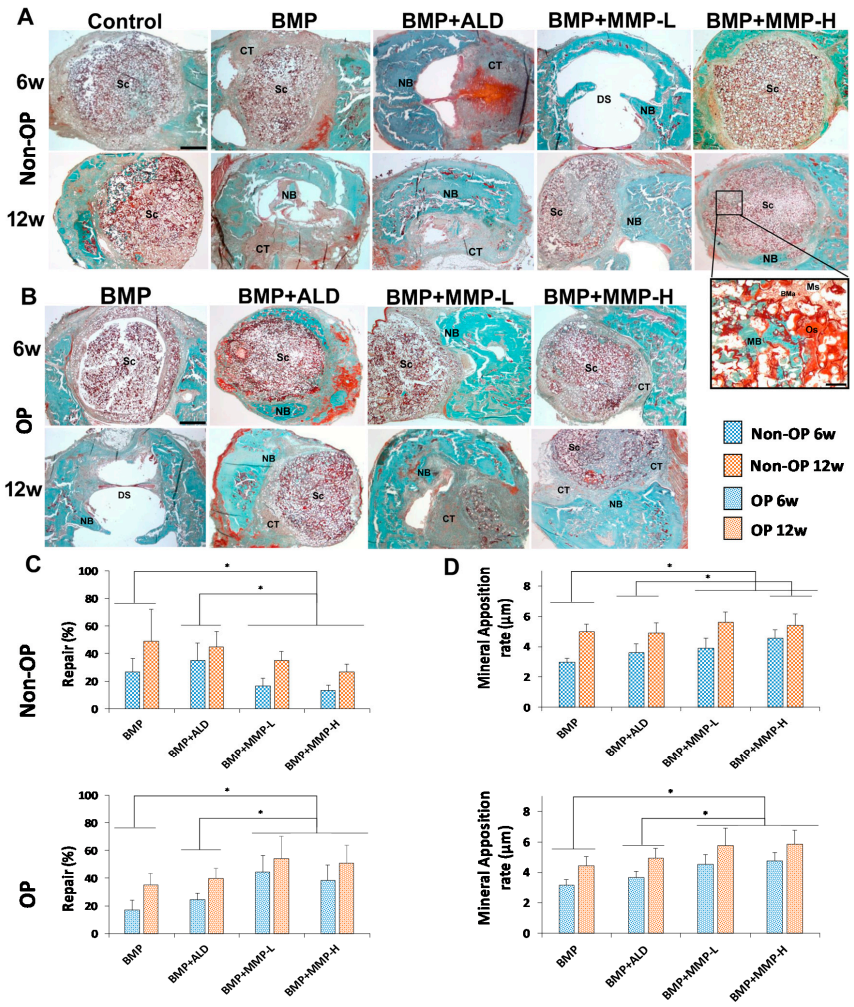

Figure 9. Representative panoramic images of the bone defect in the different experimental groups of non-OP (**A**) and OP (**B**) animals, showing the reparative response at 6 and 12 weeks post-implantation. Insert: Detail corresponding to the BMP + MMP-H group that shows active bone neoformation in the peripheral area of the scaffold (**C**,**D**). Histomorphometric analysis showing the percent of repair (**C**) and the mineral apposition rate (MAR) (**D**), six (blue) and twelve (orange) weeks post-implantation, in the different experimental groups of non-OP (squares) and OP (points) animals. Histograms represent mean ±SD values. The identical letter/symbol on different bars indicates significant differences. BMa: Bone marrow, CT: connective tissue, DS: defect site, MB: mineral bone, Ms: microspheres, NB: new bone, Os: osteoid, Sc: scaffold. Scale bars: A and B: 1 mm, inset: 80 µm. (*) denotes statistical significance differences between groups.

Scaffold's performance was also evaluated on the developed OP mice model. In osteoporotic animals the relative proportion of connective tissue in the area of the defect was similar to that observed in normal animals (Figure 9B). Following the same trend as for control animals, the obtained percentage of repair and mineral apposition rates were significantly higher at the last time point studied (12 weeks) than at 6 weeks post-

implantation (Figure 9C,D). At this point of analysis, new bone formation was observed not only in the margins but also in larger areas of the defect. However, a shift in the MMP-10 effect on tissue repair in OP animals was clearly observed when compared with control non-OP animals. In diseased animals, the combination of BMP-2 and MMP-10 at either of the doses selected promoted a significant increase in tissue repair compared with BMP-2 alone and BMP + ALD (Figure 9C). The highest percentages of repair were observed on mice implanted with BMP + MMP-L with a value of 44% after 6 weeks of implantation and 54% after 12 weeks of implantation. On the other hand, the lowest percentages of repair were obtained with scaffolds containing plain BMP showing values of 17% after six weeks of implantation and 35% after 12 weeks.

In this case, the results of mineral apposition rate match the results mentioned above for tissue repair (Figure 9D). The combination of BMP-2 and MMP-10 at either of the doses selected promoted a significant increase in the mineral apposition rate compared with the use of scaffolds including BMP-2 alone or combined with ALD.

4. Discussion

The development of biomaterials designed for bone regeneration has been one of the main objectives in the tissue engineering field for the last decades. The strategy of these scaffolds has been mostly centered on fulfilling requirements related to scaffold mechanical performance and stem cell osteogenic induction capacities recognized as crucial to ensure the recovery of the bone function. However, not only should the characteristics of the scaffold be considered but the quality of the regenerated bone should also be taken into account, especially when scaffolds are used in pathologies characterized by an impaired bone quality. Increased bone mineral content and improved microarchitecture is directly correlated with enhanced mechanical properties and is desirable for osteoporosis treatments [40]. In this study we propose to use already well-known biocompatible and biodegradable raw materials to develop sandwich-like scaffolds designed to obtain better bone quality, increasing the mechanical resistance of bone. To do so, scaffolds were doped with BMP-2 alone, with known osteogenic induction capacities, or with combinations of BMP-2 and an antiresorptive drug (ALD), or BMP-2 and metalloprotease 10 (MMP-10), at different doses.

To achieve a desirable growth factor and ALD or MMP-10 controlled release while avoiding the risk of undesirable side effects derived from high concentrations, therapeutic molecules were included on PLGA microspheres. The developed microspheres were characterized by high encapsulation efficiencies of over 60% in all cases, being even 10% higher for BMP-2 and MMP-10. The addition of chitosan in the internal phase during the synthesis of ALD-loaded PLGA microspheres aimed at increasing their drug encapsulation capacity which is a challenge due to the high aqueous solubility of the drug. Indeed, the developed microspheres presented a five-fold increase in ALD encapsulation efficiency compared with previously reported ALD-loaded PLGA microspheres prepared following a similar double emulsification method [41]. Moreover, other reports already reported lower ALD encapsulation efficiencies using a double emulsification method with levels as low as 0.2% [42].

Microspheres were then incorporated into chitosan networks serving as molds to obtain cross-linked foams with high water uptake capacity, porosity, and remarkable stability. Chitosan is a natural polymer widely used for bone tissue engineering applications due to its several advantages as easy chemical modification and high biocompatibility [43]. Plain chitosan foams have been previously tested as substrates for osteoblasts attachment indicating adequate performance [44,45]. However, chitosan is commonly combined with either ceramics and/or other polymers to improve mechanical performance and confer osteoinductive capabilities [46]. The strategy used on this study proposes to include microspheres loaded with BMP-2 and MMP-10 or ALD into chitosan foams serving as a therapeutic molecules' reservoir and conferring osteoinductive capabilities to the developed systems. In agreement with our hypothesis, the incorporation of the microspheres

to chitosan foams led to a controlled release of the therapeutic molecules both in vitro and in vivo characterized by a diffusion-controlled profile. Moreover, the incorporation of PLGA microspheres to chitosan foams could improve the mechanical performance of the systems.

The ability of the incorporated therapeutic molecules to confer osteoinductive capabilities to the developed foams was evaluated by their culture with MSC from "healthy" and OP animals and then the alkaline phosphatase activity was analyzed. The testing of scaffold performance using both cell populations is justified by the known alterations in OP MSC [47]. Cell populations were characterized by flow cytometry showing different profiles for Sca-1 and CD44 expression. Sca-1-deficient mice were previously reported to undergo osteoporosis and are characterized by a decreased self-renewal of osteogenic stem cells [48–50]. In fact, the administration of Sca-1 + sorted MSC to osteoporotic animals was able to improve bone mineral density [51]. On the other hand, similarly to Sca-1, CD44 seemed to be decreased in OP mMSC. The absence of this cell surface hyaluronan receptor has been correlated to increased osteoclastogenesis and bone loss under inflammatory environments in mice [52]. Moreover, CD44 has been described as crucial for MSC migration, a cell function reported to be decreased in OP mMSC [53,54]. Altogether, the modified positive expression of Sca-1 and CD44 observed for OP mMSC (Figure 5) could be associated to the disease instauration and the associated lower MSC migration, proliferation, and differentiation capacity [47,54]. Indeed, OP mMSC showed a lower number of ALP+ cells than non-OP mMSC for all the evaluated treatments at both of the time points selected. Analyzing the response of both cell populations to BMP-2 alone or combined with the other therapeutic molecules, clear differences were pointed out. The addition of BMP-2 significantly increased the number of ALP+ cells for both populations, but while the combination of BMP-2 + ALD and BMP-2 + MMP-10 at low dose produced an even higher number of ALP + cells for non-OP cells, no effect was observed for OP mMSC. The ability of MMP-10 to increase the number of ALP + cells under an osteogenic environment was previously described in vitro on aortic valve interstitial cells [25]. This effect has been hypothesized to be mediated mainly by the PI3K/AKT cell signaling pathway, a critical signaling pathway involved in OP [55]. This fact could explain the differences in cell response to MMP-10. On the other hand, in agreement with our findings for non-OP mMSC, ALD was previously reported to promote osteogenesis and an enhancement in ALP expression on human MSC [56].

A new strategy was used to load PLGA electrospun meshes with ALD. In this case, the drug was efficiently conjugated to different PLGA polymer chains. Thus, the obtained meshes presented a drug content directly controlled by the quantity of functionalized polymers used for electrospinning and not affected by storage. Plasma-treated electrospun meshes presented high porosity, microscale fiber diameter and, therefore, a high surface-area-to-volume ratio, which are adequate characteristics to resemble the natural extracellular matrix [57]. Indeed, osteoporotic-like cells seeded on the developed meshes showed good attachment improved by the presence of ALD on their surface. These differences could be attributed to the acid character of un-functionalized electrospun meshes due to the carboxylic acid terminal group of non-modified PLGA.

To obtain suitable scaffolds for bone regeneration, the developed chitosan foams were surrounded by two electrospun meshes generating a 3D sandwich-like scaffold. To the best of our knowledge, no previous work has been devoted to combine BMP-2 and MMP-10 on microspheres embedded in a scaffold for the regeneration of critical size bone defects in OP animals. Furthermore, the results of this combination were compared with scaffolds containing BMP-2 alone or BMP-2 + ALD. In our previous work, microspheres loaded with BMP-2 and MMP-10 were dispersed in a hydrogel and implanted on a critical size bone defect [26]. The regenerative effect of the hydrogels was evaluated after 4 and 8 weeks of implantation and the ratios tested for BMP-2: MMP-10 were 20:1 and 200:1. The obtained results suggested a higher percentage of bone repair and mineralization apposition rates for the higher MMP-10 dose (20:1; 30 ng MMP-10) after 4 weeks of implantation [26].

As described above, bone formation is impaired in OP. Moreover, our previous results revealed that a slow release rate of BMP-2 can be beneficial for bone regeneration promotion in OP animals. Furthermore, the development of solid scaffolds able to remain longer on the defect site leads to better bone repair [58]. Therefore, in the present study, scaffolds were designed to persist in the defect site for a long time and to slowly release the therapeutic molecules. In fact, the presence of the scaffolds on the defect area was evident at both six and twelve weeks of implantation. Likewise, a complete infiltration of the scaffold by connective tissue was observed, with the presence of cells both between the microspheres and inside them. However, this long-term stability of the scaffolds had a negative effect on non-OP animals, hindering the rapid regeneration observed on these animals and leading to lower regeneration percentages to those previously reported for BMP-2 + MMP-10 [26]. This fact could also explain the in vivo lack of positive response in percentage of repair for the BMP+MMP and BMP+ALD treatments compared with plain BMP-2, despite the beneficial effects in ALP activity observed for these treatments in vitro. Moreover, the dose-dependent negative effect of MMP-10 addition on the regenerative response could be attributed to a catabolic effect aimed to degrade the scaffold. Despite the decrease observed in tissue repair, the mineralization rate for BMP+MMP treatments was significantly higher than BMP-2, confirming the positive effect of MMP-10 addition on bone mineralization.

The results obtained suggested the designed sandwich-like scaffolds are a closer match for the bone tissue repair requirements in OP animals. In these animals, the combination of BMP-2 and MMP-10 induced a regenerative effect and an improved mineral apposition rate when compared with scaffolds containing BMP-2 alone or BMP-2 + ALD. These observations suggested the requirements to achieve a good bone regeneration in the osteoporotic population are different than those in healthy animals. Therefore, for bone regeneration it is clear that there are three factors that must be controlled as well as their interactions to achieve the desired effect: (1) the activity of the bone tissue to be repaired; (2) the time the scaffold stays in the defect or, in other words, the rate of scaffold degradation and; (3) the release rate and dose of the active substances as well as their combinations. Future work is necessary to improve the understanding of the underlying interactions between these three factors to exploit them and guide the development of novel therapeutic strategies for bone regeneration.

5. Conclusions

Sandwich-like scaffolds were obtained combining PLGA electrospun meshes and drug-loaded chitosan foams. Therapeutic molecules were efficiently loaded and released from microspheres embedded on the chitosan network acting in vivo and in vitro as therapeutic molecule reservoirs for the developed scaffolds. This versatile strategy for scaffold development allowed testing of the effect of BMP-2 and BMP-2 + MMP-10 or BMP-2 + ALD on osteogenic induction and bone regeneration. The obtained results point out the crucial role of the bone tissue repair activity on the treatment's success. The designed BMP-2 + MMP-10 combinations showed the desired effect of tissue repair promotion on OP animals, but the opposite effect was observed on control animals. Therefore, the development of adequate scaffolds for bone regeneration require consideration of the tissue catabolic/anabolic balance to obtain biomaterials with a degradation/release behavior suited for the existing tissue status.

Supplementary Materials: The following are available online at https://www.mdpi.com/article/10.3390/pharmaceutics13070979/s1, Figure S1, In vivo experiments timeline for osteoporotic model evaluation by bone mineral density (BMD) measurements and the assessment of scaffold performance; Figure S2, ^{1}H-NMR spectrum; Figure S3, In vitro drug release profiles of ALD from microsphere-loaded chitosan foams (ALD foam) and plain microspheres (ALD microspheres).

Author Contributions: P.G.-G.: conceptualization, methodology, investigation, writing—original draft. R.R.: methodology, investigation, writing—original draft. J.A.R.: methodology, resources, writing—original draft. T.M.: methodology, investigation, writing—original draft. C.E.: conceptual-

ization, visualization, writing—review and editing, funding acquisition. P.D.-R.: conceptualization, investigation, writing—original draft, writing—review and editing. A.D.: conceptualization, writing—review and editing, project administration, funding acquisition. All authors have read and agreed to the published version of the manuscript.

Funding: This work was supported by the FEDER/Ministerio de Ciencia e Innovación—Agencia Estatal de Investigación MAT201455657-R and by the Spanish Ministry of Science, Innovation and Universities (MICINN), State Research Agency (AEI) and the European Regional Development Funds (ERDF) (PGC2018-094503-B-C21). Patricia García-García acknowledges University of La Laguna for her fellowship grant (M-ULL).

Institutional Review Board Statement: Animal experiments were performed according to the European Union legislation on Care and Use of Animals in Experimental Procedures (2010/63/UE) and after approval by the Ethic Committee for animal care of the University of La Laguna (CEIBA2014-0128).

Informed Consent Statement: Not applicable.

Conflicts of Interest: The authors declare no conflict of interest.

References

1. Michalski, M.N.; McCauley, L.K. Macrophages and skeletal health. *Pharmacol. Ther.* **2017**, *174*, 43–54. [CrossRef] [PubMed]
2. Russow, G.; Jahn, D.; Appelt, J.; Märdian, S.; Tsitsilonis, S.; Keller, J. Anabolic Therapies in Osteoporosis and Bone Regeneration. *Int. J. Mol. Sci.* **2018**, *20*, 83. [CrossRef] [PubMed]
3. Quinlan, E.; Thompson, E.M.; Matsiko, A.; O'Brien, F.J.; López-Noriega, A. Long-term controlled delivery of rhBMP-2 from collagen-hydroxyapatite scaffolds for superior bone tissue regeneration. *J. Control. Release* **2015**, *207*, 112–119. [CrossRef] [PubMed]
4. Lyritis, G.P.; Georgoulas, T.; Zafeiris, C.P. Bone anabolic versus bone anticatabolic treatment of postmenopausal osteoporosis. *Ann. N. Y. Acad. Sci.* **2010**, *1205*, 277–283. [CrossRef] [PubMed]
5. Segredo-Morales, E.; García-García, P.; Reyes, R.; Pérez-Herrero, E.; Delgado, A.; Évora, C. Bone regeneration in osteoporosis by delivery BMP-2 and PRGF from tetronic–alginate composite thermogel. *Int. J. Pharm.* **2018**, *543*, 160–168. [CrossRef]
6. Segredo-Morales, E.; Reyes, R.; Arnau, M.R.; Delgado, A.; Évora, C. In situ gel-forming system for dual BMP-2 and 17β-estradiol controlled release for bone regeneration in osteoporotic rats. *Drug Deliv. Transl. Res.* **2018**, *8*, 1103–1113. [CrossRef]
7. García, P.; Reyes, R.; Segredo-Morales, E.; Pérez-Herrero, E.; Delgado, A.; Évora, C. PLGA-BMP-2 and PLA-17β-Estradiol Microspheres Reinforcing a Composite Hydrogel for Bone Regeneration in Osteoporosis. *Pharmaceutics* **2019**, *11*, 648. [CrossRef]
8. Hur, W.; Park, M.; Lee, J.Y.; Kim, M.H.; Lee, S.H.; Park, C.G.; Kim, S.N.; Min, H.S.; Min, H.J.; Chai, J.H.; et al. Bioabsorbable bone plates enabled with local, sustained delivery of alendronate for bone regeneration. *J. Control. Release Off. J. Control. Release Soc.* **2016**, *222*, 97–106. [CrossRef]
9. Kim, S.E.; Yun, Y.P.; Shim, K.S.; Kim, H.J.; Park, K.; Song, H.R. 3D printed alendronate-releasing poly (caprolactone) porous scaffolds enhance osteogenic differentiation and bone formation in rat tibial defects. *Biomed. Mater.* **2016**, *11*, 055005. [CrossRef]
10. Mardas, N.; Busetti, J.; de Figueiredo, J.A.; Mezzomo, L.A.; Scarparo, R.K.; Donos, N. Guided bone regeneration in osteoporotic conditions following treatment with zoledronic acid. *Clin. Oral Implant. Res.* **2017**, *28*, 362–371. [CrossRef]
11. van Houdt, C.I.A.; Gabbai-Armelin, P.R.; Lopez-Perez, P.M.; Ulrich, D.J.O.; Jansen, J.A.; Renno, A.C.M.; van den Beucken, J. Alendronate release from calcium phosphate cement for bone regeneration in osteoporotic conditions. *Sci. Rep.* **2018**, *8*, 15398. [CrossRef]
12. Wang, X.; Zeng, D.; Weng, W.; Huang, Q.; Zhang, X.; Wen, J.; Wu, J.; Jiang, X. Alendronate delivery on amino modified mesoporous bioactive glass scaffolds to enhance bone regeneration in osteoporosis rats. *Artif. Cells Nanomed. Biotechnol.* **2018**, *46*, 171–181. [CrossRef]
13. Toker, H.; Ozdemir, H.; Ozer, H.; Eren, K. A comparative evaluation of the systemic and local alendronate treatment in synthetic bone graft: A histologic and histomorphometric study in a rat calvarial defect model. *Oral Surg. Oral Med. Oral Pathol. Oral Radiol.* **2012**, *114*, S146–S152. [CrossRef]
14. Huntley, R.; Jensen, E.; Gopalakrishnan, R.; Mansky, K.C. Bone morphogenetic proteins: Their role in regulating osteoclast differentiation. *Bone Rep.* **2019**, *10*, 100207. [CrossRef] [PubMed]
15. Little, D.G.; McDonald, M.; Bransford, R.; Godfrey, C.B.; Amanat, N. Manipulation of the anabolic and catabolic responses with OP-1 and zoledronic acid in a rat critical defect model. *J. Bone Miner. Res. Off. J. Am. Soc. Bone Mineral. Res.* **2005**, *20*, 2044–2052. [CrossRef] [PubMed]
16. Raina, D.B.; Larsson, D.; Mrkonjic, F.; Isaksson, H.; Kumar, A.; Lidgren, L.; Tägil, M. Gelatin-hydroxyapatite-calcium sulphate based biomaterial for long term sustained delivery of bone morphogenic protein-2 and zoledronic acid for increased bone formation: In-Vitro and In-Vivo carrier properties. *J. Control. Release Off. J. Control. Release Soc.* **2018**, *272*, 83–96. [CrossRef] [PubMed]
17. Lee, J.H.; Baek, H.R.; Lee, K.M.; Zheng, G.B.; Shin, S.J.; Jin, Y.Z. The inhibitory effect of zoledronate on early-stage osteoinduction by recombinant human bone morphogenetic protein 2 in an osteoporosis model. *Growth Factors* **2015**, *33*, 220–228. [CrossRef]

18. Mathavan, N.; Tägil, M.; Isaksson, H. Do osteoporotic fractures constitute a greater recalcitrant challenge for skeletal regeneration? Investigating the efficacy of BMP-7 and zoledronate treatment of diaphyseal fractures in an open fracture osteoporotic rat model. *Osteoporos Int.* **2017**, *28*, 697–707. [CrossRef] [PubMed]
19. Colnot, C.; Thompson, Z.; Miclau, T.; Werb, Z.; Helms, J.A. Altered fracture repair in the absence of MMP9. *Development* **2003**, *130*, 4123–4133. [CrossRef]
20. Kosaki, N.; Takaishi, H.; Kamekura, S.; Kimura, T.; Okada, Y.; Minqi, L.; Amizuka, N.; Chung, U.-I.; Nakamura, K.; Kawaguchi, H.; et al. Impaired bone fracture healing in matrix metalloproteinase-13 deficient mice. *Biochem. Biophys. Res. Commun.* **2007**, *354*, 846–851. [CrossRef]
21. Stickens, D.; Behonick, D.J.; Ortega, N.; Heyer, B.; Hartenstein, B.; Yu, Y.; Fosang, A.J.; Schorpp-Kistner, M.; Angel, P.; Werb, Z. Altered endochondral bone development in matrix metalloproteinase 13-deficient mice. *Development* **2004**, *131*, 5883. [CrossRef]
22. Lieu, S.; Hansen, E.; Dedini, R.; Behonick, D.; Werb, Z.; Miclau, T.; Marcucio, R.; Colnot, C. Impaired remodeling phase of fracture repair in the absence of matrix metalloproteinase-2. *Dis. Model. Mech.* **2011**, *4*, 203–211. [CrossRef]
23. Bord, S.; Horner, A.; Hembry, R.M.; Compston, J.E. Stromelysin-1 (MMP-3) and stromelysin-2 (MMP-10) expression in developing human bone: Potential roles in skeletal development. *Bone* **1998**, *23*, 7–12. [CrossRef]
24. Mao, L.; Yano, M.; Kawao, N.; Tamura, Y.; Okada, K.; Kaji, H. Role of matrix metalloproteinase-10 in the BMP-2 inducing osteoblastic differentiation. *Endocr. J.* **2013**, *60*, 1309–1319. [CrossRef]
25. Matilla, L.; Roncal, C.; Ibarrola, J.; Arrieta, V.; Garciá-Penã, A.; Fernández-Celis, A.; Navarro, A.; Álvarez, V.; Gainza, A.; Orbe, J.; et al. A Role for MMP-10 (Matrix Metalloproteinase-10) in Calcific Aortic Valve Stenosis. *Arterioscler. Thromb. Vasc. Biol.* **2020**, *4*, 1370–1382. [CrossRef]
26. Reyes, R.; Rodríguez, J.A.; Orbe, J.; Arnau, M.R.; Évora, C.; Delgado, A. Combined sustained release of BMP2 and MMP10 accelerates bone formation and mineralization of calvaria critical size defect in mice. *Drug Deliv.* **2018**, *25*, 750–756. [CrossRef] [PubMed]
27. Orbe, J.; Barrenetxe, J.; Rodriguez, J.A.; Vivien, D.; Orset, C.; Parks, W.C.; Birkland, T.P.; Serrano, R.; Purroy, A.; Martinez de Lizarrondo, S.; et al. Matrix metalloproteinase-10 effectively reduces infarct size in experimental stroke by enhancing fibrinolysis via a thrombin-activatable fibrinolysis inhibitor-mediated mechanism. *Circulation* **2011**, *124*, 2909–2919. [CrossRef] [PubMed]
28. Fraker, P.J.; Speck, J.C., Jr. Protein and cell membrane iodinations with a sparingly soluble chloroamide, 1,3,4,6-tetrachloro-3a,6a-diphrenylglycoluril. *Biochem. Biophys. Res. Commun.* **1978**, *80*, 849–857. [CrossRef]
29. Del Rosario, C.; Rodríguez-Évora, M.; Reyes, R.; Simões, S.; Concheiro, A.; Évora, C.; Alvarez-Lorenzo, C.; Delgado, A. Bone critical defect repair with poloxamine-cyclodextrin supramolecular gels. *Int. J. Pharm.* **2015**, *495*, 463–473. [CrossRef] [PubMed]
30. Gundogdu, E.; Ekinci, M.; Ozgenc, E.; Ozdemir, D.I.; Asikoglu, M. Development and Evaluation of Liquid and Solid Lipid Based Drug Delivery Systems Containing Technetium-99m-Radiolabeled Alendronate Sodium. *Curr. Radiopharm.* **2018**, *11*, 100–108. [CrossRef] [PubMed]
31. De la Riva, B.; Nowak, C.; Sánchez, E.; Hernández, A.; Schulz-Siegmund, M.; Pec, M.K.; Delgado, A.; Evora, C. VEGF-controlled release within a bone defect from alginate/chitosan/PLA-H scaffolds. *Eur. J. Pharm Biopharm.* **2009**, *73*, 50–58. [CrossRef] [PubMed]
32. Dolci, L.S.; Panzavolta, S.; Torricelli, P.; Albertini, B.; Sicuro, L.; Fini, M.; Bigi, A.; Passerini, N. Modulation of Alendronate release from a calcium phosphate bone cement: An in vitro osteoblast-osteoclast co-culture study. *Int. J. Pharm.* **2019**, *554*, 245–255. [CrossRef]
33. Hernández, A.; Sánchez, E.; Soriano, I.; Reyes, R.; Delgado, A.; Évora, C. Material-related effects of BMP-2 delivery systems on bone regeneration. *Acta Biomater.* **2012**, *8*, 781–791. [CrossRef]
34. Soleimani, M.; Nadri, S. A protocol for isolation and culture of mesenchymal stem cells from mouse bone marrow. *Nat. Protoc.* **2009**, *4*, 102–106. [CrossRef]
35. Rodríguez-Évora, M.; Delgado, A.; Reyes, R.; Hernández-Daranas, A.; Soriano, I.; San Román, J.; Évora, C. Osteogenic effect of local, long versus short term BMP-2 delivery from a novel SPU–PLGA–βTCP concentric system in a critical size defect in rats. *Eur. J. Pharm. Sci.* **2013**, *49*, 873–884. [CrossRef]
36. Del Rosario, C.; Rodríguez-Évora, M.; Reyes, R.; Delgado, A.; Évora, C. BMP-2, PDGF-BB, and bone marrow mesenchymal cells in a macroporous β-TCP scaffold for critical-size bone defect repair in rats. *Biomed. Mater.* **2015**, *10*, 045008. [CrossRef]
37. De la Riva, B.; Sánchez, E.; Hernández, A.; Reyes, R.; Tamimi, F.; López-Cabarcos, E.; Delgado, A.; Evora, C. Local controlled release of VEGF and PDGF from a combined brushite-chitosan system enhances bone regeneration. *J. Control. Release Off. J. Control. Release* **2010**, *143*, 45–52. [CrossRef]
38. Rodríguez-Évora, M.; García-Pizarro, E.; del Rosario, C.; Pérez-López, J.; Reyes, R.; Delgado, A.; Rodríguez-Rey, J.C.; Évora, C. Smurf1 knocked-down, mesenchymal stem cells and BMP-2 in an electrospun system for bone regeneration. *Biomacromolecules* **2014**, *15*, 1311–1322. [CrossRef]
39. Golub, E.E.; Boesze-Battaglia, K. The role of alkaline phosphatase in mineralization. *Curr. Opin. Orthop.* **2007**, *18*, 444–448. [CrossRef]
40. Faibish, D.; Ott, S.M.; Boskey, A.L. Mineral changes in osteoporosis: A review. *Clin. Orthop. Relat. Res.* **2006**, *443*, 28–38. [CrossRef] [PubMed]
41. Deca, A.G.; Belu, I.; Croitoru, O.; Bubulică, M.V.; Manda, C.V.; Neamtu, J. Formulation and In Vitro Evaluation of Alendronate Sodium/PLGA Microspheres for Applications in Bone Related Disorders. *Curr. health Sci. J.* **2015**, *41*, 246–250. [CrossRef]

42. Nafea, E.H.; El-Massik, M.A.; El-Khordagui, L.K.; Marei, M.k.; Khalafallah, N.M. Alendronate PLGA microspheres with high loading efficiency for dental applications. *J. Microencapsul.* **2007**, *24*, 525–538. [CrossRef]
43. LogithKumar, R.; KeshavNarayan, A.; Dhivya, S.; Chawla, A.; Saravanan, S.; Selvamurugan, N. A review of chitosan and its derivatives in bone tissue engineering. *Carbohydr. Polym.* **2016**, *151*, 172–188. [CrossRef]
44. Sukul, M.; Sahariah, P.; Lauzon, H.L.; Borges, J.; Másson, M.; Mano, J.F.; Haugen, H.J.; Reseland, J.E. In vitro biological response of human osteoblasts in 3D chitosan sponges with controlled degree of deacetylation and molecular weight. *Carbohydr. Polym.* **2021**, *254*, 117434. [CrossRef] [PubMed]
45. Seol, Y.J.; Lee, J.Y.; Park, Y.J.; Lee, Y.M.; Young, K.; Rhyu, I.C.; Lee, S.J.; Han, S.B.; Chung, C.P. Chitosan sponges as tissue engineering scaffolds for bone formation. *Biotechnol. Lett.* **2004**, *26*, 1037–1041. [CrossRef] [PubMed]
46. Ikono, R.; Li, N.; Pratama, N.H.; Vibriani, A.; Yuniarni, D.R.; Luthfansyah, M.; Bachtiar, B.M.; Bachtiar, E.W.; Mulia, K.; Nasikin, M.; et al. Enhanced bone regeneration capability of chitosan sponge coated with TiO_2 nanoparticles. *Biotechnol. Rep.* **2019**, *24*, e00350. [CrossRef] [PubMed]
47. Paspaliaris, V.; Kolios, G. Stem cells in Osteoporosis: From Biology to New Therapeutic Approaches. *Stem Cells Int.* **2019**, *2019*, 1730978. [CrossRef] [PubMed]
48. Bonyadi, M.; Waldman, S.D.; Liu, D.; Aubin, J.E.; Grynpas, M.D.; Stanford, W.L. Mesenchymal progenitor self-renewal deficiency leads to age-dependent osteoporosis in Sca-1/Ly-6A null mice. *Proc. Natl. Acad. Sci. USA* **2003**, *100*, 5840–5845. [CrossRef]
49. Hidestrand, M.; Richards-Malcolm, S.; Gurley, C.M.; Nolen, G.; Grimes, B.; Waterstrat, A.; Zant, G.V.; Peterson, C.A. Sca-1-expressing nonmyogenic cells contribute to fibrosis in aged skeletal muscle. *J. Gerontol. A Biol. Sci. Med. Sci.* **2008**, *63*, 566–579. [CrossRef]
50. Holmes, C.; Khan, T.S.; Owen, C.; Ciliberti, N.; Grynpas, M.D.; Stanford, W.L. Longitudinal analysis of mesenchymal progenitors and bone quality in the stem cell antigen-1-null osteoporotic mouse. *J. Bone Miner. Res. Off. J. Am. Soc. Bone Mineral. Res.* **2007**, *22*, 1373–1386. [CrossRef]
51. Agata, H.; Sumita, Y.; Hidaka, T.; Iwatake, M.; Kagami, H.; Asahina, I. Intra-Bone Marrow Administration of Mesenchymal Stem/Stromal Cells Is a Promising Approach for Treating Osteoporosis. *Stem Cells Int.* **2019**, *2019*, 4214281. [CrossRef]
52. Hayer, S.; Steiner, G.; Görtz, B.; Reiter, E.; Tohidast-Akrad, M.; Amling, M.; Hoffmann, O.; Redlich, K.; Zwerina, J.; Skriner, K.; et al. CD44 is a determinant of inflammatory bone loss. *J. Exp. Med.* **2005**, *201*, 903–914. [CrossRef] [PubMed]
53. Zhu, H.; Mitsuhashi, N.; Klein, A.; Barsky, L.W.; Weinberg, K.; Barr, M.L.; Demetriou, A.; Wu, G.D. The Role of the Hyaluronan Receptor CD44 in Mesenchymal Stem Cell Migration in the Extracellular Matrix. *Stem Cells* **2006**, *24*, 928–935. [CrossRef]
54. Sanghani-Kerai, A.; Coathup, M.; Samazideh, S.; Kalia, P.; Silvio, L.D.; Idowu, B.; Blunn, G. Osteoporosis and ageing affects the migration of stem cells and this is ameliorated by transfection with CXCR4. *Bone Jt. Res.* **2017**, *6*, 358–365. [CrossRef] [PubMed]
55. Xi, J.-C.; Zang, H.-Y.; Guo, L.-X.; Xue, H.-B.; Liu, X.-D.; Bai, Y.-B.; Ma, Y.-Z. The PI3K/AKT cell signaling pathway is involved in regulation of osteoporosis. *J. Recept. Signal. Transduct.* **2015**, *35*, 640–645. [CrossRef]
56. Chan, J.M.; Zhang, L.; Yuet, K.P.; Liao, G.; Rhee, J.-W.; Langer, R.; Farokhzad, O.C. PLGA–lecithin–PEG core–shell nanoparticles for controlled drug delivery. *Biomaterials* **2009**, *30*, 1627–1634. [CrossRef] [PubMed]
57. Jun, I.; Han, H.-S.; Edwards, J.R.; Jeon, H. Electrospun Fibrous Scaffolds for Tissue Engineering: Viewpoints on Architecture and Fabrication. *Int. J. Mol. Sci.* **2018**, *19*, 745. [CrossRef] [PubMed]
58. García-García, P.; Reyes, R.; Pérez-Herrero, E.; Arnau, M.R.; Évora, C.; Delgado, A. Alginate-hydrogel versus alginate-solid system. Efficacy in bone regeneration in osteoporosis. *Mater. Sci. Eng.* **2020**, *115*, 111009. [CrossRef] [PubMed]

Drug Delivery and Translational Research (2021) 11:598–607
https://doi.org/10.1007/s13346-021-00926-5

ORIGINAL ARTICLE

Tailor-made oligonucleotide-loaded lipid-polymer nanosystems designed for bone gene therapy

Patricia García-García[1] · Erik Briffault[1] · Mariana Landin[2] · Carmen Evora[1,3] · Patricia Diaz-Rodriguez[1,3] · Araceli Delgado[1,3]

Accepted: 26 January 2021 / Published online: 24 February 2021

Abstract
Gene therapy has emerged as a tool for the treatment of systemic metabolic disorders as osteoporosis (OP). However, the design of a suitable vehicle able to efficiently load and release the genetic material on the target cells is still a challenge. Moreover, the internalization pathway of nanosystems has been described to be dependent on their surface characteristics and the cell type evaluated. In this study, we aim at obtaining PEGylated lipid-PLGA nanoparticles (NPs) with variable surface charge able to incorporate GapmeRs (single-strand antisense oligonucleotides) for OP treatment. Nanoparticles showing negative, positive, and neutral surface charge were obtained by modulating the lipid composition. All formulations showed a remarkably low polydispersity index with adequate size. NPs were loaded with GapmeRs showing a high encapsulation efficiency and a surface charge–independent oligonucleotide loading. All the formulations were adequately internalized by MSCs. Future experiments will be devoted to use the developed formulations to clarify if the intracellular distribution of hybrid NPs on mesenchymal stem cells (MSCs) is dependent on surface charge. This portfolio of NPs will serve as a tool to analyze the effect of NP surface charge on gene therapy efficiency.

Keywords Gene therapy · Osteoporosis · Lipid-polymer nanoparticles · Tailorable surface charge · Cell uptake

Introduction

Osteoporosis (OP) is considered a worldwide high-prevalence disease with an associated significant morbidity and mortality. This pathology is characterized by a loss in the bone mass and a weak bone microarchitecture making patients susceptible to bone fractures [1]. The current osteoporosis management is mainly based on antiresorptive drugs that, when used as long-term treatments, present risk of side effects as osteonecrosis and atypical femoral fractures. Therefore, new therapeutic strategies for OP management have been explored focused on promoting tissue anabolism instead of avoiding bone catabolism [2]. On this sense, the use of gene therapy strategies devoted to control osteoblast activity and bone homeostasis have successfully increased osteogenesis "in vitro" in osteoporotic-derived mesenchymal stem cells and promoted mature bone formation in an "in vivo" model of OP [3].

Gene silencing has emerged as a promising tool for treating complex diseases such as cancer or systemic metabolic disorders as OP [4]. Despite the huge potential of synthetic oligonucleotides as gene-silencing molecules, their efficient administration remains a challenge to beat due to their low stability, small-cell internalization, and lack of specificity [5]. Among synthetic oligonucleotides, GapmeRs are antisense oligonucleotides composed of a synthetic single strand containing a central block of DNA nucleotides flanked by locked nucleic acids on each side. This structure provides several advantages as increased stability and decreased size when compared with other

✉ Patricia Diaz-Rodriguez
pdiarodr@ull.edu.es

✉ Araceli Delgado
adelgado@ull.edu.es

[1] Department of Chemical Engineering and Pharmaceutical Technology, Universidad de La Laguna, 38200 La Laguna, Spain

[2] R+D Pharma Group (GI-1645); Strategic Grouping in Materials (AEMAT)Department of Pharmacology, Pharmacy and Pharmaceutical TechnologyFaculty of Pharmacy, Universidade de Santiago de Compostela-Campus Vida, 15782 Santiago de Compostela, Spain

[3] Institute of Biomedical Technologies (ITB), Center for Biomedical Research of the Canary Islands (CIBICAN), Universidad de La Laguna, 38200 La Laguna, Spain

synthetic oligonucleotides [6]. Nanoparticulated systems allow for the incorporation of several therapeutic molecules on their structure that, owing to their surface modification abilities, can be specifically released to the target cells [7].

The physicochemical characteristics and composition of nanoparticles (NPs) condition both their "in vivo" and "in vitro" performance. Therefore, the development of nanomaterials with tailorable characteristics based on the selected application is a crucial step in formulation development [8]. However, the establishment of the formulation characteristics (composition, formulation procedures, concentrations…) responsible for the final formulation properties is complex. The nanosize nature of NPs makes these systems highly sensitive to any minimal change during formulation leading to unexpected formulation properties [9]. In order to obtain robust and reproducible formulations, it is crucial to understand the effect of the different components on formulation characteristics. Moreover, NP surface characteristics have been recognized as a crucial factor conditioning nanoparticle-cell interactions and recognition of proteins [10]. Pegylation is a widely used strategy to reduce protein adsorption, avoid opsonization, reduce NP clearance, and increase their blood circulation permanence time [7]. However, NP surface electric charge should also be considered as it conditions nanoparticle bioavailability, absorption, and cell uptake [11]. The entrance of NPs into the cells is an important step to ensure therapeutic efficacy when designing systems aimed at intracellular delivery, usually the case for antisense oligonucleotide delivery systems. Recently, the effect of cell status as cell cycle position and cell type on NPs endocytosis has been pointed out [12]. Numerous studies indicate that different cell types use different endocytic pathways to internalize the same NPs [13]. Therefore, it is crucial to understand the cell uptake process of the designed NPs on the desired cell target.

Lipid-polymer hybrid NPs can be composed by a polymeric core surrounded by a lipid shell. They have numerous advantages combining the favorable characteristics of polymeric and lipid nanoparticles. Therefore, they possess high stability and physical integrity due to the polymeric core, and ease of functionalization, high stability in general circulation, and cell uptake due to the lipid shell [14]. These characteristics make lipid-polymer hybrid nanoparticles a promising next generation of drug delivery platforms.

The main objective of this work is to develop pegylated lipid-PLGA nanosystems able to incorporate GapmeRs suitable for OP treatment. To obtain tailor-made nanoparticles with the desired properties, we initially aimed at understanding the effect of the lipid composition on nanoparticles physicochemical properties. On a next step, we evaluated the effect of NP surface charge on GapmeR-loading efficiency and bone marrow–derived mesenchymal stem cell uptake. To this purpose, lipid-PLGA nanoparticles were prepared with a similar particle size and polyethylene glycol (PEG) density but with variable surface charges (positive, negative, and neutral).

Materials and methods

Materials

Poly(D,L-lactide-co-glycolide) (Resomer® RG 502 H, MW 7,000–17,000) was provided by Evonik (Germany), Soy L-α-phosphatidylcholine (Lecithin) was obtained from Avanti Polar Lipids (USA), DSPE-PEG_{2000} (1,2-distearoyl-sn-glycero-3-phosphoethanolamine-N-[amino(polyethylene glycol)-2000] (ammonium salt)) was provided by Nanosoft Polymers (USA), DOTAP (1,2-dioleoyl-3-trimethylammonium-propane) and Protamine sulfate were purchased from Sigma-Aldrich (M_r: 5000–10000, USA), and fluorescently labeled GapmeR was custom designed and synthesized by Integrated DNA Technologies (USA).

GapmeR condensation using protamine

The ability of the cationic protein protamine to interact with GapmeR and promote its complexation was evaluated using three different oligonucleotide/protein weight ratios (1:2, 1:1, and 1:0.5). GapmeRs were allowed to interact with the protein for 40 min at room temperature. Samples were then loaded on 15% acrylamide gels, and electrophoresis was performed for 45 min. The migration of the GapmeR was visualized by ethidium bromide staining.

Hybrid nanoparticles preparation

Lipid-polymeric hybrid nanoparticles were prepared by a modified single-step nanoprecipitation method as shown in Supplementary Fig. 1 [15–17]. Briefly, PLGA or PLGA + DOTAP at the desired concentrations (see Table 1) were dissolved in acetone (1 ml), then 50 μL of an aqueous solution of protamine or protamine + GapmeR was added and mixed. Immediately, this mixture was poured on an aqueous solution (4% ethanol in water; 10 ml) containing the required amount of DSPE-PEG_{2000} with or without lecithin (Table 1). Lecithin was previously dissolved on the aqueous phase by heating the solution to 65 °C. To obtain GapmeR-loaded nanoparticles, the oligonucleotide was condensed with the protamine at a oligonucleotide/protamine 1:2 weight ratio for 40 min before their addition.

Physicochemical characterization of hybrid nanoparticles

The physicochemical properties of the nanoparticles were characterized in terms of average diameter, polydispersity

Table 1 Lipid composition and physicochemical characteristics of the analyzed formulations. Core components were kept constant (PLGA 5 mg (0.4 µmol)/batch and protamine 45 µg (0.006 µmol)/batch). Molar ratios (MRs) are shown in brackets

	Lecithin	DOTAP	DSPE-PEG$_{2000}$	Size (nm)		PdI		ζ-potential	
	mg (MR)	mg (MR)	mg (MR)	Mean	SD	Mean	SD	Mean	SD
1	2.0 (1)	–	–	179.77	3.76	0.18	0.03	38.97	3.24
2	1.2 (1)	–	–	171.75	5.87	0.13	0.04	−6.33	28.57
3	0.6 (1)	–	0.4 (0.2)	150.77	0.78	0.11	0.01	−34.30	1.85
4	0.6 (1)	–	0.8 (0.4)	178.47	2.48	0.09	0.02	−24.47	2.91
5	0.5 (1)	–	1.4 (0.7)	161.50	0.36	0.19	0.02	−25.57	2.06
6	0.3 (1)	0.1 (0.4)	–	176.45	11.29	0.08	0.01	28.72	9.64
7	0.4 (1)	0.1 (0.3)	–	176.22	0.12	0.12	0.04	32.23	2.12
8	0.3 (1)	0.2 (0.7)	–	178.07	2.42	0.10	0.04	51.07	2.58
9	0.4 (1)	0.2 (0.5)	–	184.02	5.49	0.08	0.01	44.72	0.64
10	0.3 (1)	0.2 (0.7)	0.4 (0.4)	167.77	0.91	0.10	0.004	35.33	3.20
11	0.4 (1)	0.2 (0.5)	0.4 (0.3)	163.56	9.66	0.13	0.06	13.87	8.86
12	0.6 (1)	0.2 (0.4)	0.4 (0.2)	173.57	5.81	0.10	0.03	14.33	0.23
13	–	0.4 (1)	–	167.40	0.72	0.06	0.002	49.43	1.31
14	–	0.4 (1)	0.5 (0.3)	153.93	1.79	0.10	0.004	39.55	0.64
15	–	0.4 (1)	0.4 (0.3)	165.03	0.45	0.10	0.02	44.37	2.75
16	–	0.4 (1)	0.8 (0.5)	144.97	1.40	0.10	0.01	28.07	1.40
17	0.6 (1)	0.4 (0.7)	0.8 (0.4)	166.10	4.37	0.16	0.06	19.80	0.50
18	0.1 (1)	0.5 (5.4)	0.9 (2.5)	145.37	0.49	0.11	0.01	35.30	0.89

index (PdI), and zeta-potential (ζ-potential) on a Zetasizer Nano-ZS (Malvern Instruments, UK). Samples were adequately diluted in ultrapure Milli-Q water and sonicated for 1 min on a water bath before characterization (P Selecta, Spain). All measurements were performed in triplicate for each sample.

Analysis of composition-properties relationship

To minimize the effect of formulation procedures on NP properties, all the formulations were prepared following the same protocol and fixing the amount of PLGA (5 mg/batch) and protamine (45 µg/batch). The composition of the NPs surface was modulated by changing the lipid components as described in Table 1. To understand the effect of each lipid on NP properties and their possible interactions, the database was modeled using the Artificial Intelligence software FormRules® v4.03 (Intelligensys Ltd., UK). This software combines artificial neural networks and fuzzy logic allowing to answer "WHAT IF" questions by the set of "IF-THEN" rules generated by the model explaining the effect of the lipid composition on the NP characteristics. To generate these rules, a fuzzyfication process is necessary as described elsewhere [18].

The training parameters used for FormRules® v4.03 models were Adaptive Spline Modeling of Observation Data (ASMOD) mode, two set densities, four maximum inputs per submodel, and 15 maximum nodes per input. The quality of the independent predictive model for each NPs property was evaluated using the determination coefficient of the training or test sets (R^2) expressed in percentage (predictability) and the analysis of variance (ANOVA) (accuracy) [18].

Encapsulation efficiency of hybrid nanoparticles

To analyze the encapsulation efficiency of NPs, fluorescently labeled GapmeRs were used (IDT Technologies, Germany). Formulations were prepared as described above, and NP suspensions were filtered through 10 KDa MWCO (Millipore Amicon, USA) filters. Non-encapsulated oligonucleotide was quantified on the filtrate by measuring the fluorescence on a plate reader (Biotek, USA). Oligonucleotide concentration was assessed by means of the correspondent calibration curve. The physicochemical properties of GapmeR-loaded NPs were also analyzed as described above.

Isolation of bone marrow–derived mesenchymal stem cells

Primary murine mesenchymal stem cells (mMSCs) were isolated from the tibia and femur of 8-week-old FVB male mice as previously described with slight modifications [19]. Bones were extracted, cleaned from muscle and periosteum, and stored in DPBS (Lonza, Belgium). In sterile conditions, both epiphyses were ruptured and washed twice with 10 mL of Dulbecco's modified Eagle's medium (DMEM) (Lonza, Belgium) supplemented with 10% fetal bovine serum (FBS; Biowest, France), 2 mM L-glutamine (Sigma-Aldrich,

Germany), and 1% penicillin-streptomycin (Sigma-Aldrich, Germany). Eluates were collected and centrifuged at 1,200 rpm for 5 min; the resulting pellets were combined, resuspended in 15 mL of DPBS, and centrifuged again under the same conditions. The resulting pellet was resuspended in 1.5 mL of complete DMEM; cells were seeded on a petri dish and incubated at 37 °C and 5% CO_2. Cell culture media was changed every day for 72 h, then trypsinized (trypsin–EDTA 0.25% in HBSS free of calcium, magnesium, and phenol red, Biowest, France) and cells seeded in T-75 Flasks until confluency.

Hybrid NP cell uptake

To evaluate NP cell uptake, positive, negative, and neutral systems were loaded with 40 µg/ml coumarin-6 (Sigma-Aldrich, Germany). The obtained NP suspensions were purified by filtration and washed twice with double-distilled water to remove any free couamarin-6. mMSCs were seeded on 96-well plates at 2×10^5 cells per well and allowed to attach for 24 h. The day of the experiment culture media was removed, and cells were treated with NP suspensions diluted in complete culture media at variable concentrations for 2 h at 37 °C. Then, NP suspensions were removed, and cell monolayers were washed three times with DPBS (Lonza, USA). Afterward, cells were lysed with 1% Triton X-100, and the fluorescence of the lysate was measured on a plate reader. The dose of NPs internalized was obtained by the correlation of the obtained fluorescence with the fluorescence of NP suspensions at variable concentrations.

Statistical analysis

Results are expressed as mean ± standard deviation. SPSS software (IBM SPSS Statistics 27) was employed to perform a one-way ANOVA followed by HSD Tukey's post hoc to compare the different groups. Statistically significant differences were considered when $p < 0.05$.

Results

Protamine complexation of the selected GapmeR

Figure 1 shows the migration of GapmeRs alone (denoted as 1:0) or complexed with variable amounts of protamine. The addition of protamine to the oligonucleotide solution indeed promoted its complexation with the protein avoiding GapmeR migration. Moreover, while the GapmeR/protamine ratio 1:0.5 led to some free oligonucleotide, an increase in the protein amount (1:1 and 1:2 ratios) completely blocked oligonucleotide migration indicating its successful complexation with protamine. The selected ratio used for further experiments was 1:2 GapmeR/protamine.

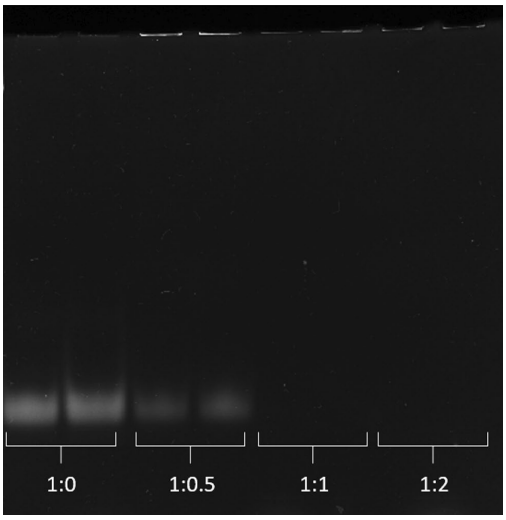

Fig. 1 Gel electrophoresis of GapmeR alone (1:0) or GapmeR/protamine complexes at 1:0.5, 1:1, and 1:2 weight rations in a 15% acrylamide gel

Analysis of composition-properties relationship

Hybrid nanoparticles with suitable physicochemical properties were successfully obtained by a modified single-step nanoprecipitation method without the need of synthetic surfactants. The physicochemical characteristics of the developed formulations are shown in Table 1. As indicated below, the core components were kept constant for all the formulations (PLGA 5 mg/batch and protamine 45 µg/batch) while the lipid components were combined in different proportions. The amount of DOTAP tested varied from 0 to 0.5 mg, DSPE-PEG_{2000} was used in variable amounts from 0 to 1.45 mg, and soy lecithin was studied using proportions from 0 to 2 mg. Further compositions were tested but discarded due to high size (> 200 nm) and/or PdI (> 0.20). All the selected formulations presented adequate size ranging from 137.6 to 179.77 nm with low standard deviation. The PdI values of the analyzed formulations were between 0.08 and 0.19 also with low standard deviation. As expected, ζ-potential values were highly variable, obtaining formulations from −34.30 to + 51.7 mV with different standard deviation depending on the composition.

To better understand the formulation components responsible for the variation in ζ-potential, we took advantage of artificial intelligence techniques. The modelization performed by FormRules® v4.03 allowed to point out the crucial role of DOTAP

on NP surface properties that mainly rules NP surface charge. The model presented good predictability (R^2=79.5) and accuracy (computed f ratio > critical f ratio at α=0.05). The complete set of "IN-THEN" rules is shown in Supplementary Materials. The obtained model also indicated, as a secondary submodel, that an increment in DSPE-PEG$_{2000}$ amount leads to a decrease in surface charge (Fig. 2, Supplementary Fig. 2). Therefore, according to the developed model, ζ-potential can be mainly modulated by just modifying the amount of DOTAP used. Consequently, to obtain NPs with different surface charge (negative (ANPs), positive (CNPs), and neutral (NNPs)) three levels of DOTAP were used (0, 0.4, and 0.2 mg respectively) while maintaining constant the total lipid content and PEG density.

Development of anionic, cationic, and neutral NPs

PEG molecules are known to shield the nanoparticle surface and decrease reticuloendothelial system (RES) capture. In vivo NP terminal half-life increases with high PEG molecule densities like 0.9 PEG/nm^2 [20]. Moreover, increasing PEG-coating densities to 1.25 PEG/nm^2 leads to a decrease in serum protein adsorption [21]. Thus, the selected PEG density for further studying NP surface charge effect on GapmeR encapsulation efficiency and mesenchymal stem cell uptake was set at 1.25 PEG/nm^2.

To determine the PEG amount required to achieve the desired density of 1.25 PEG/nm^2, we used the equation described elsewhere [22] and assumed the following: (1) all the PEG was incorporated into the NP shell, (2) NPs were completely spherical, and (3) the obtained NPs would have an average diameter of 166 nm (mean diameter of previously obtained NPs). The development of models able to correlate formulation components with not only ζ-potential but also size and PdI with excellent predictability ($R^2 > 71$) and accuracy (computed f ratio > critical f ratio at $\alpha = 0.05$) allowed to predict the characteristics of the designed negative, positive, and neutral NPs as described on Table 2.

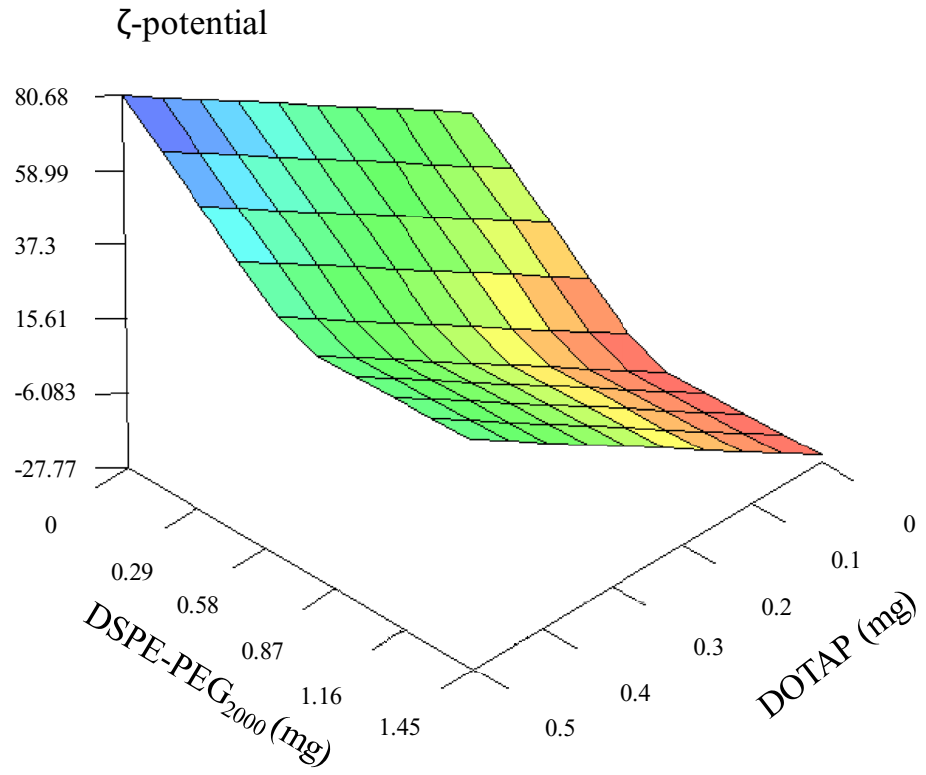

Fig. 2 Effect of DSPE-PEG$_{2000}$ and DOTAP amount on hybrid NP surface charge according to FormRules® v4.03

Table 2 Lipid composition and predicted physicochemical characteristics of the selected positive (CNPs), negative (ANPs), and neutral (NNPs). Core components were kept constant (PLGA 5 mg/batch and protamine 45 μg/batch)

	DOTAP	DSPE-PEG$_{2000}$	Lecithin	Size	PdI	ζ-potential
	mg	mg	mg	nm		mV
ANPs	0.0	1.1	0.4	155.77	0.134	−26.917
CNPs	0.4	1.1	0.0	139.82	0.085	25.391
NNPs	0.2	1.1	0.2	153.68	0.109	−0.763

Six batches of each of the designed formulations were prepared in order to analyze the reproducibility of the physicochemical characteristics of the NPs. All the developed NPs present a monodisperse distribution with mean PdI values of 0.12 ± 0.01 for ANPs, 0.09 ± 0.01 for CNPs, and 0.08 ± 0.01 for NNPs. Interestingly, ANP presented significantly higher PdI values when compared with CNPs and NNPs ($p < 0.036$). Figure 3 shows the distribution of size and zeta-potential of the three formulations selected. No significant differences in size ($p > 0.8$) were observed between the three formulations (Fig. 3a). The mean size was 170.34 ± 20.81 nm for ANPs, 162.90 ± 14.97 nm for CNPs, and 168.85 ± 21.96 nm for NNPs. On the other hand, as expected, significant differences were obtained in the surface charge of the developed formulations ($p \leq 0.002$) (Fig. 3b). ANPs presented a ζ-potential of -20.68 ± 5.70 mV; CNPs showed a surface potential of 25.08 ± 6.89 mV, and NNPs were characterized by a neutral potential ($0{,}30 \pm 11{,}46$ mV). Remarkably, the developed formulations presented the desired surface properties showing values close to those predicted by the model not only for surface charge properties but also for size and PdI, pointing out the reliability of the developed models (Table 2).

After NP characterization, PEG densities were calculated based on the real NP diameter leading to the following values: 1.28 PEG/nm^2 for ANP, 1.23 PEG/nm^2 for CNP, and 1.27 PEG/nm^2 for NNP.

Encapsulation efficiency of ANPs, CNPs, and NNPs

The capacity of the developed ANPs, CNPs, and NNPs to incorporate oligonucleotides was determined (Fig. 4a). All nanoparticles showed high GapmeR encapsulation efficiency with no significant differences between the samples being of $83.27 \pm 1.14\%$ for ANPs, $84.47 \pm 0.52\%$ for CNPs, and $84.55 \pm 0.41\%$ for NNPs. Moreover, no significant effect of GapmeR incorporation was observed on NP size (Fig. 4b). The incorporation of GapmeR-modified NP surface charge depends on the composition of the NPs, as shown in Fig. 4c. While not much effect was observed for negatively charged NPs (ANPs) and positively charged (CNPs), neutral (NNPs) NPs significantly decreased their ζ-potential with the incorporation of GapmeR ($p = 0.000$).

Cell uptake

NP cell uptake was analyzed using bone marrow–derived mesenchymal stem cells, crucial for controlling bone metabolism (Fig. 5). No statistical differences were observed between the three formulations tested, but a slight decrease in cellular uptake was visible for nanoparticles prepared only with DOTAP (CNPs) despite their clear positive charge.

Discussion

The use of artificial intelligence techniques successfully allowed to predict the properties of lipid-polymer hybrid nanoparticles. This utility of artificial intelligence techniques has been previously described for other type of pharmaceutical formulations as hydrogels, microspheres, and lipid nanoparticles, allowing to select the formulation conditions/components suitable to obtain the desired properties [9, 23, 24]. However, to the best of our knowledge,

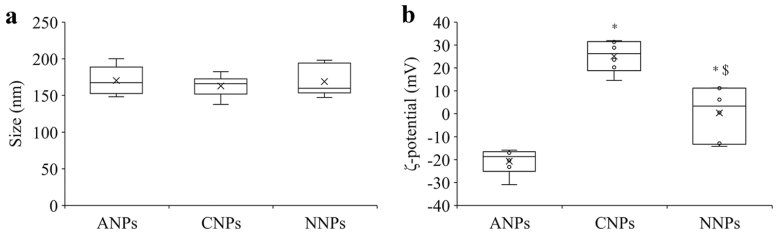

Fig. 3 Distribution of size and surface charge of the selected formulations cationic NPs (CNPs), anionic NPs (ANPs), and neutral (NNPs). *Denotes statistical differences to ANPs ($p = 0.000$), $statistical differences to CNPs ($p \leq 0.002$)

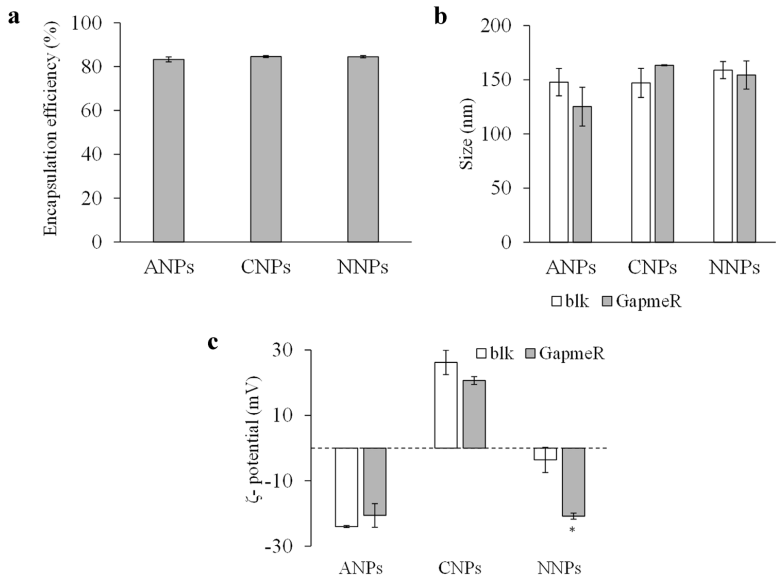

Fig. 4 **a** Encapsulation efficiency of designed anionic, cationic, and neutral NPs. **b**, **c** Size and zeta potential of empty (blk) and loaded (GapmeR) nanoparticle formulations. *Statistical differences compared with blk formulations ($p = 0.000$)

no studies concerning hybrid nanoparticles using artificial intelligence tools have been reported before. In this study, the modelization of the experimental results with excellent predictability and accuracy indicated that the surface charge of PEGylated PLGA hybrid nanoparticles is mainly controlled by the cationic lipid DOTAP (Fig. 2). Despite using a negatively charged PEG-modified lipid (DSPE-PEG_{2000}) on the formulation, the effect of this component on the surface charge only appears as a secondary submodel. The lower effect of DSPE-PEG on surface charge compared with DOTAP could be related to the presence of the PEG chain on the molecule that could shield the DSPE phosphate group negative charge. The effect of PEG addition on NP charge decrease has been already pointed out [25].

Based on the obtained models, we can modify NP surface charge by just tuning the amount of DOTAP used during the formulation procedure allowing to maintain the PEG density constant, crucial in most of the NP surface phenomena. This fact could be highly valuable when correlating surface properties with NP biological performance.

PEGylated lipid-polymer hybrid nanoparticles were obtained without requiring the use of surfactants, other than soy lecithin, showing a monodisperse distribution with an adequate diameter (Fig. 3). In fact, cationic nanoparticles were obtained even without the addition of lecithin. This behavior can be explained by the formulation method selected: a one-step self-assembly nanoprecipitation method. Remarkably, the formulations we prepared following our developed protocol presented similar size or even lower than those reported by other authors for hybrid PLGA nanoparticles following similar methodology [26, 27]. Surfactants are commonly included in nanoparticulated systems during the formulation step to control the formation, morphology, and surface properties of NPs [28]. Moreover, their use as stabilizers to avoid particle aggregation is a common practice for both metallic and polymeric NPs [29, 30]. However, the presence of synthetic surfactants on NPs surface hinders their interaction with the surrounding components while conditioning cell binding and target recognition [29]. Furthermore, synthetic surfactants are highly toxic and compromise the cytocompatibility of the final formulations. In this context, natural surfactants as lecithins

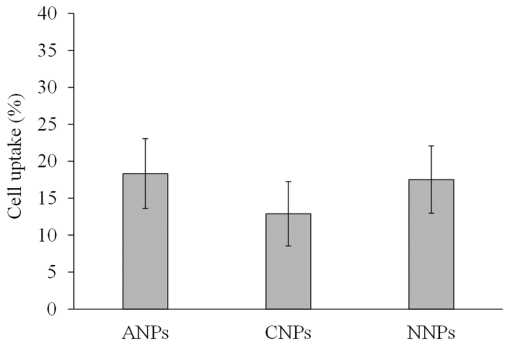

Fig. 5 Bone marrow–derived mesenchymal stem cell uptake of selected anionic, cationic, and neutral NPs after 2 h of incubation

have been proposed as alternatives in NP formulation due to their high biocompatibility and amphiphilicity, presenting great emulsifying properties [31]. Therefore, the NPs designed in this work presented adequate characteristics evading the drawbacks of synthetic surfactants.

Surface PEGylation is a widely used strategy to decrease unspecific protein adsorption and promote RES evasion. The PEG grafting density modulates NP pharmacokinetics, migration trough biological matrices, and mucus [22]. Some authors have pointed out that PEG density should be at least 0.2 PEG/nm^2 to prolong blood circulation time independently of the NP size [32]. Moreover, the use of PEG densities above 0.64 PEG/nm^2 leads to a decrease in macrophage uptake. In this case, NPs are internalized by a mechanism independent of surface protein adsorption [21]. The NPs prepared in this work presented a PEG density close to 1.25 PEG/nm^2; this characteristic could decrease unspecific macrophage internalization while ensuring long circulation time.

The lipid/polymer ratio of hybrid nanoparticles affects their encapsulation efficiency, drug loading, and release [33]. To avoid variability caused by different lipid/polymer ratios, we fixed the total amount of lipid used. The selected formulations (ANPs, CNPs, and NNPs) indeed presented negative, positive, and neutral charge with similar size. NPs were loaded with nucleic acid (GapmeR) for this; oligonucleotides were condensed with the cationic protein (protamine) showing adequate complexation (Fig. 1). This approach led to high encapsulation efficiencies for all the formulations tested (Fig. 4). Hybrid nanoparticles have been already tested as gene delivery systems. However, these NPs were superficially loaded with oligonucleotides based on a surface charge–dependent mechanism through electrostatic complexation [33]. This strategy entangles the risk of nucleic acid desorption during storage or administration and higher exposure to nucleases in the extracellular space [34, 35]. On the other hand, the method followed on this work, unlike superficial ionic loading, allowed to reach an adequate oligonucleotide incorporation independent of NP surface charge.

Bone marrow mesenchymal stem cells (MSCs) are highly involved in osteogenesis. During this process, they migrate, proliferate, and commit to actively proliferating pre-osteoblasts followed by their differentiation to mature osteoblasts. However, in OP, MSC functionality is impaired: their self-renewal capacity is decreased, and they tend to shift to an adipogenic differentiation commitment [36]. The development of therapeutic systems able to revert this altered behavior is an attractive alternative to promote a healthy bone homeostasis. Gene therapy strategies, transfecting MSCs with oligonucleotides aimed at controlling their differentiation pathway followed by their "in vivo" implantation, have been used to promote osteogenesis with successful outcomes [3, 37–39]. As a step forward, in this study, we propose to develop NPs for in vivo transfection of MSCs in OP. This approach should allow to achieve systemic effects while avoiding cell isolation, "in vitro" expansion, and later implantation. Moreover, the proposed strategy eludes the risk of MSC mortality after implantation. The developed gene delivery systems should be internalized by the target cells (MSCs), allowing for the subsequent release of the nucleic acid inside them. Therefore, NP cell uptake by MSCs is a key step to ensure therapeutic performance.

NP surface charge together with size, shape, composition, and surface hydrophobicity modulates cell uptake [40]. In this study, we aimed at analyzing the effect of surface charge in the cell uptake of hybrid NPs with the same PEG density. Literature generally points out cationic NPs tend to be more easily internalized than anionic NPs, while this behavior depends on the cell type and many other factors [40, 41]. In our work, PEGylated lipid-polymer PLGA NPs were internalized in a similar extend independently of their surface charge (Fig. 4). Similar results have been already described for mesoporous silica nanoparticles and PLGA nanoparticles [42, 43]. This performance could be explained by the high NP uptake efficiency of MSCs. As reported by Chung and coworkers, the lack of correlation between NP surface charge and cell uptake in MSCs could be caused by a switch in the internalization pathway from a clathrin- and actin-dependent endocytosis, when neutral and negative NPs are used, to a different mechanism when highly positive NPs are used (+19 mV). The use of different internalization pathways would determine NP intracellular fate and distribution. Indeed, for other cell lines (fibroblasts, epithelial cells, endothelial cells, and blood cells), the intracellular trafficking of NPs showed a charge-dependent behavior. Positively charged NPs could escape the lysosomes after internalization, showing perinuclear localization, while negative and neutral NPs were mainly located within lysosomes [26]. It is still unknown whether varying NP surface charge promotes a similar change in NP intracellular distribution in MSCs to those described in other cell types. The surface tailorable properties of the NPs developed in this work may help to clarify this point, which conditions gene-silencing efficiency.

Conclusions

For the first time, PEGylated PLGA lipid-polymer hybrid nanoparticles with tailorable surface charge were obtained to analyze the effect of surface charge on GapmeR loading and MSC uptake. The obtained negative, positive, and neutral NPs showed a remarkably low polydispersity index with adequate size and allowed a surface charge–independent loading of GapmeR. All the formulations were adequately internalized by MSCs. Future experiments will be devoted to use ANPs, CNPs, and NNPs to clarify if the intracellular

distribution of hybrid NPs on MSCs is dependent on surface charge. This portfolio of NPs will serve as a tool to analyze the effect of NP surface charge on gene therapy efficiency.

Supplementary information The online version contains supplementary material available at https://doi.org/10.1007/s13346-021-00926-5.

Acknowledgements PGG thanks Universidad de La Laguna and Ministerio de Ciencia, Innovación y Universidades for her Ph.D. fellowship (Contratos M-ULL para la formación de Doctores convocatoria 2019).

Author contributions Conceptualization: PGG, ML, CE, PDR, and AD; methodology and investigation: PGG, EB, and PDR; formal analysis: ML, CE, PDR and AD; writing, draft preparation, review, and editing: CE, PDR, and AD; funding acquisition: CE and AD.

Funding This work was supported by Ministerio de Ciencia, Innovación y Universidades (RTI2018-097324).

Data availability Full database will be available after request.

Declarations

Competing interests The authors declare that they have no conflict of interest.

References

1. Kanis JA, Cooper C, Rizzoli R, Reginster JY. European guidance for the diagnosis and management of osteoporosis in postmenopausal women. Osteoporosis international : a journal established as result of cooperation between the European Foundation for Osteoporosis and the National Osteoporosis Foundation of the USA. 2019;30(1):3–44. https://doi.org/10.1007/s00198-018-4704-5.
2. Cheng C, Wentworth K, Shoback DM. New frontiers in osteoporosis therapy. Annu Rev Med. 2020;71:277–88. https://doi.org/10.1146/annurev-med-052218-020620.
3. García-García P, Ruiz M, Reyes R, Delgado A, Évora C, Riancho JA et al. Smurf1 silencing using a LNA-ASOs/lipid nanoparticle system to promote bone regeneration. 2019;8(12):1306–17. https://doi.org/10.1002/sctm.19-0145.
4. Lundin KE, Gissberg O, Smith CI. Oligonucleotide therapies: the past and the present. Hum Gene Ther. 2015;26(8):475–85. https://doi.org/10.1089/hum.2015.070.
5. Juliano RL. The delivery of therapeutic oligonucleotides. Nucleic Acids Res. 2016;44(14):6518–48. https://doi.org/10.1093/nar/gkw236.
6. Abewe H, Deshmukh S, Mukim A, Beliakova-Bethell N. Use of GapmeRs for gene expression knockdowns in human primary resting CD4+ T cells. J Immunol Methods. 2020;476:112674. https://doi.org/10.1016/j.jim.2019.112674.
7. Machado Cruz R, Santos-Martinez MJ, Tajber L. Impact of polyethylene glycol polymers on the physicochemical properties and mucoadhesivity of itraconazole nanoparticles. European journal of pharmaceutics and biopharmaceutics : official journal of Arbeitsgemeinschaft fur Pharmazeutische Verfahrenstechnik eV. 2019;144:57–67. https://doi.org/10.1016/j.ejpb.2019.09.004.
8. Patra JK, Das G, Fraceto LF, Campos EVR, Rodriguez-Torres MDP, Acosta-Torres LS, et al. Nano based drug delivery systems: recent developments and future prospects. J Nanobiotechnol. 2018;16(1):71. https://doi.org/10.1186/s12951-018-0392-8.
9. Rouco H, Diaz-Rodriguez P, Rama-Molinos S, Remuñán-López C, Landin M. Delimiting the knowledge space and the design space of nanostructured lipid carriers through Artificial Intelligence tools. Int J Pharm. 2018;553(1):522–30. https://doi.org/10.1016/j.ijpharm.2018.10.058.
10. Godara S, Lather V, Kirthanashri SV, Awasthi R, Pandita D. Lipid-PLGA hybrid nanoparticles of paclitaxel: Preparation, characterization, in vitro and in vivo evaluation. Mater Sci Eng C Mater Biol Appl. 2020;109:110576. https://doi.org/10.1016/j.msec.2019.110576.
11. Du XJ, Wang JL, Iqbal S, Li HJ, Cao ZT, Wang YC, et al. The effect of surface charge on oral absorption of polymeric nanoparticles. Biomater Sci. 2018;6(3):642–50. https://doi.org/10.1039/c7bm01096f.
12. Rees P, Wills JW, Brown MR, Barnes CM, Summers HD. The origin of heterogeneous nanoparticle uptake by cells. Nat Commun. 2019;10(1):2341. https://doi.org/10.1038/s41467-019-10112-4.
13. Behzadi S, Serpooshan V, Tao W, Hamaly MA, Alkawareek MY, Dreaden EC, et al. Cellular uptake of nanoparticles: journey inside the cell. Chem Soc Rev. 2017;46(14):4218–44. https://doi.org/10.1039/c6cs00636a.
14. Mukherjee A, Waters AK, Kalyan P, Achrol AS, Kesari S, Yenugonda VM. Lipid-polymer hybrid nanoparticles as a next-generation drug delivery platform: state of the art, emerging technologies, and perspectives. Int J Nanomed. 2019;14:1937–52. https://doi.org/10.2147/ijn.s198353.
15. Chan JM, Zhang L, Yuet KP, Liao G, Rhee J-W, Langer R, et al. PLGA–lecithin–PEG core–shell nanoparticles for controlled drug delivery. Biomaterials. 2009;30(8):1627–34. https://doi.org/10.1016/j.biomaterials.2008.12.013.
16. Zhang L, Chan JM, Gu FX, Rhee JW, Wang AZ, Radovic-Moreno AF, et al. Self-assembled lipid–polymer hybrid nanoparticles: a robust drug delivery platform. ACS Nano. 2008;2(8):1696–702. https://doi.org/10.1021/nn800275r.
17. Tahir N, Madni A, Correia A, Rehman M, Balasubramanian V, Khan MM, et al. Lipid-polymer hybrid nanoparticles for controlled delivery of hydrophilic and lipophilic doxorubicin for breast cancer therapy. Int J Nanomed. 2019;14:4961–74. https://doi.org/10.2147/IJN.S209325.
18. Díaz-Rodríguez P, Landin M. Smart design of intratumoral thermosensitive β-lapachone hydrogels by artificial neural networks. Int J Pharm. 2012;433(1):112–8. https://doi.org/10.1016/j.ijpharm.2012.05.008.
19. Soleimani M, Nadri S. A protocol for isolation and culture of mesenchymal stem cells from mouse bone marrow. Nat Protoc. 2009;4(1):102–6. https://doi.org/10.1038/nprot.2008.221.
20. Du XJ, Wang JL, Liu WW, Yang JX, Sun CY, Sun R, et al. Regulating the surface poly(ethylene glycol) density of polymeric nanoparticles and evaluating its role in drug delivery in vivo. Biomaterials. 2015;69:1–11. https://doi.org/10.1016/j.biomaterials.2015.07.048.
21. Walkey CD, Olsen JB, Guo H, Emili A, Chan WCW. Nanoparticle size and surface chemistry determine serum protein adsorption and macrophage uptake. J Am Chem Soc. 2012;134(4):2139–47. https://doi.org/10.1021/ja2084338.
22. Xu Q, Ensign LM, Boylan NJ, Schön A, Gong X, Yang JC, et al. Impact of surface polyethylene glycol (PEG) density on biodegradable nanoparticle transport in mucus ex vivo and distribution in vivo. ACS Nano. 2015;9(9):9217–27. https://doi.org/10.1021/acsnano.5b03876.
23. Garcia-del Rio L, Diaz-Rodriguez P, Landin M. New tools to design smart thermosensitive hydrogels for protein rectal delivery in IBD. Mater Sci Eng, C. 2020;106:110252. https://doi.org/10.1016/j.msec.2019.110252.

24. Kazazi-Hyseni F, Landin M, Lathuile A, Veldhuis GJ, Rahimian S, Hennink WE, et al. Computer modeling assisted design of monodisperse plga microspheres with controlled porosity affords zero order release of an encapsulated macromolecule for 3 months. Pharm Res. 2014;31(10):2844–56. https://doi.org/10.1007/s11095-014-1381-8.
25. Kumar V, Qin J, Jiang Y, Duncan RG, Brigham B, Fishman S, et al. Shielding of lipid nanoparticles for siRNA delivery: impact on physicochemical properties, cytokine induction, and efficacy. Mol Ther Nucleic Acids. 2014;3(11):e210. https://doi.org/10.1038/mtna.2014.61.
26. Yue Z-G, Wei W, Lv P-P, Yue H, Wang L-Y, Su Z-G, et al. Surface charge affects cellular uptake and intracellular trafficking of chitosan-based nanoparticles. Biomacromolecules. 2011;12(7):2440–6. https://doi.org/10.1021/bm101482r.
27. Ling G, Zhang P, Zhang W, Sun J, Meng X, Qin Y, et al. Development of novel self-assembled DS-PLGA hybrid nanoparticles for improving oral bioavailability of vincristine sulfate by P-gp inhibition. J Control Release. 2010;148(2):241–8. https://doi.org/10.1016/j.jconrel.2010.08.010.
28. Wang W, Gu B, Liang L. Effect of surfactants on the formation, morphology, and surface property of synthesized SiO2 nanoparticles. J Dispersion Sci Technol. 2005;25(5):593–601. https://doi.org/10.1081/DIS-200027309.
29. Khan R, Inam MA, Khan S, Jiménez AN, Park DR, Yeom IT. The influence of ionic and nonionic surfactants on the colloidal stability and removal of CuO nanoparticles from water by chemical coagulation. Int J Environ Res Public Health. 2019;16(7). https://doi.org/10.3390/ijerph16071260.
30. Kennedy PJ, Perreira I, Ferreira D, Nestor M, Oliveira C, Granja PL, et al. Impact of surfactants on the target recognition of Fab-conjugated PLGA nanoparticles. Eur J Pharm Biopharm. 2018;127:366–70. https://doi.org/10.1016/j.ejpb.2018.03.005.
31. Vater C, Adamovic A, Ruttensteiner L, Steiner K, Tajpara P, Klang V, et al. Cytotoxicity of lecithin-based nanoemulsions on human skin cells and ex vivo skin permeation: comparison to conventional surfactant types. Int J Pharm. 2019;566:383–90. https://doi.org/10.1016/j.ijpharm.2019.05.078.
32. Bertrand N, Grenier P, Mahmoudi M, Lima EM, Appel EA, Dormont F, et al. Mechanistic understanding of in vivo protein corona formation on polymeric nanoparticles and impact on pharmacokinetics. Nat Commun. 2017;8(1):777. https://doi.org/10.1038/s41467-017-00600-w.
33. Dave V, Tak K, Sohgaura A, Gupta A, Sadhu V, Reddy KR. Lipid-polymer hybrid nanoparticles: Synthesis strategies and biomedical applications. J Microbiol Methods. 2019;160:130–42. https://doi.org/10.1016/j.mimet.2019.03.017.
34. Roberts TC, Langer R, Wood MJA. Advances in oligonucleotide drug delivery. Nat Rev Drug Discov. 2020;19(10):673–94. https://doi.org/10.1038/s41573-020-0075-7.
35. Yang Z, Qian Y, Yang F, Chen C, Tang X, Jin J. Investigating adsorption/desorption of DNA on ZIF-8 surface by fluorescently labeled oligonucleotides. Langmuir. 2019;35(49):16290–6. https://doi.org/10.1021/acs.langmuir.9b02692.
36. Infante A, Rodríguez CI. Osteogenesis and aging: lessons from mesenchymal stem cells. Stem Cell Res Ther. 2018;9(1):244. https://doi.org/10.1186/s13287-018-0995-x.
37. Sun Y, Xu J, Xu L, Zhang J, Chan K, Pan X, et al. MiR-503 promotes bone formation in distraction osteogenesis through suppressing Smurf1 expression. Sci Rep. 2017;7(1):409. https://doi.org/10.1038/s41598-017-00466-4.
38. Xie Q, Wei W, Ruan J, Ding Y, Zhuang A, Bi X, et al. Effects of miR-146a on the osteogenesis of adipose-derived mesenchymal stem cells and bone regeneration. Sci Rep. 2017;7(1):42840. https://doi.org/10.1038/srep42840.
39. Xie Q, Wang Z, Zhou H, Yu Z, Huang Y, Sun H, et al. The role of miR-135-modified adipose-derived mesenchymal stem cells in bone regeneration. Biomaterials. 2016;75:279–94. https://doi.org/10.1016/j.biomaterials.2015.10.042.
40. Fröhlich E. The role of surface charge in cellular uptake and cytotoxicity of medical nanoparticles. Int J Nanomed. 2012;7:5577–91. https://doi.org/10.2147/ijn.s36111.
41. Verma A, Stellacci F. Effect of surface properties on nanoparticle-cell interactions. Small. 2010;6(1):12–21. https://doi.org/10.1002/smll.200901158.
42. Chung T-H, Wu S-H, Yao M, Lu C-W, Lin Y-S, Hung Y, et al. The effect of surface charge on the uptake and biological function of mesoporous silica nanoparticles in 3T3-L1 cells and human mesenchymal stem cells. Biomaterials. 2007;28(19):2959–66. https://doi.org/10.1016/j.biomaterials.2007.03.006.
43. Almeida B, Wang Y, Shukla A. Effects of nanoparticle properties on kartogenin delivery and interactions with mesenchymal stem cells. Ann Biomed Eng. 2020;48(7):2090–102. https://doi.org/10.1007/s10439-019-02430-x.